University of Sussex

Beyond the standard model in effective couplings

The charm contribution to mixing and decay of the B meson

Kirsten Leslie

Submitted for the degree of Doctor of Philosophy

School of Mathematical and Physical Sciences

University of Sussex

July 2019

Declaration

I hereby declare that this thesis has not been and will not be submitted in whole or in part to another University for the award of any other degree. The research in this Thesis has been carried out in collaboration with my supervisor Prof. S. Jäger and Prof . A. Lenz, Dr. M. Kirk and Dr. L. Vale-Silva. The parts of this Thesis which contain research performed collaboratively are detailed as follows:

- Chapters 3, 4, 5 and 6 contain work with Prof. S. Jäger, Dr. M. Kirk and Prof. A. Lenz based on "Charming new physics in rare b decays and mixing?" published in Physical Reviews D [1].

- Chapters 3, 4, 5 and 6 contain work with Prof. S. Jäger, Prof. A. Lenz, Dr. M. Kirk based on "Charming New B-Physics" submitted to JHEP [2].

- Chapter 6 is based on work with Prof. S. Jäger and Dr. L.Vale-Silva [3].

Signature:

Kirsten Leslie

UNIVERSITY OF SUSSEX

KIRSTEN LESLIE, DOCTOR OF PHILOSOPHY

BEYOND THE STANDARD MODEL IN EFFECTIVE COUPLINGS
THE CHARM CONTRIBUTION TO MIXING AND DECAY OF THE B MESON

SUMMARY

This thesis performs a comprehensive and systematic study of Beyond the Standard Model (BSM) physics in $b \to c\bar{c}s$ couplings, using an Effective Field Theory (EFT) framework. The weak effective Hamiltonian is constructed from a complete set of twenty, dimension six four quark operators and their respective Wilson coefficients. The phenomenological impact of these operators upon B-physics observables is investigated. Conservation and violation of CP (where C is the charge conjugation symmetry and P is the parity symmetry) are both considered.

Where CP is conserved, couplings take real values. In this case, the following quantities are calculated; from mixing processes the $B_s^{(0)} - \bar{B}_s^{(0)}$ decay rate difference and flavour specific CP asymmetry, the $B_s^{(0)}$ to $B_d^{(0)}$ meson lifetime ratio, the branching ratio for the inclusive $B \to X_s\gamma$ decay rate and the partonic transition amplitude for the rare decay $b \to s\mu^+\mu^-$. Subsequently, effects potentially detectable in real valued Wilson coefficients are predicted and presented for the full basis of twenty operators. Bounds upon the energy scale at which such operators are generated and which indicate the energy at which new heavy quanta could be present, are found to be in the TeV range.

Where CP is violated couplings take complex values, and hence carry new weak phases. Here, the above set of observables is expanded to include the time dependent $B_d^{(0)} \to J/\psi K_S$ CP asymmetry and the $B_d^{(0)} \to J/\psi K_d^{(0)}$ branching ratio. These quantities are calculated for a subset of coefficients. It is found that a small CP violating shift to SM coefficients is attainable within constraints from data.

In addition to the above findings, the Renormalization Group Equation (RGE) is solved for the complete set of Wilson coefficients, and the evolution matrix governing the change of coefficients with energy scale is obtained and presented.

Finally, a separate technical result regarding one and two loop diagrams which forms part of an ongoing project on anomalous dimensions in the Standard Model Effective Field Theory (SMEFT), are presented.

Acknowledgements

I would like to express my thanks to my supervisor Sebastian Jäger for his time, discussion and experience and for giving me this opportunity. I thank Alex Lenz for discussion, experience and support and Matthew Kirk for being such a good collaborator and for reading some chapters of my thesis for me. I would like to thank Luiz Vale Silva for his time, experience and discussion. I warmly and sincerely thank all those who have given me encouragement at various times during my PhD, it has made such a difference.
I would like to thank Susan, Anoushka and Alexie for their unwavering support, for believing in me and for giving me the time to write this thesis. I would like to express my heartfelt thanks to Elliot Leslie for encouragement, inspiration and for giving me a reason to be the best I can be.

Contents

List of Tables

List of Figures

Chapter 1

Introduction

1.1 Prelude

Motivation for belief in and the study of physics beyond the standard model (BSM) is twofold; on the theoretical side the Standard Model (SM) of particle physics is extremely successful in predicting many of the phenomena observed in nature. However it is long believed to be incomplete due to its inability to explain outstanding questions such as the hierarchy/naturalness problem and the reason for the observed pattern of masses and mixing angles of quarks and leptons. These problems lead theorists to believe that the SM is the low energy limit of a more fundamental theory offering a complete description of nature. On the experimental side, experiments have reached high levels of sensitivity to flavour observables. Such levels of sensitivity offer two advantages; the first is when reported values of measurements deviate from the SM prediction, there is an obvious motivation for theorists to explain such a deviation by constructing well motivated extensions to the SM. The second is the power to constrain or falsify models going beyond the SM.

The flavour sector of the SM concerns interactions which differentiate between different flavours of matter particles. It is known to be sensitive to indirect effects which could occur due to the presence of new non standard particles. Effects produced by new particles, too heavy to be produced at energies currently within experimental reach, may effect flavour observables. Hence, this sector of the SM has the potential to probe indirectly the underlying structure of possible completions of the SM. Some observable quantities in the B physics sector are suppressed due to small Cabibbo Kobayashi Masakawa (CKM) matrix elements, or because some processes are forbidden at tree level in the SM and

hence the leading perturbative contributions are suppressed by loop factors such as Flavour Changing Neutral Current (FCNC) interactions. Other B meson processes are sensitive probes of CP violation; a phenomenon which is thought to arise in the SM purely due to the CKM matrix, but which is much more prominent in the universe than can be explained through this alone.

In this thesis we consider those processes in B physics which are triggered by the quark level $b \to c\bar{c}s$ transition. This transition contributes to a wide range of B physics processes and thus offers a selection of complimentary observables one can use to constrain predicted signals of physics beyond the standard model (BSM).

In particular, this transition contributes at loop level to the suppressed rare B decays triggered by the $b \to s\mu^+\mu^-$ transition. This decay mode is one for which there exist tensions between experiment and theory [4, 5, 6, 7, 8, 9, 10, 11, 12, 13]. Interestingly, such tensions may indicate a beyond the SM contact interaction, which could cause a negative shift to the SM Wilson coefficient C_{9V}, as has been studied previously [14, 15, 16, 17, 18, 19, 20]. The significance of such an effect is somewhat unclear, due to hadronic uncertainties [21, 22, 23, 24]. However, as short distance virtual charm contributions constitute a portion of C_{9V} in the SM, in this thesis we consider whether such rare decay anomalies could be explained by new heavy degrees of freedom affecting the quark level $b \to c\bar{c}s$ transitions. Such an effect, if indeed responsible for the anomalies, would also be captured as a negative $\mathcal{O}(1)$ shift to C_{9V}.

If there exist BSM effects in rare decay, affecting B physics observables through a charm loop, such effects will also show up in mixing and lifetime processes, offering the exciting prospect of investigating these effects in $\bar{B}^0_s - B^0_s$ mixing and B^0_s lifetimes [1]. In addition, we extend our study to include radiative processes triggered by the quark level $b \to s\gamma$ transition, as well as the hadronic $B \to J/\psi K_{(S)}$ decay, to which $b \to c\bar{c}s$ transitions also contribute, at loop and at tree level respectively [2].

Using the standard EFT framework, we go beyond research previously carried out by constructing the most general weak effective Hamiltonian of $b \to c\bar{c}s$ operators, and perform a comprehensive evaluation of new physics effects in B physics observables related to the processes mentioned above [1],[2]. Namely, the mass eigenstate decay rate difference $\Delta\Gamma_s$ and flavour specific CP asymmetry a^s_{fs} from $B^0_s - \bar{B}^0_s$ mixing, the inclusive radiative decay branching ratio $\mathcal{B}(B \to X_s\gamma)$, the time dependent $B^0_d \to J/\psi K_S$ CP asymmetry observables $S_{J\psi K_S}$ and $C_{J/\psi K_S}$, and the branching ratio $\mathcal{B}(B^0_d \to J/\psi K^0_d)$.

Further, we consider the impact of operators containing a right-handed strange quark, associated with the chirality conjugate partners of our basis. We then ask the question as to whether $B_d^0 \to J/\psi K_{(S)}$ observables can impose extra constraints upon BSM shifts to SM coefficients, through the introduction of coefficients carrying weak CP violating phases. Finally, we determine the resultant constraints of all these quantities upon each Wilson coefficient in the Hamiltonian and speculate upon what type of new physics could have generated this at the TeV scale.

As an additional separate chapter we include a technical result which is a part of an ongoing project. Here, we include a set of two loop and one loop Feynman diagrams which contribute to the anomalous dimension matrix element governing the mixing of dimension six operators with dipole operators in the Standard Model Effective Field Theory (SMEFT), and present the methodology employed to perform the calculations [3].

1.2 Layout of thesis

The remainder of this thesis is laid out as follows; In Chapter 2 we review the SM of particle physics and introduce some of the existing formalism for meson mixing and CP violation, the concept and practical application of renormalization, the EFT framework, and the necessary theoretical tools required for the following chapters such as heavy quark effective theory (HQET) and the heavy quark expansion (HQE). In Chapter 3 the Charming Beyond the Standard Model (CBSM) scenario is introduced, motivated and the operator basis and weak Hamiltonian defined. In Chapter 4 the full renormalization group evolution for our scenario is presented, in Chapter 5 the observables considered in our work are defined mathematically and their expressions in terms of Wilson coefficients given. In Chapter 6 the phenomenological implications of our mechanism are presented and discussed. In Chapter 7, results of the set of two, and one-loop diagrams contributing to the Anomalous Dimension Matrix (ADM) element which governs mixing of certain operators with dipole operators in SMEFT are presented and technical details shown [3]. Finally, Chapter 8 contains our conclusions.

Chapter 2

Preliminaries

In this chapter we lay the foundation for our novel results by reviewing the standard model of particle physics in 2.1 with a focus on the flavour sector. In section 2.2 we review the basics of neutral meson mixing and derive some expressions for later chapters and in section 2.3 we define some transformation properties and highlight relevant CP violating processes. In section 2.4 we review the standard treatment of divergences which appear in quantum field theory calculations focusing on regularization, the concept and application of renormalizat $SU_W(2)$ion and introduce the renormalization group. In section 2.5 we review the EFT framework and give a simple illustrative example. In sections 2.6 and 2.7 we introduce the Heavy Quark Effective Theory (HQET) and Heavy Quark Expansion (HQE), respectively.

2.1 The standard model

The Standard Model (SM) of particle physics is described by the Lagrangian density [25, 26, 27, 28, 29, 30]

$$\begin{aligned}\mathcal{L}_{SM} = &-\frac{1}{4}\sum_{A=1\ldots8} G^A_{\mu\nu}G^{A,\mu\nu} - \frac{1}{4}\sum_{I=1\ldots3} W^I_{\mu\nu}W^{I,\mu\nu} - \frac{1}{4}B_{\mu\nu}B^{\mu\nu} + \sum_{\psi=q,u,d,l,e}\bar{\psi}i\not{D}\psi \\ &+ (D_\mu H^\dagger)(D^\mu H) - \lambda\left(H^\dagger H - \frac{\mu^2}{2\lambda}\right)^2 \\ &- \left[\bar{q}_j Y_d d H_j + \bar{q}_j Y_u u \tilde{H}_j + \bar{\ell}_j Y_e e H_j + \text{h.c}\right] \end{aligned} \tag{2.1}$$

which is specified by the gauge group $SU_C(3) \times SU_W(2) \times U_Y(1)$ and it's matter content. The first line contains the gauge and fermion terms and the second and third lines are comprised of terms involving the Higgs field. The field content of the SM and the

transformation properties of the fields under the gauge group are given in table 2.1. The

Table 2.1: SM field content and transformation properties of fields under the gauge group.

Fermion fields			
$q_1 = \begin{pmatrix} u \\ d \end{pmatrix}_L$	$q_2 = \begin{pmatrix} c \\ s \end{pmatrix}_L$	$q_3 = \begin{pmatrix} t \\ b \end{pmatrix}_L$	$(\mathbf{3}, \mathbf{2}, \frac{1}{6})$
u_R	c_R	t_R	$(\mathbf{3}, \mathbf{1}, \frac{2}{3})$
d_R	s_R	b_R	$(\mathbf{3}, \mathbf{1}, -\frac{1}{3})$
$\ell_1 = \begin{pmatrix} \nu_e \\ e^- \end{pmatrix}_L$	$\ell_2 = \begin{pmatrix} \nu_\mu \\ \mu^- \end{pmatrix}_L$	$\ell_3 = \begin{pmatrix} \nu_\tau \\ \tau^- \end{pmatrix}_L$	$(\mathbf{1}, \mathbf{2}, -\frac{1}{2})$
e_R^-	μ_R^-	τ_R^-	$(\mathbf{1}, \mathbf{1}, \text{-1})$
Gauge boson fields			
G_μ^A			$(\mathbf{8}, \mathbf{1}, 0)$
W_μ^I			$(\mathbf{1}, \mathbf{3}, 0)$
B_μ			$(\mathbf{1}, \mathbf{1}, 0)$
Scalar boson fields			
$H = \begin{pmatrix} H^+ \\ H^0 \end{pmatrix}$			$(\mathbf{1}, \mathbf{2}, \frac{1}{2})$
$\tilde{H} = \begin{pmatrix} H^{0*} \\ -H^{+*} \end{pmatrix}$			$(\mathbf{1}, \mathbf{2}, -\frac{1}{2})$

fermion fields make up the first five rows of 2.1, with the upper three being the quark fields and the lower two the lepton fields. The first three columns contain the individual generations of the quark and lepton fields. The sixth to eighth rows which comprise the gauge bosons have only two columns, similarly for the last last two rows which contain the scalar boson fields. The fourth column contains the transformation properties of the fields under the gauge group. These properties are given in terms of the representation of the gauge group under which the fields transform. To summarise how these transform with respect to each individual group, there are three entries in the row vector in the last column. The representations of the gauge groups are labelled by their dimension. The 3-dimensional representation of $SU_C(3)$ is written as **3**, and this is the fundamental representation. The 2-dimensional representation of $SU_W(2)$ is written **2**, and the trans-

formation properties with respect to $U_Y(1)$ are labelled by the eigenvalue of the generator Y which is called the weak hypercharge. If a field does not transform, then this is written as **1** which denotes the trivial invariant representation.

We define the field strength tensors to be

$$G^A_{\mu\nu} = \partial_\mu A^A_\nu - \partial_\nu A^A_\mu + g_s f^{ABC} A^B_\mu A^C_\nu, \qquad A = 1...8 \tag{2.2}$$

$$W^I_{\mu\nu} = \partial_\mu W^I_\nu - \partial_\nu W^I_\mu + g_2 \epsilon^{IJK} W^J_\mu W^K_\nu, \qquad I = 1...3 \tag{2.3}$$

$$B_{\mu\nu} = \partial_\mu B_\nu - \partial_\nu B_\mu \tag{2.4}$$

where G_μ, W_μ and B_μ are the gauge fields for the $SU_C(3), SU_L(2)$ and $U_Y(1)$ gauge groups respectively. The covariant derivative is

$$D_\mu = \partial_\mu + i g_s T^A A^A_\mu + i g_2 t^I W^I_\mu + i g_1 Y B_\mu, \tag{2.5}$$

The contraction $\not{D}$ in (2.1) is defined as $\not{D} = \gamma^\mu D_\mu$ where the 4×4 Dirac matrices obey the anti-commutation relations

$$\{\gamma^\mu, \gamma^\nu\} = 2g^{\mu\nu}, \tag{2.6}$$

with $g^{\mu\nu}$ the Minkowski metric defined in (A.6). An explicit representation of the Dirac matrices is the Dirac-Pauli representation wherein

$$\gamma^0 = \begin{pmatrix} \mathbb{1} & 0 \\ 0 & -\mathbb{1} \end{pmatrix}, \qquad \gamma^i = \begin{pmatrix} 0 & \sigma^i \\ -\sigma^i & 0 \end{pmatrix}, \qquad \gamma^5 = \begin{pmatrix} 0 & \mathbb{1} \\ \mathbb{1} & 0 \end{pmatrix}, \tag{2.7}$$

where γ^0 and γ^5 are hermitian and γ^i is anti-hermitian and the σ^i with $i = 1, 2, 3$ are the 2×2 Pauli matrices defined below in (2.15). Here $\mathbb{1}$ denotes the 2×2 identity matrix, and the matrix γ^5 obeys

$$\{\gamma^5, \gamma^\mu\} = 0, \qquad (\gamma^5)^2 = \mathbb{1}. \tag{2.8}$$

The other commonly used representation is the Chiral or Weyl representation and this and its relation with the above representation is given in Appendix A.

Moreover, in (2.5) the T^A are the $SU_C(3)$ generators, which obey

$$[T^A, T^B] = i f^{ABC} T^C, \tag{2.9}$$

and the structure constants f^{ABC} are totally anti-symmetric. The matrices T^A are conventionally defined as

$$T^A = \frac{1}{2}\lambda^A, \tag{2.10}$$

and satisfy

$$\mathrm{Tr}(T^A T^B) = \frac{1}{2}\delta^{AB}. \tag{2.11}$$

In the conventional basis the 3×3 hermitian traceless matrices λ^A are the Gell-Mann matrices:

$$\lambda^1 = \begin{pmatrix} 0 & 1 & 0 \\ 1 & 0 & 0 \\ 0 & 0 & 0 \end{pmatrix}, \qquad \lambda^2 = \begin{pmatrix} 0 & -i & 0 \\ i & 0 & 0 \\ 0 & 0 & 0 \end{pmatrix}$$

$$\lambda^3 = \begin{pmatrix} 1 & 0 & 0 \\ 0 & -1 & 0 \\ 0 & 0 & 0 \end{pmatrix}, \qquad \lambda^4 = \begin{pmatrix} 0 & 0 & 1 \\ 0 & 0 & 0 \\ 1 & 0 & 0 \end{pmatrix}$$

$$\lambda^5 = \begin{pmatrix} 0 & 0 & -i \\ 0 & 0 & 0 \\ i & 0 & 0 \end{pmatrix}, \qquad \lambda^6 = \begin{pmatrix} 0 & 0 & 0 \\ 0 & 0 & 1 \\ 0 & 1 & 0 \end{pmatrix}$$

$$\lambda^7 = \begin{pmatrix} 0 & 0 & 0 \\ 0 & 0 & -i \\ 0 & i & 0 \end{pmatrix}, \qquad \lambda^8 = \frac{1}{\sqrt{3}} \begin{pmatrix} 1 & 0 & 0 \\ 0 & 1 & 0 \\ 0 & 0 & -2 \end{pmatrix}.$$

Similarly, t^I are the $SU_W(2)$ generators, obeying

$$[t^I, t^J] = i\epsilon^{IJK} t^K, \tag{2.12}$$

again the structure constants ϵ^{IJK}, are totally anti-symmetric. The t^I are defined as

$$t^I = \frac{1}{2}\sigma^I, \tag{2.13}$$

satisfying

$$\mathrm{Tr}(t^I t^J) = \frac{1}{2}\delta^{IJ}. \tag{2.14}$$

The traceless, hermitian 2×2 matrices σ^I are the Pauli-Sigma matrices, and are given by

$$\sigma^1 = \begin{pmatrix} 0 & 1 \\ 1 & 0 \end{pmatrix}, \qquad \sigma^2 = \begin{pmatrix} 0 & -i \\ i & 0 \end{pmatrix}, \qquad \sigma^3 = \begin{pmatrix} 1 & 0 \\ 0 & -1 \end{pmatrix}. \tag{2.15}$$

and Y is the $U_Y(1)$ hyper-charge generator. The couplings in (2.5) are as follows: g_s is the $SU_C(3)$ gauge coupling, g_2 is the $SU_W(2)$ gauge coupling and g_1 is the $U_Y(1)$ gauge coupling. The fermion fields $\psi = \{q_L, u_R, d_R, l_L, e_R\}$ all have flavour indices $p = 1, 2, 3$ for each generation in flavour space. These are suppressed in (2.1) for clarity. Explicitly

$$\bar{q}_j Y_d d H_j = \bar{q}^p_{Lj} Y_d^{pn} d^n_R H_j, \qquad p = 1, 2, 3. \tag{2.16}$$

the index j is an $SU_W(2)$ index and Y_d, Y_u and Y_e are Yukawa matrices in flavour (generation) space. The field $\tilde{H}$ is defined

$$\tilde{H}_j = \epsilon_{jk} H^\dagger_k, \tag{2.17}$$

and ϵ_{jk} is the $SU_W(2)$ invariant tensor which is defined by $\epsilon_{12} = 1, \epsilon_{jk} = -\epsilon_{kj}$.

2.1.1 Spontaneous symmetry breaking

The Lagrangian in (2.1) is expressed in the gauge eigenstate basis such that its fields have definite gauge quantum numbers and transformation properties. However, the mass spectrum of the theory is brought about by spontaneous symmetry breaking (SSB) when the Higgs field acquires a non zero vacuum expectation value (VEV) [26, 27, 28]:

$$\langle 0|H|0\rangle = \begin{pmatrix} 0 \\ \frac{v}{\sqrt{2}} \end{pmatrix}, \qquad v = \sqrt{\frac{\mu^2}{\lambda}}. \tag{2.18}$$

Working in the unitary gauge we can parameterize the Higgs field in terms of its VEV value and a real valued field $h(x)$

$$H = \begin{pmatrix} 0 \\ \frac{v+h(x)}{\sqrt{2}} \end{pmatrix}. \tag{2.19}$$

When the field H is replaced with (2.19) in (2.1), the covariant derivative given by (2.5), in terms of the three weak gauge bosons in the mass eigenstate basis, becomes [30, 25]

$$D_\mu = \partial_\mu + i\frac{g_2}{\sqrt{2}}(W_\mu^+ t^+ + W_\mu^- t^-) + i\frac{g_2}{\cos\theta_W} Z_\mu (t^3 - Q\sin^2\theta_W) + ieQA_\mu \qquad (2.20)$$

where the matrices $t^\pm = (t^1 \pm it^2)$ with $t^I = \frac{1}{2}\sigma^I \quad I = 1, 2, 3$ with σ^I the Pauli sigma matrices, as given in (2.15). The electromagnetic coupling e and the Weinberg angle θ_W are

$$e = \frac{g_2 g_1}{\sqrt{g_2^2 + g_1^2}}, \qquad \sin\theta_W = \frac{g_1}{\sqrt{g_2^2 + g_1^2}}, \qquad \cos\theta_W = \frac{g_2}{\sqrt{g_2^2 + g_1^2}}, \qquad (2.21)$$

and the $U(1)$ generator Y is related to t^3 and Q through $Q = (t^3 + Y)$. In 2.1.2 we will briefly explain the origin of the fermion masses in the SM after spontaneous symmetry breaking (SSB).

2.1.2 The flavour sector

The masses and mixings of the fermions are determined from the Yukawa term in the SM Lagrangian (2.1) which couples the Higgs field to the fermions before SSB. For the quarks, we will need to alter notation to make clear the difference between the gauge interaction and mass eigenstate bases. Let us make the substitutions

$$q \to q' = \left(\begin{pmatrix} u' \\ d' \end{pmatrix}_L, \begin{pmatrix} c' \\ s' \end{pmatrix}_L, \begin{pmatrix} t' \\ b' \end{pmatrix}_L \right) \qquad (2.22)$$

$$\ell \to \ell' = \left(\begin{pmatrix} \nu_e' \\ e' \end{pmatrix}_L, \begin{pmatrix} \nu_\mu' \\ \mu' \end{pmatrix}_L, \begin{pmatrix} \nu_\tau' \\ \tau' \end{pmatrix}_L \right) \qquad (2.23)$$

$$u_R \to u_R' \qquad \forall\ u_R \in \{u_R, c_R, t_R\} \qquad (2.24)$$

$$d_R \to d_R' \qquad \forall\ d_R \in \{d_R, s_R, b_R\} \qquad (2.25)$$

$$e_R \to e_R' \qquad \forall\ e_R \in \{e_R, \mu_R, \tau_R\} \qquad (2.26)$$

so that it is clear that when we are referring to gauge interaction eigenstate fields, we mean those with a prime in the superscript.

Fermion masses

For the quarks, the Yukawa terms, after replacing H with (2.19) lead to non diagonal mass matrices of the form

$$M^{(f)}_{pq} = -\frac{v}{\sqrt{2}} Y^{(f)}_{pq}, \qquad f = e, u, d. \tag{2.27}$$

In the quark sector, in order to obtain mass matrices which are diagonal, we make the field re-definitions letting

$$u_{L(R)} = V^u_{L(R)} u'_{L(R)}, \qquad d_{L(R)} = V^d_{L(R)} d'_{L(R)}, \tag{2.28}$$

where the matrices $V^q_{L(R)}, q = u, d$ are unitary matrices which are chosen in such a way as to ensure that the diagonalized mass matrices have real and positive eigenvalues. Upon this change the quark mass matrices become

$$\widetilde{M}^u = -\frac{v}{\sqrt{2}} \mathrm{diag}(y^u, y^c, y^t) \qquad \widetilde{M}^d = -\frac{v}{\sqrt{2}} \mathrm{diag}(y^d, y^s, y^b) \tag{2.29}$$

with the diagonalized quark mass matrices given in terms of the Yukawa matrices as

$$\widetilde{M}^f = V^f_L Y^f (V^f_R)^\dagger \qquad f = u, d. \tag{2.30}$$

We can do the same for the leptons, however because there are no right handed neutrinos there is only one Yukawa matrix to diagonalize and the two components of the $SU(2)$ doublet ℓ require the same field redefinition. The result is that the transformation matrices commute with the $SU(2)$ interactions arising in the covariant derivative and so in the mass eigenstate basis the lepton mass matrix is

$$\widetilde{M}^\ell = -\frac{v}{\sqrt{2}} \mathrm{diag}(y_e, y_\mu, y_\tau), \qquad \widetilde{M}^\ell = V^e_L Y_e (V^e_R)^\dagger \tag{2.31}$$

Fermion-gauge interactions

In terms of interactions, we must then apply the field redefinitions to the fermion kinetic term in the Lagrangian to obtain the interactions between the gauge bosons and the fermions, in the mass eigenstate basis. Interactions involving quarks and leptons and the electro weak gauge bosons are present in the standard electroweak theory of Glashow,Weinberg and Salam [25],[30]. The gauge - fermion interaction Lagrangian consists of a neutral

and a charged current.

$$\mathcal{L}_{gf} = \mathcal{L}_{cc} + \mathcal{L}_{nc}, \tag{2.32}$$

where $\mathcal{L}_{cc}$ contains the charged current interactions between quark and lepton currents mediated by the charged gauge bosons $W^{\pm}$ and $\mathcal{L}_{nc}$ the neutral current interactions between quark and lepton currents mediated by the neutral gauge bosons Z^0 and A. The charged current Lagrangian, in terms of the physical $W^{\pm}$ fields reads

$$\mathcal{L}_{cc} = -\frac{g_2}{\sqrt{2}}(\mathcal{J}_{\mu}^{+}W^{+\mu} + \mathcal{J}_{\mu}^{-}W^{-\mu}), \tag{2.33}$$

The neutral current Lagrangian reads

$$\mathcal{L}_{NC} = -e\mathcal{J}_{\mu}^{\mathrm{em}}A^{\mu} + \frac{g_2}{\cos\theta_W}\mathcal{J}_{\mu}^{0}Z^{\mu}, \tag{2.34}$$

where the electromagnetic and neutral currents are given by

$$\mathcal{J}_{\mu}^{em} = \sum_{f} Q_f \bar{f}^p \gamma_\mu f^p, \tag{2.35}$$

$$\mathcal{J}_{\mu}^{0} = \sum_{f} (\bar{f}_L^p \gamma_\mu g_L^f f_L^p + \bar{f}_R^p \gamma_\mu g_R^f f_R^p), \tag{2.36}$$

when $f = \nu_e, e, u, d$ is a fermion field and with $p = 1, 2, 3$ a generation index. The g_L^f is the 2×2 matrix $t^3 - Q_f \sin\theta_W$ which acts on the $SU_W(2)$ doublets f_L^p, where t^3 is defined in (2.13) and (2.15) for index $I = 3$. The g_R^f acts on the right handed $SU_W(2)$ singlets f_R^p. They are given below as

$$g_L^f = \begin{pmatrix} \frac{1}{2} - Q_f \sin^2\theta_W & 0 \\ 0 & -\frac{1}{2} - Q_f \sin^2\theta_W \end{pmatrix}, \tag{2.37}$$

$$g_R^f = -Q_f \sin^2\theta_W. \tag{2.38}$$

Applying the transformations given in (2.28) to the fields in the neutral current Lagrangian leads to the cancelling of the matrices $V_{L(R)}^q, q = u, d$ because the neutral current is flavour diagonal. This is due to the matrix t^3 having zero off diagonal elements and hence the components of the $SU_W(2)$ doublets do not get mixed up. This is the reason why there are no flavour changing neutral currents at tree level in the SM. Applying the field re-definitions in (2.28) to the fields in the charged current (2.33), leads to the explicit

definition of the quark mixing matrix

$$J_\mu^+ = \begin{pmatrix} \bar{u}_L, & \bar{c}_L, & \bar{t}_L \end{pmatrix} \gamma_\mu V_L^u (V_L^d)^\dagger \begin{pmatrix} d_L \\ s_L \\ b_L \end{pmatrix} \tag{2.39}$$

$$\mathcal{J}_\mu^- = (\mathcal{J}_\mu^+)^\dagger. \tag{2.40}$$

the transformation matrix $V_L^u(V_L^d)^\dagger$ in (2.39) is the Cabibbo Kobayashi Masakawa (CKM) matrix [31], [32] and originates from the Yukawa term in (2.1) in that

$$V_{CKM} = V_L^u V_L^{d\dagger}. \tag{2.41}$$

The weak interaction eigenstates of (2.39) are connected to the mass eigenstates through the Unitary transformation

$$\begin{pmatrix} d' \\ s' \\ b' \end{pmatrix} = \begin{pmatrix} V_{ud} & V_{us} & V_{ub} \\ V_{cd} & V_{cs} & V_{cb} \\ V_{td} & V_{ts} & V_{tb} \end{pmatrix} \begin{pmatrix} d \\ s \\ b \end{pmatrix}, \tag{2.42}$$

The CKM matrix is a complex 3×3 matrix predicted by the SM to be unitary, $\hat{U}^\dagger = \hat{U}^{-1}$ and therefore $\hat{U}^\dagger \hat{U} = U\hat{U}^\dagger = \mathbb{1}$. Some of the complex phases of the CKM matrix do not have physical meaning. It is possible to re-phase the quark fields

$$u_p = e^{i\phi_p}\tilde{u}_p, \tag{2.43}$$

$$d_n = e^{i\phi_n}\tilde{d}_n \tag{2.44}$$

when n, p are generation indices, with a CKM matrix element transforming under this re phasing as

$$\tilde{V}_{CKM} = e^{i(\phi_n - \phi_p)} V_{CKM}. \tag{2.45}$$

Through this re-phasing of the fields, it is possible to eliminate the phases of $2N_g - 1$ V_{CKM} elements where $N_g = 3$ is the number of generations. The number of physical parameters of the CKM matrix may be counted as follows. The number of parameters are

$$N_{param} = N_g^2 - (2N_g - 1) = (N_g - 1)^2 \tag{2.46}$$

that is the number of elements minus the number of phases which can be eliminated. These parameters can be expressed in terms of Euler angles and phases. A unitary matrix has

$$N_{angle} = \frac{1}{2} N_g (N_g - 1) \tag{2.47}$$

rotation angles. Then the number of phases we require to parameterize V_{CKM} are

$$N_{phase} = N_{param} - N_{angle} = \frac{1}{2}(N_g - 2)(N_g - 1) \tag{2.48}$$

That is for $N_g = 3$ generations the CKM matrix can be parameterized in terms of 3 Euler angles and 1 phase. It is given in the standard KM parameterization in [33] as

$$V_{CKM} = \begin{pmatrix} c_{12}c_{13} & s_{12}c_{13} & s_{13}e^{-i\delta} \\ -s_{12}c_{23} - c_{12}s_{23}s_{13}e^{i\delta} & c_{12}c_{23} - s_{12}s_{23}s_{13}e^{i\delta} & s_{23}c_{13} \\ s_{12}s_{23} - c_{12}c_{23}s_{13}e^{i\delta} & -c_{12}s_{23} - s_{12}c_{23}s_{13}e^{i\delta} & c_{23}c_{13} \end{pmatrix}. \tag{2.49}$$

where $s_{ij} = \sin\theta_{ij}, \quad c_{ij} = \cos\theta_{ij}$ and $\theta_{ij} \in [0, \frac{\pi}{2}]$ is chosen such that $s_{ij}c_{ij} \geq 1$. δ is the CP violating phase which accounts for all CP violation in flavour changing transitions. The complex elements of V_{CKM} display a hierarchy which is most transparently displayed in the Wolfenstein parameterization [34] which is related to the standard parameterization through the relations [33]

$$s_{12} = \lambda = \frac{|V_{us}|}{\sqrt{|V_{ud}|^2 + |V_{us}|^2}} \tag{2.50}$$

$$s_{23} = A\lambda^2 = \lambda \left| \frac{V_{cb}}{V_{us}} \right| \tag{2.51}$$

$$s_{13}e^{i\delta} = A\lambda^3(\rho + i\eta) = \frac{A\lambda^3(\bar{\rho} + i\bar{\eta})\sqrt{1 - A^2\lambda^4}}{\sqrt{1 - \lambda^2}[1 - A^2\lambda^4(\bar{\rho} + i\bar{\eta})]} = V_{ub}^* \tag{2.52}$$

The reason for the introduction of the barred $\bar{\rho}, \bar{\eta}$ is to ensure i) that $\bar{\rho} + i\bar{\eta} = -\frac{V_{ud}V_{ub}^*}{V_{cd}V_{cb}^*}$ is phase convention independent and ii) that V_{CKM} when written in terms of $\lambda, A, \bar{\rho}, \bar{\eta}$ is unitary to all orders in the expansion parameter λ. In terms of the un barred parameters ρ, η, where $\bar{\rho} \equiv \rho(1 - \frac{1}{2}\lambda^2 + \cdots)$, $\bar{\eta} \equiv \eta(1 - \frac{1}{2}\lambda^2 + \cdots)$, the CKM matrix can be written

in the Wolfenstein parameterization as

$$V_{CKM} = \begin{pmatrix} 1-\frac{\lambda^2}{2} & \lambda & A\lambda^3(\rho - i\eta) \\ -\lambda & 1-\frac{\lambda^2}{2} & A\lambda^2 \\ A\lambda^3(1-\rho-i\eta) & -A\lambda^2 & 1 \end{pmatrix} + \mathcal{O}(\lambda^4). \tag{2.53}$$

This highlights that interactions between quarks will be suppressed to varying degrees depending upon their CKM structure. The unitarity condition yields 3 normalization relations and 6 orthogonality relations, these are

$$\sum_{k=1\ldots3} V_{ik}^* V_{ki} = 1 \qquad\qquad \sum_{k=1\ldots3} V_{ik}^* V_{kj\neq i} = 0 \tag{2.54}$$

For the purposes of this thesis, the relation we will use most often is the one governing the $b \to s$ transitions namely

$$V_{cb}V_{cs}^* + V_{tb}V_{ts}^* + V_{ub}V_{us}^* = 0, \tag{2.55}$$

which may be expressed as

$$\frac{V_{ub}V_{us}^*}{V_{tb}V_{ts}^*} + \frac{V_{cb}V_{cs}^*}{V_{tb}V_{ts}^*} + 1 = 0. \tag{2.56}$$

The latest values of the CKM elements are to be found in [33]. Throughout this thesis we employ the standard phase convention, and calculate the CKM elements from inputs shown in Table 6.1 using (2.49).

2.2 Neutral meson mixing

In this section we follow the development of [35]. Using a simplification first shown by Wigner and Weisskopf [36], [37], in the Wigner-Weisskopf approximation, the time evolution of a beam of neutral mesons which are both oscillating and decaying, is expressible in the rest frame of the $\bar{P}^0 - P^0$ system as a superposition of meson anti meson states

$$|\psi(t)\rangle = P^0(t)|P^0\rangle + \bar{P}^0(t)|\bar{P}^0\rangle. \tag{2.57}$$

The conditions being that i) at time $t = 0$ only the wave functions above are non zero, ii) it is only these functions we are interested in, and iii) t is much larger than the strong interaction scale. Here we denote $P^0(t)$,$\bar{P}^0(t)$ as the the wave functions associated with

the states $|P^0\rangle$,$|\bar{P}^0\rangle$ which are the meson states prepared at time $t = 0$ labelled by their quark flavour quantum numbers. In this thesis we are considering $P^{(0)} = B_q^{(0)}, K_q^{(0)}$ meson mixing with $q = s, d$ flavours. The wave functions in (2.57) obey a Schrödinger type equation

$$i\hbar\frac{d}{dt}\begin{pmatrix} P^0(t) \\ \bar{P}^0(t) \end{pmatrix} = \begin{pmatrix} H_{11} & H_{12} \\ H_{21} & H_{22} \end{pmatrix}\begin{pmatrix} P^0(t) \\ \bar{P}^0(t) \end{pmatrix}. \tag{2.58}$$

The Hamiltonian governing this mixing and decay of flavour eigenstates is not Hermitian but it can be decomposed into two separately hermitian matrices $\hat{M}$, and $\hat{\Gamma}$ in the following way

$$\hat{H} = \hat{M} - \frac{i}{2}\hat{\Gamma}, \tag{2.59}$$

where $\hat{M} = \hat{M}^\dagger$, $\hat{\Gamma} = \hat{\Gamma}^\dagger$. In order to diagonalize a non hermitian matrix $\hat{H}$ with a unitary similarity transformation, $\hat{M}$ and $\hat{\Gamma}$ must be simultaneously so diagonalized. The necessary and sufficient condition for this is that $\hat{M}$ and $\hat{\Gamma}$ commute, which is possible if and only if $\hat{H}$ is normal, i.e $[\hat{H}, \hat{H}^\dagger] = 0$. The discrete symmetries CP and CPT constrain the elements of the mixing matrix so that $M_{11} = M_{22} = M$ and $\Gamma_{11} = \Gamma_{22} = \Gamma$ and hermicity of $\hat{M}$ and $\hat{\Gamma}$ ensure $M_{21} = M_{12}^*$ and $\Gamma_{21} = \Gamma_{12}^*$. This gives for the mass and decay rate matrices

$$\hat{\Gamma} = \begin{pmatrix} \Gamma & \Gamma_{12} \\ \Gamma_{12}^* & \Gamma \end{pmatrix}, \qquad \hat{M} = \begin{pmatrix} M & M_{12} \\ M_{12}^* & M \end{pmatrix}. \tag{2.60}$$

The requirement that $\hat{H}$ be normal in order to be diagonalized by a unitary similarity transformation is satisfied because the diagonal elements of $\hat{M}$ and $\hat{\Gamma}$ are real.
The eigenstates of $\hat{H}$, which we shall label $|p_A\rangle$ and $|p_B\rangle$, are states of definite mass and decay rates. They can be expressed in terms of the flavour eigenstates $|P^0\rangle$ and $|\bar{P}^0\rangle$ as

$$\begin{pmatrix} |P_A\rangle \\ |P_B\rangle \end{pmatrix} = \begin{pmatrix} p_A & q_A \\ p_B & q_B \end{pmatrix}\begin{pmatrix} |P^0\rangle \\ |\bar{P}^0\rangle \end{pmatrix}, \tag{2.61}$$

and evolve in a simple way according to

$$i\hbar\frac{d}{dt}\begin{pmatrix} |P_A(t)\rangle \\ |P_B(t)\rangle \end{pmatrix} = \begin{pmatrix} M_A - \frac{i}{2}\Gamma_A & 0 \\ 0 & M_B - \frac{i}{2}\Gamma_B \end{pmatrix}\begin{pmatrix} |P_A(t)\rangle \\ |P_B(t)\rangle \end{pmatrix}. \tag{2.62}$$

The diagonal elements are the eigenvalues of $\hat{H}$ which we label A, B in accordance with the eigenstates of $\hat{H}$. They are

$$\mu_A = M_A - \frac{i}{2}\Gamma_A, \qquad \mu_B = M_B - \frac{i}{2}\Gamma_B. \tag{2.63}$$

Let us introduce and define the mass and decay rate differences as the difference between the masses and decay rates of the physical eigenstates

$$\Delta M = M_A - M_B \tag{2.64}$$

$$\Delta\Gamma = \Gamma_A - \Gamma_B \tag{2.65}$$

The sign of these mass and decay rate difference has physical significance and is different for different mesons. In order to extract expressions for these observable quantities it is useful to define the eigenvalue difference as

$$\Delta\mu = \Delta M - \frac{i}{2}\Delta\Gamma. \tag{2.66}$$

Diagonalization of (2.59) gives the eigenvalues of (2.59)

$$\mu_A = M - \frac{i}{2}\Gamma + \sqrt{|M_{12}|^2 - \frac{1}{4}|\Gamma_{12}|^2 - i\mathrm{Re}(M_{12}^*\Gamma_{12})}, \tag{2.67}$$

$$\mu_B = M - \frac{i}{2}\Gamma - \sqrt{|M_{12}|^2 - \frac{1}{4}|\Gamma_{12}|^2 - i\mathrm{Re}(M_{12}^*\Gamma_{12})}. \tag{2.68}$$

In terms of the individual elements of the mass and decay rate matrices in the flavour eigenstate basis, from (2.66), (2.67) and (2.68) we deduce that

$$\Delta\mu = 2\sqrt{|M_{12}|^2 - \frac{1}{4}|\Gamma_{12}|^2 - i\mathrm{Re}(M_{12}^*\Gamma_{12})}. \tag{2.69}$$

As a consequence of assuming CPT to be a good symmetry of (2.59), the ratios

$$\frac{q_A}{p_A} = \frac{q_B}{p_B} \equiv \frac{q}{p}. \tag{2.70}$$

Upon diagonalization of $\hat{H}$, in the way described above, comparison of (2.61) with the transformation matrix formed of the eigenvectors of $\hat{H}$, fixes the ratio q/p to be

$$\frac{q}{p} = \frac{2(M_{12}^* - \frac{i}{2}\Gamma_{12}^*)}{\sqrt{|M_{12}|^2 - \frac{1}{4}|\Gamma_{12}|^2 - i\mathrm{Re}(M_{12}^*\Gamma_{12})}}. \tag{2.71}$$

$B_s^{(0)} - \bar{B}_s^{(0)}$ mixing

Let us specialise to $B_s^{(0)} - \bar{B}_s^{(0)}$ mixing. For this process we have $A = H, B = L$ where H stands for the heavy eigenstate and L stands for the light eigenstate. The quantity $\Delta M > 0$ by definition, and since in the SM B_L is the short lived eigenstate it means that $\Gamma_L > \Gamma_H$. We define the mass and decay rate difference in the following sense.

$$\Delta M_s = M_H^s - M_L^s \tag{2.72}$$

$$\Delta\Gamma_s = \Gamma_L^s - \Gamma_H^s \tag{2.73}$$

which means that the eigenvalue difference is

$$\Delta\mu = \Delta M + \frac{i}{2}\Delta\Gamma. \tag{2.74}$$

It is convenient in what follows to express M_{12}^s, Γ_{12}^s as

$$M_{12}^s = |M_{12}^s| e^{i\theta_M} \tag{2.75}$$

$$\Gamma_{12}^s = |\Gamma_{12}^s| e^{i\theta_\Gamma}. \tag{2.76}$$

To fix the expressions for ΔM_s and $\Delta\Gamma_s$ that are needed for construction of the mixing observables we may equate the LHS of (2.69) with the LHS of (2.66) and notice that the smallness of the ratio of the magnitude of $|\Gamma_{12}^s/M_{12}^s|$ in the SM [38]

$$\left|\frac{\Gamma_{12}^s}{M_{12}^s}\right| \approx 5 \times 10^{-3} \tag{2.77}$$

allows for an expansion in powers of $\left|\frac{\Gamma_{12}^s}{M_{12}^s}\right|$, so that

$$\begin{aligned}
\Delta M_s + \frac{i}{2}\Delta\Gamma &= 2\sqrt{|M_{12}|^2 - \frac{1}{4}|\Gamma_{12}|^2 - i\mathrm{Re}(M_{12}^*\Gamma_{12})} \\
&= 2|M_{12}|\sqrt{1 - \frac{1}{4}\left|\frac{\Gamma_{12}}{M_{12}}\right|^2 - i\frac{\mathrm{Re}(M_{12}^*\Gamma_{12})}{|M_{12}|^2}} \\
&= 2|M_{12}|\sqrt{1 - i\left|\frac{\Gamma_{12}}{M_{12}}\right|\left(\cos(\theta_\Gamma - \theta_M) - \frac{i}{4}\left|\frac{\Gamma_{12}}{M_{12}}\right|\right)} \\
&= 2|M_{12}|\left[1 - \frac{i}{2}\left|\frac{\Gamma_{12}}{M_{12}}\right|\left(\cos(\theta_\Gamma - \theta_M) - \frac{i}{4}\left|\frac{\Gamma_{12}}{M_{12}}\right|\right)\right. \\
&\qquad \left. + \frac{1}{8}\left|\frac{\Gamma_{12}}{M_{12}}\right|^2\left(\cos(\theta_\Gamma - \theta_M) - \frac{i}{4}\left|\frac{\Gamma_{12}}{M_{12}}\right|\right)^2\right.
\end{aligned}$$

$$+\frac{i}{16}\left|\frac{\Gamma_{12}}{M_{12}}\right|^3\left(\cos(\theta_\Gamma-\theta_M)-\frac{i}{4}\left|\frac{\Gamma_{12}}{M_{12}}\right|\right)^3+\cdots\Bigg]. \quad (2.78)$$

Let θ_{12} be the relative phase of M_{12}^s and Γ_{12}^s, defined as

$$\theta_{12}^s=\arg\left(-\frac{M_{12}^s}{\Gamma_{12}^s}\right):=\pi+\theta_M-\theta_\Gamma, \quad (2.79)$$

then

$$\Delta M_s+\frac{i}{2}\Delta\Gamma=2|M_{12}|\left[1+\frac{i}{2}\left|\frac{\Gamma_{12}}{M_{12}}\right|\cos\theta_{12}-\frac{1}{8}\left|\frac{\Gamma_{12}}{M_{12}}\right|^2\sin^2\theta_{12}\right.$$
$$\left.+\frac{i}{16}\left|\frac{\Gamma_{12}}{M_{12}}\right|^3\cos\theta_{12}\sin^2\theta_{12}+\mathcal{O}\left(\left|\frac{\Gamma_{12}}{M_{12}}\right|^4\right)\right] \quad (2.80)$$

Equating real and imaginary parts yields

$$\Delta M=2|M_{12}|\left(1-\frac{1}{8}\left|\frac{\Gamma_{12}}{M_{12}}\right|^2\sin^2\theta_{12}+\mathcal{O}\left(\left|\frac{\Gamma_{12}}{M_{12}}\right|^4\right)\right),$$

$$\Delta\Gamma=2|\Gamma_{12}|\cos\theta_{12}\left(1+\frac{1}{8}\left|\frac{\Gamma_{12}}{M_{12}}\right|^2\sin^2\theta_{12}+\mathcal{O}\left(\left|\frac{\Gamma_{12}}{M_{12}}\right|^4\right)\right).$$

Then neglecting the small corrections, we find

$$\Delta M^s=2|M_{12}| \quad (2.81)$$

$$\Delta\Gamma^s=2|\Gamma_{12}|\cos\theta_{12}$$
$$=-2\mathrm{Re}(\Gamma_{12}e^{-i\theta_M}) \quad (2.82)$$

where to a good approximation in the SM, the dominant contribution to the phase of M_{12}^s gives $e^{i\theta_M}\approx\frac{V_{ts}^*V_{tb}}{V_{ts}V_{tb}^*}$ [38], and the second line of (2.82) is shown for later convenience. In addition, for our study of effects in hadronic decay we will need to define the B_s^0 mixing parameter $\left(\frac{q}{p}\right)_{B_s}$ of (2.71), which is given by

$$\left(\frac{q}{p}\right)_{B_s}=\frac{(|M_{12}^s|e^{-i\theta_M}-\frac{i}{2}|\Gamma_{12}^s|e^{-i\theta_\Gamma})}{\sqrt{|M_{12}^s|^2-i\mathrm{Re}(\Gamma_{12}M_{12}^*)-\frac{1}{4}|\Gamma_{12}|^2}}$$
$$=(e^{-i\theta_M}-\frac{i}{2}\left|\frac{\Gamma_{12}}{M_{12}}\right|e^{-i\theta_\Gamma})(1+\frac{i}{2}\left|\frac{\Gamma_{12}}{M_{12}}\right|\cos(\theta_\Gamma-\theta_M)+\mathcal{O}\left(\left|\frac{\Gamma_{12}}{M_{12}}\right|^2\right))$$
$$=(e^{-i\theta_M}-\frac{i}{2}\left|\frac{\Gamma_{12}}{M_{12}}\right|e^{-i\theta_\Gamma})(1+\frac{i}{2}\left|\frac{\Gamma_{12}}{M_{12}}\right|\cos(\theta_\Gamma-\theta_M)+\mathcal{O}\left(\left|\frac{\Gamma_{12}}{M_{12}}\right|^2\right))$$

$$= e^{-i\theta_M}\left(1+\frac{1}{2}\left|\frac{\Gamma_{12}}{M_{12}}\right|\sin(\theta_M-\theta_\Gamma)\right)+\mathcal{O}\left(\left|\frac{\Gamma_{12}}{M_{12}}\right|^2\right).$$

$$= e^{-i\theta_M}\left(1-\frac{1}{2}\left|\frac{\Gamma_{12}}{M_{12}}\right|\sin\theta_{12}\right)+\mathcal{O}\left(\left|\frac{\Gamma_{12}}{M_{12}}\right|^2\right). \tag{2.83}$$

2.3 CP violation

In this section we provide a brief review of some of the basic formalism describing CP violation in the SM and introduce some notation, define some transformation properties necessary for later chapters. Where known results are stated, they will be done so following the development in [35].

2.3.1 Symmetries and transformation properties

Generically, let us define the decay amplitudes for a pseudo-scalar meson P^0 and its CP conjugate $\bar{P}^0$ to decay to a final multi particle state F, and its CP conjugate $\bar{F}$ as

$$A_F = \langle F|\mathcal{H}|P^0\rangle, \qquad \bar{A}_F = \langle F|\mathcal{H}|\bar{P}^0\rangle, \tag{2.84}$$

$$A_{\bar{F}} = \langle \bar{F}|\mathcal{H}|P^0\rangle, \qquad \bar{A}_{\bar{F}} = \langle \bar{F}|\mathcal{H}|\bar{P}^0\rangle \tag{2.85}$$

The operators representing the transformations C charge conjugation and P Parity are denoted here as $\mathcal{C}, \mathcal{P}$, and the action of these operators on the meson and final states is

$$(\mathcal{CP})|P^0\rangle = e^{i\xi_P}|\bar{P}^0\rangle \qquad (\mathcal{CP})|F\rangle = e^{i\xi_F}|\bar{F}\rangle \tag{2.86}$$

$$(\mathcal{CP})|\bar{P}^0\rangle = e^{-i\xi_P}|P^0\rangle \qquad (\mathcal{CP})|\bar{F}\rangle = e^{-i\xi_F}|F\rangle \tag{2.87}$$

$$(\mathcal{CP})^2 = 1 \tag{2.88}$$

The phases ξ_F, ξ_P are flavour dependent and non- physical. We also define the CP eigenstates as F_{CP} as

$$(\mathcal{CP})|F_{CP}\rangle = \eta_{CP}|F_{CP}\rangle, \qquad \eta_{CP} = \pm 1. \tag{2.89}$$

If CP is conserved then

$$[(\mathcal{CP}), \mathcal{H}] = 0, \tag{2.90}$$

and hence due to (2.90) and from (2.84)-(2.85) we deduce that in the absence of CP violation

$$\bar{A}_{\bar{F}} = e^{i(\xi_F - \xi_P)} A_F, \tag{2.91}$$

$$\bar{A}_F = e^{-i(\xi_P + \xi_F)} A_{\bar{F}}. \tag{2.92}$$

In addition, the action of the parity operator on the odd parity neutral mesons $P^0 = K_q^0, B_q^0$ is as follows

$$\mathcal{P}|P^0\rangle = -|P^0\rangle. \tag{2.93}$$

2.3.2 CP violation in the SM

Complex parameters in any Hamiltonian term which contribute to the decay amplitude will appear as their complex conjugate form after a CP transformation is performed. There are three sources of complex parameters arising in the SM; i) spurious flavour dependent transformation phases, ii) weak phases and iii) strong phases. The spurious phases are those shown above and are un-physical and arbitrary. We chose in this thesis to set them to zero for convenience. The weak phases are associated with the charged current interactions shown in (2.39) and violate CP. These phases are associated with the CKM matrix elements and are the only source of CP violation in the SM. The strong phases are CP conserving and in general, are non-perturbative in origin.
In this thesis the processes which are studied and which are used in the SM as a measure of CP violation are i) CP violation in B_s^0 meson mixing and ii) CP violation in the interference between mixing and decay.

CP violation in mixing: B_s^0 system

CP violation in mixing is associated with the relative phase of mixing quantities M_{12}^s and Γ_{12}^s given as θ_{12}^s and defined in (2.79). This effect is calculated in the SM as the flavour specific CP asymmetry and given by

$$a_{fs}^s = \mathrm{Im}\left(\frac{\Gamma_{12}^s}{M_{12}^s}\right) = \left|\frac{\Gamma_{12}^s}{M_{12}^s}\right| \sin\theta_{12}^s \tag{2.94}$$

by examining (2.83) it is clear that for CP violation in mixing, we will find that

$$\left|\frac{q}{p}\right|_{B_s} \neq 1. \tag{2.95}$$

CP violation in the interference between mixing and decay: B_d^0 system

This class of CP violation occurs when B_d^0 and $\bar{B}_d^0$ can decay to the same common final state which is a CP eigenstate. For this we define the quantity λ_F generically to be

$$\lambda_{F_{CP}} = \left(\frac{q}{p}\right)_B \frac{\bar{A}_{F_{CP}}}{A_{F_{CP}}}. \tag{2.96}$$

It can be measured by studying the decay of an initially pure B_d^0 meson state to a CP eigenstate and with an initially pure $\bar{B}_d^0$ meson decaying to the same CP eigenstate. In the SM this class of decay can happen when

$$\left|\frac{q}{p}\right| = 1, \qquad \mathrm{Im}(\lambda_{F_{CP}}) \neq 0. \tag{2.97}$$

2.4 Renormalization

In Quantum Field Theory (QFT), decay rates and cross sections related to interactions between combinations of quantum fields contained in (2.1), can be approximated using perturbation theory. One can calculate the leading order or "Tree level" amplitude for an interaction by obtaining the invariant matrix element of the term in the Lagrangian calculated between the desired initial and final states. The accuracy can be systematically improved by including higher order corrections in the perturbative expansion, as long as this is performed at an energy scale for which the expansion parameter is small. However, the accuracy in such computations is ultimately limited by non perturbative power corrections.

In practice, this involves the calculation of integrals over four momenta which represent the presence of virtual particles at the so called "Loop level" and often these integrals diverge. Such divergent integrals must be regulated in some way so that the divergence can be contained in a particular parameter which typically will be associated with the divergence in some limit. There are various methods of doing this, and in this thesis we will employ the gauge invariant method of dimensional regularization.

2.4.1 Dimensional regularization

In Dimensional Regularization [39, 40, 41, 42, 43] scheme the number of spacetime dimensions is continued to $d = 4 - 2\epsilon$ and singularities arising in loop integrals are contained in $\frac{1}{\epsilon}$ poles. As an illustration let us consider the diagram associated with the quark field renormalization

$$\begin{aligned} -i\Sigma_{\alpha\beta}(p) &= -g^2\mu^{4-d}(T^A T^A)_{\alpha\beta}\int \frac{d^dk}{(2\pi)^d}\frac{\gamma^\nu \not{k}\gamma_\nu}{(k^2+i\epsilon)((p-k)^2+i\epsilon)} \\ &= -g^2\mu^{4-d}C_F\delta_{\alpha\beta}\int \frac{d^d\ell}{(2\pi)^d}\int_0^1 dx \frac{\gamma^\nu(\not{\ell}+(1-x)\not{p})\gamma_\nu}{(\ell^2-\Delta+i\epsilon)^2} \\ &= -g^2\mu^{4-d}C_F\delta_{\alpha\beta}\int \frac{d^d\ell}{(2\pi)^d}\int_0^1 dx \frac{(2-d)(\not{\ell}+(1-x)\not{p})}{(\ell^2-\Delta+i\epsilon)^2} \end{aligned} \tag{2.98}$$

where we have shifted $k = \ell + (1-x)p$ and $\Delta = -x(1-x)p^2$, $T^A, A = 1, ..., 8$ are $SU_C(3)$ group generators, and μ is a parameter with dimensions of mass, introduced in order to ensure the strong coupling is dimensionless in d dimensions. In the last line the Dirac algebra in d dimensions gives

$$\gamma^\nu\gamma_\rho\gamma_\nu = (2-d)\gamma_\rho \tag{2.99}$$

$$\gamma^\nu\gamma_\nu = d \tag{2.100}$$

The two integrals over ℓ arising in (2.98) are evaluated in dimensional regularization to be

$$\int \frac{d^d\ell}{(2\pi)^d}\frac{1}{(\ell^2-\Delta+i\epsilon)^2} = \frac{i}{(4\pi)^{\frac{d}{2}}}\frac{\Gamma(2-\frac{d}{2})}{\Gamma(2)}\left(\frac{1}{\Delta}\right)^{2-\frac{d}{2}} \tag{2.101}$$

$$\int \frac{d^d\ell}{(2\pi)^d}\frac{\not{\ell}}{(\ell^2-\Delta+i\epsilon)^2} = 0 \tag{2.102}$$

The second integral (2.102) is zero by symmetry and the (2.101) is expressed in terms of Gamma functions.

$$\begin{aligned} -i\Sigma_{\alpha\beta}(p) &= -ig^2\mu^{4-d}C_F\delta_{\alpha\beta}\int_0^1 dx(1-x)\frac{(2-d)\not{p}}{(4\pi)^{d/2}}\frac{\Gamma(2-\frac{d}{2})}{\Gamma(2)}\left(\frac{1}{\Delta}\right)^{2-\frac{d}{2}} \\ &= -2ig^2\frac{C_F}{(4\pi)^2}\delta_{\alpha\beta}\not{p}\int_0^1 dx(1-x)(\epsilon-1)\Gamma(\epsilon)\left(\frac{4\pi\mu^2}{\Delta}\right)^\epsilon \end{aligned} \tag{2.103}$$

with $C_F = \frac{N^2-1}{2N}$ and N is the number of colours. For $d = 4-2\epsilon$, the Γ function has a pole at $\epsilon = 0$ so we expand for ϵ close to zero. The quantities in parentheses raised to the

power ϵ and the Gamma function close to its pole may be expanded under the integral in ϵ about zero, where

$$\Gamma(\epsilon) = \frac{1}{\epsilon} - \gamma_E + \mathcal{O}(\epsilon), \qquad A^\epsilon = 1 + \epsilon \ln A + \mathcal{O}(\epsilon^2), \tag{2.104}$$

where γ_E is the Euler Gamma constant. This gives for the integral (2.98) in dimensional regularization scheme

$$\begin{aligned}\Sigma_{\alpha\beta}(p) &= \frac{g^2 C_F}{(4\pi)^2}\delta_{\alpha\beta}\not{p}\left(1 - \frac{1}{\epsilon} - \ln\left(\frac{\mu^2}{-p^2}\right) + \gamma_E \right.\\ &\qquad\qquad \left. - \ln 4\pi + 2\int_0^1 dx x \ln\left(x(1-x)\right) + \mathcal{O}(\epsilon)\right)\\ &= \frac{\alpha_s}{4\pi} C_F \delta_{\alpha\beta}\not{p}\left(1 - \frac{1}{\epsilon} - \ln\left(\frac{\mu^2}{-p^2}\right) + \gamma_E - \ln 4\pi\right) + \text{finite}.\end{aligned} \tag{2.105}$$

This integral has now been regulated, and the divergence is now contained in the $\frac{1}{\epsilon}$ pole, which diverges as $\epsilon \to 0$.

Renormalization is the practice of removing these divergences, represented by the $\frac{1}{\epsilon}$ poles, order by order in perturbation theory so that one may obtain finite results in the limit as $\epsilon \to 0$ in $d = 4$ dimensions. These renormalized quantities can then be safely used in the theoretical prediction of observables such as cross sections and decay rates.

For a concrete example of how the procedure of renormalization works consider the theory of Quantum Chromodynamics (QCD). Following the development of [44], upon first fixing the gauge via the method of Fadeev and Popov [45], the Lagrangian density is given by

$$\begin{aligned}\mathcal{L}_{qcd} = &-\frac{1}{4}(\partial_\mu G^A_\nu - \partial_\nu G^A_\mu)(\partial^\mu G^{\nu A} - \partial^\nu G^{\mu A}) - \frac{1}{2\xi}(\partial^\mu G^A_\mu)^2\\ &+ \bar{q}(i\not{\partial} - m_q)q + \chi^{A*}\partial^\mu\partial_\mu\chi^A\\ &- \frac{g}{2}f^{ABC}(\partial_\mu G^A_\nu - \partial_\nu G^A_\mu)G^{B\mu}G^{C\nu} - \frac{g^2}{4}f^{ABC}f^{CDE}G^A_\mu G^B_\nu G^{C\mu}G^{D\nu}\\ &+ g\bar{q}_i T^A_{ij}\gamma^\mu q_j G^A_\mu + g f^{ABC}(\partial^\mu\chi^{A*})\chi^B G^C_\mu,\end{aligned} \tag{2.106}$$

where T^A, f^{ABC} with $A, B, C = (1, 2, ..., 8)$ are the generators and structure constants of $SU(3)_c$ respectively, G^A_μ are the gluon fields, $q = (q_1, q_2, q_3)$ are the $SU(3)$ colour triplet of the quark field of flavour q_i where $i = (u, d, c, s, t, b)$. χ^A is the ghost field, ξ is the gauge parameter and g is the strong coupling.

The procedure for renormalization of the theory is to write the bare Lagrangian as the sum of the Lagrangian of (2.109) and a counter term Lagrangian.

$$\mathcal{L}_{qcd,b} = \mathcal{L}_{qcd} + \mathcal{L}_{qcd,CT}, \tag{2.107}$$

One then expresses the bare Lagrangian containing the bare quantities in terms of renormalization constants and renormalizad quantities, via the following prescription:

$$\begin{aligned} G^A_{b\mu} &= \sqrt{Z}_3 G^A_\mu, \qquad q_b = \sqrt{Z_2} q, \qquad \chi^A_b = \tilde{Z}_3 \chi^A, \\ g_b &= Z_g \mu^\epsilon g, \qquad m_b = Z_m m, \qquad \xi_b = Z_3 \xi. \end{aligned} \tag{2.108}$$

where the quantities with a subscript b are the bare unrenormalized ones and the Z_i are the renormalization constants. The quantity μ is introduced to the strong coupling in order to make it dimensionless in d dimensions. By comparing the RHS of (2.107) given by

$$\begin{aligned} \mathcal{L}_{qcd} + \mathcal{L}_{qcd,CT} = &-\frac{(1+\delta_3)}{4}(\partial_\mu G^A_\nu - \partial_\nu G^A_\mu)(\partial^\mu G^{\nu A} - \partial^\nu G^{\mu A}) - \frac{1}{2\xi}(\partial^\mu G^A_\mu)^2 \\ &+ i(1+\delta_2)\bar{q}\partial\!\!\!/ q - (1+\delta_m) m_q \bar{q} q + (1+\tilde{\delta}_3)\chi^{A*}\partial^\mu\partial_\mu\chi^A \\ &- (1+\delta_3^{3g})\frac{g}{2} f^{ABC}(\partial_\mu G^A_\nu - \partial_\nu G^A_\mu) G^{B\mu} G^{C\nu} \\ &- (1+\delta_3^{4g})\frac{g^2}{4} f^{ABC} f^{CDE} G^A_\mu G^B_\nu G^{C\mu} G^{D\nu} \\ &+ (1+\delta_1 g)\bar{q}_i T^A_{ij}\gamma^\mu q_j G^A_\mu + (1+\tilde{\delta}_1) g f^{ABC}(\partial^\mu \chi^{A*})\chi^B G^C_\mu, \end{aligned} \tag{2.109}$$

with the LHS expressed in terms of (2.108)

$$\begin{aligned} \mathcal{L}_{qcd,b} = &-\frac{Z_3}{4}(\partial_\mu G^A_\nu - \partial_\nu G^A_\mu)(\partial^\mu G^{\nu A} - \partial^\nu G^{\mu A}) - \frac{1}{2\xi}(\partial^\mu G^A_\mu)^2 \\ &+ Z_2 \bar{q}\partial\!\!\!/ q - Z_2 Z_m m_q \bar{q} q + \tilde{Z}_3 \chi^{A*}\partial^\mu\partial_\mu\chi^A \\ &- Z_3^{\frac{3}{2}} Z_g \frac{g}{2} f^{ABC}(\partial_\mu G^A_\nu - \partial_\nu G^A_\mu) G^{B\mu} G^{C\nu} \\ &- Z_3^2 Z_g^2 \frac{g^2}{4} f^{ABC} f^{CDE} G^A_\mu G^B_\nu G^{C\mu} G^{D\nu} \\ &+ Z_2 Z_g Z_3^{\frac{1}{2}} g \bar{q}_i T^A_{ij}\gamma^\mu q_j G^A_\mu + Z_2 Z_g \tilde{Z}_3^{\frac{1}{2}} g f^{ABC}(\partial^\mu \chi^{A*})\chi^B G^C_\mu, \end{aligned} \tag{2.110}$$

the parameters for the counter terms are found to be

$$\delta_3 = Z_3 - 1, \qquad \delta_2 = Z_2 - 1, \qquad \tilde{\delta}_3 = \tilde{Z}_3 - 1,$$

$$\begin{aligned}
\delta_m &= Z_2 Z_m - 1, \qquad \delta_3^{3g} = Z_3^{\frac{3}{2}} Z_g - 1, \qquad \delta_3^{4g} = Z_3^2 Z_g^2 - 1, \\
\delta_1 &= Z_2 Z_3^{\frac{1}{2}} Z_g - 1, \qquad \tilde{\delta}_1 = \tilde{Z}_3 Z_3^{\frac{1}{2}} Z_g - 1.
\end{aligned} \tag{2.111}$$

The counter terms are then treated as interaction terms in the Lagrangian and have corresponding Feynman rules. These then contribute to the calculation of Green functions at the desired order in perturbation theory. To fix the renormalization constants Z_i one then determines their value such that they cancel the divergences which arise in computing the Green functions, in accordance with the selected renormalization scheme. In this thesis we use the $\overline{MS}$ scheme, for which only the divergent $\frac{1}{\epsilon}$ poles are subtracted, and not any of the other finite parts of the calculated loop diagrams. In this scheme the quantity μ introduced in (2.109) is re-expressed as

$$\mu_{\overline{MS}} = \frac{e^{\gamma_E/2}}{\sqrt{4\pi}}\mu \tag{2.112}$$

So for example from the result given by (2.105), the quark field renormalization constant Z_2 will renormalize the theory at $\mathcal{O}(\alpha_s)$ in $\overline{MS}$ for

$$Z_2 = 1 - \frac{\alpha_s}{4\pi} C_F \frac{1}{\epsilon}. \tag{2.113}$$

2.4.2 Renormalization group

The Renormalization Group [46, 47] is the group of transformations between different choices of renormalization scale μ. The renormalization group equations (RGE) govern the change in renormalized quantities such as Greens functions and parameters (masses, couplings) with μ, in differential form. Let us consider the strong coupling in (2.108) and derive the differential equations it obeys, keeping in mind that the bare parameters are μ independent. Consider the strong coupling which depends upon μ through the rescaling performed in order to obtain a dimensionless coupling in d spacetime dimensions. We re-express g in (2.108) as

$$g(\mu) = Z_g^{-1} \mu^{-\epsilon} g_b \tag{2.114}$$

and take the derivative of $g(\mu)$ with respect to μ

$$\begin{aligned}
\mu \frac{d}{d\mu} g(\mu) &= Z_g^{-1} g_b \left(\mu \frac{d}{d\mu} \mu^{-\epsilon} \right) + \mu^{-\epsilon} g_b \left(\mu \frac{d}{d\mu} Z_g^{-1} \right), \\
&= -\epsilon \mu^{-\epsilon} Z_g^{-1} g_b - \mu^{-\epsilon} g_b Z_g^{-2} \left(\mu \frac{d}{d\mu} Z_g \right),
\end{aligned}$$

$$= -\epsilon g(\mu) - g(\mu)\frac{1}{Z_g}\left(\frac{d}{d\ln\mu}Z_g\right).$$

This can be written in terms of the QCD beta function

$$\mu\frac{d}{d\mu}g(\mu) = \beta(\epsilon, g(\mu)), \tag{2.115}$$

where the definition of $\beta(\epsilon, g(\mu))$ valid in d dimensions is explicitly

$$\beta(\epsilon, g(\mu)) = -\epsilon g(\mu) - g(\mu)\frac{1}{Z_g}\left(\frac{d}{d\ln\mu}Z_g\right). \tag{2.116}$$

For Z_g in the $\overline{MS}$ scheme to L.O given as

$$Z_g = 1 + \frac{g_b^2}{32\pi^2}\frac{1}{\epsilon}(-11 + \frac{2N_f}{3}), \tag{2.117}$$

where N_f is the number of active quark flavours and where it is understood that in the dimensional regularization scheme, the $\frac{1}{\epsilon}$ pole is pre-multiplied by the same factor as the logarithm of μ appearing in the calculation of Z_g. Then differentiating with respect to (2.117) and taking the limit as $\epsilon \to 0$ in $d \to 4$ of (2.116) gives

$$\beta(g) = -\beta_0\frac{g^3}{16\pi^2}, \tag{2.118}$$

with $\beta_0 = \frac{11N-2N_f}{3}$, and N is the number of colours. Then at leading order, the RGE for the strong coupling is given by

$$\mu\frac{d}{d\mu}g(\mu) = -\beta_0\frac{g(\mu)^3}{16\pi^2}, \tag{2.119}$$

and solving this will give the value of the strong coupling at scale μ at leading order in perturbation theory. We give this example here as it will be useful in explaining how the RG is used in renormalization group improved effective field theory.

2.5 Effective Field Theory

2.5.1 Weak effective Hamiltonian

An Effective Field Theory (EFT) is a framework adopted in order to find the simplest way to encapsulate the most important physics for the problem. The type of EFT applicable to B meson processes is a "top down" EFT in that we have knowledge of the theory

at higher energy scales, but for greater simplicity in calculations, it is useful to obtain a theory valid at lower energies containing only the relevant degrees of freedom. The guiding principle in such an endeavour is that in order to describe physics at a scale μ, we need not have detailed knowledge of the dynamics at much higher scales $\Lambda \gg \mu$ thus we may remove from the lower energy theory the degrees of freedom not relevant, and focus on interactions involving those that are. In B meson decays there is a wide variation in scales within the problem. These include Λ_{QCD}, m_b, M_W where $\Lambda_{QCD} \ll m_b \ll M_W$. Λ_{QCD} is the so called "soft scale" and this is the scale at which perturbation theory breaks down and non perturbative methods must be applied. The natural scale in the decay of a B meson is the b quark mass, given that the b quark is the "heavy" quark in the meson and when the meson decays at rest the most energy which can go into decay products will be proportional to this. Then M_W is the so called "hard scale" at which we "integrate out " the mass of the W boson. In QCD the relevant expansion parameter is the strong coupling $\alpha_s(\mu)$ which is a valid expansion parameter down to scales $\mu \sim 1\mathrm{GeV}$. If we consider a b decay $b \to c\bar{c}s$ then the appropriate scale at which to renormalize the effective operators is the characteristic scale of the problem $\mu = \mathcal{O}(m_b)$. Figure 2.1 depicts the reduction of a full amplitude to an effective amplitude in diagrammatic from, and is a generalization of the Fermi theory for β decays [48, 49, 50].

Mathematically, according to the momentum space Feynman rues the full amplitude for

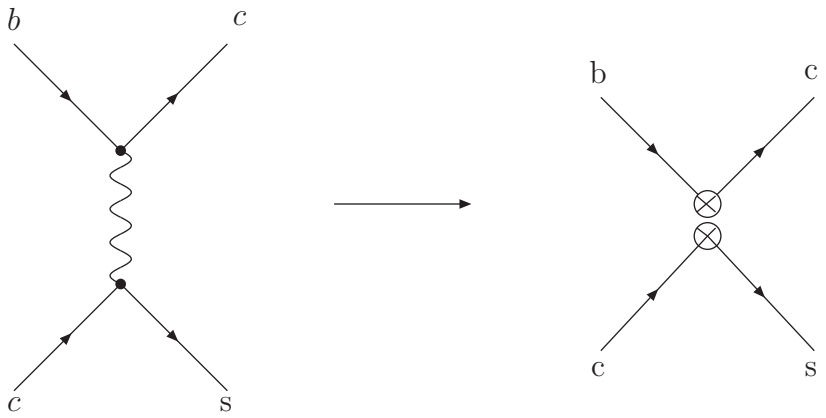

Figure 2.1: Full theory to effective theory

the diagram on the lhs is

$$\mathcal{A}_{\text{full}} = ig_2^2 \frac{V_{cs}^* V_{cb}}{8} \bar{u}_s^\alpha \gamma_\mu (1-\gamma_5) u_c^\alpha \left(\frac{\eta^{\mu\nu}}{q^2 - M_W^2 + i\epsilon} \right) \bar{u}_c^\beta \gamma_\nu (1-\gamma_5) u_b^\beta. \tag{2.120}$$

with q^2 the momentum squared of the W boson, u_q the spinors for the quark fields, $\alpha, \beta = 1, 2, 3$ $SU_C(3)$ colour indices. As this process really describes a $b \to c\bar{c}s$ transition, the momentum release available is of the order $q^2 \sim m_b^2 \ll M_W^2$. We can perform a Taylor expansion in $\frac{q^2}{M_W^2}$ on the propagator to give

$$-i\frac{\eta^{\mu\nu}}{q^2 - M_W^2 + i\epsilon}|_{q^2 \ll M_W^2} = \frac{i\eta^{\mu\nu}}{M_W^2} + \mathcal{O}\left(\frac{q^2}{M_W^2}\right). \tag{2.121}$$

This makes the propagator at LO effectively a constant and removes the heavy W degree of freedom from the theory. We can write this now as an effective interaction valid for $q^2 \ll M_W^2$

$$\mathcal{A}_{\text{full}} \to -ig_2^2\frac{V_{cs}^* V_{cb}}{8M_W^2}[\bar{u}_s^\alpha \gamma^\mu(1-\gamma_5)u_c^\alpha][\bar{u}_c^\beta(p)\gamma_\mu(1-\gamma_5)u_b^\beta] + \mathcal{O}\left(\frac{q^2}{M_W^2}\right). \tag{2.122}$$

We can obtain the identical result by writing down an Effective $\Delta B = 1$ Hamiltonian comprised of only two four fermion operators

$$\mathcal{H}_{\text{eff}} = \frac{G_F}{\sqrt{2}} V_{cbV_{cs}} \sum_{i=1}^{2} C_i Q_i \tag{2.123}$$

where the Fermi constant G_F is

$$\frac{G_F}{\sqrt{2}} = \frac{g_2^2}{8M_W^2}, \qquad\qquad G_F = 1.16639 \times 10^{-5}\text{GeV}^{-2}, \tag{2.124}$$

and where the operators Q_i are defined as

$$Q_1 = (\bar{c}_L^\alpha \gamma_\mu b_L^\beta)(\bar{s}_L^\beta \gamma^\mu c_L^\alpha), \qquad\qquad Q_2 = (\bar{c}_L^\alpha \gamma_\mu b_L^\alpha)(\bar{s}_L^\beta \gamma^\mu c_L^\beta). \tag{2.125}$$

We obtain the same amplitude as given in (2.122) by calculating the rhs of Figure 2.1 where the circled crosses denote the vector minus axial vector $(V - A)$ currents in operators Q_i.

$$\mathcal{A}_{\text{eff}} = \frac{G_F}{\sqrt{2}} V_{cs}^* V_{cb} \left[C_1 \langle Q_1 \rangle_p^{\text{Tree}} + C_2 \langle Q_2 \rangle_p^{\text{Tree}}\right] \tag{2.126}$$

We define the tree level matrix elements to be

$$\langle Q_i \rangle_p^{Tree} = \langle s(\vec{p}'), c(\vec{p}_c')|Q_1(0)|c(\vec{p}_c), b(\vec{p})\rangle + \mathcal{O}(\alpha_s) \tag{2.127}$$

and explicitly at tree level they are simple products of quark field bilinears

$$\langle Q_1 \rangle_p^{\text{Tree}} = [\bar{u}_s^\alpha \gamma^\mu (1-\gamma^5) u_c^\beta][\bar{u}_c^\beta \gamma_\mu (1-\gamma_5) u_b^\alpha] \tag{2.128}$$

$$\langle Q_2 \rangle_p^{\text{Tree}} = [\bar{u}_s^\alpha \gamma^\mu (1-\gamma^5) u_c^\alpha][\bar{u}_c^\beta \gamma_\mu (1-\gamma_5) u_b^\beta] \tag{2.129}$$

Therefore the effective amplitude corresponding to the rhs in figure 2.1 is

$$\begin{aligned}\mathcal{A}_{\text{eff}} = -\frac{G_F}{\sqrt{2}} V_{cs}^* V_{cb} \Big(& C_1 [\bar{u}_s^\alpha \gamma^\mu (1-\gamma^5) u_c^\beta][\bar{u}_c^\beta \gamma_\mu (1-\gamma_5) u_b^\alpha] + \\ & + C_2 [\bar{u}_s^\alpha \gamma^\mu (1-\gamma^5) u_c^\alpha][\bar{u}_c^\beta \gamma_\mu (1-\gamma_5) u_b^\beta] \Big)\end{aligned} \tag{2.130}$$

Then by matching (2.122) onto i times (2.130) we can determine the Wilson coefficients C_1 and C_2 at tree level to be

$$C_1(M_W) = 0, \qquad\qquad C_2(M_W) = 1. \tag{2.131}$$

The reason that C_1 is zero at tree level is because there are no gluonic colour index changing contributions. The weak W boson does not change colour and so the two quark currents have the same $SU_C(3)$ index. The weak effective Hamiltonian in (2.123) is the starting point of the effective theory and is an Operator Product Expansion (OPE), first introduced by [51, 52, 53, 54]. In the following section, we discuss this in greater detail.

2.5.2 Operator Product Expansion

The Operator Product Expansion was proposed as a generalization the equal time commutator of two fields $X(x)$ and $Y(y)$ by [51]. This approach is applied to the time ordered product of operators under similar conditions as was later introduced in [52]. Following [55], in position space, the bi-local time ordered product (defined in (A.14)) of operators placed at different space time points a distance z apart, can be systematically expanded in local operators multiplied by coefficient functions, in the limit as $z \to 0$. That is

$$T[Q_a(z) Q_b(0)] = \sum_k C_{abk}(z) \mathcal{O}_k(0). \tag{2.132}$$

The coefficients $C_{abk}(z)$ are independent of the matrix elements of the operators on the left hand side and right hand sides, under the condition that the external states have momentum components which are small compared to the inverse separation. Moreover, the coefficients are calculated in perturbation theory in an expansion in the QCD coupling α_s

due to the "short distance" effects being contained in the coefficients and all non perturbative "long distance" effects occurring at scales much larger than z. Or, to cast this in a slightly different light, the momentum space expression for the OPE is

$$\int d^4z e^{iq\cdot z} T[Q_a(z)Q_b(0)] = \sum_k C_{abk}(q)\mathcal{O}_k(0) \tag{2.133}$$

In this case, the limit is $q \to \infty$, which the Fourier transform relates to $z \to 0$. Thus we can think of the expansion in terms of matrix elements representing "low energy" non perturbative parts and coefficient functions containing the "high energy" scales. Since again the strong coupling becomes asymptotically small for high scales the coefficients can be computed in perturbation theory.

The method of moving from a high energy theory to a low energy effective theory depicted in Figure 2.1 and discussed in subsection 2.5.1 can be viewed as an OPE as was introduced in [54]. As long as the momentum scale relevant for the decaying meson is much lower than the mass of the particle we wish to " integrate out", we can express the amplitude describing the weak decay of a meson as

$$\mathcal{A} = \langle \mathcal{H}_{\text{eff}} \rangle = \frac{G_F}{\sqrt{2}} V_{CKM} \sum_i C_i(\mu, M_W)\langle Q_i(\mu)\rangle. \tag{2.134}$$

Here the factor V_{CKM} is schematic, it will be different for different operators and contain a combination of CKM matrix elements. In (2.134) the application of the OPE formalism has again achieved a separation of scales, the short distance, high energy physics belongs to the perturbatively calculable Wilson coefficients $C_i(\mu)$ and the long distance, low energy physics to the non perturbative matrix elements of local operators $\langle Q_i(\mu)\rangle$ and μ is the scale of separation between the two regimes. Degrees of freedom with mass higher than μ are removed from the theory, but their existence is remembered by the Wilson coefficients.

The physical amplitude cannot depend upon the factorization scale, which therefore should cancel out in between the Wilson coefficients and the operator matrix elements. The Wilson coefficients, as has been mentioned above, can be calculated perturbatively, however large logarithms of the form $\ln\left(\frac{M_W}{\mu}\right)$ spoil the perturbative expansion due to the large separation of scales present on weak meson decays. In order to address this problem, we must employ the Renormalization Group formalism to sum up these large logarithms to all orders in perturbation theory. After this, one may use this " renormalization

group improved perturbation theory" to calculate the coefficients. The operator matrix elements can be treated separately and these require non perturbative methods such as Lattice gauge theory , Heavy Quark Effective Theory (HQET), Heavy Quark Expansion (HQE), $\frac{1}{N}$ counting rules and so on.

2.5.3 Operator renormalization

The operators in the Weak effective Hamiltonian are renormalized in a way analogous to that of the quark fields, they are rescaled by a multiplicative renormalization constant, which is adjusted according to a renormalization condition to remove ultra violet divergences order by order in perturbation theory. In the case of an operator basis, the renormalization constant is replaced with a renormalization matrix which leads to operator mixing. Here and in what follows, where initial and final states are not explicitly labelled, we denote the matrix elements of operators with hadronic initial and final states I, F as

$$\langle F|Q|I\rangle := \langle Q\rangle, \tag{2.135}$$

and the matrix elements of operators with partonic initial and final states i, f as

$$\langle f|Q|i\rangle := \langle Q\rangle_p, \tag{2.136}$$

where in the latter case, the subscript p stands for partonic. In this section, the expectation value of an operator given by (2.136) denotes amputated Greens functions with operator insertion. In the partonic case this is evaluated using LSZ reduction formula or by computing Feynman diagrams. in the hadronic case as in (2.135) which will become relevant in later sections, this represents a non perturbative quantity and as such will be parameterised in terms of non perturbative quantities such as decay constants, form factors and bag factors computed using Lattice QCD (LQCD), Light Cone Sum Rules (LCSR), or QCD Factorization (QCDF) etc.

To illustrate this let us consider an example of the $\mathcal{O}(\alpha_s)$ corrections to tree level matrix elements of Q_1^c and Q_2^c shown already in subsection 2.5.1. Considering the Hamiltonian given in (2.123), the QCD corrections to the matrix elements of Q_1 and Q_2 are calculated by evaluating and summing up the 6 diagrams shown in figure 2.2.

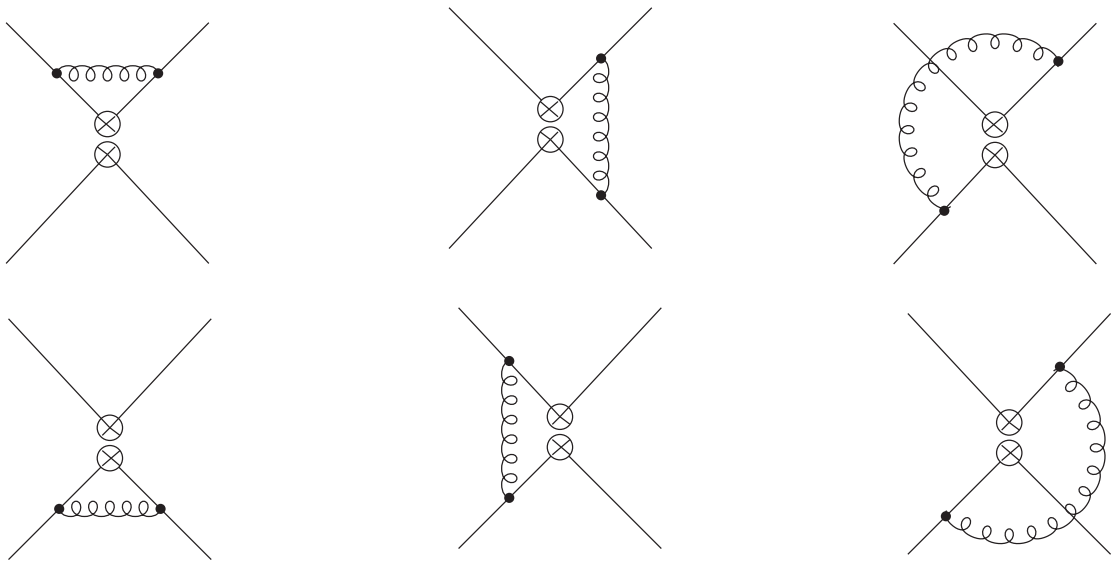

Figure 2.2: QCD corrections to effective $b \to c\bar{c}s$ operators. Circled crosses denote the current current operator structure.

That is

$$\mathcal{A}(b \to c\bar{c}s) = \frac{4G_F}{\sqrt{2}} V_{cb}V_{cs}^* \langle s\bar{c}c|(C_1(\mu)Q_1(\mu) + C_2(\mu)Q_2(\mu))|b\rangle + \mathcal{O}(\alpha_s^2). \quad (2.137)$$

The corresponding divergent amputated Green functions of (2.137) are then obtained, assuming all quarks have the same momenta p and setting all quark masses to zero, as

$$\begin{aligned}
\langle Q_1\rangle_p &= \langle Q_1\rangle_p^{\text{Tree}} + 2C_F\frac{\alpha_s}{4\pi}\left(\frac{1}{\epsilon} + \ln\left(\frac{\mu^2}{-p^2}\right)\right)\langle Q_1\rangle_p^{\text{Tree}} \\
&\quad - 3\frac{\alpha_s}{4\pi}\left(\frac{1}{\epsilon} + \ln\left(\frac{\mu^2}{-p^2}\right)\right)\langle Q_2\rangle_p^{\text{Tree}} + \frac{3}{N}\frac{\alpha_s}{4\pi}\left(\frac{1}{\epsilon} + \ln\left(\frac{\mu^2}{-p^2}\right)\right)\langle Q_1\rangle_p^{\text{Tree}} \\
&\quad + 4\frac{\alpha_s}{4\pi}\left(\frac{1}{\epsilon} + \ln\left(\frac{\mu^2}{-p^2}\right)\right)\left[\langle E_2^2\rangle_p^{\text{Tree}} - \langle E_1^1\rangle_p^{\text{Tree}}\right] \\
\langle Q_2\rangle_p &= \langle Q_2\rangle_p^{\text{Tree}} + 2C_F\frac{\alpha_s}{4\pi}\left(\frac{1}{\epsilon} + \ln\left(\frac{\mu^2}{-p^2}\right)\right)\langle Q_2\rangle_p^{\text{Tree}} \\
&\quad - 3\frac{\alpha_s}{4\pi}\left(\frac{1}{\epsilon} + \ln\left(\frac{\mu^2}{-p^2}\right)\right)\langle Q_1\rangle_p^{\text{Tree}} + \frac{3}{N}\frac{\alpha_s}{4\pi}\left(\frac{1}{\epsilon} + \ln\left(\frac{\mu^2}{-p^2}\right)\right)\langle Q_2\rangle_p^{\text{Tree}} \\
&\quad + \frac{\alpha_s}{4\pi}\left(\frac{1}{\epsilon} + \ln\left(\frac{\mu^2}{-p^2}\right)\right)\left[\langle E_1^1\rangle_p^{\text{Tree}} - 4\langle E_2^1\rangle_p^{\text{Tree}} + \frac{1}{N}(\langle E_2^2\rangle_p^{\text{Tree}} - 4\langle E_2^1\rangle_p^{\text{Tree}})\right]
\end{aligned} \quad (2.138)$$

The evanescent operators $E_{1(2)}^{1(2)}$ will only yield constant and finite contributions and are not relevant for finding the leading order anomalous dimension matrix. So dropping finite

and constant terms leaves

$$\langle Q_1\rangle_p = \left(1 + 2C_F\frac{\alpha_s}{4\pi}\left(\frac{1}{\epsilon} + \ln\left(\frac{\mu^2}{-p^2}\right)\right)\right)\langle Q_1\rangle_p^{\text{Tree}} - 3\frac{\alpha_s}{4\pi}\left(\frac{1}{\epsilon} + \ln\left(\frac{\mu^2}{-p^2}\right)\right)\langle Q_2\rangle_p^{\text{Tree}} + \frac{3}{N}\frac{\alpha_s}{4\pi}\left(\frac{1}{\epsilon} + \ln\left(\frac{\mu^2}{-p^2}\right)\right)\langle Q_1\rangle_p^{\text{Tree}} \tag{2.139}$$

$$\langle Q_2\rangle_p = \left(1 + 2C_F\frac{\alpha_s}{4\pi}\left(\frac{1}{\epsilon} + \ln\left(\frac{\mu^2}{-p^2}\right)\right)\right)\langle Q_2\rangle_p^{\text{Tree}} - 3\frac{\alpha_s}{4\pi}\left(\frac{1}{\epsilon} + \ln\left(\frac{\mu^2}{-p^2}\right)\right)\langle Q_1\rangle_p^{\text{Tree}} + \frac{3}{N}\frac{\alpha_s}{4\pi}\left(\frac{1}{\epsilon} + \ln\left(\frac{\mu^2}{-p^2}\right)\right)\langle Q_2\rangle_p^{\text{Tree}} \tag{2.140}$$

To renormalize the operators a similar procedure is performed as that for fields and parameters except for composite operators an extra renormalization must be performed. This is because at $\mathcal{O}(\alpha_s)$ the colour structure of the interactions generate linear combinations of operators Q_1 and Q_2 and so counter terms for both operators are required. This comes about by the QCD coupling to quarks involving an $SU_C(3)$ matrix which generates an extra colour structure. In analogy with (2.108) the relation between bare and renormalized operators is

$$Q_i^b = Z_{ij}Q_j \qquad\qquad i,j = 1,2 \tag{2.141}$$

and it is understood that the composite operator is comprised of bare quark fields. The corresponding relation for the amputated Greens functions is

$$\langle Q_i\rangle_p^b = Z_2^2 Z_{ij}\langle Q_j\rangle_p \qquad\qquad i,j = 1,2 \tag{2.142}$$

with Z_2 the quark field renormalization constant which in $\overline{MS}$ scheme is given by (2.113). Expressing then the amputated Green functions of (2.139) and (2.140) as prescribed in (2.142)

$$\langle Q_1\rangle_p^{(b)} = \left(1 + 2C_F\frac{\alpha_s}{4\pi}\ln\left(\frac{\mu^2}{-p^2}\right)\right)\langle Q_1\rangle_p^{\text{Tree}} - 3\frac{\alpha_s}{4\pi}\left(\frac{1}{\epsilon} + \ln\left(\frac{\mu^2}{-p^2}\right)\right)\langle Q_2\rangle_p^{\text{Tree}} + \frac{3}{N}\frac{\alpha_s}{4\pi}\left(\frac{1}{\epsilon} + \ln\left(\frac{\mu^2}{-p^2}\right)\right)\langle Q_1\rangle_p^{\text{Tree}}, \tag{2.143}$$

$$\langle Q_2\rangle_p^{(b)} = \left(1 + 2C_F\frac{\alpha_s}{4\pi}\ln\left(\frac{\mu^2}{-p^2}\right)\right)\langle Q_2\rangle_p^{\text{Tree}} - 3\frac{\alpha_s}{4\pi}\left(\frac{1}{\epsilon} + \ln\left(\frac{\mu^2}{-p^2}\right)\right)\langle Q_1\rangle_p^{\text{Tree}} + \frac{3}{N}\frac{\alpha_s}{4\pi}\left(\frac{1}{\epsilon} + \ln\left(\frac{\mu^2}{-p^2}\right)\right)\langle Q_2\rangle_p^{\text{Tree}}. \tag{2.144}$$

the quark field renormalization factor has removed the pole in the first term of (2.143) and (2.144) and we can read off the expression for the renormalization matrix in the $\overline{MS}$ scheme to be

$$Z = 1 + \frac{\alpha_s}{4\pi}\frac{1}{\epsilon}\begin{pmatrix} \frac{3}{N} & -3 \\ -3 & \frac{3}{N}\end{pmatrix}. \tag{2.145}$$

So that the renormalized amputated Green functions on the RHS of (2.142) are now finite in the limit as $\epsilon \to 0$ and are given to $\mathcal{O}(\alpha_s^2)$ by

$$\langle Q_1\rangle_p = \left(1 + 2C_F\frac{\alpha_s}{4\pi}\ln\left(\frac{\mu^2}{-p^2}\right)\right)\langle Q_1\rangle_p^{\text{Tree}} - 3\frac{\alpha_s}{4\pi}\ln\left(\frac{\mu^2}{-p^2}\right)\langle Q_2\rangle_p^{\text{Tree}} + \frac{3}{N}\frac{\alpha_s}{4\pi}\ln\left(\frac{\mu^2}{-p^2}\right)\langle Q_1\rangle_p^{\text{Tree}}, \tag{2.146}$$

$$\langle Q_2\rangle_p = \left(1 + 2C_F\frac{\alpha_s}{4\pi}\ln\left(\frac{\mu^2}{-p^2}\right)\right)\langle Q_2\rangle_p^{\text{Tree}} - 3\frac{\alpha_s}{4\pi}\ln\left(\frac{\mu^2}{-p^2}\right)\langle Q_1\rangle_p^{\text{Tree}} + \frac{3}{N}\frac{\alpha_s}{4\pi}\ln\left(\frac{\mu^2}{-p^2}\right)\langle Q_2\rangle_p^{\text{Tree}}. \tag{2.147}$$

Finally, the renormalized amplitude in the effective theory is given by

$$\mathcal{A}_{\text{eff}} = \frac{4G_F}{\sqrt{2}}V_{cb}V_{cs}^*\left[C_1(\mu)\left(d_1\langle Q_1\rangle_p^{\text{Tree}} + d_2\langle Q_2\rangle_p^{\text{Tree}}\right) + C_2(\mu)\left(d_1\langle Q_2\rangle_p^{\text{Tree}} + d_2\langle Q_1\rangle_p^{\text{Tree}}\right)\right] + \mathcal{O}(\alpha_s^2) \tag{2.148}$$

with the coefficients d_1, d_2

$$d_1 = 1 + 2C_F\frac{\alpha_s}{4\pi}\ln\left(\frac{\mu^2}{-p^2}\right) + \frac{3}{N}\frac{\alpha_s}{4\pi}\ln\left(\frac{\mu^2}{-p^2}\right), \tag{2.149}$$

$$d_2 = -3\frac{\alpha_s}{4\pi}\ln\left(\frac{\mu^2}{-p^2}\right). \tag{2.150}$$

We have calculated the QCD corrections to the matrix elements of the operators in the effective Hamiltonian (2.123) and obtained their renormalization matrix and subsequently know the renormalized amputated Green functions and renormalized amplitude in the effective theory at some scale μ. However, in order to calculate the Wilson coefficients

C_1 and C_2, one needs to compute the $\mathcal{O}(\alpha_s)$ corrections to $\mathcal{A}_{\text{full}}$ given in (2.120), and "match" this onto the result $\mathcal{A}_{\text{eff}}$ given in (2.148). We do not do this here, however it is detailed in [44]. The coefficients so obtained will contain μ dependent logarithms of the form $\alpha_s(\mu)\ln\left(\frac{M_W^2}{\mu^2}\right)$ which are only small, if the subtraction point is $\mu \approx M_W$. However the characteristic scale of the problem in $b \to c\bar{c}s$ transitions is $\mu \approx m_b$ and hence the natural scale at which to obtain results. In the next section we will introduce the application of renormalization group to improve the EFT outlined above, such that large logarithms are resummed by solving the renormalization group equations.

2.5.4 Renormalization group improvement of EFT

The renormalization group equation for the amputated Green functions is analogous to (2.119) shown in 2.4 and is obtained by the same principles. It is written as

$$\mu\frac{d}{d\mu}\langle Q(\mu)\rangle_{p,i} = -\gamma_{ij}\langle Q(\mu)\rangle_{p,j} \tag{2.151}$$

with the anomalous dimension matrix (ADM) given as an expansion in the strong coupling to be

$$\hat{\gamma} = \frac{\alpha_s}{4\pi}\hat{\gamma}^{(0)} + \mathcal{O}(\alpha_s^2). \tag{2.152}$$

Where our notational conventions are that where the symbol is shown with a 'hat' as in $\hat{\gamma}$, we are referring to a matrix, and where the symbol is given without the 'hat' but with indices as in γ_{ij}, we are referring to the component of $\hat{\gamma}$ with indices i, j. Having prior knowledge of the renormalization matrix of (2.145) leads to a simple way of obtaining the anomalous dimension. Since the coefficients of the $\frac{1}{\epsilon}$ poles in (2.139) and (2.140) are the same coefficients of the μ^2 dependent logarithms when using the dimensional regularization scheme, we obtain the anomalous dimension matrix by direct differentiation of the divergent parts of (2.143) and (2.144),with respect to μ. That is

$$\mu\frac{d}{d\mu}\begin{pmatrix}\langle Q_1\rangle_p^b\\ \langle Q_2\rangle_p^b\end{pmatrix} = \frac{\alpha_s}{4\pi}\begin{pmatrix}\frac{6}{N} & -6\\ -6 & \frac{6}{N}\end{pmatrix}\begin{pmatrix}\langle Q_1\rangle_p^{tree}\\ \langle Q_2\rangle_p^{tree}\end{pmatrix} + \mathcal{O}(\alpha_s^2) \tag{2.153}$$

by comparison with (2.151) then

$$\hat{\gamma}^{(0)} = \begin{pmatrix}-\frac{6}{N} & 6\\ 6 & -\frac{6}{N}\end{pmatrix}. \tag{2.154}$$

Due to the μ independence of the Hamiltonian, the RGE of (2.151) holds also for the Wilson coefficients. For later chapters, it will be instructive here to demonstrate in this relatively simple case how the solution to this differential equation will give the evolution of the coefficients with scale μ. At leading logarithmic order, the RGE for the Wilson coefficients is

$$\mu\frac{d}{d\mu}\vec{C}(\mu) = \frac{\alpha_s}{4\pi}(\hat{\gamma}^{(0)})^T\vec{C}(\mu). \tag{2.155}$$

and the initial conditions are the Wilson coefficients renormalized at the scale μ_0, obtained by the matching the full theory on to the effective theory at $\mathcal{O}(\alpha_s)$. We solve (2.155) by transforming to a basis in which the ADM is diagonal. The coefficients in the new basis are

$$C_+(\mu) = \frac{1}{\sqrt{2}}(C_1(\mu) + C_2(\mu)), \qquad C_-(\mu) = \frac{1}{\sqrt{2}}(C_1(\mu) - C_2(\mu)), \tag{2.156}$$

so that in this basis the RGE becomes

$$\mu\frac{d}{d\mu}C_\pm(\mu) = \frac{\alpha_s}{4\pi}\lambda_\pm C_\pm(\mu), \tag{2.157}$$

with the eigenvalues of (2.154) given by $\lambda_\pm = -6(\frac{1}{N} \pm 1)$. Solving (2.157) is straight forward, using the relation between the strong coupling and the QCD beta function

$$\mu\frac{d}{d\mu} = \mu\frac{d}{d\alpha_s}\frac{d\alpha_s}{d\mu} = \beta(\alpha_s)\frac{d}{d\alpha_s} = -2\beta^{(0)}\frac{\alpha_s^2}{4\pi}\frac{d}{d\alpha_s} + \mathcal{O}(\alpha_s^3), \tag{2.158}$$

we may write

$$\int_{C_\pm(\mu_0)}^{C_\pm(\mu)} \frac{dC'_\pm(\mu')}{C'_\pm(\mu')} = -\frac{\lambda_\pm}{2\beta_0}\int_{\alpha(\mu_0)}^{\alpha(\mu)} \frac{d\alpha'(\mu')}{\alpha'(\mu')} \tag{2.159}$$

and upon integration and exponentiation obtain the solution

$$C_\pm(\mu) = \left(\frac{\alpha(\mu_0)}{\alpha(\mu)}\right)^{\frac{\lambda_\pm}{2\beta_0}} C_\pm(\mu_0). \tag{2.160}$$

Transforming back to the original basis gives the leading logarithmic relation between the coefficients at scale μ in terms of the coefficients at the scale μ_0

$$\begin{pmatrix} C_1(\mu) \\ C_2(\mu) \end{pmatrix} = \frac{1}{2}\begin{pmatrix} \eta^+ + \eta^- & \eta^+ - \eta^- \\ \eta^+ - \eta^- & \eta^+ + \eta^- \end{pmatrix}\begin{pmatrix} C_1(\mu_0) \\ C_2(\mu_0) \end{pmatrix}, \tag{2.161}$$

where

$$\eta^{\pm} = \left(\frac{\alpha(\mu_0)}{\alpha(\mu)}\right)^{\frac{\lambda_{\pm}}{2\beta_0}}. \tag{2.162}$$

This result enables the accurate calculation of Wilson coefficients at a scale μ in terms of the coefficients of operators renormalized at scale μ_0. The Wilson coefficients $C_i(\mu_0)$ contain no large logarithms.

2.6 Heavy Quark Effective Theory

Here we briefly describe the Heavy Quark Effective Theory (HQET) [56, 57, 58] and state some results and make some definitions required for later chapters. Where known results are stated we refer to the development in [59]. In Heavy Quark Effective Theory one considers a single heavy quark inside a hadron which moves with a velocity comparable to that of the hadron and interacts softly with light degrees of freedom inside the hadron. The momentum of an on shell heavy quark is $p = m_Q v$ and the momentum of an off shell heavy quark is $p = m_Q v + k$ where k is the residual momentum, which determines the amount by which the quark is "off shell" due to interaction. v^μ is a four velocity and $v^2 = 1$. It is convenient to define a heavy quark field as

$$Q(x) = e^{-im_Q v\cdot x}\left[h_v(x) + H_v(x)\right] \tag{2.163}$$

where the new fields are

$$h_v(x) = e^{im_Q v\cdot x}P^+Q(x) \qquad\qquad H_v(x) = e^{im_Q v\cdot x}P^-Q(x), \tag{2.164}$$

and with the velocity dependent projectors defined as

$$P^{\pm} = \frac{\mathbb{1} \pm \not{v}}{2}. \tag{2.165}$$

The following relations hold due to the projectors

$$\not{v}h_v(x) = h_v(x), \qquad\qquad \not{v}H_v(x) = -H_v(x). \tag{2.166}$$

The HQET is obtained from the QCD Lagrangian by substitution of (2.163) in to the part of the Lagrangian for the heavy quark

$$\mathcal{L}_{\text{eff}} = \bar{Q}(x)(i\not{D} - m_Q)Q(x) \tag{2.167}$$

$$\begin{aligned}\mathcal{L}_{\text{eff}} &= (e^{im_Q v\cdot x}(\bar{h}_v(x)+\bar{H}_v(x)))(i\not{D}-m_Q)(e^{-im_Q v\cdot x}(h_v(x)+H_v(x))) \\ &= \bar{h}_v(x)(m_Q\not{v}+i\not{D})h_v(x)+\bar{h}_v(x)(m_Q\not{v}+i\not{D})H_v(x)+ \\ &\quad +\bar{H}_v(x)(m_Q\not{v}+i\not{D})h_v(x)+\bar{H}_v(x)(m_Q\not{v}+i\not{D})H_v(x) \\ &\quad -m_Q(\bar{h}(x)_v h_v(x)+\bar{H}(x)_v h_v(x)+\bar{h}(x)_v H_v(x)+\bar{H}(x)_v H_v(x)) \end{aligned} \tag{2.168}$$

using (2.166) we find the mass terms for the h_v field cancel and acting with P^+ and P^- either side of the derivatives in the terms only involving $h_v(x)$ and $H_v(x)$ respectively, gives

$$\begin{aligned}\mathcal{L}_{\text{eff}} &= \bar{h}_v(x)(iv\cdot D)h_v(x)-\bar{H}_v(x)(iv\cdot D+2m_Q)H_v(x)+\bar{h}_v(x)i\not{D}H_v(x) \\ &\quad +\bar{H}_v(x)i\not{D}h_v(x). \end{aligned} \tag{2.169}$$

Already we can see from (2.169) that H_v appears to have a mass term with a mass parameter of twice the heavy quark mass, and the field h_v does not have such a term. To remove the field H_v from the Lagrangian at tree level we solve the equations of motion. These are derived in a similar manner as the Lagrangian. Given

$$(i\not{D}-m_Q)Q(x)=0 \tag{2.170}$$

we find, substituting (2.163) into (2.170) and acting with the covariant derivatives on the exponential factors gives

$$[(i\not{D}+m_Q\not{v})h_v(x)+(i\not{D}+m_Q\not{v})H_v(x)-m_Q(h_v(x)+H_v(x))]=0 \tag{2.171}$$

and application of (2.166) leads to

$$i\not{D}h_v(x)+(i\not{D}-2m_Q)H_v(x)=0. \tag{2.172}$$

To further reduce this we act from the left with the projector P^- of (2.165) and commute the $\not{v}$ terms with the covariant derivatives where

$$\not{v}\not{D}=2v\cdot D-\not{D}\not{v} \tag{2.173}$$

It is also convenient to project four vectors onto components parallel and perpendicular to the heavy quark velocity v. The we define the perpendicular component of any four

vector x to be

$$x_\perp^\mu = x^\mu - x \cdot v v^\mu \tag{2.174}$$

then (2.172) becomes

$$\begin{aligned}
&\frac{1}{2}(1-\not{v})\left(i\not{D}h_v(x) + (i\not{D} - 2m_Q)H_v(x)\right) = \\
&\frac{1}{2}\left((i\not{D}h_v(x) + (i\not{D} - 2m_Q)H_v(x)) - \left(i(2v\cdot D - \not{D}\not{v})(h_v(x) + H_v(x)) + 2m_Q\not{v})H_v(x)\right)\right) \\
&= i\not{D}_\perp h_v(x) - (iv\cdot D + 2m_Q)H_v(x).
\end{aligned} \tag{2.175}$$

$$\Rightarrow H_v(x) = \frac{i\not{D}_\perp}{(iv\cdot D + 2m_Q)} h_v(x) \tag{2.176}$$

This demonstrates that the effects of the $H_v(x)$ field are $\mathcal{O}(\frac{1}{m_Q})$ suppressed relative to $h_v(x)$. Now, let us substitute (2.176) into (2.163) to give

$$\mathcal{L}_{\text{eff}} = \bar{h}_v(x)\left((iv\cdot D) + i\not{D}_\perp \frac{1}{(iv\cdot D + 2m_Q)}\not{D}_\perp\right) h_v(x) \tag{2.177}$$

because the derivatives acting on the field h_v bring down powers of the residual momentum which by definition is $\mathcal{O}(\lambda_{QCD}) \ll m_Q$ we may express the inverse operator $(iv\cdot D + 2m_Q)^{-1}$ as a derivative expansion as

$$\frac{1}{(iv\cdot D + 2m_Q)} = \frac{1}{2m_Q}\sum_{k=0}^{\infty}\left(\frac{-iv\cdot D}{2m_Q}\right)^k, \tag{2.178}$$

further using the fact that $P^+ h_v(x) = h)v(x)$ we use the identity

$$P_+ i\not{D}_\perp i\not{D}_\perp P^+ = P^+\left[(i\not{D}_\perp)^2 + \frac{g_s}{2}\sigma_{\mu\nu}G^{\mu\nu}\right]P^+ \tag{2.179}$$

to give the HQET Lagrangian is to $\mathcal{O}\left(\frac{1}{m_Q^2}\right)$as

$$\mathcal{L}_{\text{eff}} = \bar{h}_v(x)(iv\cdot D)h_v(x) - \bar{h}_v(x)\frac{(\not{D}_\perp)^2}{2m_Q}h_v(x) - \bar{h}_v(x)\frac{g_s}{4m_Q}\sigma_{\mu\nu}G^{\mu\nu}h_v(x). \tag{2.180}$$

In the heavy quark limit $m_Q \to \infty$

$$\mathcal{L}_{\text{eff}}\,|_{m_b\to\infty} = \bar{h}_v(iv\cdot D)h_v(x). \tag{2.181}$$

2.7 Heavy Quark Expansion

2.7.1 An expansion in inverse powers of the heavy quark mass

The Heavy Quark Expansion (HQE) was introduced in [60], [61], [62], [63]. Here we will follow the reviews [64] ,[65] and [66]. To begin a quark is considered heavy if its mass term in the QCD Lagrangian has $m_Q \gg \Lambda_{QCD}$.The hadron itself, denoted H_Q is comprised of a heavy quark Q and a light anti quark $\bar{q}$ and a cloud of quarks and gluons which acts to keep all the constituent parts together in a colourless bound state. In order to introduce the HQE it is taken as understood that the light constituents of the hadron have soft momenta of $\mathcal{O}(\Lambda_{QCD})$. The heavy quark is treated as a non relativistic object submerged in a soft gluon background field.

The HQE is an extension of the OPE and as such we begin with the transition operator which is the imaginary part of the bi-local product of the weak effective Hamiltonian $\mathcal{H}_W$

$$\mathcal{T}(Q \to F \to Q) = \mathrm{Im}\left\{ i \int d^4x T[\mathcal{H}_W(x)\mathcal{H}_W(0)] \right\}. \tag{2.182}$$

If the energy released in the decay $H_Q \to F$ is sufficiently large, $\mathcal{T}$ may be expressed as an infinite sum of local operators of increasing dimension, suppressed by inverse powers of the heavy quark mass

$$\begin{aligned}\mathcal{T} &= G_F^2 m_Q^5 |\hat{V}_{CKM}|^2 \sum_j \frac{c_j^f(\mu)}{m_Q^{d_j-3}} \mathcal{O}_j \\ &= G_F^2 m_Q^5 |\hat{V}_{CKM}|^2 \left(c_3^{(f)}(\mu)\bar{Q}Q + \frac{c_5^{(f)}(\mu)}{m_Q^2}\bar{Q}\frac{1}{2}\sigma \cdot GQ + \frac{c_6^{(f)}(\mu)}{m_Q^3}\mathcal{O}_6 \right. \\ &\qquad \left. + \frac{c_7^{(f)}(\mu)}{m_Q^4}\mathcal{O}_7 + \mathcal{O}\left(\frac{1}{m_Q^5}\right)\right)\end{aligned} \tag{2.183}$$

where $\hat{V}_{CKM}$ schematically represents the relevant CKM matrix elements, d_j is the dimension of the operator $\mathcal{O}_j$ and μ is the renormalization scale. There is no $\frac{1}{m_Q}$ term. The operators of dimension $d = 6, 7$ depend upon the spectator quark and are different depending upon terms arising in the bi-local product of Hamiltonians on the left hand side. For semi-leptonic and non leptonic decays, the HQE predicts that the the total inclusive rate for the decay of a heavy hadron to final state f is given by

$$\Gamma = \frac{G_F^2 m_Q^5}{192\pi^3}|\hat{V}_{CKM}|^2 \left[c_3^f(\mu)\frac{\langle H_Q|\bar{Q}Q|H_Q\rangle(\mu)}{2M_{H_Q}} + \frac{c_5^f(\mu)}{m_Q^2}\frac{\langle H_Q|\bar{Q}\frac{1}{2}\sigma \cdot GQ|H_Q\rangle(\mu)}{2M_{H_Q}} + \right.$$

$$\sum_j \frac{c^f_{6,j}(\mu)}{m_Q^3}\frac{\langle H_Q|\mathcal{O}^{(6)}_j|H_Q\rangle(\mu)}{2M_{H_Q}} + \sum_j \frac{c^f_{7,j}(\mu)}{m_Q^4}\frac{\langle H_Q|\mathcal{O}^{(7)}_j|H_Q\rangle(\mu)}{2M_{H_Q}} + \mathcal{O}\left(\frac{1}{m_Q^5}\right)\Bigg] \quad . \tag{2.184}$$

2.7.2 Individual terms in the HQE

The individual terms require some explanation. The first term is universal to all Q flavoured Hadron decay and is associated with the decay of a free quark. In HQET

$$\langle H_Q|\bar{Q}Q|H_Q\rangle = 1 - \frac{\mu_\pi(H_Q)^2 - \mu_G(H_Q)^2}{2m_Q^2} + \mathcal{O}\left(\frac{1}{m_q^3}\right) \tag{2.185}$$

The two contributions are the matrix element of the kinetic operator μ_π^2 and the matrix element of the chromomagnetic operator μ_G^2 and are defined in the rest frame of the heavy hadron H_Q to be

$$\mu_\pi^2(H_Q) = \frac{1}{2M_{H_Q}}\langle H_Q|\bar{Q}(i\vec{D})^2Q|H_Q\rangle, \tag{2.186}$$

$$\mu_G^2(H_Q) = \frac{1}{2M_{H_Q}}\langle H_Q|\bar{Q}\frac{g_s}{2}\sigma_{\mu\nu}G^{\mu\nu}Q|H_Q\rangle. \tag{2.187}$$

Here $(i\vec{D})^2 = (iv\cdot D)^2 - (iD)^2$. The kinetic part is analogous to the Lorenz factor because the lifetime for a particle in motion will increase due to time dilation. The chromomagnetic part is due describes the colour magnetic interaction of the heavy quark inside the hadron, with the gluon field. The second term is again associated with the chromomagnetic operator and arises from a two loop diagram involving the emission of a gluon from an internal quark like, it results in the chromomagnetic operator which again, due to its dimension, is suppressed by two powers of the heavy quark mass.
The third term contains dimension $d = 6$ operators of the form

$$\mathcal{O}^{(6)}_j = (\bar{Q}\Gamma_j q)(\bar{q}\Gamma_j Q) \tag{2.188}$$

where Γ_j denotes generic Dirac and chiral structure. This term is associated with a one-loop diagram which called a weak annihilation diagram (for example the annihilation $bs \to c\bar{c}$ in the case of $H_Q = B_s^{(0)}$ [67]) and this is the first term in the HQE that is sensitive to the flavour of the spectator quark. The fourth term is associated with dimension $d =$

7 operators which are comprised either of dimension 6 operators such as those above multiplied by a power of the spectator quark mass or contain additional derivatives.

Chapter 3

Beyond the standard model in $b \to c\bar{c}s$ transitions

Chapters 1-2 have focused upon known results, and now in this chapter we begin our presentation of novel research as detailed in[1, 2]. To begin, we motivate our novel study of BSM in $b \to \bar{c}cs$ transitions in section 3.1 and give definitions of the weak Hamiltonian and operator basis constructed to perform the investigation in 3.2.

3.1 Why study new physics in $b \to c\bar{c}s$

The quark level $b \to c\bar{c}s$ transition contributes to a range of both CP conserving and CP violating processes providing a number of different ways to theoretically test for signs of physics beyond the standard model (BSM). One set of processes which have received a lot of attention in recent years are the rare semi-leptonic decays triggered by the $b \to s\bar{\ell}\ell$ transition. Anomalies exist in between theory and experiment in observables associated with these decays [4, 5, 6, 7, 8, 9, 10, 11, 12, 13, 14, 15, 16, 17, 18, 19, 20], and have been the cause of much excitement due to their potential to be explained by the presence of new degrees of freedom.

In contrast, $b \to c\bar{c}s$ transitions also affect $B_s^{(0)} - \bar{B}_s^{(0)}$ mixing for which theoretical predictions of observables such as $\Delta\Gamma_s$ are currently in perfect agreement with experiment [68]. Another observable which provides a precise theoretical prediction in good agreement with experiment is the branching ratio for the total inclusive $\bar{B} \to X_s\gamma$ decay [69]. The purpose of this research is to determine effects produced by a complete set of dimension 6 four quark operators in a full compliment of processes to which they contribute in

order to both offer possible explanations for anomalies, and to obtain phenomenological constraints upon the couplings that accompany them in the effective Hamiltonian.
More precisely, we construct the most general set of $\Delta B = 1$ dimension 6 effective operators which are allowed by the symmetries of the theory, and which mimic the $b \to c\bar{c}s$ transition in the effective theory, and add this to the SM weak effective Hamiltonian. These operators differ from those of the SM by their Dirac and chiral structure, and thus are used to calculate BSM contributions to observables associated with the following processes, which proceed at loop level: Rare semi leptonic decay through $b \to s\mu^+\mu^-$ transitions, Radiative decay through $b \to s\gamma$ transitions, $B_s^{(0)} - \bar{B}_s^{(0)}$ mixing and $B_s^{(0)}$ lifetimes. In addition we consider the $B_d^0 \to J/\psi K_S$ hadronic decay through tree level $b \to c\bar{c}s$ transitions. Signs of new physics appear in three forms in our explorative study: i) as shifts to SM Wilson coefficients C_1^c and C_2^c, ii) in the form of non zero BSM Wilson coefficients which accompany our new operators in the extended weak Hamiltonian, and iii) as complex parts of SM Wilson coefficients. In what follows, we define the weak Hamiltonian constructed of the SM and BSM $b \to c\bar{c}s$ operators as detailed above, and their corresponding Wilson coefficients in terms of their SM and BSM parts, and together call this the 'Charming Beyond the Standard Model' (CBSM) scenario as presented in works [1] and [2].

3.2 Weak Hamiltonian and operator Basis

In what follows we use from the unitarity relation of the CKM matrix (2.55)

$$\frac{V_{cb}V_{cs}^*}{V_{tb}V_{ts}^*} + \frac{V_{ub}V_{us}^*}{V_{tb}V_{ts}^*} = -1, \tag{3.1}$$

and neglect the small ratio

$$\frac{V_{ub}V_{us}^*}{V_{tb}V_{ts}^*} \approx \mathcal{O}(10^{-3}), \tag{3.2}$$

so that in the following definitions we have worked with the approximation that

$$\frac{V_{cb}V_{cs}^*}{V_{tb}V_{ts}^*} \approx -1. \tag{3.3}$$

In the CP conserving case, the observable which would be affected by neglecting the small ratio (3.2) is the flavour specific CP asymmetry a^s_{fs}, which currently has an experimental value of roughly ~ 130 times that of the SM central value, so that the above approximation yields reasonable results. In the CP violating case, we find that the BSM complex Wilson coefficients can take values much larger than the error we make in neglecting this quantity, so that the impact of doing so does not appreciably affect our results.

We define the weak effective Hamiltonian governing $b \to c\bar{c}s$ transitions as

$$\mathcal{H}^{c\bar{c}}_{\text{eff}} = \frac{4G_F}{\sqrt{2}}\left[V_{cb}V^*_{cs}\sum_{\ell=1}^{10}(C^c_\ell(\mu)Q^c_\ell(\mu) + C'^c_\ell(\mu)Q'^c_\ell(\mu))\right] + \text{h.c}, \tag{3.4}$$

The full basis of dimension $d = 6$ four quark operators is given by [1]

$$\begin{aligned}
Q^c_1 &= (\bar{c}^i_L\gamma_\mu b^j_L)(\bar{s}^j_L\gamma^\mu c^i_L), & Q^c_2 &= (\bar{c}^i_L\gamma_\mu b^i_L)(\bar{s}^j_L\gamma^\mu c^j_L),\\
Q^c_3 &= (\bar{c}^i_R b^j_L)(\bar{s}^j_L c^i_R), & Q^c_4 &= (\bar{c}^i_R b^i_L)(\bar{s}^j_L c^j_R),\\
Q^c_5 &= (\bar{c}^i_R\gamma_\mu b^j_R)(\bar{s}^j_L\gamma^\mu c^i_L), & Q^c_6 &= (\bar{c}^i_R\gamma_\mu b^i_R)(\bar{s}^j_L\gamma^\mu c^j_L),\\
Q^c_7 &= (\bar{c}^i_L b^j_R)(\bar{s}^j_L c^i_R), & Q^c_8 &= (\bar{c}^i_L b^i_R)(\bar{s}^j_L c^j_R),\\
Q^c_9 &= (\bar{c}^i_L\sigma_{\mu\nu} b^j_R)(\bar{s}^j_L\sigma^{\mu\nu} c^i_R), & Q^c_{10} &= (\bar{c}^i_L\sigma_{\mu\nu} b^i_R)(\bar{s}^j_L\sigma^{\mu\nu} c^j_R),
\end{aligned}$$

and there are a further 10 primed four fermion operators can be obtained by letting $P_{L/R} \to P_{R/L}$ in the above expressions, where we define the left and right projection operators as $P_{L(R)} = \frac{(1\mp\gamma^5)}{2}$. The roman indices $i, j = 1..3$ are colour indices. To describe the rare and radiative decay processes we will need to introduce the weak Hamiltonian triggering the $b \to s\bar{\ell}\ell$ and $b \to s\gamma$ transitions as

$$\begin{aligned}
\mathcal{H}^{rsl}_{\text{eff}} = \frac{4G_F}{\sqrt{2}}\,[&V_{cb}V^*_{cs}(C_{7\gamma}(\mu)Q_{7\gamma}(\mu) + C_{9V}(\mu)Q_{9V}(\mu)\\
&+C'_{7\gamma}(\mu)Q'_{7\gamma}(\mu) + C'_{9V}(\mu)Q'_{9V}(\mu))\big] + \text{h.c.}
\end{aligned} \tag{3.5}$$

The electromagnetic dipole and semileptonic operators, along with their chirality conjugates are given by

$$\begin{aligned}
Q_{7\gamma} &= \frac{em_b}{16\pi^2}(\bar{s}_L\sigma_{\mu\nu}b_R)F^{\mu\nu}, & Q_{9V} &= \frac{\alpha}{4\pi}(\bar{s}_L\gamma_\mu b_L)(\bar{\mu}\gamma^\mu\mu)\\
Q'_{7\gamma} &= \frac{em_b}{16\pi^2}(\bar{s}_R\sigma_{\mu\nu}b_L)F^{\mu\nu}, & Q'_{9V} &= \frac{\alpha}{4\pi}(\bar{s}_R\gamma_\mu b_R)(\bar{\mu}\gamma^\mu\mu).
\end{aligned}$$

Where m_b is the b-quark mass, e is the electromagnetic coupling, and $\alpha = \frac{e^2}{4\pi}$.

To calculate the ADM and subsequent mixing of the CBSM operators and their mixing with the dipole and semileptonic operators one should also include the section of the SM Effective Hamiltonian which contains the QCD penguin operators and the chromomagnetic dipole operator.

$$\mathcal{H}_{\text{eff}}^{qcd} = \frac{4G_F}{\sqrt{2}}\Bigg[V_{cb}V_{cs}^*\sum_{\ell=3}^{6}(C_\ell^p(\mu)Q_\ell^p(\mu) + C_\ell^{\prime p}(\mu)Q_\ell^{\prime p}(\mu)) + C_{8g}(\mu)Q_{8g}(\mu) + C'_{8g}(\mu)Q'_{8g}(\mu)\Big] + \text{h.c} \tag{3.6}$$

The basis of QCD penguin operators is taken from [70]

$$Q_3^p = (\bar{s}_L\gamma_\mu b_L)\sum_q(\bar{q}\gamma^\mu q) \tag{3.7}$$

$$Q_4^p = (\bar{s}_L\gamma_\mu T^a b_L)\sum_q(\bar{q}\gamma^\mu T^a q) \tag{3.8}$$

$$Q_5^p = (\bar{s}_L\gamma_\nu\gamma_\mu\gamma_\rho b_L)\sum_q(\bar{q}\gamma^\nu\gamma^\mu\gamma^\rho q) \tag{3.9}$$

$$Q_6^p = (\bar{s}_L\gamma_\nu\gamma_\mu\gamma_\rho T^a b_L)\sum_q(\bar{q}\gamma^\nu\gamma^\mu\gamma^\rho T^a q) \tag{3.10}$$

where q runs over all active quark flavours in the effective theory. Again, the primed operators corresponding to the above set are obtained by letting $\psi_{L(R)} \rightarrow \psi_{R(L)}$ for $\psi \in \{s, c, b\}$.

In addition to the dipole and semileptonic operators, in order to obtain the correct evolution for the $b \rightarrow c\bar{c}s$ basis, we also need to include the chromomagnetic dipole operator given by

$$Q_{8g} = \frac{g_s}{16\pi^2}(\bar{s}\sigma^{\mu\nu}T^a P_R b)G^a_{\mu\nu}. \tag{3.11}$$

Further, to isolate the BSM contribution we define the Wilson coefficients for the charmed four quark operators to be split into SM parts and NP parts which are expressed as

$$C_\ell^c(\mu) = \begin{cases} C_\ell^{SM}(\mu) + \Delta C_\ell(\mu), & \ell = 1, 2 \\ \Delta C_\ell(\mu), & \ell = 3, .., 10 \end{cases}$$
$$C_\ell^{c\prime}(\mu) = \Delta C'_\ell(\mu) \qquad \ell = 1, ..., 10 \qquad . \tag{3.12}$$

As will be described next, RG evolution then generates BSM contributions to the penguin and dipole operators, which play a crucial role in the phenomenology of the CBSM scenario. The CBSM scenario should be viewed as a partial effective description of a more complete UV scenario, which will in general also involve nonzero initial values for the other ΔC_ℓ.

Chapter 4

Renormalization group improvement of CBSM

In Chapter 1 the notion of renormalization in QFT, and further in EFT was introduced and in Section 2.4 it was explained how renormalization group can be used to sum up large logarithms appearing in the perturbative expansion. The RGE for operator matrix elements and for their Wilson coefficients was introduced in 2.5 for the simple case of QCD corrections to the effective amplitude involving SM operators Q_1^c and Q_2^c. Here we now wish to present our novel extension to this known result, by considering the special and somewhat more complicated case of the renormalization group evolution for full CBSM operator basis.

The chapter is laid out as follows: In section 4.1 the renormalization group equation in terms of the full set of Wilson coefficients used in this study and the full anomalous dimension matrix governing their respective change of scale is given. In section 4.2 a derivation of the solution to the RGE is outlined and we present two individual cases in which we solve the RGE and subsequently obtain the evolved $b \to c\bar{c}s$ coefficients. Finally in section 4.3 the full evolution matrix is given.

4.1 Renormalization group equation

4.1.1 Effective coefficients

To obtain the renormalization group evolution for the full basis of operators we will be using the Hamiltonian

$$\mathcal{H}_{\text{eff}} = \mathcal{H}_{\text{eff}}^{c\bar{c}} + \mathcal{H}_{\text{eff}}^{\text{qcd}} + \mathcal{H}_{\text{eff}}^{\text{r,sl}}, \tag{4.1}$$

where the $\mathcal{H}_{\rm eff}^{c\bar{c}}$, $\mathcal{H}_{\rm eff}^{\rm qcd}$ and $\mathcal{H}_{\rm eff}^{\rm r,sl}$ and the operator basis are defined in chapter 3. Instead of using the coefficients for the electromagnetic and chromomagnetic dipole operators it is convenient and conventional to use certain linear combinations of them which are termed "effective coefficients". We extend the formalism of [71] and [70] and express the coefficients of the electromagnetic and chromomagnetic dipole operators in terms of a linear combination of the QCD penguin coefficients and our CBSM coefficients. In the SM, only the penguin coefficients and the C_1, C_2 SM coefficients contribute, however here we present a novel result which necessarily includes all contributing Wilson coefficients contained in (4.1). Let us define the effective coefficients as

$$C_{7\gamma}^{\rm eff}(\mu) = C_{7\gamma}(\mu) + \vec{y}\cdot\vec{C}(\mu), \tag{4.2}$$

$$C_{8g}^{\rm eff}(\mu) = C_{8g}(\mu) + \vec{z}\cdot\vec{C}(\mu). \tag{4.3}$$

here $\vec{C}(\mu) = (\vec{C}^c(\mu), \vec{C}^p(\mu))$ is a column vector with components

$$\vec{C}^c(\mu) = (C_1^c(\mu), C_2^c(\mu), ..., C_{10}^c(\mu)), \tag{4.4}$$

$$\vec{C}^p(\mu) = (C_3^p(\mu), C_4^p(\mu), ..., C_6^p(\mu)), \tag{4.5}$$

with the coefficients $C_i^c(\mu)$ as defined in (3.12). The vectors $\vec{z}$ and $\vec{y}$ are

$$\vec{y} = \left(0,0,0,0,\frac{2N}{3}x_c,\frac{2}{3}x_c,0,0,0,0,-\frac{1}{3},-\frac{4}{9},-\frac{20}{3},-\frac{80}{9}\right), \tag{4.6}$$

$$\vec{z} = \left(0,0,0,0,0,x_c,0,0,0,0,1,-\frac{1}{6},20,-\frac{10}{3}\right), \tag{4.7}$$

where N is the number of colours and $x_c = \frac{m_c}{m_b}$. The first two and the final four components of equations (4.6) and (4.7) are known SM results which are taken from [70] [1], and the components y_i, z_i for $i = 3...10$ are novel results calculated for the first time here [2]. There are a further six equations which correspond to the primed parity conjugate operators defined in chapter 3 which take the same structural form and can be obtained from those above by simply adding a prime in superscript. This is due to the Q_i^c and their chirality flipped counterparts $Q_i^{c\prime}$ not mixing under renormalization.

The need to express the magnetic dipole coefficients in this way arises due to a regularization scheme dependence which is particular to $b \to s\gamma$ decay. In Naive Dimensional Regularization (NDR) scheme, which is dimensional regularization with fully anti-

[1] Note that the authors use a different basis for the four fermion operators however the result is the same in our basis.

commuting γ^5, when computing the 1 loop matrix elements of the four quark operators in $b \to s\gamma$ decay it is found that there are terms arising which are finite in the limit $\epsilon \to 0$. It was found in [71] that such terms are zero when doing the same calculations in the 't Hooft-Veltman (HV) scheme. In the SM these terms arise in the calculation of matrix elements of penguin operators. In the CBSM scenario extra terms arise which are associated with the 1 loop matrix elements of $Q^c_{5,6}$. The matrix element of $\mathcal{H}_{\rm eff}$ between the appropriate initial and final states at order $\alpha_s^{(0)}$ is

$$\langle s\gamma|\mathcal{H}_{\rm eff}|b\rangle = C_{7\gamma}(\mu)\langle s\gamma|Q_{7\gamma}(\mu)|b\rangle^{tree} + \sum_{i=1}^{14} C_i^a(\mu)\langle s\gamma|Q_i^a(\mu)|b\rangle^{1-loop} \tag{4.8}$$

when (4.8) is renormalized, there will remain some finite terms which are scheme dependent. We then express (4.8) as

$$\langle s\gamma|\mathcal{H}_{\rm eff}|b\rangle = C_7^{\rm eff}(\mu)\langle s\gamma|Q_{7\gamma}(\mu)|b\rangle^{tree} \tag{4.9}$$

with $C_{7\gamma}^{\rm eff}(\mu)$ as defined in (4.2). This corresponds to a finite renormalization of the operators such that the renormalized operators are the same in either NDR or HV scheme. There are analogous expressions in terms of Q_{8g}

$$\langle sg|\mathcal{H}_{\rm eff}|b\rangle = C_{8g}(\mu)\langle sg|Q_{8g}(\mu)|b\rangle^{tree} + \sum_{i=1}^{14} C_i^a(\mu)\langle sg|Q_i^a(\mu)|b\rangle^{1-loop} \tag{4.10}$$

$$\langle sg|\mathcal{H}_{\rm eff}|b\rangle = C_{8g}^{\rm eff}(\mu)\langle sg|Q_{8g}(\mu)|b\rangle^{tree}. \tag{4.11}$$

4.1.2 RGE for the effective coefficients

The evolution of the effective coefficients is governed by their renormalization group equation

$$\mu\frac{d}{d\mu}C_i^{\rm eff}(\mu) = \gamma_{ji}^{\rm eff}(\mu)C_j^{\rm eff}(\mu), \tag{4.12}$$

where $\hat{\gamma}^{\rm eff}$ is a 17×17 matrix, and the 17×1 column vector upon which it acts is

$$\vec{C}^{\rm eff}(\mu) = (\vec{C}^c(\mu), \vec{C}^p(\mu), C_{7\gamma}^{\rm eff}(\mu), C_{8g}^{\rm eff}(\mu), C_{9V}(\mu)), \tag{4.13}$$

and the 10×1 and 4×1 vectors $\vec{C}^c(\mu)$ and $\vec{C}^p(\mu)$, corresponding to the CBSM coefficients and the penguin coefficients respectively are defined in (4.4) and (4.5). The relation between the effective ADM and the ADM governing the evolution of the non effective

coefficients is extended beyond that given in [70], such that the terms involving components y_i, z_i now contain novel results [2]

$$\gamma_{ji}^{(0)\text{eff}} = \gamma_{j7\gamma}^{(0)} + \sum_{k=1}^{14} y_k \gamma_{jk}^{(0)} - \gamma_{7\gamma 7\gamma}^{(0)} y_j - \gamma_{8g7\gamma}^{(0)} z_j \qquad i = 7\gamma, j = 1, ..., 14 \tag{4.14}$$

$$\gamma_{ji}^{(0)\text{eff}} = \gamma_{j8g}^{(0)} + \sum_{k=1}^{14} z_k \gamma_{jk}^{(0)} - \gamma_{8g8g}^{(0)} z_j \qquad i = 8g, j = 1, ..., 14 \tag{4.15}$$

$$\gamma_{ji}^{(0)\text{eff}} = \gamma_{ji}^{(0)} \qquad \text{otherwise} \tag{4.16}$$

The effective ADM and in addition the QCD beta function both have a perturbative expansion in $\alpha_s(\mu)$

$$\hat{\gamma}^{\text{eff}}(\mu) = \frac{\alpha_s(\mu)}{4\pi}\hat{\gamma}^{(0)\text{eff}} + \left(\frac{\alpha_s(\mu)}{4\pi}\right)^2 \hat{\gamma}^{(1)\text{eff}} + \cdots \tag{4.17}$$

$$\beta(\mu) = -2\beta_0 \frac{\alpha_s(\mu)^2}{4\pi} - 2\beta_1 \frac{\alpha_s(\mu)^3}{(4\pi)^2} + \cdots \tag{4.18}$$

we will work to leading order in both, in what follows.

4.2 Solutions to the RGE

4.2.1 The solution to the RGE

The solution to the RGE gives the direct relation between the coefficients renormalized at a given high scale μ_0 which is the initial condition for the solutions, and a lower energy scale μ which is the scale of interest. It is

$$C_i^{\text{eff}}(\mu) = U_{ij}(\mu, \mu_0) C_j^{\text{eff}}(\mu_0), \tag{4.19}$$

Let us solve (4.12) in order to obtain the evolution operator and hence the full evolution of the coefficients in (4.13). We truncate (4.17) and (4.18) at L.O. then,

$$\mu \frac{d}{d\mu} C_i^{\text{eff}}(\mu) = \frac{\alpha_s}{4\pi} \gamma_{ji}^{(0)\text{eff}} C_j^{\text{eff}}(\mu). \tag{4.20}$$

We will use (2.158) to change variables such that (4.20) becomes

$$\frac{d}{d\alpha_s} C_i^{\text{eff}}(\mu) = -\frac{1}{\alpha_s} \frac{1}{2\beta^{(0)}} \gamma_{ji}^{(0)\text{eff}} C_j^{\text{eff}}(\mu) \tag{4.21}$$

To solve this differential equation we have to diagonalize $\hat{\gamma}^{(0)}$ and solve (4.20) in the basis of coefficients for which $\hat{\gamma}^{(0)}$ is diagonal. That is we seek a matrix $\hat{X}$ with $\det\hat{X} \neq 0$ such that

$$C_i'(\mu) = (X^{-1})_{ij} C_j^{\text{eff}}(\mu) \tag{4.22}$$

because $\hat{X}$ is non singular it has an inverse and satisfies

$$\hat{X}\hat{X}^{-1} = \hat{X}^{-1}\hat{X} = \hat{\mathbb{1}} \tag{4.23}$$

where $\hat{\mathbb{1}}$ is the 17×17 identity matrix. Then inserting (4.22) into the lhs of (4.21) gives

$$\frac{d}{d\alpha_s}(X^{-1})_{ik} C_k^{\text{eff}}(\mu) = -\frac{1}{\alpha_s}\frac{1}{2\beta^{(0)}}(X^{-1})_{jk}\gamma_{km}^{(0)\text{eff}} X_{mi}(X^{-1})_{jl} C_l^{\text{eff}}(\mu) \tag{4.24}$$

where the identity matrix has been inserted on the rhs. Then, in the new basis we have

$$\frac{d}{d\alpha_s} C_i'(\mu) = -\frac{1}{\alpha_s}\frac{1}{2\beta^{(0)}}(X^{-1}(\gamma^{(0)\text{eff}})^T X)_{ij} C_j'(\mu), \tag{4.25}$$

where the change of basis matrices diagonalize $(\hat{\gamma}^{(0)\text{eff}})^T$ so that

$$(\hat{X}^{-1}(\hat{\gamma}^{(0)\text{eff}})^T \hat{X}) = \text{Diag}(\lambda_1, \lambda_2, ..., \lambda_n), \tag{4.26}$$

with $\lambda_1, ..., \lambda_n$ the eigenvalues of $(\hat{\gamma}^{(0)\text{eff}})^T$ and $\hat{X}$ is the matrix whose columns are the eigenvectors of $(\hat{\gamma}^{(0)\text{eff}})^T$. Further it is convenient to define a vector $\vec{\gamma}_D^{(0)} = (\lambda_1, \lambda_2, ..., \lambda_n)^T$ containing the diagonal elements of (4.26). So now the differential equation is decoupled and we have a set of $n = 17$ ODE's to be solved for each coefficient in $\vec{C}'$. This is straight forward at L.O:

$$\int_{C'(\mu)}^{C'(\mu_0)} \frac{dC_i'(\mu')}{C_i'(\mu')} = -\frac{(\gamma_D^{(0)})_i}{2\beta^{(0)}} \int_{\alpha_s(\mu)}^{\alpha_s(\mu_0)} \frac{d\alpha_s'}{\alpha_s'} \tag{4.27}$$

where no sum over i is implied. Upon integrating (4.27) and exponentiating, componentwise the solution in the diagonal basis is

$$C_i'(\mu) = \left(\frac{\alpha_s(\mu)}{\alpha_s(\mu_0)}\right)^{\frac{-((\gamma^{(0)})_D)_i}{2\beta^{(0)}}} C_i'(\mu_0), \tag{4.28}$$

again, no sum implied.Transforming back to our original basis then we must left multiply (4.28) with $\hat{X}$ to give in matrix notation

$$\vec{C}^{\text{eff}}(\mu) = \left(\hat{X} \left[\left(\frac{\alpha_s(\mu)}{\alpha_s(\mu_0)} \right)^{\frac{-\vec{\gamma}_D^{(0)}}{2\beta^{(0)}}} \right]_D \hat{X}^{-1} \right) \vec{C}^{\text{eff}}(\mu_0) \tag{4.29}$$

where what is meant by the subscript D on the matrix between the $\hat{X}$ and its inverse is that this is a diagonal matrix whose diagonal elements are precisely the pre-factor to $C_i'(\mu_0)$ in (4.28). Comparing with (4.19), we obtain the LO solution for the evolution matrix

$$\hat{U}^{(0)}(\mu, \mu_0) = \left(\hat{X} \left[\left(\frac{\alpha_s(\mu)}{\alpha_s(\mu_0)} \right)^{-\frac{\vec{\gamma}_D^{(0)}}{2\beta^{(0)}}} \right]_D \hat{X}^{-1} \right). \tag{4.30}$$

Solving the RGE in practice for the full set of coefficients contains a degree of complexity, owing to the fact that at 1-loop level, the contributions from matrix elements of the operators in our basis enter at differing orders in the strong coupling - that being $\alpha_s^{(0)}, \alpha_s^{(1)}$, however the leading order term in the expansion (4.17) is of order $\alpha_s^{(1)}$. In addition, operator matrix elements of the electromagnetic dipole vanish at 1 loop and contribute at two loop but order $\alpha_s^{(1)}$. In this section it is shown that the solution to (4.20) is found by considering two separate cases, categorised as Case I and Case II, for which we must rescale some of the operators and coefficients in our basis differently, in order to obtain a solution to (4.20) which is expressible in the form (4.19). For the purposes of solving in each case, we split the vector of CBSM coefficients as

$$\vec{C}^c(\mu) = (\vec{C}_I^c(\mu), \vec{C}_{II}^c(\mu)), \tag{4.31}$$

$$\vec{C}_I^c(\mu) = (C_1^c(\mu), ..., C_6^c(\mu)), \tag{4.32}$$

$$\vec{C}_{II}^c(\mu) = (C_7^c(\mu), ..., C_{10}^c(\mu)). \tag{4.33}$$

and accordingly in what follows, the ADM which governs the 1-loop mixing of the $b \to c\bar{c}s$ amongst themselves is split as

$$\hat{\gamma}_{cc}^{(0)} = \left[\begin{array}{c|c} \hat{\gamma}_{cc,I}^{(0)} & 0 \\ \hline 0 & \hat{\gamma}_{cc,II}^{(0)} \end{array} \right].$$

For the effective dipole coefficients we split the $\vec{y}, \vec{z}$ vectors as:

$$\vec{y} = (\vec{y}^c_I, \vec{y}^c_{II}, \vec{y}^p) \tag{4.34}$$

$$\vec{z} = (\vec{z}^c_I, \vec{z}^c_{II}, \vec{z}^p) \tag{4.35}$$

$$\vec{y}^p = \left(-\frac{1}{3}, -\frac{4}{9}, -\frac{20}{3}, -\frac{80}{9}\right), \qquad \vec{z}^p = \left(0, 1, -\frac{1}{6}, 20, -\frac{10}{3}\right), \tag{4.36}$$

$$\vec{y}^c_I = (0, 0, 0, 0, 2x_c, \frac{2}{3}x_c), \qquad \vec{z}^c_I = (0, 0, 0, 0, 0, x_c), \tag{4.37}$$

$$\vec{y}^c_{II} = (0, 0, 0, 0), \qquad \vec{z}^c_{II} = (0, 0, 0, 0). \tag{4.38}$$

4.2.2 Case I: $C^c_1(\mu) - C^c_6(\mu)$

In this case we consider only the first 6 CBSM Wilson coefficients, and so $\vec{C}_I(\mu) = (\vec{C}^c_I(\mu), \vec{C}^p(\mu), C^{\text{eff}}_{7,I}(\mu), C^{\text{eff}}_{8,I}(\mu), C_{9V}(\mu))^T$. The effective coefficients are defined through

$$C^{\text{eff}}_{7,I}(\mu) = C_{7\gamma}(\mu) + \vec{y}_I \cdot \vec{C}^{cp}_I(\mu), \tag{4.39}$$

$$C^{\text{eff}}_{8,I}(\mu) = C_{8g}(\mu) + \vec{z}_I \cdot \vec{C}^{cp}_I(\mu). \tag{4.40}$$

with $\vec{y}_I = (\vec{y}^c_I, \vec{y}^p)$,$\vec{z}_I = (\vec{z}^c_I, \vec{z}^p)$ and $\vec{C}^{cp}_I(\mu) = (\vec{C}^c_I(\mu), \vec{C}^p(\mu))$. To understand how the rescaling works and how to scale back after solving the RGE, it is most transparent to look at the individual coupled equations. For the purpose of clarity in what follows, we will omit the zero superscript on the ADM.

$$\mu\frac{d}{d\mu}\vec{C}^c_I(\mu) = \frac{\alpha_s}{4\pi}\hat{\gamma}^T_{cc,I}\vec{C}^c_I(\mu) \tag{4.41}$$

$$\mu\frac{d}{d\mu}\vec{C}^p(\mu) = \frac{\alpha_s}{4\pi}\left(\hat{\gamma}^T_{cp,I}\vec{C}^c_I(\mu) + \hat{\gamma}^T_{pp}\vec{C}^p(\mu)\right) \tag{4.42}$$

$$\mu\frac{d}{d\mu}C^{\text{eff}}_{7,I}(\mu) = \frac{\alpha_s}{4\pi}\left((\vec{\gamma}^{\text{eff}}_{c7,I})^T \cdot \vec{C}^c_I(\mu) + (\vec{\gamma}^{\text{eff}}_{p7})^T \cdot \vec{C}^p(\mu) + \gamma_{77}C^{\text{eff}}_{7,I}(\mu) + \gamma_{87}C^{\text{eff}}_{8,I}(\mu)\right) \tag{4.43}$$

$$\mu\frac{d}{d\mu}C^{\text{eff}}_{8,I}(\mu) = \frac{\alpha_s}{4\pi}\left((\vec{\gamma}^{\text{eff}}_{c8,I})^T \cdot \vec{C}^c_I(\mu) + (\vec{\gamma}^{\text{eff}}_{p8})^T \cdot \vec{C}^p(\mu) + \gamma_{88}C^{\text{eff}}_{8,I}(\mu)\right) \tag{4.44}$$

The differential equations above are all proportional to one power of the strong coupling, because the partonic matrix elements of their operators, between the relevant states involve 2 interaction vertices which contribute a power of α_s. However, at 1-loop the entries $\vec{\gamma}^{(0)}_{c9}$ are $\mathcal{O}(\alpha, \alpha_s^{(0)})$ and so right hand side of the DE below is not proportional to

α_s as it does not originate from QCD corrections. It is therefore necessary to rescale Q_{9V} and C_{9V} so that we bring $\vec{\gamma}^{(0)}_{c9}$ into the full leading order ADM and solve the RGE in a straight forward manner. Then

$$\tilde{Q}_{9V} = \frac{4\pi}{\alpha_s} Q_{9V}, \qquad \tilde{C}_{9V} = \frac{\alpha_s}{4\pi} C_{9V}. \tag{4.45}$$

The coefficient $C_{9V}(\mu)$ obeys

$$\mu \frac{d}{d\mu} C_{9V}(\mu) = \vec{\gamma}^T_{c9,I} \vec{C}^c_I(\mu) + \vec{\gamma}^T_{p9} \vec{C}^p(\mu), \tag{4.46}$$

now rescaling C_9 in accordance with (4.45) gives the expression

$$\mu \frac{d}{d\mu} \tilde{C}_{9V}(\mu) = \frac{\alpha_s}{4\pi} \left(\vec{\gamma}^T_{c9,I} \vec{C}^c(\mu) + \vec{\gamma}^T_{p9} \vec{C}^p(\mu) - 2\beta_0 \tilde{C}_{9V}(\mu) \right) \tag{4.47}$$

Now it is possible to solve the RGE in matrix form, with a single ADM given symbolically below and numerically in (4.48) [1, 2] .

$$\mu \frac{d}{d\mu} \begin{pmatrix} \vec{C}^c_I(\mu) \\ \vec{C}^p(\mu) \\ C^{\text{eff}}_{7,I}(\mu) \\ C^{\text{eff}}_{8,I}(\mu) \\ \tilde{C}_{9V}(\mu) \end{pmatrix} = \frac{\alpha_s}{4\pi} \begin{pmatrix} \hat{\gamma}_{cc,I} & \hat{\gamma}_{cp,I} & \vec{\gamma}^{\text{eff}}_{c7,I} & \vec{\gamma}^{\text{eff}}_{c8,I} & \vec{\gamma}_{c9,I} \\ 0 & \hat{\gamma}_{pp} & \vec{\gamma}^{\text{eff}}_{p7} & \vec{\gamma}^{\text{eff}}_{p8} & \vec{\gamma}_{p9} \\ 0 & 0 & \gamma_{77} & 0 & 0 \\ 0 & 0 & \gamma_{87} & \gamma_{88} & 0 \\ 0 & 0 & 0 & 0 & \gamma_{99} \end{pmatrix}^T \begin{pmatrix} \vec{C}^c_I(\mu) \\ \vec{C}^p(\mu) \\ C^{\text{eff}}_{7,I}(\mu) \\ C^{\text{eff}}_{8,I}(\mu) \\ \tilde{C}_{9V}(\mu) \end{pmatrix}.$$

$$\hat{\gamma}^{\text{eff}}_I = \begin{pmatrix} -2 & 6 & 0 & 0 & 0 & 0 & 0 & 0 & 0 & 0 & 0 & 3 & -\frac{8}{3} \\ 6 & -2 & 0 & 0 & 0 & 0 & 0 & \frac{4}{3} & 0 & 0 & \frac{416}{81} & \frac{70}{27} & -\frac{8}{9} \\ 0 & 0 & 2 & -6 & 0 & 0 & 0 & 0 & 0 & 0 & 0 & 0 & \frac{4}{3} \\ 0 & 0 & 0 & -16 & 0 & 0 & 0 & -\frac{2}{3} & 0 & 0 & \frac{224}{81} & \frac{1}{9} & \frac{4}{9} \\ 0 & 0 & 0 & 0 & -16 & 0 & 0 & 0 & 0 & 0 & -\frac{160\text{xc}}{3} & 0 & 0 \\ 0 & 0 & 0 & 0 & -6 & 2 & 0 & 0 & 0 & 0 & -\frac{128\text{xc}}{9} & -\frac{22\text{xc}}{3} & 0 \\ 0 & 0 & 0 & 0 & 0 & 0 & 0 & -\frac{52}{3} & 0 & 2 & -\frac{176}{81} & \frac{14}{27} & -\frac{16}{9} \\ 0 & 0 & 0 & 0 & 0 & 0 & -\frac{40}{9} & -\frac{100}{9} & \frac{4}{9} & \frac{5}{6} & -\frac{152}{243} & -\frac{587}{162} & \frac{32}{27} \\ 0 & 0 & 0 & 0 & 0 & 0 & 0 & -\frac{256}{3} & 0 & 20 & -\frac{6272}{81} & \frac{6596}{27} & -\frac{112}{9} \\ 0 & 0 & 0 & 0 & 0 & 0 & -\frac{256}{9} & \frac{56}{9} & \frac{40}{9} & -\frac{2}{3} & \frac{4624}{243} & \frac{4772}{81} & \frac{512}{27} \\ 0 & 0 & 0 & 0 & 0 & 0 & 0 & 0 & 0 & 0 & \frac{32}{3} & 0 & 0 \\ 0 & 0 & 0 & 0 & 0 & 0 & 0 & 0 & 0 & 0 & -\frac{32}{9} & \frac{28}{3} & 0 \\ 0 & 0 & 0 & 0 & 0 & 0 & 0 & 0 & 0 & 0 & 0 & 0 & -2\beta 0 \end{pmatrix} \tag{4.48}$$

To construct the ADM we have extracted elements from our own calculations detailed in chapter 5 using the procedure outlined in section 2.5 and for the remaining elements used known entries calculated by the following authors [72], [70], [73], [74]. The full details of which are given in appendix B and in [2].

The evolution matrix $\hat{U}(\mu, \mu_0)$ is calculated as prescribed in 4.1, with help from Mathematica for diagonalization of the large matrices. Eigenvalues and eigenvectors are extracted accordingly and the evolved coefficients are given below after rescaling back the scaled coefficient $\tilde{C}_{9V}$. The values of the coefficients at the Weak scale are all zero except for the coefficients in $\vec{C}_I^c(\mu)$.

$$C_1^c(\mu_b) = \frac{1}{2}(\eta^{\frac{6}{23}} + \eta^{-\frac{12}{23}})\, C_1^c(M_W) + \frac{1}{2}(\eta^{\frac{6}{23}} - \eta^{-\frac{12}{23}})\, C_2^c(M_W) \tag{4.49}$$

$$C_2^c(\mu_b) = \frac{1}{2}(\eta^{\frac{6}{23}} - \eta^{-\frac{12}{23}})\, C_1^c(M_W) + \frac{1}{2}(\eta^{\frac{6}{23}} + \eta^{-\frac{12}{23}})\, C_2^c(M_W) \tag{4.50}$$

$$C_3^c(\mu_b) = \eta^{\frac{3}{23}}\, C_3^c(M_W) \tag{4.51}$$

$$C_4^c(\mu_b) = \frac{1}{3}(\eta^{-\frac{24}{23}} - \eta^{\frac{3}{23}})\, C_3^c(M_W) + \eta^{-\frac{24}{23}}\, C_4^c(M_W) \tag{4.52}$$

$$C_5^c(\mu_b) = \eta^{-\frac{24}{23}}\, C_5^c(M_W) + \frac{1}{3}(\eta^{-\frac{24}{23}} - \eta^{\frac{3}{23}})\, C_6^c(M_W) \tag{4.53}$$

$$C_6^c(\mu_b) = \eta^{\frac{3}{23}}\, C_6^c(M_W) \tag{4.54}$$

$$\begin{aligned} C_{7,I}^{\text{eff}}(\mu_b) = {} & h_i\eta^{a_i}\, C_1^c(M_W) + g_i\eta^{a_i}\, C_2^c(M_W) + f_i\eta^{b_i}\, C_3^c(M_W) \\ & + k_i\eta^{b_i}\, C_4^c(M_W) + l_i\eta^{b_i}\, C_5^c(M_W) + n_i\eta^{b_i}\, C_6^c(M_W)) \end{aligned} \tag{4.55}$$

$$\begin{aligned} C_{9V}(\mu_b) = {} & \frac{4\pi}{\alpha(\mu_b)} \big\{ m_i\eta^{c_i}\, C_1^c(M_W) + q_i\eta^{c_i}\, C_2^c(M_W) + r_i\eta^{d_i}\, C_3^c(M_W) \\ & + s_i\eta^{d_i}\, C_4^c(M_W) \big\} \end{aligned} \tag{4.56}$$

where $\eta = \frac{\alpha_s(M_W)}{\alpha_s(\mu_b)}$ and the coefficients and exponents given by alphabetical letters are

$$\vec{a} = \left(\tfrac{16}{23} \;, \tfrac{14}{23} \;, \tfrac{6}{23} \;, -\tfrac{12}{23} \;, 0.899 \;, 0.423 \;, 0.409 \;, 0.146 \right)$$

$$\vec{b} = \left(\tfrac{16}{23} \;, \tfrac{14}{23} \;, \tfrac{3}{23} \;, -\tfrac{24}{23} - 0.899 \;, -0.423 \;, 0.409 \;, 0.146 \right)$$

$$\vec{c} = \left(\tfrac{6}{23} \;, -\tfrac{12}{23} \;, -0.90 \;, -0.42 \;, 0.41 \;, 0.15 \;, -1 \right)$$

$$\vec{d} = \left(\tfrac{3}{23} \;, -\tfrac{24}{23} \;, -0.90 \;, -0.42 \;, 0.41 \;, 0.15 \;, -1 \right)$$

$$\vec{h} = \left(-\tfrac{59331}{51730} \;, \tfrac{58186}{30253} \;, -\tfrac{3}{7} \;, \tfrac{1}{14} \;, 0.009 \;, 0.051 \;, -0.471 \;, -0.008 \right)$$

$$\vec{g} = \left(-\tfrac{56281}{51730} \;, 2.30 \;, -\tfrac{3}{7} \;, -\tfrac{1}{14} \;, -0.019 \;, 0.038 \;, -0.65 \;, -0.006 \right)$$

$$\vec{f} = \left(-\frac{18818}{144105} \ , 0.1133 \ , \frac{1330}{11583} \ , -\frac{986}{38475} \ , -0.014 \ , 0.005 \ , -0.08 \ , 0.017 \right)$$
$$\vec{k} = \left(\frac{18818}{99765} \ , -0.1138 \ , 0, -\frac{986}{12825} \ , -0.037 \ , 0.007 \ , 0.057 \ , -0.001 \right)$$
$$\vec{l} = \left(-\frac{92417}{209000} \ , 0 \ , 0 \ , \frac{92417}{209000} \ , 0 \ , 0 \ , 0 \ , 0 \right)$$
$$\vec{n} = \left(\frac{92417}{209000} \ , -\frac{92417}{156750} \ , 0 \ , \frac{92417}{627000} \ , 0 \ , 0 \ , 0 \ , 0 \right)$$
$$\vec{m} = \left(-\frac{20}{203}, -\frac{2}{33}, -0.02, -0.05, 0.01, -0.003, 0.22 \right)$$
$$\vec{q} = \left(-\frac{20}{203}, \frac{2}{33}, 0.04, 0.03, 0.01, -0.002, -0.05 \right)$$
$$\vec{r} = \left(\frac{4}{65}, -\frac{1}{5}, 0.03, -0.01, 0.001, 0.006, 0.11 \right)$$
$$\vec{s} = \left(0, -\frac{3}{5}, -0.08, -0.01, -0.001 - 0.002, \frac{41378}{78647} \right)$$

In (4.56) it is made explicit the rescaling back of $C_{9V}(\mu_b)$ and that this coefficient therefore receives an enhancement of $\frac{4\pi}{\alpha_s(\mu_b)}$ which is the reason for strong RG effects in the phenomenology section. Below, in matrix form and with numerical evolution matrix entries is the full mixing of the coefficients to leading order for case I.

$$\begin{pmatrix} C_1^c(\mu_b) \\ C_2^c(\mu_b) \\ C_3^c(\mu_b) \\ C_4^c(\mu_b) \\ C_5^c(\mu_b) \\ C_6^c(\mu_b) \\ C_{7,I}^{\text{eff}}(\mu_b) \\ C_{9V}(\mu_b) \end{pmatrix} = \begin{pmatrix} 1.12 & -0.267 & 0 & 0 & 0 & 0 \\ -0.267 & 1.12 & 0 & 0 & 0 & 0 \\ 0 & 0 & 0.922 & 0 & 0 & 0 \\ 0 & 0 & 0.331 & 1.92 & 0 & 0 \\ 0 & 0 & 0 & 0 & 1.92 & 0.331 \\ 0 & 0 & 0 & 0 & 0 & 0.922 \\ 0.0171 & -0.185 & -0.0147 & -0.131 & 0.560 & 0.166 \\ 8.49 & 2.05 & -4.26 & -1.97 & 0 & 0 \end{pmatrix} \begin{pmatrix} C_1^c(M_W) \\ C_2^c(M_W) \\ C_3^c(M_W) \\ C_4^c(M_W) \\ C_5^c(M_W) \\ C_6^c(M_W) \\ 0 \\ 0 \end{pmatrix} . \quad (4.57)$$

4.2.3 Case II: $C_7^c(\mu) - C_{10}^c(\mu)$

In this case we consider only the last 4 CBSM Wilson coefficients, and so $\vec{C}_{II}(\mu) = (\vec{C}_{II}^c(\mu), \vec{C}^p(\mu), C_{7,II}^{\text{eff}}(\mu), C_{8,II}^{\text{eff}}(\mu), C_{9V}(\mu))^T$. This time, we will need to rescale the dipole and magnetic penguin operators and coefficients in the following way:

$$\tilde{Q}_{7\gamma} = \frac{4\pi}{\alpha_s} Q_{9V}, \qquad \tilde{C}_7 = \frac{\alpha_s}{4\pi} C_7 \quad (4.58)$$
$$\tilde{Q}_{8g} = \frac{4\pi}{\alpha_s} Q_8, \qquad \tilde{C}_8 = \frac{\alpha_s}{4\pi} C_8 \quad (4.59)$$

We keep expressing the coefficients in terms of the effective combinations, but the $C_{7\gamma}, C_{8g}$ parts are rescaled

$$\tilde{C}_{7,II}^{\text{eff}}(\mu) = \tilde{C}_{7\gamma}(\mu) + \vec{y}_{II} \cdot \vec{C}_{II}^{cp}(\mu), \quad (4.60)$$

$$\tilde{C}^{\text{eff}}_{8,II}(\mu) = \tilde{C}_{8g}(\mu) + \vec{z}_{II} \cdot \vec{C}^{cp}_{II}(\mu). \tag{4.61}$$

here $\vec{y}_{II} = (\vec{y}^{c}_{II}, \vec{y}^{p})$,$\vec{z}_{II} = (\vec{z}^{c}_{II}, \vec{z}^{p})$ and $\vec{C}^{cp}_{II}(\mu) = (\vec{C}^{c}_{II}(\mu), \vec{C}^{p}(\mu))$. The coupled equations this time are (note that $\gamma_{78} = \gamma_{79} = \gamma_{89} = \gamma_{99} = \vec{\gamma}_{p7} = \vec{\gamma}_{p8=}0$)

$$\mu\frac{d}{d\mu}\vec{C}^{c}_{II}(\mu) = \frac{\alpha_s}{4\pi}(\hat{\gamma}_{cc,II})^T\vec{C}^{c}_{II}(\mu) \tag{4.62}$$

$$\mu\frac{d}{d\mu}\vec{C}^{p}(\mu) = \frac{\alpha_s}{4\pi}\left((\hat{\gamma}_{cp,II})^T\vec{C}^{c}_{II}(\mu) + \hat{\gamma}^T_{pp}\vec{C}^{p}(\mu)\right) \tag{4.63}$$

$$\mu\frac{d}{d\mu}\tilde{C}^{\text{eff}}_{7,II}(\mu) = \frac{\alpha_s}{4\pi}\left((\vec{\gamma}^{\text{eff}}_{c7,II})^T \cdot \vec{C}^{c}_{II}(\mu) + (\vec{\gamma}^{\text{eff}}_{p7,II})^T \cdot \vec{C}^{p}(\mu) + (\gamma_{77} - 2\beta_0)\tilde{C}_{7\gamma}(\mu) + \gamma_{87}\tilde{C}_{8g}(\mu)\right) \tag{4.64}$$

$$\mu\frac{d}{d\mu}\tilde{C}^{\text{eff}}_{8,II}(\mu) = \frac{\alpha_s}{4\pi}\left((\vec{\gamma}^{\text{eff}}_{c8,II})^T \cdot \vec{C}^{c}_{II}(\mu) + (\vec{\gamma}^{\text{eff}}_{p8,II})^T \cdot \vec{C}^{p}(\mu) + (\gamma_{88} - 2\beta_0)\tilde{C}_{8g}(\mu)\right) \tag{4.65}$$

$$\mu\frac{d}{d\mu}\tilde{C}_{9}(\mu) = \frac{\alpha_s}{4\pi}\left(\vec{\gamma}^T_{p9}\vec{C}^{p}(\mu) - 2\beta_0\tilde{C}_{9}(\mu)\right) \tag{4.66}$$

The full RGE in matrix form is then

$$\mu\frac{d}{d\mu}\begin{pmatrix} \vec{C}^{c}_{II}(\mu) \\ \vec{C}^{p}(\mu) \\ \tilde{C}^{\text{eff}}_{7,II}(\mu) \\ \tilde{C}^{\text{eff}}_{8,II}(\mu) \\ \tilde{C}_{9V,II}(\mu) \end{pmatrix} = \frac{\alpha_s}{4\pi}\begin{pmatrix} \hat{\gamma}_{cc,II} & \hat{\gamma}_{cp,II} & \vec{\gamma}^{\text{eff}}_{c7,II} & \vec{\gamma}^{\text{eff}}_{c8,II} & 0 \\ 0 & \hat{\gamma}_{pp} & \vec{\gamma}^{\text{eff}}_{p7,II} & \vec{\gamma}^{\text{eff}}_{p8,II} & \vec{\gamma}_{p9,II} \\ 0 & 0 & \gamma_{77,II} & 0 & 0 \\ 0 & 0 & \gamma_{87,II} & \gamma_{88,II} & 0 \\ 0 & 0 & 0 & 0 & \gamma_{99,II} \end{pmatrix}^T \begin{pmatrix} \vec{C}^{c}_{I}(\mu) \\ \vec{C}^{p}(\mu) \\ \tilde{C}^{\text{eff}}_{7,II}(\mu) \\ \tilde{C}^{\text{eff}}_{8,II}(\mu) \\ \tilde{C}_{9V,II}(\mu) \end{pmatrix}.$$

where, again, the ADM contains elements extracted from our own calculations [2] and the remaining elements are known results from [72], [70], [73], [74], see appendix B for

full details. The L.O ADM matrix being explicitly given by

$$\hat{\gamma}_{II}^{\text{eff}} = \begin{pmatrix} 2 & -6 & -\frac{7}{6} & -\frac{1}{2} & 0 & 0 & 0 & 0 & 2\text{xc} & 0 & 0 \\ 0 & -16 & -1 & \frac{1}{3} & 0 & 0 & 0 & 0 & \frac{2\text{xc}}{3} & \text{xc} & 0 \\ -56 & -24 & -\frac{38}{3} & 6 & 0 & 0 & 0 & 0 & -8\text{xc} & 0 & 0 \\ -48 & 16 & 0 & \frac{16}{3} & 0 & 0 & 0 & 0 & -\frac{8\text{xc}}{3} & -4\text{xc} & 0 \\ 0 & 0 & 0 & 0 & 0 & -\frac{52}{3} & 0 & 2 & -\frac{218}{27} & \frac{20}{9} & -\frac{16}{9} \\ 0 & 0 & 0 & 0 & -\frac{40}{9} & -\frac{100}{9} & \frac{4}{9} & \frac{5}{6} & -\frac{536}{81} & \frac{68}{27} & \frac{32}{27} \\ 0 & 0 & 0 & 0 & 0 & -\frac{256}{3} & 0 & 20 & -\frac{2696}{27} & \frac{608}{9} & -\frac{112}{9} \\ 0 & 0 & 0 & 0 & -\frac{256}{9} & \frac{56}{9} & \frac{40}{9} & -\frac{2}{3} & -\frac{5696}{81} & \frac{1124}{27} & \frac{512}{27} \\ 0 & 0 & 0 & 0 & 0 & 0 & 0 & 0 & \frac{32}{3} - 2\beta 0 & 0 & 0 \\ 0 & 0 & 0 & 0 & 0 & 0 & 0 & 0 & -\frac{32}{9} & \frac{28}{3} - 2\beta 0 & 0 \\ 0 & 0 & 0 & 0 & 0 & 0 & 0 & 0 & 0 & 0 & -2\beta 0 \end{pmatrix} \tag{4.67}$$

Once again, the coefficients at each scale are related via the evolution operator. Upon solving the RGE with initial conditions at the weak scale M_W and rescaling back, the individual expressions for evolution of the NP coefficients are

$$\begin{aligned} C_7^c(\mu_b) = &\left(0.427\eta^{0.718} + \frac{0.427}{\eta^{0.064}} + \frac{0.073}{\eta^{0.631}} + \frac{0.073}{\eta^{1.414}}\right) C_7^c(M_W) \\ &+ \left(0.028\eta^{0.718} + \frac{0.117}{\eta^{0.064}} - \frac{0.278}{\eta^{0.631}} + \frac{0.133}{\eta^{1.414}}\right) C_8^c(M_W) \\ &+ \left(-1.932\eta^{0.718} - \frac{0.773}{\eta^{0.064}} + \frac{1.932}{\eta^{0.631}} + \frac{0.773}{\eta^{1.414}}\right) C_9^c(M_W) \\ &\left(-3.529\eta^{0.718} + \frac{2.949}{\eta^{0.064}} + \frac{0.529}{\eta^{0.631}} + \frac{0.051}{\eta^{1.414}}\right) C_{10}^c(M_W) \end{aligned} \tag{4.68}$$

$$\begin{aligned} C_8^c(\mu_b) = &\left(0.966\eta^{0.718} - \frac{0.193}{\eta^{0.064}} - \frac{0.966}{\eta^{0.631}} + \frac{0.193}{\eta^{1.414}}\right) C_{10}^c(M_W) \\ &+ \left(-0.117\eta^{0.718} - \frac{0.028}{\eta^{0.064}} - \frac{0.133}{\eta^{0.631}} + \frac{0.278}{\eta^{1.414}}\right) C_7^c(M_W) \\ &+ \left(-0.008\eta^{0.718} - \frac{0.008}{\eta^{0.064}} + \frac{0.508}{\eta^{0.631}} + \frac{0.508}{\eta^{1.414}}\right) C_8^c(M_W) \\ &+ \left(0.529\eta^{0.718} + \frac{0.051}{\eta^{0.064}} - \frac{3.529}{\eta^{0.631}} + \frac{2.949}{\eta^{1.414}}\right) C_9^c(M_W) \end{aligned} \tag{4.69}$$

$$\begin{aligned} C_9^c(\mu_b) = &\left(0.133\eta^{0.718} - \frac{0.278}{\eta^{0.064}} + \frac{0.117}{\eta^{0.631}} + \frac{0.028}{\eta^{1.414}}\right) C_{10}^c(M_W) \\ &+ \left(-0.016\eta^{0.718} - \frac{0.040}{\eta^{0.064}} + \frac{0.016}{\eta^{0.631}} + \frac{0.040}{\eta^{1.414}}\right) C_7^c(M_W) \end{aligned}$$

$$+\left(-0.001\eta^{0.718}-\frac{0.011}{\eta^{0.064}}-\frac{0.061}{\eta^{0.631}}+\frac{0.074}{\eta^{1.414}}\right)C_8^c(M_W)$$
$$+\left(0.073\eta^{0.718}+\frac{0.073}{\eta^{0.064}}+\frac{0.427}{\eta^{0.631}}+\frac{0.427}{\eta^{1.414}}\right)C_9^c(M_W) \tag{4.70}$$

$$C_{10}^c(\mu_b)=\left(0.508\eta^{0.718}+\frac{0.508}{\eta^{0.064}}-\frac{0.008}{\eta^{0.631}}-\frac{0.008}{\eta^{1.414}}\right)C_{10}^c(M_W)$$
$$+\left(-0.061\eta^{0.718}+\frac{0.074}{\eta^{0.064}}-\frac{0.001}{\eta^{0.631}}-\frac{0.011}{\eta^{1.414}}\right)C_7^c(M_W)$$
$$+\left(-0.004\eta^{0.718}+\frac{0.020}{\eta^{0.064}}+\frac{0.004}{\eta^{0.631}}-\frac{0.020}{\eta^{1.414}}\right)C_8^c(M_W)$$
$$+\left(0.278\eta^{0.718}-\frac{0.133}{\eta^{0.064}}-\frac{0.028}{\eta^{0.631}}-\frac{0.117}{\eta^{1.414}}\right)C_9^c(M_W) \tag{4.71}$$

$$C_{7,II}^{\text{eff}}(\mu_b)=\frac{4\pi}{\alpha(\mu_b)}\left(-0.121\eta^{0.72}+\frac{0.493}{\eta^{0.064}}-\frac{0.590}{\eta^{7/23}}+\frac{0.157}{\eta^{9/23}}+\frac{0.062}{\eta^{0.63}}-\frac{0.001}{\eta^{1.41}}\right)C_{10}^c(M_W)$$
$$+\left(0.015\eta^{0.72}+\frac{0.071}{\eta^{0.06}}-\frac{0.118}{\eta^{7/23}}+\frac{0.025}{\eta^{9/23}}+\frac{0.009}{\eta^{0.63}}-\frac{0.002}{\eta^{1.41}}\right)C_7^c(M_W)$$
$$+\left(0.001\eta^{0.72}+\frac{0.02}{\eta^{0.06}}-\frac{0.096}{\eta^{7/23}}+\frac{0.111}{\eta^{9/23}}-\frac{0.033}{\eta^{0.631}}-\frac{0.003}{\eta^{1.41}}\right)C_8^c(M_W)$$
$$+\left(-0.067\eta^{0.72}-\frac{0.13}{\eta^{0.06}}+\frac{0.452}{\eta^{7/23}}-\frac{0.467}{\eta^{9/23}}+\frac{0.226}{\eta^{0.631}}-\frac{0.015}{\eta^{1.41}}\right)C_9^c(M_W) \tag{4.72}$$

It was possible to rescale (4.72) because 1) the penguin and CBSM coefficients do not mix into each other and 2) the entries to $\vec{y}_{II}^{\,c}$ are all zero. This means that $\tilde{C}_{7,II}^{\text{eff}}(\mu_b)=\tilde{C}_{7\gamma}(\mu_b)$. Again, after rescaling, the full evolution numerically is given below.

$$\begin{pmatrix} C_7^c(\mu_b) \\ C_8^c(\mu_b) \\ C_9^c(\mu_b) \\ C_{10}^c(\mu_b) \\ C_{7,II}^{\text{eff}}(\mu_b) \\ C_{9V}(\mu_b) \end{pmatrix} = \begin{pmatrix} 1.0 & 0.049 & 2.7 & 1.7 \\ 0.37 & 2.0 & 2.3 & -0.55 \\ 0.069 & 0.074 & 1.8 & 0.037 \\ 0.0091 & -0.024 & -0.28 & 0.82 \\ -1.0 & -0.47 & 4.0 & 0.70 \\ 0 & 0 & 0 & 0 \end{pmatrix} \begin{pmatrix} C_7^c(M_W) \\ C_8^c(M_W) \\ C_9^c(M_W) \\ C_{10}^c(M_W) \\ 0 \\ 0 \end{pmatrix}. \tag{4.73}$$

4.3 Complete evolution

Finally in this section we present the full evolution matrix which governs the mixing of the CBSM operators with renormalization through the solving of the RGE. In subsection

4.2.2 and 4.2.3 we showed that the evolution for the Wilson coefficients was calculated separately for two sets of coefficients due to the different order at which they appear in the perturbative expansion. The final result can be recombined into one expression, due to the dependence of the dipole and semi leptonic coefficients only upon the CBSM coefficients, and the block diagonal nature of the evolution matrix corresponding to the mixing of charm coefficients amongst themselves. As explained above, we have

$$\begin{pmatrix} \vec{c}^{\,c}_I(\mu_b) \\ \vec{c}^{\,c}_{II}(\mu_b) \end{pmatrix} = \left(\begin{array}{c|c} \hat{U}_{cc,I} & 0 \\ \hline 0 & \hat{U}_{cc,II} \end{array}\right) \begin{pmatrix} \vec{c}^{\,c}_I(M_W) \\ \vec{c}^{\,c}_{II}(M_W) \end{pmatrix}.$$
$$\Rightarrow \vec{C}^c(\mu_b) = \hat{U}_{cc} \cdot \vec{C}^c(M_W) \tag{4.74}$$

Similarly for the dipole and semileptonic coefficients

$$\begin{pmatrix} C_7^{\rm eff}(\mu_b) \\ C_{9V}(\mu_b) \end{pmatrix} = \left(\begin{array}{c|c} \vec{U}_{c7,I} & \vec{U}_{c7,II} \\ \hline \vec{U}_{c9,I} & \vec{U}_{c9,II} \end{array}\right) \begin{pmatrix} \vec{c}^{\,c}_I(M_W) \\ \vec{c}^{\,c}_{II}(M_W) \end{pmatrix}.$$
$$\Rightarrow C_7^{\rm eff}(\mu_b) = \vec{U}_{c7} \cdot \vec{C}^c(M_W) \tag{4.75}$$
$$C_{9V}(\mu_b) = \vec{U}_{c9} \cdot \vec{C}^c(M_W) \tag{4.76}$$

The full evolution matrix for all the coefficients in our study is given below [2].

$$\hat{U} = \begin{pmatrix} 1.1 & -0.27 & 0 & 0 & 0 & 0 & 0 & 0 & 0 & 0 \\ -0.27 & 1.1 & 0 & 0 & 0 & 0 & 0 & 0 & 0 & 0 \\ 0 & 0 & 0.92 & 0 & 0 & 0 & 0 & 0 & 0 & 0 \\ 0 & 0 & 0.33 & 1.9 & 0 & 0 & 0 & 0 & 0 & 0 \\ 0 & 0 & 0 & 0 & 1.9 & 0.33 & 0 & 0 & 0 & 0 \\ 0 & 0 & 0 & 0 & 0 & 0.92 & 0 & 0 & 0 & 0 \\ 0 & 0 & 0 & 0 & 0 & 0 & 1.0 & 0.05 & 2.70 & 1.70 \\ 0 & 0 & 0 & 0 & 0 & 0 & 0.37 & 2.0 & 2.30 & -0.55 \\ 0 & 0 & 0 & 0 & 0 & 0 & 0.07 & 0.07 & 1.80 & 0.04 \\ 0 & 0 & 0 & 0 & 0 & 0 & 0.01 & -0.02 & -0.29 & 0.82 \\ 0.02 & -0.19 & -0.015 & -0.13 & 0.56 & 0.17 & -1.0 & -0.47 & 4.00 & 0.70 \\ 8.50 & 2.10 & -4.30 & -2.00 & 0 & 0 & 0 & 0 & 0 & 0 \end{pmatrix}. \tag{4.77}$$

The computation carried out in this chapter has been performed with only partial knowledge of the contribution to the evolution of coefficients $C_7^{\rm eff}$ and C_{9V} from operators Q_5^c and Q_6^c. These operators do not contribute at all to the evolution of $C_{9V}(\mu)$ at leading order and contribute to the evolution of $C_7^{\rm eff}(\mu)$ only through finite pieces which enter

the effective anomalous dimension matrix. Therefore to reliably trust the dependence of $C_7^{\rm eff}(\mu_b)$ upon $C_5^c(M_W)$ and $C_6^c(M_W)$ which is calculated in (4.77), it would be required to perform a higher order calculation to obtain the leading anomalous dimension matrix entries governing the mixing of $C_5^c(\mu)$ and $C_6^c(\mu)$ into $C_7^{\rm eff}(\mu)$.

Chapter 5

Observables

In this chapter we introduce a set of observables used to constrain BSM effects generated by the CBSM operator basis given in (3.2). The results we present here are novel and are obtained in sections 5.1, 5.2, 5.3.1, 5.4 by inserting all of the operators in (3.2) into the expressions for each of the following observables; the rare semileptonic decay coefficient $\bar{C}_{9V}^{(\prime)}$[1], the inclusive radiative decay branching ratio $\mathcal{B}(B \to X_s\gamma)$, the B_s^0 meson width difference $\Delta\Gamma_s$, the flavour specific CP asymmetry a_{fs}^s, and the B_s^0 to B_d^0 lifetime ratio $\frac{\tau_{B_s}}{\tau_{B_d}}$, respectively. We thus provide a new BSM theoretical prediction for each individual observable, in the form of a function of all of the Wilson coefficients present in the CBSM Hamiltonian $\mathcal{H}_{\text{eff}}^{c\bar{c}}$. In section 5.5 we also provide a novel BSM prediction which in addition to including all operators in (3.2), allows all Wilson coefficients in $\mathcal{H}_{\text{eff}}^{c\bar{c}}$ to be complex for the quantities $S_{J/\psi K_S}$ and $C_{J/\psi K_S}$ associated with the observable $B \to J/\psi K_S$ CP asymmetry, and for the branching ratio observable $\mathcal{B}(B_d^{(0)} \to J/\psi K_d^{(0)})$. These predictions have not been calculated before, form part of the novel research presented in this thesis and may be found in articles [1, 2]. We show the calculations carried out in order to determine contributions from the operators to each observable and show the methods used in order to achieve this.

5.1 The rare decay $b \to s\mu^+\mu^-$

5.1.1 The partonic amplitude $\mathcal{A}(b \to s\mu^+\mu^-)$

We study here the $b \to c\bar{c}s$ contribution to the Flavour Changing Neutral Current (FCNC) decay $b \to s\bar{\ell}\ell$ for $\ell = \mu$. This quark level decay would contribute to the hadronic

[1] This coefficient is extracted from the partonic amplitude $\mathcal{A}(b \to s\bar{\mu}\mu)$

$B \to K^{(*)}\bar{\mu}\mu$ process. This decay is not present in the SM at tree level and so the LO contribution begins at the 1-loop level at $\mathcal{O}(\alpha, \alpha_s^{(0)})$ in the electromagnetic and strong couplings respectively. The Feynman diagram in Figure 5.1 describes the process by which a beauty quark decays to a strange quark and a di-muon pair with invariant mass squared q^2, via a charm quark loop and an off shell photon.

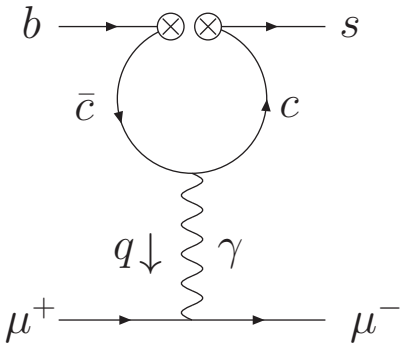

Figure 5.1: Feynman diagram for $b \to s\bar{\ell}\ell$ quark level decay

The circled crosses here denote electromagnetic quark currents which make up the dim 6 operators of (3.2). We define the individual four quark operators generically as

$$Q_i^c = C_{\alpha\beta\gamma\delta} \left(\bar{c}^\alpha \Gamma_i^A b^\beta\right) \left(\bar{s}^\gamma \Gamma_i^B c^\delta\right), \tag{5.1}$$

where $C^{\alpha\beta\gamma\delta}$ are colour factors, $i = 1, ..., 10$, Γ^X; $X = A, B$ are Dirac structures and left - right projection operators. At tree level + 1-loop we express the amplitude for a free b quark to decay to a strange quark and a photon as

$$\mathcal{A}(b \to s\bar{\mu}\mu) = \mathcal{A}^{(0)}(b \to s\bar{\mu}\mu) + \mathcal{A}^{(1)}(b \to s\bar{\mu}\mu) + \mathcal{O}(\alpha_s, \alpha\alpha_s), \tag{5.2}$$

where the leading order tree level and the 1-loop contributions are defined as follows

$$\begin{aligned}\mathcal{A}^{(0)}(b \to s\bar{\mu}\mu) = \frac{4G_F V_{cb} V_{cs}^*}{\sqrt{2}} \big(&C_{7\gamma}\langle Q_{7\gamma}\rangle_p^{(0)} + C_{9V}\langle Q_{9V}\rangle_p^{(0)} \\ &+ C'_{7\gamma}\langle Q'_{7\gamma}\rangle_p^{(0)} + C'_{9V}\langle Q'_{9V}\rangle_p^{(0)}\big)\end{aligned} \tag{5.3}$$

$$\mathcal{A}^{(1)}(b \to s\bar{\mu}\mu) = \frac{4G_F V_{cb} V_{cs}^*}{\sqrt{2}} \sum_{i=1}^{10} \left(C_i^c \langle Q_i^c\rangle_p^{(1,0)} + C_i'^c \langle Q_i'^c\rangle_p^{(1,0)}\right). \tag{5.4}$$

To make clear what is meant by these tree level and loop level matrix elements we define the following tree level matrix element of the effective operator Q_X for $X =$

$1, ...10, 7\gamma, 9V$ as

$$\langle Q_X \rangle_p^{(0)} = C_X(\alpha', \beta') \langle s(p', \alpha'), \bar{\mu}(r), \mu(r') | Q_X(0) | b(p; \beta') \rangle, \tag{5.5}$$

where the indices α', β' are colour indices and the contractions of these with colour factor is $C_X(\alpha', \beta')$ ensures the whole object is colourless. The 1-loop matrix element of the effective operator is the third order term in the perturbative expansion of the S matrix which contains two interaction terms from the neutral current Lagrangian and one insertion of the operator,

$$\begin{aligned}\langle Q_X \rangle_p^{(1,0)} = C_X(\alpha', \beta') \int d^4x \int d^4y \times \\ \langle \bar{\mu}(r), \mu(r') | s(p'; \alpha') | T\{(-ie\mathcal{J}_\mu^l(x) A^\mu(x)) (-ie\mathcal{J}_\nu^c(y) A^\nu(y)) Q_X(0)\} | b(p; \beta') \rangle.\end{aligned} \tag{5.6}$$

Where $\mathcal{J}_\mu^l$ is the muon vector current and $\mathcal{J}_\nu^c$ is the charm vector current as defined in (2.35) with $Q_f = -1$ for the left handed muon and $Q_f = \frac{2}{3}$ for the left handed charm quark, and e is the electromagnetic coupling. Only the four quark operators survive (5.6) and upon employing the LSZ reduction formula [75] and performing the Wick contractions yields the loop integrals

$$\langle Q_i \rangle_p^{(1,0)} = i\frac{2}{3}\frac{\mu^{4-d}e^2}{Z_q Z_e} \int \frac{d^dk}{(2\pi)^d} \frac{[\bar{u}_s(p')\Gamma_i^B((\not{k} - \not{q}) + m_c)\gamma_\nu(\not{k} + m_c)\Gamma_i^A u_b(p)]}{((k-q)^2 - m_c^2 + i\epsilon)(k^2 - m_c^2 + i\epsilon)} \frac{[\bar{u}(r')\gamma^\nu v(r)]}{(q^2 + i\epsilon)}, \tag{5.7}$$

where the quark and lepton field renormalization factors are defined in Section 2.4. To reduce the integrand for all Dirac structures it is convenient to define the numerator as

$$N = \Gamma_i^B((\not{k} - \not{q}) + m)\gamma_\nu(\not{k} + m)\Gamma_i^A \otimes \gamma^\nu \tag{5.8}$$

where it is understood that the tensor product symbol means that the Dirac matrices on either side are contracted with spinor fields. Upon expanding (5.8) simplifies as

$$\begin{aligned}N &= \Gamma_i^B(\not{k}\gamma_\nu\not{k} + m_c(\not{k}\gamma_\nu + \gamma_\nu\not{k}) - \not{q}\gamma_\nu\not{k} - \not{q}\gamma_\nu m_c + m_c^2\gamma_\nu)\Gamma_i^A \otimes \gamma^\nu \\ &= \Gamma_i^B(\gamma_{\rho\nu\sigma}k^\rho k^\sigma + (2m_c\eta_{\nu\sigma} - \gamma_{\rho\nu\sigma}q^\rho)k^\sigma + (m_c^2\gamma_\nu - m_c\gamma_{\sigma\nu}q^\sigma))\Gamma_i^A \otimes \gamma^\nu\end{aligned} \tag{5.9}$$

Employing the method of Veltman and Passarino (VP) [76], the tensor integrals are reduced to the product of scalar 1-loop integrals over loop momenta k and Dirac structures

contracted with spinor fields. We can express (5.7) as a master expression

$$\begin{aligned}\langle Q_i\rangle_p^{(1,0)} = i\frac{2}{3}\frac{\mu^{4-d}e^2}{Z_q Z_e}\Big\{\big[&(2-d)B_{00}(m_c^2,m_c^2,q^2)+m_c^2 B_0(m_c^2,m_c^2,q^2)\\ &+q^2(B_1(m_c^2,m_c^2,q^2)-B_{11}(m_c^2,m_c^2,q^2))\,\big)\big]\langle Q_i^V\rangle_p\\ &+m_c B_0(m_c^2,m_c^2,q^2)\langle Q_i^T\rangle_p\Big\}\frac{1}{q^2},\end{aligned} \tag{5.10}$$

which can then be evaluated for each operator Q_i^c in the basis. Here d is the number of spacetime dimensions and the Veltman and Passarino (VP) integrals are given in Appendix C. We define the tree level matrix elements which depend upon the Dirac structure of each operator for each $i = 1, ..., 10$ as

$$\langle Q_i^V\rangle_p = [\bar{u}_s(p')\Gamma_i^B\gamma_\nu\Gamma_i^A u_b(p)][\bar{u}(r')\gamma^\nu v(r)], \tag{5.11}$$

$$\langle Q_i^T\rangle_p = [\bar{u}_s(p')\Gamma_i^B q^\mu i\sigma_{\mu\nu}\Gamma_i^A u_b(p)][\bar{u}(r')\gamma^\nu v(r)]. \tag{5.12}$$

no sum implied, and the basis integrals evaluated in the dimensional regularization scheme are

$$B_0(m_c^2,q^2) = \frac{i}{(4\pi)^2}\left[\frac{1}{\epsilon}+\ln\left(\frac{\mu^2}{m_c^2}\right)+2-2\sqrt{|z-1|}\begin{cases}\arctan\left(\frac{1}{\sqrt{z-1}}\right) & z>1\\ \ln\left(\frac{1+\sqrt{1-z}}{\sqrt{z}}\right)-\frac{i\pi}{2} & z\leqslant 1\end{cases}\right]. \tag{5.13}$$

$$A(m_c^2) = \frac{im_c^2}{(4\pi)^2}\left[\frac{1}{\epsilon}+1+\ln\left(\frac{\mu^2}{m_c^2}\right)\right]+\mathcal{O}(\epsilon), \tag{5.14}$$

where $z = \frac{4m_c^2}{q^2}$. As expressed in Section 2.4 parameter $\mu^2 = \frac{e^\gamma\tilde{\mu}^2}{4\pi}$ is the usual dimension-full quantity which is introduced into the calculation so as to give a dimensionless electromagnetic coupling e, but which is also the renormalization scale. The meaning of the two branches to $B_0(m^2,m^2,q^2)$ is that below the charm pair production threshold energy where $q^2 < 4m_c^2$ we have $z > 1$ and at or above the threshold where $q^2 \geq 4m_c^2$ the loop function develops an imaginary part and we have $z \leq 1$. At the threshold we will have a resonance where there is enough energy for charmonium states to be produced. For the purposes of the study of $b \to s\bar{\ell}\ell$ we will always stay below threshold. In what follows we construct an observable $\bar{C}_{9V}^{(\prime)}$ which is an ingredient of the the forward backward (FB) asymmetry observable in $\bar{B} \to \bar{K}^*\ell^+\ell^-$, as calculated in [77] using the QCD factorization approach. For low q^2, such observables contain uncertainties due to power suppressed non perturbative charm effects. In this thesis we neglect these uncertainties

and work instead, directly with the coefficient $\bar{C}_{9V}^{(\prime)}$.

5.1.2 The pseudo observable $\bar{C}_{9V}$ and $\bar{C}_{7\gamma}$

Returning now to (5.2), (5.3) and (5.4), at the tree level there is nothing to be done but at the loop level we must sum up all contributions from each of the $i = 1, ..., 10$ operators and their chirality conjugates in the basis introduced in subsection 3.2. For the sum over operator matrix elements in (5.4) we find for the primed and the unprimed case that these are expressible in terms of a linear combination of tree level matrix elements of the dipole and semi leptonic operators. That is

$$\sum_{i=1}^{10} C_i^{(\prime)c} \langle Q_i^{(\prime)c} \rangle_p^{(1,0)} = \mathcal{C}_{7\gamma}^{(\prime)} \langle Q_{7\gamma}^{(\prime)} \rangle_p^{(0)} + \mathcal{C}_{9V}^{(\prime)} \langle Q_{9V}^{(\prime)} \rangle_p^{(0)}. \tag{5.15}$$

Let us define the coefficients $\mathcal{C}_{9V}^{(\prime)}, \mathcal{C}_{7\gamma}^{(\prime)}$as

$$\mathcal{C}_{7\gamma}^{(\prime)} = \sum_{i=1}^{10} C_i^{c(\prime)} \kappa_{7\gamma}^i(\mu, q^2) \qquad\qquad \mathcal{C}_{9V}^{(\prime)} = \sum_{i=1}^{10} C_i^{c(\prime)} \kappa_{9V}^i(\mu, q^2), \tag{5.16}$$

and the κ^X are functions of the VP integrals from (5.10) and whatever relations result from the Dirac reduction in (5.11) and (5.12). In (5.2) then we can write for the full amplitude at tree + 1-loop

$$\begin{aligned} \mathcal{A}(b \to s\bar{\mu}\mu) = \frac{4G_F V_{cb} V_{cs}^*}{\sqrt{2}} \big[& (C_{7\gamma} + \mathcal{C}_{7\gamma}) \langle Q_{7\gamma} \rangle_p^{(0)} + (C_{9V} + \mathcal{C}_{9V}) \langle Q_{9V} \rangle_p^{(0)} \\ & + (C'_{7\gamma} + \mathcal{C}'_{7\gamma}) \langle Q'_{7\gamma} \rangle_p^{(0)} + (C'_{9V} + \mathcal{C}'_{9V}) \langle Q'_{9V} \rangle_p^{(0)} \big] \\ & + \mathcal{O}(\alpha_s, \alpha\alpha_s). \end{aligned} \tag{5.17}$$

The coefficients $\mathcal{C}_{9V}^{(\prime)}$ and $\mathcal{C}_{7\gamma}^{(\prime)}$ as defined in (5.16) are

$$\mathcal{C}_{9V}^{(\prime)}(q^2, \mu, m_c) = \left(\Delta C_{1,2}^{(\prime)} - \frac{\Delta C_{3,4}^{(\prime)}}{2} \right) h - \frac{2}{9} \Delta C_{3,4}^{(\prime)}, \tag{5.18}$$

$$\mathcal{C}_{7\gamma}^{(\prime)}(q^2, \mu, m_c) = \frac{m_c}{m_b} \left[\left(4\Delta C_{9,10}^{(\prime)} - C_{7,8}^{(\prime)} \right) y - \frac{\Delta C_{7,8}^{(\prime)}}{6} \right], \tag{5.19}$$

with $\Delta C_{x,y} = 3\Delta C_x + \Delta C_y$, and the loop functions

$$h(q^2, m_c, \mu) = -\frac{4}{9} \left[\ln \frac{m_c^2}{\mu^2} - \frac{2}{3} + (2 + z) a(z) - z \right], \tag{5.20}$$

$$y(q^2, m_c, \mu) = -\frac{1}{3}\left[\ln\frac{m_c^2}{\mu^2} - \frac{3}{2} + 2a(z)\right], \tag{5.21}$$

where $a(z) = \sqrt{|z-1|}\arctan\frac{1}{\sqrt{z-1}}$, and the $\Delta C_{x,y}$ are just short hand for the linear combinations $3\Delta C_x + \Delta C_y$, where the BSM coefficients ΔC_x are defined in (3.12) in chapter 3, and always appear in this combination due to the differing colour structure of pairs of operators with the same Dirac structure. For this thesis we will find it convenient to further express these tree level and loop level induced coefficients in a single coefficient for both the dipole and semileptonic operators.

$$\bar{C}_{9V}^{(\prime)}(\mu) = C_{9V}^{(\prime)\mathrm{BSM}}(\mu) + \mathcal{C}_{9V}^{(\prime)}(q^2, \mu, m_c) \tag{5.22}$$

$$\bar{C}_{7\gamma}^{(\prime)\mathrm{eff}}(\mu) = C_{7\gamma}^{(\prime)\mathrm{eff,BSM}}(\mu) + \mathcal{C}_{7\gamma}^{(\prime)}(q^2, \mu, m_c), \tag{5.23}$$

where the first term on the right hand side (RHS) will mix with the four fermion coefficients $\Delta C_i(\mu)$ through renormalization group evolution if we wish to consider scales above the scale of the B meson mass $\mu > \mu_b \approx m_b$ and the second term will contain the evolved coefficients themselves in addition to a q^2 dependent piece. In Chapter 6 we will explore the q^2 dependence and study the different constraints we obtain upon rare decay at the B scale and the weak scale.

5.2 The radiative decay $b \to s\gamma$

In this subsection we introduce the $b \to c\bar{c}s$ operator contribution to the $b \to s\gamma$ decay amplitude and show how this contributes to the observable $\mathcal{B}(\bar{B} \to X_s\gamma)$.

5.2.1 The partonic amplitude $\mathcal{A}(b \to s\gamma)$

The Feynman diagram for a b quark to decay to a strange quark and a photon via a charm loop is given in Figure 5.2.

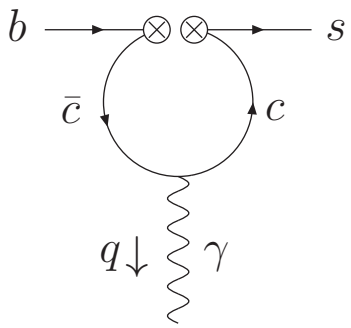

Figure 5.2: Feynman diagram for $b \to s\gamma$ quark level decay

Again, we split the amplitude into tree and 1-loop level contributions as

$$\mathcal{A}(b \to s\gamma) = \mathcal{A}^{(0)}(b \to s\gamma) + \mathcal{A}^{(1)}(b \to s\gamma) + \mathcal{O}(\alpha_s, \alpha\alpha_s), \tag{5.24}$$

where the individual tree level and 1-loop contributions are proportional to

$$\mathcal{A}^{(0)}(b \to s\gamma) = \frac{4G_F V_{cb}V_{cs}^*}{\sqrt{2}}(C_{7\gamma}\langle Q_{7\gamma}\rangle_p^{(0)} + C'_{7\gamma}\langle Q'_{7\gamma}\rangle_p^{(0)}), \tag{5.25}$$

$$\mathcal{A}^{(1)}(b \to s\gamma) = \frac{4G_F V_{cb}V_{cs}^*}{\sqrt{2}} \sum_{i=1}^{10} \left(C_i^c\langle Q_i^c\rangle_p^{(1,0)} + C_i'^c\langle Q_i'^c\rangle_p^{(1,0)}\right). \tag{5.26}$$

The one-loop $\mathcal{O}(\alpha_s^{(0)})$ contributions from SM operator Q_1^c, Q_2^c and from Q_3^c, Q_4^c vanish for an on shell photon with $q^2 = 0$. However, operators $Q_5^c - Q_{10}^c$ do contribute at 1 loop at order $\alpha_s^{(0)}$. We do not repeat the steps shown above but state the acquired result for the master expression, which is

$$\langle Q_i\rangle_p^{(1,0)} = i\frac{2}{3}\frac{\mu^{4-d}e^2}{Z_q Z_e} m B_0(m^2, m^2, 0)\langle Q_i^T\rangle, \tag{5.27}$$

This is none other than the result which contributes to the $b \to s\mu\mu$ amplitude for operators $Q_5^c - Q_{10}^c$. Thus we write

$$\mathcal{A}(b \to s\gamma) = \frac{4G_F V_{cb}V_{cs}^*}{\sqrt{2}}\left[(C_{7\gamma} + \mathcal{C}_{7\gamma})\langle Q_{7\gamma}\rangle_p^{(0)} + (C'_{7\gamma} + \mathcal{C}'_{7\gamma})\langle Q'_{7\gamma}\rangle_p^{(0)}\right] + \mathcal{O}(\alpha_s, \alpha\alpha_s). \tag{5.28}$$

and for the calligraphic coefficients $\mathcal{C}^{(\prime)}$ and loop function we have

$$\mathcal{C}_{7\gamma}^{(\prime)}(0, \mu, m_c) \;=\; \frac{m_c}{m_b}\left[\left(4\Delta C_{9,10}^{(\prime)} - C_{7,8}^{(\prime)}\right) y - \frac{\Delta C_{7,8}^{(\prime)}}{6}\right], \tag{5.29}$$

$$y(0, m_c, \mu) = -\frac{1}{3}\left[\ln\frac{m_c^2}{\mu^2} + \frac{1}{2}\right]. \tag{5.30}$$

It is customary, as explained in chapter 4 to define a scheme independent effective coefficient.

5.2.2 The inclusive branching Ratio $\mathcal{B}(\bar{B} \to X_s\gamma)$

It is well known that weak radiative B meson decays are sensitive to BSM physics. The Standard-Model prediction of the branching ratio for $\mathcal{B}(\bar{B} \to X_s\gamma)^{\rm SM} = (3.36 \pm 0.23) \times 10^{-4}$ [69] is in good agreement with the current experimental average of $\mathcal{B}(\bar{B} \to X_s\gamma)^{\rm exp} = (3.32 \pm 0.15) \times 10^{-4}$[78]. In accordance with Heavy Quark Effective Theory (HQET) we may express the inclusive decay rate for a B meson into a charmless hadron and a photon as

$$\Gamma(\bar{B} \to X_s\gamma) \simeq \Gamma(b \to X_s^{\rm parton}\gamma) + \delta^{\rm np}, \tag{5.31}$$

Here the nonperturbative term $\delta^{\rm np}$, for $E_\gamma > E_0$ with the lower cut off of the photon energy $E_0 = 1.6{\rm GeV}$, is estimated to be at the $(3 \pm 5)\%$ level [79, 80]. Following the approach of [81, 82] the branching ratio $\mathcal{B}(\bar{B} \to X_s\gamma)$ can be expressed as

$$\mathcal{B}(\bar{B} \to X_s\gamma)_{E_0>E_\gamma} = \mathcal{B}(\bar{B} \to X_c e\bar{\nu})^{\rm exp} \left|\frac{V_{ts}^* V_{tb}}{V_{cb}}\right|^2 \frac{6\alpha_{em}}{\pi C}\left[P(E_0) + N(E_0)\right], \tag{5.32}$$

where $P(E_0)$ and $N(E_0)$ denote, respectively, the leading-power perturbative contribution and non-perturbative corrections, and C is defined as

$$C = \left|\frac{V_{ub}}{V_{cb}}\right|^2 \frac{\Gamma(\bar{B} \to X_c e\bar{\nu})}{\Gamma(\bar{B} \to X_u e\bar{\nu})}. \tag{5.33}$$

The semi-leptonic branching ratio and the ratio C are taken from [81]:

$$\mathcal{B}(\bar{B} \to X_c e\bar{\nu})^{\rm exp} = 0.1061 \pm 0.0017\,, \tag{5.34}$$

$$C = 0.580 \pm 0.016\,. \tag{5.35}$$

We neglect BSM corrections to the non-perturbative part and split the perturbative term $P(E_0)$ into an SM part and a BSM part,

$$P(E_0) = P^{\rm SM}(E_0) + \Delta P(E_0). \tag{5.36}$$

We similarly split the branching ratio,

$$\mathcal{B}(\bar{B} \to X_s\gamma) = \mathcal{B}(\bar{B} \to X_s\gamma)_{SM} + \Delta\mathcal{B}_{NP}. \tag{5.37}$$

To zeroth order in α_s and neglecting the strange quark mass, we have

$$\Delta P(E_0) = 2C_{7\gamma}^{\text{eff,SM}}\text{Re}(\bar{C}_{7\gamma}^{\text{eff}}) + |\bar{C}_{7\gamma}^{\text{eff}}|^2 + |\bar{C}_{7\gamma}^{\prime\text{eff}}|^2, \tag{5.38}$$

which follows from substituting $C_{7\gamma}^{\text{eff}} \to C_{7\gamma}^{\text{eff,SM}} + \bar{C}_{7\gamma}^{\text{eff}}$ in the SM expression. The SM contribution to $B \to X_s\gamma$ which interferes with our BSM contribution is given by [83]

$$C_{7\gamma}^{\text{eff,SM}}(m_b) = -0.385\,. \tag{5.39}$$

The barred coefficients are defined as below, where the first term comes from the evolution detailed in 4 and the second term is the LO result of (5.29).

$$\bar{C}_{7\gamma}^{\text{eff}}(\mu) = C_{7\gamma}^{\text{eff,BSM}}(\mu) + \mathcal{C}_{7\gamma}(0,\mu,z) \tag{5.40}$$

$$\bar{C}_{7\gamma}^{\prime\text{eff}}(\mu) = C_{7\gamma}^{\prime\text{eff,BSM}}(\mu) + \mathcal{C}_{7\gamma}^{\prime}(0,\mu,z), \tag{5.41}$$

With expressions (5.32) and (5.38) we determine the shift to the SM branching ratio in terms of the charmed four fermion coefficients and in Chapter 6 find this leads, in many cases, to stringent constraints upon the possible size of BSM effects.

5.3 B_s^0 mixing observables $\Delta\Gamma_s$ and a_{sl}^s

5.3.1 The calculation of Γ_{12}^s

The quantity we wish to compute is Γ_{12}^s, the off diagonal matrix element of the $B_s^{(0)} - \bar{B}_s^{(0)}$ decay rate matrix given in eq (2.60) in section 2.2. This quantity is the absorptive part of the $B_s^{(0)}$ meson mixing matrix in that contributions to Γ_{12}^s are associated with intermediate states for which there is enough energy to actually be produced. As there is no top quark contribution, the charm will give the leading effect. Following [67], [84] Γ_{12} may be expressed as [2]

$$\Gamma_{12}^s = \frac{1}{2M_B}\langle B_s^0|\mathcal{T}|\bar{B}_s^0\rangle, \tag{5.42}$$

[2] Our operator basis is the hermitian conjugate of those used the literature cited, so we are computing Γ_{12} and not Γ_{21}.

where we use the relativistic normalization of states $\langle B_s|B_s\rangle = 2EV$ and the transition operator $\mathcal{T}$ is formed of the imaginary part of the bi-local time ordered product of the two $\Delta B = 1$ Hamiltonians at different spacetime points as detailed in section 2.7.

$$\mathcal{T} = \mathrm{Im}\left\{ i \int d^4x T\left[\mathcal{H}_{\mathrm{eff}}(x)\mathcal{H}_{\mathrm{eff}}(0)\right]\right\}. \tag{5.43}$$

with the Hamiltonian being the weak effective Hamiltonian which mediates b quark decay. We split Γ_{12}^s into the SM part and a NP part

$$\Gamma_{12}^s = \Gamma_{12}^{SM} + \Gamma_{12}^{c\bar{c}}, \tag{5.44}$$

where the second term contains the effects of $b \to c\bar{c}s$ operators. The time ordered product of the Hamiltonian is given by (3.4) expands into four terms which contribute to different processes.

$$\begin{aligned} T(\mathcal{H}^{c\bar{c}}(x)\mathcal{H}^{c\bar{c}}(0)) = 8G_F^2 \sum_n \sum_m \big\{ & V_{cb}^2 (V_{cs}^*)^2 C_m C_n T[Q_m(x)Q_n(0)] \\ & + |V_{cb}|^2 |V_{cs}|^2 C_m C_n^* T[Q_m(x)Q_n^\dagger(0)] \\ & + |V_{cb}|^2 |V_{cs}|^2 C_m^* C_n T[Q_m^\dagger(x)Q_n(0)] \\ & + (V_{cb}^*)^2 (V_{cs}^*)^2 C_m^* C_n^* T[Q_m^\dagger(x)Q_n^\dagger(0)]\big\}. \end{aligned} \tag{5.45}$$

The part of which contributes to Γ_{12}^s and does not vanish between the given initial and final states is

$$\mathcal{T}|_{\Gamma_{12}^{c\bar{c}}} = 8G_F^2 V_{cb}^2 (V_{cs}^*)^2 \sum_{m=1}^{20}\sum_{n=1}^{20} C_m^c C_n^c \mathrm{Im}\left\{ i \int d^4x T\left[Q_m^c(x)Q_n^c(0)\right]\right\}, \tag{5.46}$$

where here, operators with indices $m = 11, ..., 20$ are the primed operators of (3.4) with indices $m = 1, ..., 10$. Thus we express the second term in (5.44) as

$$\Gamma_{12}^{c\bar{c}} = \sum_{m=1}^{20}\sum_{n=1}^{20} \mathcal{N}_{mn} \langle B_s^0 | \mathrm{Im}\left\{ i \int d^4x T\left[Q_m^c(x)Q_n^c(0)\right]\right\} |\bar{B}_s^0\rangle, \tag{5.47}$$

for brevity expressing the normalization factor as

$$\mathcal{N}_{mn} = \frac{4G_F^2 V_{cb}^2 (V_{cs}^*)^2 C_m^c C_n^c}{M_B}. \tag{5.48}$$

The leading contribution to Γ_{12} occurs at third order in the HQE such that the dimension 6 operators arising in (5.43) are local $\Delta B = 2$ operators

$$\langle B_s^0|\text{Im}\left\{i\int d^4x T[Q_m^c(x)Q_n^c(0)]\right\}|\bar{B}_s^0\rangle = \frac{m_b^2}{16\pi}\left[G(m,n)(z)\langle Q\rangle + F(m,n)(z)\langle\tilde{Q}_S\rangle\right]. \tag{5.49}$$

To compute these quantities, the matrix element of the transition operator is evaluated between partonic initial and final states - and once the coefficients $F(m,n), G(m,n)$ of the new basis of operators are found, the matrix elements of these are expressed between the full meson (non perturbative) states. That is to say, we may compute the coefficients $F(m,n), G(m,n)$ using perturbative methods, but when this is done, we will need to use matrix elements of the $\Delta B = 2$ operators computed using QCD Sum rules or Lattice Field theory to obtain a prediction. First let us define the shorthand notation

$$\langle\hat{A}\rangle_p^{mix} := \langle\bar{b}_2(p_{b2}), s_2(p_{s2})|\hat{A}|b_1(p_{b1}), \bar{s}_1(p_{s1})\rangle, \tag{5.50}$$

where p stands for partonic, $p_{qj}, j = 1,2, q = b,s$ are the four momentum of the initial and final state particles, and $\hat{A}$ is any operator, and the superscript "mix" indicates that the initial and final states are associated with $\bar{B}$ and a B meson respectively. Consider the partonic matrix element of the T-product of $\Delta B = 1$ operators on the lhs of (5.49). Straight forward application of the LSZ reduction formula [75] gives

$$\begin{aligned}\int d^4x\langle T[Q_m(x)Q_n(0)]\rangle_p^{mix} = Z_f\int d^4x\int d^4x_2\int d^4y_2\int d^4x_1\int d^4y_1\,\{\\ (-i)e^{ip_{s2}\cdot y_2}[\bar{u}_{s_2}(p_{s2})(i\overleftarrow{\not\partial}_{y_2} - m)]_{\beta_2} ie^{-ip_{s1}\cdot y_1}[\bar{v}_{s_1}(p_{s1})(i\not\partial_{y_1} - m)]_{\beta_1}\times\\ \langle 0|T[\bar{\psi}^i_{\alpha_2}(x_2)\psi^j_{\beta_2}(y_2)\bar{\psi}^k_{\alpha_1}(x_1)\psi^l_{\beta_1}(y_1)Q_m(x)Q_n(0)]|0\rangle\times\\ (-i)[(-i\overleftarrow{\not\partial}_{x_1} - m)u_{b_1}(p_{b1})]_{\alpha_1}e^{-ip_{b1}\cdot x_1} i[(-i\overleftarrow{\not\partial}_{x_2} - m)v_{b_2}(p_{b2})]_{\alpha_2}e^{ip'\cdot x_2}\Big\}\end{aligned} \tag{5.51}$$

here $\psi^i_\alpha(x)$ are anti commuting fermion fields, greek letters α and β are Dirac indices, roman letters i,j,k,l are colour indices and $u(p), v(p)$ are spinors. Since the time ordered product of operators is

$$T[\hat{A}\hat{B}...\hat{Z}] = N[\hat{A}\hat{B}...\hat{Z} + \text{all possible contractions}] \tag{5.52}$$

and between the vacuum states, a product of un-contracted fields in normal order vanishes, that is

$$\langle 0|N(\text{anything uncontracted})|0\rangle = 0 \tag{5.53}$$

there are only actually 4 non vanishing contractions, and two of those are related by symmetry. We find for the correlation function in (5.51)

$$\begin{aligned}
&\langle 0|T[\bar{\psi}^i_{\alpha_2}(x_2)\psi^j_{\beta_2}(y_2)\bar{\psi}^k_{\alpha_1}(x_1)\psi^l_{\beta_1}(y_1)Q_m(x)Q_n(0)]|0\rangle = \\
&= (S^F(y_2)\Gamma^B_n S^F(-x)\Gamma^A_m S^F(x-x_2))_{\beta_2\alpha_2}(S^F(y_1-x)\Gamma^B_m S^F(x)\Gamma^A_n S^F(-x_1))_{\beta_1\alpha_1} \\
&- (S^F(y_1)\Gamma^B_n S^F(-x)\Gamma^A_m S^F(x-x_2))_{\beta_1\alpha_2}(S^F(y_2-x)\Gamma^B_m S^F(x)\Gamma^A_n S^F(-x_1))_{\beta_2\alpha_1} \\
&+ n \leftrightarrow m
\end{aligned} \tag{5.54}$$

where $S^F(x)$ are Dirac Feynman propagators and are given in (A.13) in Appendix A. Now let us substitute these results back in to (5.51) this gives

$$\text{Im}\left\{ i\int d^4x \langle T[Q_m(x)Q_n(0)]\rangle^{mix}_p \right\} = Z_F \text{Im}\left[i(I_1(m,n) - I_2(m,n) + n \leftrightarrow m)\right] \tag{5.55}$$

After some simplification, the integrals over loop momenta are

$$I_1(m,n) = C^{ijkl}_{uv}\int \frac{d^4k}{(4\pi)^4}\frac{[\bar{u}^i_{s2}\Gamma^B_n(\not{k}+m)\Gamma^A_m v^j_{b2}]}{(k^2-m^2+i\epsilon)}\frac{[\bar{v}^k_{s1}\Gamma^B_m((\not{k}+\not{p}^-)+m)\Gamma^A_n u^l_{b1}]}{((k+p^-)^2-m^2+i\epsilon)} \tag{5.56}$$

$$I_2(m,n) = C^{ijkl}_{uu}\int \frac{d^4k}{(4\pi)^4}\frac{[\bar{v}^k_{s1}\Gamma^B_n(\not{k}+m)\Gamma^A_m v^l_{b2}]}{(k^2-m^2+i\epsilon)}\frac{[\bar{u}^i_{s2}\Gamma^B_m((\not{k}+\not{p}^+)+m)\Gamma^A_n u^j_{b1}]}{((k+p^+)^2-m^2+i\epsilon)} \tag{5.57}$$

where $C^{ijkl}_{uu(v)}$ are colour factors and depend upon n and m. Momentum conserving Dirac Delta functions (see appendix) give the external momentum conservation relations $p^- = p_{b1} - p_{s2} = p_{b2} - p_{s1}$ and $p^+ = p_{b1} + p_{s1} = p_{b2} + p_{s2}$. In the same way as was done in Section 5.1 the integrals in (5.56) and (5.57) are reduced to the product of a scaler loop integral and some tree level matrix elements which are given below. Upon expanding out and taking the imaginary part (5.56) and (5.57) reduce to

$$\begin{aligned}
\text{Im}(iI_1) = \frac{\sqrt{1-\xi}}{192\pi}\big[&(p^-)^2(1-\xi^-)\langle Q^{uv}_V\rangle^{mix}_p + (\xi^-+2)\langle Q^{uv}_{PP}\rangle^{mix}_p \\
&-6m_c(\langle Q^{uv}_{PR}\rangle^{mix}_p - \langle Q^{uv}_{PL}\rangle^{mix}_p) - 12m_c^2\langle Q^{uv}_S\rangle^{mix}_p\big]
\end{aligned} \tag{5.58}$$

$$\text{Im}(iI_2) = \frac{\sqrt{1-\xi}}{192\pi}\big[(p^+)^2(1-\xi^+)\langle Q^{uu}_V\rangle^{mix}_p + (\xi^+2)\langle Q^{uu}_{PP}\rangle^{mix}_p$$

$$-6m_c(\langle Q^{uu}_{PR}\rangle^{mix}_p - \langle Q^{uu}_{PL}\rangle^{mix}_p) - 12m_c^2\langle Q^{uu}_S\rangle^{mix}_p\big] \tag{5.59}$$

where $\xi^{\pm}$ are defined as $\xi^{\pm} = \frac{4m_c^2}{(p^{\pm})^2}$, and the matrix elements $\langle Q^{xy}_X\rangle^{mix}_p$ with $x, y = uu, uv$ and $X \in \{V, PP, PR, PL, S\}$ are comprised of spinors and Dirac structure and include colour factors, colour indices and dependence upon n, m are suppressed for clarity. In fact we can further simplify (5.58) and (5.59) as in this work we do not keep terms of $\mathcal{O}(\frac{m_s}{m_b})$ or higher. Expanding the external momenta in inverse powers of the b quark mass gives

$$\frac{(p^-)^2}{m_b^2} = 1 + \frac{m_s^2}{m_b^2} - \frac{2p_{b1}\cdot p_{s2}}{m_b^2} \tag{5.60}$$

$$\frac{(p^+)^2}{m_b^2} = 1 + \frac{m_s^2}{m_b^2} + \frac{2p_{b1}\cdot p_{s1}}{m_b^2} \tag{5.61}$$

In this work we approximate $(p^+)^2 = (p^-)^2 \approx p_b^2$ and this gives $\xi^+ = \xi^- = \xi \approx 4\frac{m_c^2}{m_b^2}$. For the lhs, the master integral is

$$\begin{aligned}\mathrm{Im}(iI(m,n)) = \frac{\sqrt{1-\xi}}{96\pi}\big[&p_b^2(1-\xi)\langle Q_V\rangle^{mix}_p + (\xi+2)\langle Q_{PP}\rangle^{mix}_p \\ &-6m_c(\langle Q_{PR}\rangle^{mix}_p - \langle Q_{PL}\rangle^{mix}_p) - 12m_c^2\langle Q_S\rangle^{mix}_p\big]\end{aligned} \tag{5.62}$$

where a symmetry factor of 2 has been included as the above expression is symmetric under interchange of labels $n \leftrightarrow m$. Finally, taking the imaginary part, the result for the lhs of (5.49) in terms of perturbative quantities is

$$\begin{aligned}\mathrm{Im}\left\{i\int d^4x\langle T[Q_m(x)Q_n(0)]\rangle^{mix}_p\right\} = \frac{\sqrt{\xi-1}}{96\pi}\big[&p^2(1-\xi)\langle Q_V(m,n)\rangle^{mix}_p \\ &+(\xi+2)\langle Q_{PP}(m,n)\rangle^{mix}_p \\ &-6m_c(\langle Q_{PR}(m,n)\rangle^{mix}_p - \langle Q_{PL}(m,n)\rangle^{mix}_p) \\ &-12m_c^2\langle Q_S(m,n)\rangle^{mix}_p\big].\end{aligned} \tag{5.63}$$

When using the above expression and performing the reduction of Dirac matrices using their anti commuting properties, the terms dependent upon external momentum may be reduced using the equations of motion for the b and s quark spinor fields. These are

$$(\not{p}_b - m_b)u_b = 0 \qquad (\not{p}_b + m_b)v_b = 0, \tag{5.64}$$

$$\bar{u}_s(\not{p}_s - m_s) = 0 \qquad \bar{v}_s(\not{p}_s + m_s) = 0. \tag{5.65}$$

Again, neglecting the mass of the strange quark achieves simplification and in addition, we do not keep terms dependent upon the strange quark momentum - these lead to higher dimensional operators but are also proportional again to the strange quark mass (see operator basis definitions (R operators)). The dictionary for the above quantities is given below in table 5.1, where colour indices on spinors and colour factors $C^{xy}, xy = uu, uv$ have again been suppressed for clarity.

Table 5.1: Intermediate bilinears : Mixing

Quantity	Expression
$\langle Q_V(m,n)\rangle_p^{mix}$	$C^{uv}(\bar{u}_{s2}\Gamma_n^B\gamma_\nu\Gamma_m^A v_{b2})(\bar{v}_{s1}\Gamma_m^B\gamma^\nu\Gamma_n^A u_{b1}) - C^{uu}(\bar{u}_{s2}\Gamma_n^B\gamma_\nu\Gamma_m^A u_{b1})(\bar{v}_{s1}\Gamma_m^B\gamma^\nu\Gamma_n^A v_{b2})$
$\langle Q_P(m,n)\rangle_p^{mix}$	$C^{uv}(\bar{u}_{s2}\Gamma_n^B\not{p}\Gamma_m^A v_{b2})(\bar{v}_{s1}\Gamma_m^B\not{p}\Gamma_n^A u_{b1}) - C^{uu}(\bar{u}_{s2}\Gamma_n^B\not{p}\Gamma_m^A u_{b1})(\bar{v}_{s1}\Gamma_m^B\not{p}\Gamma_n^A v_{b2})$
$\langle Q_{PL}(m,n)\rangle_p^{mix}$	$C^{uv}(\bar{u}_{s2}\Gamma_n^B\not{p}\Gamma_m^A v_{b2})(\bar{v}_{s1}\Gamma_m^B\Gamma_n^A u_{b1})) - C^{uu}(\bar{u}_{s2}\Gamma_n^B\Gamma_m^A u_{b1})(\bar{v}_{s1}\Gamma_m^B\not{p}\Gamma_n^A v_{b2})$
$\langle Q_{PR}(m,n)\rangle_p^{mix}$	$C^{uv}(\bar{u}_{s2}\Gamma_n^B\Gamma_m^A v_{b2})(\bar{v}_{s1}\Gamma_m^B\not{p}\Gamma_n^A u_{b1}) - C^{uu}(\bar{u}_{s2}\Gamma_n^B\Gamma_m^A u_{b1})(\bar{v}_{s1}\Gamma_m^B\not{p}\Gamma_n^A v_{b2})$
$\langle Q_S(m,n)\rangle_p^{mix}$	$C^{uv}(\bar{u}_{s2}\Gamma_n^B\Gamma_m^A v_{b2})(\bar{v}_{s1}\Gamma_m^B\Gamma_n^A u_{b1}) - C^{uu}(\bar{u}_{s2}\Gamma_n^B\Gamma_m^A u_{b1})(\bar{v}_{s1}\Gamma_m^B\Gamma_n^A v_{b2}))$

Evaluating (5.63) for each n, m results in a new expression in terms of partonic matrix elements of $\Delta B = 2$ operators.

$$\mathrm{Im}\left\{i\int d^4x\langle T[Q_m(x)Q_n(0)]\rangle_p^{mix}\right\} = \frac{m_b^2}{16\pi}\left[G(m,n)(z)\langle Q\rangle_p^{mix} + F(m,n)(z)\langle\tilde{Q}_S\rangle_p^{mix}\right]. \tag{5.66}$$

Now the dependence upon m and n has been placed into the coefficients $G(m,n)$ and $F(m,n)$ and depending upon the different combination of Dirac structures these will be proportional to one of two operator matrix elements which are identified as in Table 5.2

Table 5.2: Spinorial form of $\Delta B = 2$ matrix elements

Quantity	Expression
$\langle Q\rangle_p^{mix}$	$2C^{uv}((\bar{u}_{s2}\gamma_\nu(1-\gamma^5)v_{b2})(\bar{v}_{s1}\gamma^\nu(1-\gamma^5)u_{b1})$ $-C^{uu}(\bar{u}_{s2}\gamma_\nu(1-\gamma^5)u_{b1})((\bar{v}_{s1}\gamma^\nu(1-\gamma^5)v_{b2}))$
$\langle Q_S\rangle_p^{mix}$	$2C^{uv}((\bar{u}_{s2}(1+\gamma^5)v_{b2})(\bar{v}_{s1}(1+\gamma^5)u_{b1}) - C^{uu}(\bar{u}_{s2}(1+\gamma^5)u_{b1})((\bar{v}_{s1}(1+\gamma^5)v_{b2}))$

To summarise the calculation steps

1. we evaluate the LHS of (5.49) using equations of motion and anti commuting properties of Dirac matrices for each m, n

2. match this onto the RHS to obtain the coefficients $F(m,n), G(m,n)$ for each m,n

3. Return to the full expression for Γ_{12} and identify the perturbative matrix elements with the non perturbative ones and use non perturbative methods to express the evaluation of these.

Expressing Γ_{12} in terms of non perturbative objects having performed the integration and Dirac reduction we find

$$\Gamma_{12}^{c\bar{c}} = \frac{G_F^2 V_{cb}^2 (V_{cs}^*)^2 m_b^2}{4 M_B \pi} \left[G(\xi)\langle Q \rangle + F(\xi)\langle \tilde{Q}_S \rangle \right] + \mathcal{O}\left(\frac{m_s}{m_b}\right) + \mathcal{O}(\alpha_s) \tag{5.67}$$

The coefficients $F(\xi)$ and $G(\xi)$ are sums over individual coefficients which depend upon the m,n operators inserted.

$$F(\xi) = \sum_{m=1}^{20} \sum_{n=m}^{20} F_{m,n}^{(0)}(\xi) C_m^c C_n^c - F_{SM}^{(0)} + \mathcal{O}(\alpha_s) \tag{5.68}$$

$$G(\xi) = \sum_{m=1}^{20} \sum_{n=m}^{20} G_{m,n}^{(0)}(\xi) C_m^c C_n^c - G_{SM}^{(0)} + \mathcal{O}(\alpha_s) \tag{5.69}$$

At leading order and neglecting dimension 7 operators, the two primed and unprimed sectors do not mix. I.e. there are not terms in (5.67) proportional to combinations of Wilson Coefficients such as $C_m^c C_n^{c'}$ or $C_m^{c'} C_n^c$.
Below are given the coefficients $F_{m,n}^{(0)}$, and $G_{m,n}^{(0)}$ with $\xi = \frac{4m_c^2}{m_b^2}$, and following this is the prescription for obtaining the further coefficients not given below, which are associated with terms quadratic in the primed Wilson coefficients. To reconstruct (5.67), substitute the below coefficients and the further set obtained through relations (5.70) and (5.71), in to (5.68) and (5.69) and subtract off all terms quadratic in coefficients $C_i^{SM} C_j^{SM} \quad i,j = 1,2$. This is necessary to avoid over counting because the SM part of the observables will already be included in Γ_{12}^{SM}.

$F^{(0)}_{1,1} = \frac{N_c}{12}\sqrt{1-\xi}(\xi+2)$ $F^{(0)}_{1,2} = \frac{1}{6}\sqrt{1-\xi}(\xi+2)$ $F^{(0)}_{2,2} = -\frac{1}{12}\sqrt{1-\xi}(\xi+2)$

$F^{(0)}_{3,3} = \frac{N_c}{48}\sqrt{1-\xi}(\xi+2)$ $F^{(0)}_{3,4} = \frac{1}{24}\sqrt{1-\xi}(\xi+2)$ $F^{(0)}_{4,4} = -\frac{1}{48}\sqrt{1-\xi}(\xi+2)$

$F^{(0)}_{5,7} = \frac{N_c}{4}\sqrt{1-\xi}(\xi-2)$ $F^{(0)}_{5,8} = \frac{1}{4}\sqrt{1-\xi}(\xi-2)$ $F^{(0)}_{5,9} = 3N_c\sqrt{1-\xi}(\xi-2)$

$F^{(0)}_{5,10} = 3\sqrt{1-\xi}(\xi-2)$ $F^{(0)}_{6,7} = \frac{1}{4}\sqrt{1-\xi}(\xi-2)$ $F^{(0)}_{6,8} = -\frac{1}{4}\sqrt{1-\xi}(\xi-2)$

$F^{(0)}_{6,9} = 3N_c\sqrt{1-\xi}(\xi-2)$ $F^{(0)}_{6,10} = -3\sqrt{1-\xi}(\xi-2)$

$F^{(0)}_{1,5} = -\frac{1}{2}N_c\sqrt{\xi(1-\xi)}$ $F^{(0)}_{1,6} = -\frac{1}{2}\sqrt{\xi(1-\xi)}$ $F^{(0)}_{1,9} = 2N_c\sqrt{\xi(1-\xi)}$

$F_{1,10} = 2\sqrt{\xi(1-\xi)}$ $F^{(0)}_{2,5} = -\frac{1}{2}\sqrt{\xi(1-\xi)}$ $F^{(0)}_{2,6} = \frac{1}{2}\sqrt{\xi(1-\xi)}$

$F^{(0)}_{2,9} = 2\sqrt{\xi(1-\xi)}$ $F^{(0)}_{2,10} = -2\sqrt{\xi(1-\xi)}$ $F^{(0)}_{3,5} = -\frac{N_c}{4}\sqrt{\xi(1-\xi)}$

$F^{(0)}_{3,6} = -\frac{1}{4}\sqrt{\xi(1-\xi)}$ $F^{(0)}_{3,7} = \frac{N_c}{8}\sqrt{\xi(1-\xi)}$ $F^{(0)}_{3,8} = \frac{1}{8}\sqrt{\xi(1-\xi)}$

$F^{(0)}_{3,9} = \frac{N_c}{2}\sqrt{\xi(1-\xi)}$ $F^{(0)}_{3,10} = \frac{1}{2}\sqrt{\xi(1-\xi)}$ $F^{(0)}_{4,5} = -\frac{1}{4}\sqrt{\xi(1-\xi)}$

$F^{(0)}_{4,6} = \frac{1}{4}\sqrt{\xi(1-\xi)}$ $F^{(0)}_{4,7} = \frac{1}{8}\sqrt{\xi(1-\xi)}$ $F^{(0)}_{4,8} = -\frac{1}{8}\sqrt{\xi(1-\xi)}$

$F^{(0)}_{4,9} = \frac{1}{2}\sqrt{\xi(1-\xi)}$ $F^{(0)}_{4,10} = -\frac{1}{2}\sqrt{\xi(1-\xi)}$ $F^{(0)}_{5,5} = \frac{N_c}{2}\sqrt{1-\xi}\xi$

$F^{(0)}_{5,6} = \sqrt{1-\xi}\xi$ $F^{(0)}_{6,6} = -\frac{1}{2}\xi\sqrt{1-\xi}$ $F^{(0)}_{7,7} = \frac{N_c}{16}\sqrt{1-\xi}\xi$

$F^{(0)}_{7,8} = \frac{1}{8}\sqrt{1-\xi}\xi$ $F^{(0)}_{7,9} = \frac{N_c}{2}\xi\sqrt{1-\xi}$ $F^{(0)}_{7,10} = \frac{1}{2}\sqrt{1-\xi}\xi$

$F^{(0)}_{8,8} = -\frac{1}{16}\sqrt{1-\xi}\xi$ $F^{(0)}_{8,9} = \frac{1}{2}\xi\sqrt{1-\xi}$ $F^{(0)}_{8,10} = -\frac{1}{2}\sqrt{1-\xi}\xi$

$F^{(0)}_{9,9} = 5N_c\sqrt{1-\xi}\xi$ $F^{(0)}_{9,10} = 10\xi\sqrt{1-\xi}$ $F^{(0)}_{10,10} = -5\sqrt{1-\xi}\xi$

The coefficients $G^{(0)}_{m,n}$

$G^{(0)}_{1,1} = -\frac{N_c}{12}(1-\xi)^{\frac{3}{2}}$ $G^{(0)}_{1,2} = -\frac{1}{6}(1-\xi)^{\frac{3}{2}}$ $G^{(0)}_{3,3} = -\frac{N_c}{48}(1-\xi)^{\frac{3}{2}}$

$G^{(0)}_{3,4} = -\frac{1}{24}(1-\xi)^{\frac{3}{2}}$ $G^{(0)}_{2,2} = \frac{1}{24}\sqrt{1-\xi}(\xi-4)$ $G^{(0)}_{4,4} = \frac{1}{96}\sqrt{1-\xi}(\xi-4)$

$G^{(0)}_{5,7} = \frac{N_c}{8}\sqrt{1-\xi}(\xi-2)$ $G^{(0)}_{5,8} = \frac{1}{8}\sqrt{1-\xi}(\xi-2)$ $G^{(0)}_{5,9} = \frac{3N_c}{2}\sqrt{1-\xi}(\xi-2)$

$G^{(0)}_{5,10} = \frac{3}{2}\sqrt{1-\xi}(\xi-2)$ $G^{(0)}_{6,7} = \frac{1}{8}\sqrt{1-\xi}(\xi-2)$ $G^{(0)}_{6,9} = \frac{3}{2}\sqrt{1-\xi}(\xi-2)$

$G^{(0)}_{1,3} = \frac{N_c}{8}\sqrt{1-\xi}\xi$ $G^{(0)}_{1,4} = \frac{1}{8}\sqrt{1-\xi}\xi$ $G^{(0)}_{2,3} = \frac{1}{8}\sqrt{1-\xi}\xi$

$G^{(0)}_{2,4} = \frac{1}{8}\sqrt{1-\xi}\xi$ $G^{(0)}_{5,5} = \frac{N_c}{4}\sqrt{1-\xi}\xi$ $G^{(0)}_{5,6} = \frac{1}{2}\sqrt{1-\xi}\xi$

$G^{(0)}_{7,9} = \frac{N_c}{2}\sqrt{1-\xi}\xi$ $G^{(0)}_{7,10} = \frac{1}{2}\sqrt{1-\xi}\xi$ $G^{(0)}_{8,8} = -\frac{1}{32}\sqrt{1-\xi}\xi$

$G^{(0)}_{8,9} = \frac{1}{2}\sqrt{1-\xi}\xi$ $G^{(0)}_{8,10} = \frac{1}{4}\sqrt{1-\xi}\xi$ $G^{(0)}_{9,9} = 2N_c\sqrt{1-\xi}\xi$

$G^{(0)}_{9,10} = 4\sqrt{1-\xi}\xi$ $G^{(0)}_{10,10} = -\frac{1}{2}\sqrt{1-\xi}\xi$ $G^{(0)}_{1,6} = -\frac{1}{4}\sqrt{\xi(1-\xi)}$

$G^{(0)}_{1,8} = \frac{1}{8}\sqrt{\xi(1-\xi)}$ $G^{(0)}_{1,9} = \frac{N_c}{2}\sqrt{\xi(1-\xi)}$ $G^{(0)}_{1,10} = \frac{1}{2}\sqrt{\xi(1-\xi)}$

$G^{(0)}_{2,5} = -\frac{1}{4}\sqrt{\xi(1-\xi)}$ $G^{(0)}_{2,7} = \frac{1}{8}\sqrt{\xi(1-\xi)}$ $G^{(0)}_{2,8} = \frac{1}{8}\sqrt{\xi(1-\xi)}$

$G^{(0)}_{2,9} = \frac{1}{2}\sqrt{\xi(1-\xi)}$ $G^{(0)}_{2,10} = -\frac{1}{2}\sqrt{\xi(1-\xi)}$ $G^{(0)}_{3,5} = -\frac{N_c}{8}\sqrt{\xi(1-\xi)}$

$G^{(0)}_{3,6} = -\frac{1}{8}\sqrt{\xi(1-\xi)}$ $G^{(0)}_{3,9} = \frac{N_c}{2}\sqrt{\xi(1-\xi)}$ $G^{(0)}_{3,10} = \frac{1}{2}\sqrt{\xi(1-\xi)}$

$$G^{(0)}_{4,5} = -\tfrac{1}{8}\sqrt{\xi(1-\xi)} \qquad G^{(0)}_{4,8} = -\tfrac{1}{16}\sqrt{\xi(1-\xi)} \qquad G^{(0)}_{4,9} = \tfrac{1}{2}\sqrt{\xi(1-\xi)}$$
$$G^{(0)}_{4,10} = \tfrac{1}{4}\sqrt{\xi(1-\xi)} \qquad G^{(0)}_{1,5} = -\tfrac{N_c}{4}\sqrt{\xi(1-\xi)} \qquad G^{(0)}_{1,7} = \tfrac{N_c}{8}\sqrt{\xi(1-\xi)}$$

To obtain other coefficients use the prescription

$$F^{(0)}_{m,n} = \begin{cases} F^{(0)}_{m-10,n-10} & n > 10, m > 10 \\ 0 & \text{otherwise} \end{cases} \tag{5.70}$$

$$G^{(0)}_{m,n} = \begin{cases} G^{(0)}_{m-10,n-10} & n > 10, m > 10 \\ 0 & \text{otherwise} \end{cases} \tag{5.71}$$

and all others are zero.

5.3.2 Matrix elements of $\Delta B = 2$ basis

We use the $\Delta B = 2$ basis in accordance with the SM calculations performed in [84], [85], [86]

$$Q = (\bar{s}^\alpha \gamma_\mu (1-\gamma_5) b^\alpha) \times (\bar{s}^\beta \gamma^\mu (1-\gamma_5) b^\beta) \tag{5.72}$$
$$Q_S = (\bar{s}^\alpha (1+\gamma_5) b^\alpha) \times (\bar{s}^\beta (1+\gamma_5) b^\beta) \tag{5.73}$$
$$\tilde{Q}_S = (\bar{s}^\alpha (1+\gamma_5) b^\beta) \times (\bar{s}^\beta (1+\gamma_5) b^\alpha) \tag{5.74}$$
$$R_1 = \frac{m_s}{m_b} (\bar{s}^\alpha (1+\gamma^5) b^\alpha) \times (\bar{s}^\beta (1-\gamma^5) b^\beta) \tag{5.75}$$
$$\tilde{R}_1 = \frac{m_s}{m_b} (\bar{s}^\alpha (1+\gamma^5) b^\beta) \times (\bar{s}^\beta (1-\gamma^5) b^\alpha) \tag{5.76}$$

However, as we do not include $\mathcal{O}(\frac{m_s}{m_b})$ contributions which correspond to the $d = 7$ operators arising at $\mathcal{O}\left(\frac{1}{m_b^4}\right)$ in the HQE, so the operator matrix elements of R_1 and $\tilde{R}_1$ are not required. As found in [67] the above set of operators is not independent and we can eliminate Q_S through

$$Q_S = -\tilde{Q}_S - \frac{1}{2} Q + \mathcal{O}\left(\frac{\Lambda}{m_b}\right). \tag{5.77}$$

The non perturbative matrix elements of the operators Q and $\tilde{Q}_S$ are parameterized in terms of decay constants and bag factors and are given by

$$\langle Q \rangle = \frac{8}{3} m_B^2 f_B^2 B, \qquad \langle \tilde{Q}_S \rangle = \frac{1}{3} m_B^2 f_{B_s}^2 \tilde{B}', \tag{5.78}$$

with the modified bag parameter defined in [38] as

$$B'(\mu) = \frac{M_{B_s}^2}{(\overline{m}_b(\overline{m}_b) + \overline{m}_s(\overline{m}_b))^2} B(\mu). \tag{5.79}$$

5.3.3 The width difference $\Delta\Gamma_s$

Using the conventions of [38], in the SM the width difference $\Delta\Gamma_s$ may be expressed as

$$\Delta\Gamma_s = 2|\Gamma_{12}^s| \cos\theta_{12}^s, \tag{5.80}$$

where the relative phase is defined in (2.79). For phenomenological purposes as we are considering NP only in Γ_{12}^s, it is more convenient to use the following form, in which we split the SM and NP parts as defined in (5.44) and assume a SM like M_{12}^s

$$\Delta\Gamma_s = -2\mathrm{Re}\left((\Gamma_{12}^{SM} + \Gamma_{12}^{c\bar{c}}) e^{-i\mathrm{Arg}(M_{12}^s)}\right) \tag{5.81}$$

with the SM value of $e^{i\mathrm{Arg}(M_{12}^{s,SM})} = \frac{V_{ts}V_{tb}^*}{V_{ts}^*V_{tb}}$ as given in [38].

5.3.4 The flavour specific asymmetry a_{sl}^s

Using the same conventions and as found in [**?**], in the SM the flavour specific CP asymmetry may be expressed again in terms of the mixing angle θ_{12} as

$$a_{fs}^s = \left|\frac{\Gamma_{12}^s}{M_{12}^s}\right| \sin\theta_{12}. \tag{5.82}$$

Again, to separate cleanly the SM and NP contributions of Γ_{12} and for ease of calculation in the study of complex Wilson coefficients we use the following expression, again assuming SM like M_{12}^s and experimentally determined value of ΔM. It is

$$a_{fs}^s = \frac{2\mathrm{Im}\left((\Gamma_{12}^{SM} + \Gamma_{12}^{c\bar{c}}) e^{-i\mathrm{Arg}(M_{12}^s)}\right)}{\Delta M}. \tag{5.83}$$

5.4 Lifetime ratio $\left(\frac{\tau_{B_s}}{\tau_{B_d}}\right)$

5.4.1 Calculation of the total inclusive width Γ_s

As is shown in the decay rate matrix in (2.60), the diagonal elements of the decay rate matrix in the Hamiltonian governing mixing and decay of the neutral B mesons is the total width Γ_{B_s}. We can compute the contribution of the $b \to c\bar{c}s$ operator basis to this width using again the HQE, to which the dimension 6 operators enter at $\mathcal{O}\left(\frac{1}{m_b^3}\right)$ as shown in (2.184) with $H_Q = B_s^{(0)}$. The total inclusive width is again expressed as the imaginary part of the forward matrix element of the transition operator

$$\Gamma_{B_s} = \frac{1}{2M_B}\langle B_s^{(0)} \mid \mathcal{T} \mid B_s^{(0)}\rangle. \tag{5.84}$$

The ratio of the B_s^0 meson to B_d^0 meson lifetimes is proportional to the ratio of the B_d^0 meson to B_s^0 meson total widths and so we may express it as

$$\begin{aligned}\frac{\tau_{B_s}}{\tau_{B_d}} &= 1 + \frac{\Gamma_{B_d} - \Gamma_{B_s}}{\Gamma_{B_s}} = 1 + \frac{\Gamma_{B_d}^{SM} - \Gamma_{B_s}^{SM}}{\Gamma_{B_s}^{SM}} - \frac{\Gamma_{B_s}^{c\bar{c}}}{\Gamma_{B_s}} \\ &= \frac{\tau_{B_s}^{SM}}{\tau_{B_d}^{SM}} - \tau_{B_s}^{exp}\Gamma_{B_s}^{c\bar{c}}\end{aligned} \tag{5.85}$$

In (5.85) we assume no BSM effects in Γ_{B_d} and for the part to which we introduce the BSM effects of our operators we use the experimental value of the B_s meson lifetime. In terms of the individual operator insertions, the terms in (5.45) which will contribute to the transition operator for the B_s lifetime are the second and third terms

$$\begin{aligned}\mathcal{T}\mid_{\tau_{B_s}^{c\bar{c}}} = 8G_F^2 \mid V_{cb}\mid^2 \mid V_{cs}\mid^2 \mathrm{Im}\Bigg\{ i\int d^4x \sum_{m=1}^{20}\sum_{n=1}^{20} \Big(C_m C_n^* T\left[Q_m^c(x)Q_n^{c\dagger}(0)\right] \\ + C_m^* C_n T\left[Q_m^{c\dagger}(x)Q_n^c(0)\right]\Big)\Bigg\}\end{aligned} \tag{5.86}$$

However, the second term in (5.86) can be simplified using translational invariance, under the assumption that the initial and final B_s meson momenta are equal. Take the matrix element of the integral in the second term in (5.86), sandwiched between between meson initial and final B_s^0 states

$$I = \int d^4x \sum_{m=1}^{20}\sum_{n=1}^{20} C_m^* C_n \langle B_s^0 | T\left[Q_m^{c\dagger}(x)Q_n^c(0)\right] | B_s^0\rangle \tag{5.87}$$

and make a change of variables where $x^\mu \to x'^\mu = -x^\mu$, then the Jacobean is

$$\begin{aligned}\mathcal{J} &= \text{Det}\left[\frac{\partial x'^\mu}{\partial x^\nu}\right] \\ &= \text{Det}(\text{Diag}(-1,-1,-1,-1)) \\ &= 1 \end{aligned} \tag{5.88}$$

so $d^4x \to d^4x' = d^4x$. Then I becomes

$$I = \int d^4x \sum_{m=1}^{20}\sum_{n=1}^{20} C_m^* C_n \langle B_s^0 | T\left[Q_m^{c\dagger}(-x) Q_n^c(0)\right] | B_s^0\rangle \tag{5.89}$$

Inserting the translation operator defined through

$$U(a) = e^{-iPa} \qquad \text{with} \qquad U(a)\phi(x)U^\dagger(a) = \phi(x+a) \tag{5.90}$$

$$U^\dagger(a) = e^{iPa} \qquad \text{with} \qquad U^\dagger(a)\phi(x)U(a) = \phi(x-a) \tag{5.91}$$

whose action on the B meson momentum eigenstates is

$$U(x)|B_s^0\rangle = e^{-iPx}|B_s^0\rangle = |B_s^0\rangle e^{-ipx} \tag{5.92}$$

$$\begin{aligned} I &= \int d^4x \sum_{m=1}^{20}\sum_{n=1}^{20} C_m^* C_n \langle B_s^0 | T\left[U^\dagger(x)U(x)Q_m^{c\dagger}(-x)U^\dagger(x)U(x)Q_n^c(0)U^\dagger(x)U(x)\right] | B_s^0\rangle \\ &= \int d^4x \sum_{m=1}^{20}\sum_{n=1}^{20} C_m^* C_n \langle B_s^0 | e^{iPx} T\left[Q_m^{c\dagger}(0) Q_n^c(x))\right] e^{-iPx} | B_s^0\rangle \\ &= \int d^4x e^{i(p-p)x} \sum_{m=1}^{20}\sum_{n=1}^{20} C_m^* C_n \langle B_s^0 | T\left[Q_n^c(x) Q_m^{c\dagger}(0)\right] | B_s^0\rangle \\ &= \int d^4x \sum_{n=1}^{20}\sum_{m=1}^{20} C_n^* C_m \langle B_s^0 | T\left[Q_m^c(x) Q_n^{c\dagger}(0)\right] | B_s^0\rangle \end{aligned} \tag{5.93}$$

In the last step it was used that dummy indices which are summed over can be relabelled, and it is assumed that the initial and final B meson momenta are equal. So, then

$$\mathcal{T}|_{\mathcal{T}_{B_s}^{c\bar{c}}} = 16 G_F^2 \mid V_{cb} \mid^2 \mid V_{cs} \mid^2 \text{Im}\left\{ i \int d^4x \sum_{m=1}^{20}\sum_{n=1}^{20} C_m C_n^* T\left[Q_m^c(x) Q_n^{c\dagger}(0)\right]\right\} \tag{5.94}$$

and the quantity which we would like to calculate, and which contributes to the lifetime ratio, is then

$$\Gamma_{B_s}^{c\bar{c}} = \sum_{m=1}^{20}\sum_{n=1}^{20}\tilde{\mathcal{N}}_{m,n}\langle B_s \mid \mathrm{Im}\left\{ i\int d^4x T\left[Q_m(x)Q_n^{\dagger}(0)\right]\right\} \mid B_s\rangle. \tag{5.95}$$

$$\tilde{\mathcal{N}}_{mn} = \frac{8G_F^2 \mid V_{cb}\mid^2 \mid V_{cs}\mid^2}{M_B} C_m^c C_n^{c*} \tag{5.96}$$

The calculation is carried out in a similar way to the calculation which was performed to obtain Γ_{12} except the resulting basis of $d = 6$ operators will be of the $\Delta B = 0$ quark structure. The RHS of (5.95) is matched onto a linear combination of coefficients and $\Delta B = 0$ opaerator matrix elements

$$\begin{aligned}\langle B_s^0|\mathrm{Im}\left\{ i\int d^4x T[Q_m^c(x)Q_n^{c\dagger}(0)]\right\}|B_s^0\rangle = \frac{m_b^2}{16\pi}\Big[&H(m,n)(z)\langle Q_{LL}\rangle + \tilde{H}(m,n)(z)\langle\tilde{Q}_{LL}\rangle \\ &+K(m,n)(z)\langle Q_{LR}\rangle + \tilde{K}(m,n)(z)\langle\tilde{Q}_{LR}\rangle \\ &+H^S(m,n)(z)\langle Q_{LL}^S\rangle + \tilde{H}^S(m,n)(z)\langle\tilde{Q}_{LL}^S\rangle \\ &+K^S(m,n)(z)\langle Q_{LR}^S\rangle + \tilde{K}^S(m,n)(z)\langle\tilde{Q}_{LR}^S\rangle\Big].\end{aligned} \tag{5.97}$$

Define the short hand notation for the matrix element of operator $\hat{A}$ between partonic $\bar{b}$ and s initial and final states as

$$\langle\hat{A}\rangle_p^{lt} := \langle\bar{b}(p_{b_1}), s(p_{s_1}) \mid \hat{A} \mid \bar{b}(p_{b_2}), s(p_{s_2})\rangle \tag{5.98}$$

where p stands for partonic and $\hat{A}$ is any operator of our considered basis, and the superscript "lt" indicates that the initial and final states are both those quark level states associated with a $B_s^{(0)}$ meson. There is only one contraction possible for the double insertion between these initial and final states and so

$$\mathrm{Im}\left\{ i\int d^4x\langle T[Q_m^c(x)Q_n^{c\dagger}(0)]\rangle_p^{lt}\right\} = Z_F\mathrm{Im}\left[i(I(m,n)\right] \tag{5.99}$$

where the imaginary part of the integration over loop momenta yields a similar set of intermediate spinor bilinears as shown below and given explicitly in table 5.4.

$$\begin{aligned}\mathrm{Im}(iI(m,n)) = \frac{\sqrt{1-\xi}}{192\pi}\Big[&p^2(1-\xi)\langle\mathcal{O}_V\rangle_p^{lt} + (\xi+2)\langle\mathcal{O}_{PP}\rangle_p^{lt} - 6m_c(\langle\mathcal{O}_{PR}\rangle_p^{lt} - \langle\mathcal{O}_{PL}\rangle_p^{lt}) \\ &-12m_c^2\langle\mathcal{O}_S\rangle_p^{lt}\Big]\end{aligned} \tag{5.100}$$

Table 5.4: Intermediate bilinears : Lifetimes

$\langle\mathcal{O}_V\rangle_p^{lt} = (\bar{v}_{b1}\Gamma_n^{B\dagger}\gamma_\nu\Gamma_m^A v_{b2})(\bar{u}_{s2}\Gamma_m^B\gamma^\nu\Gamma_n^{A\dagger}u_{s1})$	$\langle\mathcal{O}_P\rangle_p^{lt} = (\bar{v}_{b1}\Gamma_n^{B\dagger}\not{p}\Gamma_m^A v_{b2})(\bar{v}_{s1}\Gamma_m^B\not{p}\Gamma_n^{A\dagger}u_{s1})$
$\langle\mathcal{O}_{PL}\rangle_p^{lt} = (\bar{v}_{b1}\Gamma_n^{B\dagger}\not{p}\Gamma_m^A v_{b2})(\bar{v}_{s1}\Gamma_m^B\Gamma_n^A u_{s1}))$	$\langle\mathcal{O}_{PR}\rangle_p^{lt} = (\bar{v}_{b1}\Gamma_n^{B\dagger}\Gamma_m^A v_{b2})(\bar{v}_{s1}\Gamma_m^B\not{p}\Gamma_n^{A\dagger}u_{s1})$
$\langle\mathcal{O}_S\rangle_p^{lt} = (\bar{v}_{b1}\Gamma_n^{B\dagger}\Gamma_m^A v_{b2})(\bar{v}_{s1}\Gamma_m^B\Gamma_n^{A\dagger}u_{s1})$	

Again after performing the Dirac reduction, applying the equations of motion and using the fierz relations given in Appendix A the result is a linear combination of the following operator matrix elements in table 5.5.

Table 5.5: Spinorial form of $\Delta B = 0$ perturbative matrix elements

$\langle\mathcal{O}_{LL}\rangle_p^{lt} = (\bar{v}_{b1}\gamma_\mu P_L u_{s1})(\bar{u}_{s2}\gamma^\mu P_L v_{b2})$	$\langle\tilde{\mathcal{O}}_{LL}\rangle_p^{lt} = (\bar{v}_{b1}^\alpha\Gamma_\mu P_L u_{s1}^\beta)(\bar{u}_{s2}^\beta\gamma^\mu P_L v_{b2}^\alpha)$
$\langle\mathcal{O}_{LR}\rangle_p^{lt} = (\bar{v}_{b1}\gamma_\mu P_L u_{s1})(\bar{u}_{s2}\gamma^\mu P_R v_{b2})$	$\langle\tilde{\mathcal{O}}_{LR}\rangle_p^{lt} = (\bar{v}_{b1}^\alpha\Gamma_\mu P_L u_{s1}^\beta)(\bar{u}_{s2}^\beta\gamma^\mu P_R v_{b2}^\alpha)$
$\langle\mathcal{O}_{LL}^S\rangle_p^{lt} = (\bar{v}_{b1}P_L u_{s1})(\bar{u}_{s2}P_L v_{b2})$	$\langle\tilde{\mathcal{O}}_{LL}^S\rangle_p^{lt} = (\bar{v}_{b1}^\alpha P_L u_{s1}^\beta)(\bar{u}_{s2}^\beta P_L v_{b2}^\alpha)$
$\langle\mathcal{O}_{LR}^S\rangle_p^{lt} = (\bar{v}_{b1}P_L u_{s1})(\bar{u}_{s2}P_R v_{b2})$	$\langle\tilde{\mathcal{O}}_{LR}^S\rangle_p^{lt} = (\bar{v}_{b1}^\alpha P_L u_{s1}^\beta)(\bar{u}_{s2}^\beta P_R v_{b2}^\alpha)$

Having shown the procedure used for calculating the results in perturbation theory, it is now possible to express the full inclusive width in terms of the coefficients calculated through (5.97) and replace the matrix elements of the $\Delta B = 0$ operators which have arisen naturally during the calculation and have been found and are expressed on a perturbative level in table 5.5, with their full hadronic form which need to be calculated using Sum rules. The full result for the inclusive width is then expressed up to $\frac{1}{m_b}$ corrections as

$$\begin{aligned}\Gamma_{B_s}^{c\bar{c}} = \frac{G_F^2|V_{cb}|^2|V_{cs}|^2 m_b^2}{2M_B\pi}\Big[&H(\xi)\langle Q_{LL}\rangle + \tilde{H}(\xi)\langle\tilde{Q}_{LL}\rangle + K(\xi)\langle Q_{LR}\rangle + \tilde{K}(z)\langle\tilde{Q}_{LR}\rangle \\ &+H^S(\xi)\langle Q_{LL}^S\rangle + \tilde{H}^S(\xi)\langle\tilde{Q}_{LL}^S\rangle + K^S(\xi)\langle Q_{LR}^S\rangle \\ &+\tilde{K}^S(\xi)\langle\tilde{Q}_{LR}^S\rangle\Big] + \mathcal{O}\left(\frac{m_s}{m_b}\right) + \mathcal{O}(\alpha_s)\end{aligned} \tag{5.101}$$

$$\begin{aligned}R(\xi) &= \sum_{m=1}^{20}\sum_{n=m}^{20} R_{m,n}^{(0)}(\xi)2\mathrm{Re}(C_m^c(C_n^c)^*) - R_{SM}^{(0)} \\ R^{(S)}(\xi) &\in \{H^{(S)}(\xi), K^{(S)}(\xi), \tilde{H}^{(S)}(\xi), \tilde{K}^{(S)}(\xi)\}\end{aligned} \tag{5.102}$$

Below are listed the coefficients in (5.101) and following this, relations one can use to obtain the remaining coefficients related by symmetry. In (5.102), all parts which are quadratic in the SM Wilson coefficients are once more subtracted. To reconstruct the total width, substitute into (5.102), the coefficients below and use the following rules (5.103) and (5.104) for obtaining the remaining coefficients not listed in the minimal set below. Then one may calculate the CBSM contribution to given in (5.101) to the lifetime ratio in (5.85).

$$H^{(0)}_{1,1} = \tfrac{N_c}{12}\sqrt{1-\xi}(\xi-4) \qquad H^{(0)}_{3,3} = \tfrac{N_c}{48}\sqrt{1-\xi}(\xi-4) \qquad H^{(0)}_{7,7} = -\tfrac{N_c}{48}\sqrt{1-\xi}(\xi+2)$$
$$H^{(0)}_{7,9} = \tfrac{N_c}{6}\sqrt{1-\xi}(\xi+2) \qquad H^{(0)}_{9,9} = -\tfrac{N_c}{3}\sqrt{1-\xi}(\xi+2) \qquad H^{(0)}_{1,3} = \tfrac{N_c}{4}\xi\sqrt{1-\xi}$$
$$H^{(0)}_{1,7} = \tfrac{N_c}{4}\sqrt{\xi(1-\xi)} \qquad H^{(0)}_{1,9} = -N_c\sqrt{\xi(1-\xi)} \qquad H^{(0)}_{3,7} = -\tfrac{N_c}{8}\sqrt{\xi(1-\xi)}$$
$$H^{(0)}_{3,9} = \tfrac{N_c}{2}\sqrt{\xi(1-\xi)} \qquad H^{(0)}_{1,2} = \tfrac{1}{6}\sqrt{1-\xi}(\xi-4) \qquad H^{(0)}_{3,4} = \tfrac{1}{24}\sqrt{1-\xi}(\xi-4)$$
$$H^{(0)}_{7,8} = -\tfrac{1}{24}\sqrt{1-\xi}(\xi+2) \qquad H^{(0)}_{9,10} = -\tfrac{2}{3}\sqrt{1-\xi}(\xi+2) \qquad H^{(0)}_{5,5} = H^{(0)}_{5,6} = 0$$

$$H^{(0)}_{m,n} = 0, m \leq 10, n > 10$$

$$K^{(0)}_{1,13} = -\tfrac{N_c}{12}\sqrt{1-\xi}(\xi-4) \qquad K^{(0)}_{1,11} = -\tfrac{N_c}{2}\xi\sqrt{1-\xi} \qquad K^{(0)}_{3,13} = -\tfrac{N_c}{8}\xi\sqrt{1-\xi}$$
$$K^{(0)}_{3,19} = \tfrac{N_c}{2}\sqrt{\xi(1-\xi)} \qquad K^{(0)}_{7,17} = -\tfrac{N_c}{8}\xi\sqrt{1-\xi} \qquad K^{(0)}_{7,19} = \tfrac{N_c}{2}\xi\sqrt{1-\xi}$$
$$K^{(0)}_{9,19} = -2N_c\xi\sqrt{1-\xi} \qquad K^{(0)}_{3,17} = -\tfrac{N_c}{8}\sqrt{\xi(1-\xi)} \qquad K^{(0)}_{1,17} = \tfrac{N_c}{4}\sqrt{\xi(1-\xi)}$$
$$K^{(0)}_{1,19} = -N_c\sqrt{\xi(1-\xi)}$$

$$K^{(0)}_{m,n} = 0, m, n \leq 10$$

$$H^{S(0)}_{1,13} = -\tfrac{N_c}{6}\sqrt{1-\xi}(\xi+2) \qquad H^{S(0)}_{1,15} = N_c\sqrt{\xi(1-\xi)} \qquad H^{S(0)}_{1,17} = -\tfrac{N_c}{2}\sqrt{\xi(1-\xi)}$$
$$H^{S(0)}_{1,19} = -2N_c\sqrt{\xi(1-\xi)} \qquad H^{S(0)}_{3,15} = \tfrac{N_c}{2}\sqrt{\xi(1-\xi)} \qquad H^{S(0)}_{3,19} = -2N_c\sqrt{\xi(1-\xi)}$$
$$H^{S(0)}_{5,17} = -\tfrac{N_c}{2}\sqrt{1-\xi}(\xi-2) \qquad H^{S(0)}_{5,19} = -6N_c\sqrt{1-\xi}(\xi-2) \qquad H^{S(0)}_{5,15} = -2N_c\xi\sqrt{1-\xi}$$
$$H^{S(0)}_{7,19} = -2N_c\sqrt{1-\xi}\xi \qquad H^{S(0)}_{9,19} = -16N_c\sqrt{1-\xi}\xi$$

$$H^{S(0)}_{m,n} = 0, m, n \leq 10$$

$K^{S(0)}_{9,9} = \frac{2N_c\sqrt{1-\xi}}{3}(28-13\xi)$ $K^{S(0)}_{7,9} = \frac{N_c\sqrt{1-\xi}}{3}(8-5\xi)$ $K^{S(0)}_{3,3} = \frac{N_c}{24}\sqrt{1-\xi}(\xi+2)$

$K^{S(0)}_{1,1} = \frac{N_c}{6}\sqrt{1-\xi}(\xi+2)$ $K^{S(0)}_{1,5} = -N_c\sqrt{\xi(1-\xi)}$ $K^{S(0)}_{1,9} = 4N_c\sqrt{\xi(1-\xi)}$

$K^{S(0)}_{3,5} = -\frac{1}{2}N_c\sqrt{\xi(1-\xi)}$ $K^{S(0)}_{3,7} = \frac{N_c}{4}\sqrt{\xi(1-\xi)}$ $K^{S(0)}_{3,9} = N_c\sqrt{\xi(1-\xi)}$

$K^{S(0)}_{5,7} = -\frac{1}{2}N_c\xi\sqrt{1-\xi}$ $K^{S(0)}_{5,9} = -6N_c\xi\sqrt{1-\xi}$ $K^{S(0)}_{5,5} = -N_c\sqrt{1-\xi}(\xi-2)$

$K^{S(0)}_{7,7} = -\frac{N_c}{24}\sqrt{1-\xi}(\xi-4)$ $K^{S(0)}_{9,10} = \frac{4\sqrt{1-\xi}}{3}(28-13\xi)$ $K^{S(0)}_{3,4} = \frac{1}{12}\sqrt{1-\xi}(\xi+2)$

$K^{S(0)}_{1,2} = \frac{1}{3}\sqrt{1-\xi}(\xi+2)$ $K^{S(0)}_{5,6} = -2\sqrt{1-\xi}(\xi-2)$ $K^{S(0)}_{7,8} = -\frac{1}{12}\sqrt{1-\xi}(\xi-4)$

$K^{S(0)}_{m,n} = 0, m \leq 10, n > 10$

To obtain the other coefficients the following relations hold for the non tilde operators

$$R^{(S)}_{m,n} = \begin{cases} 0 & m,n \quad \text{even} \\ R^{(S)}_{m-10,n-10} & m,n = 11,...20 \\ \frac{1}{N_c}R^{(S)}_{m,n-1} & m \quad \text{odd}, n = m+3,...,20 \quad \text{even} \\ \frac{1}{N_c}R^{(S)}_{m-1,n} & m \quad \text{even}, n \quad \text{odd} \quad n > m \\ R^{(S)}_{n-10,m+10} & m \leq 10, n > 10 \end{cases} \tag{5.103}$$

and the remaining relations which determine the tilde coefficients are associated with colour factors. They are

$$\tilde{R}^{(S)}_{m,n} = \begin{cases} \frac{1}{N_c}R^{(S)}_{m-1,n-1} & m,n \quad \text{even}, \quad n > m \end{cases} \tag{5.104}$$

$\Delta B = 0$ **Basis**

Operators arising in the calculation of the B^0_s lifetime are given below.

$Q_{LL} = (\bar{b}^\alpha\gamma_\mu P_L s^\alpha)(\bar{s}^\beta\gamma^\mu P_L b^\beta)$ $\tilde{Q}_{LL} = (\bar{b}^\alpha\gamma_\mu P_L s^\beta)(\bar{s}^\beta\gamma^\mu P_L b^\alpha)$

$Q_{LR} = (\bar{b}^\alpha\gamma_\mu P_L s^\alpha)(\bar{s}^\beta\gamma^\mu P_R b^\beta)$ $\tilde{Q}_{LR} = (\bar{b}^\alpha\gamma_\mu P_L s^\beta)(\bar{s}^\beta\gamma^\mu P_R b^\alpha)$

$Q^S_{LR} = (\bar{b}^\alpha P_L s^\alpha)(\bar{s}^\beta P_R b^\beta)$ $\tilde{Q}^S_{LR} = (\bar{b}^\alpha P_L s^\beta)(\bar{s}^\beta P_R b^\alpha)$

$Q^S_{LL} = (\bar{b}^\alpha P_L s^\alpha)(\bar{s}^\beta P_L b^\beta)$ $\tilde{Q}^S_{LL} = (\bar{b}^\alpha P_L s^\beta)(\bar{s}^\beta P_L b^\alpha)$

$Q^T_{LL} = (\bar{b}^\alpha\sigma^{\mu\nu} P_L s^\alpha)(\bar{s}^\beta\sigma_{\mu\nu} P_L b^\beta)$ $\tilde{Q}^T_{LL} = (\bar{b}^\alpha\sigma^{\mu\nu} P_L s^\beta)(\bar{s}^\beta\sigma_{\mu\nu} P_L b^\alpha)$

5.4.2 Reduction of $\Delta B = 0$ operators in heavy quark limit

There are a further 10 operators found by taking the parity conjugate of the above set, however the matrix elements of the above operators are found to be equal to those of their parity conjugates. All in all the counting gives 10 independent matrix elements, however the number of linearly independent operator matrix elements between B meson states decreases in the heavy quark limit.

Defining the heavy b quark field as

$$b(x) = e^{-im_b v\cdot x}[b_v(x) + B_v(x)] \tag{5.105}$$

In the heavy quark limit, the $B_v(x)$ field is integrated out of the theory. In order to reduce the number of linearly independent operators arising in the calculation we use the remaining component of the heavy quark field in our $\Delta B = 0$ operators. We work in the fierzed basis expressing our operators generically as

$$Q_\Gamma = (\bar{b}_v \Gamma b_v)(\bar{s}\Gamma s) + \mathcal{O}\left(\frac{1}{m_b}\right), \tag{5.106}$$

with $\Gamma \in \{\mathbb{1}, P_L(R), \gamma_\mu P_{L(R)}, \sigma_{\mu\nu} P_{L(R)}\}$. We form a list of all linearly independent heavy and light bilinears possible. Working in the rest frame of the heavy quark, in the Dirac-Pauli basis we reduce the number of independent heavy bilinears by one and then determine all possible heavy-light operators we can construct which respect the parity symmetry of QCD.

We find that in the heavy quark limit, there are four non vanishing linearly independent $\Delta B = 0$ operators which can be formed from the heavy-light bilinears.

$$\mathcal{H}_1 = (\bar{b}_v b_v)(\bar{s}s) \qquad \mathcal{H}_2 = (\bar{b}_v b_v)(\bar{s}\not{v}s) \tag{5.107}$$

$$\mathcal{H}_3 = (\bar{b}_v \gamma^\mu \gamma^5 b_v)(\bar{s}\gamma^\mu\gamma^5 s) \qquad \mathcal{H}_4 = (\bar{b}_v \sigma^{\mu\nu} b_v)(\bar{s}\sigma^{\mu\nu} s) \tag{5.108}$$

To reduce the number of operators in out chiral basis we express their matrix elements in terms of matrix elements of operators in the basis found in the HQ limit. These are

$$\langle B_s^0|Q_{LL}|B_s^0\rangle = \frac{1}{4}(\langle B_s^0|\mathcal{H}_2|B_s^0\rangle + \langle B_s^0|\mathcal{H}_3|B_s^0\rangle) \tag{5.109}$$

$$\langle B_s^0|Q_{LR}|B_s^0\rangle = -\frac{1}{2}\langle B_s^0|\mathcal{H}_1|B_s^0\rangle \tag{5.110}$$

$$\langle B_s^0|Q_{LR}^S|B_s^0\rangle = \frac{1}{8}(\langle B_s^0|\mathcal{H}_3|B_s^0\rangle - \langle B_s^0|\mathcal{H}_2|B_s^0\rangle) \tag{5.111}$$

$$\langle B_s^0|Q_{LL}^S|B_s^0\rangle = -\frac{1}{16}(\langle B_s^0|\mathcal{H}_4|B_s^0\rangle + 2\langle B_s^0|\mathcal{H}_1|B_s^0\rangle) \tag{5.112}$$

$$\langle B_s^0|Q_{LL}^T|B_s^0\rangle = \frac{1}{4}(\langle B_s^0|\mathcal{H}_4|B_s^0\rangle - 6\langle B_s^0|\mathcal{H}_1|B_s^0\rangle) \tag{5.113}$$

From the above relations we can deduce that the relation we require is

$$\langle B_s^0|Q_{LR}|B_s^0\rangle = \langle B_s^0|Q_{LL}^S|B_s^0\rangle + \frac{1}{4}\langle B_s^0|Q_{LL}^T|B_s^0\rangle. \tag{5.114}$$

The stronger statement that this holds at the operator level is given below

$$Q_{LL}^T = 4(Q_{LR} - Q_{LL}^S) \tag{5.115}$$

and is used to remove the tensor operators Q_{LL}^T and $\tilde{Q}_{LL}^T$ from the above basis thus reducing the number of linearly independent operators from 10 to 8.

Matrix elements

The hadronic matrix elements of the above set of operators, evaluated between B meson states are non-perturbative objects and thus have to be parameterised in some form such that our ignorance of the hadronic effects are hidden in some small number of parameters. Using the colour singlet and colour rearranged operator basis below, the parameters B,$\tilde{B}_i$ are defined following conventions in [87] such that

$$\begin{aligned}
\frac{1}{2M_B}\langle B_s|Q_{LL}|B_s\rangle &= \frac{1}{8}B_1(\mu)f_B^2M_B, & \frac{1}{2M_B}\langle B_s|\tilde{Q}_{LL}|B_s\rangle &= \frac{1}{8}\tilde{B}_1(\mu)f_B^2M_B,\\
\frac{1}{2M_B}\langle B_s|Q_{LR}^s|B_s\rangle &= \frac{1}{8}B_2'(\mu)f_B^2M_B, & \frac{1}{2M_B}\langle B_s|\tilde{Q}_{LR}^s|B_s\rangle &= \frac{1}{8}\tilde{B}_2'(\mu)f_B^2M_B,\\
\frac{1}{2M_B}\langle B_s|Q_{LR}|B_s\rangle &= \frac{1}{8}B_3(\mu)f_B^2M_B, & \frac{1}{2M_B}\langle B_s|\tilde{Q}_{LR}|B_s\rangle &= \frac{1}{8}\tilde{B}_3(\mu)f_B^2M_B,\\
\frac{1}{2M_B}\langle B_s|Q_{LL}^s|B_s\rangle &= \frac{1}{8}B_4'(\mu)f_B^2M_B, & \frac{1}{2M_B}\langle B_s|\tilde{Q}_{LL}^s|B_s\rangle &= \frac{1}{8}\tilde{B}_4'(\mu)f_B^2M_B
\end{aligned}$$

where we define the modified bag parameter B_i' is defined in (5.79). In the Vacuum insertion approximation in which the matrix elements of the operators are evaluated by inserting the vacuum state, the following values for the bag parameters of the BSM operator matrix elements hold

$$B_3 = -1, \qquad B_4 = -1,$$

$$\tilde{B}_3 = -\frac{1}{N_c}, \qquad \tilde{B}_4 = -\frac{1}{N_c}.$$

For the bag parameters of the SM operator matrix elements we use recently calculated results from HQET sum rules in [88] which uses non perturbative inputs from [89], [90], and which are calculated in a different basis. The relation between the different operators is given as

$$Q_1 = 4Q_{LL}\,, \qquad Q_2 = 4Q^S_{LR}\,, \tag{5.116}$$

$$T_1 = 2\tilde{Q}_{LL} - \frac{2}{N_c}Q_{LL}\,, \qquad T_2 = 2\tilde{Q}^S_{LR} - \frac{2}{N_c}Q^S_{LR}\,. \tag{5.117}$$

and the matrix elements in the basis of [88] are defined as

$$\langle B_s|Q_i|B_s\rangle = A_i f^2_{B_s} M^2_{B_s} B_i\,, \qquad \langle B_s|T_i|B_s\rangle = A_i f^2_{B_s} M^2_{B_s} \epsilon_i\,, \tag{5.118}$$

with the coefficients

$$A_1 = 1\,, \qquad A_2 = \frac{M^2_{B_s}}{(m_b + m_s)^2}\,. \tag{5.119}$$

The SM values for the non perturbative inputs, including the meson decay constant taken from FLAG [91], are

$$f_{B_s} = (227.2 \pm 3.4)\,\text{MeV}, \tag{5.120}$$

$$\bar{B}_1(\bar{m}_b) = 1.028^{+0.064}_{-0.056}\,, \qquad \bar{B}_2(\bar{m}_b) = 0.988^{+0.087}_{-0.079}\,, \tag{5.121}$$

$$\bar{\epsilon}_1(\bar{m}_b) = -0.107^{+0.028}_{-0.029}\,, \qquad \bar{\epsilon}_2(\bar{m}_b) = -0.033^{+0.021}_{-0.021}\,. \tag{5.122}$$

5.5 The hadronic decay $B^0_d \to J/\psi K_S$

5.5.1 Operator basis and factorization

Another process to which the $b \to c\bar{c}s$ operators contribute is the hadronic decay of a neutral B_d meson into a charmonium state J/ψ and the short lived flavour eigenstate K_S. This process is interesting because in the SM it may be used to predict the value of the CKM matrix angle β as it violates CP and the only source of CP violation in the SM comes from the CKM matrix. This allows for the introduction of new weak CP violating phases via the $b \to c\bar{c}s$ Wilson coefficients as a measure of possible new sources of CP violation

not coming from the SM. For the study of CP violating processes we use the fierzed basis as it is more convenient when we wish to consider the computation of hadronic matrix elements in the naive factorization hypothesis. In this basis the operators are

$$\begin{aligned}
O_1^c &= (\bar{s}_L^i \gamma_\mu b_L^i)(\bar{c}_L^j \gamma^\mu c_L^j), & O_2^c &= (\bar{s}_L^i \gamma_\mu b_L^j)(\bar{c}_L^j \gamma^\mu c_L^i), \\
O_3^c &= (\bar{s}_L^i \gamma_\mu b_L^i)(\bar{c}_R^j \gamma^\mu c_R^j), & O_4^c &= (\bar{s}_L^i \gamma_\mu b_L^j)(\bar{c}_R^j \gamma^\mu c_R^i), \\
O_5^c &= (\bar{s}_L^i b_R^i)(\bar{c}_R^j c_L^j), & O_6^c &= (\bar{s}_L^i b_R^j)(\bar{c}_R^j c_L^i), \\
O_7^c &= (\bar{s}_L^i b_R^i)(\bar{c}_L^j c_R^j), & O_8^c &= (\bar{s}_L^i b_R^j)(\bar{c}_L^j c_R^i), \\
O_9^c &= (\bar{s}_L^i \sigma_{\mu\nu} b_R^j)(\bar{c}_L^j \sigma^{\mu\nu} c_R^i), & O_{10}^c &= (\bar{s}_L^i \sigma_{\mu\nu} b_R^i)(\bar{c}_L^j \sigma^{\mu\nu} c_R^j).
\end{aligned}$$

The transformation matrix $\hat{\mathcal{F}}$ which converts the $(\bar{c}b)(\bar{s}c)$ basis introduced in chapter 3, into the above $(\bar{c}c)(\bar{s}b)$ basis is given by

$$\hat{\mathcal{F}} = \begin{pmatrix}
1 & 0 & 0 & 0 & 0 & 0 & 0 & 0 & 0 & 0 \\
0 & 1 & 0 & 0 & 0 & 0 & 0 & 0 & 0 & 0 \\
0 & 0 & -\frac{1}{2} & 0 & 0 & 0 & 0 & 0 & 0 & 0 \\
0 & 0 & 0 & -\frac{1}{2} & 0 & 0 & 0 & 0 & 0 & 0 \\
0 & 0 & 0 & 0 & -2 & 0 & 0 & 0 & 0 & 0 \\
0 & 0 & 0 & 0 & 0 & -2 & 0 & 0 & 0 & 0 \\
0 & 0 & 0 & 0 & 0 & 0 & -\frac{1}{2} & 0 & -\frac{1}{8} & 0 \\
0 & 0 & 0 & 0 & 0 & 0 & 0 & -\frac{1}{2} & 0 & -\frac{1}{8} \\
0 & 0 & 0 & 0 & 0 & 0 & -6 & 0 & \frac{1}{2} & 0 \\
0 & 0 & 0 & 0 & 0 & 0 & 0 & -6 & 0 & \frac{1}{2}
\end{pmatrix}. \tag{5.123}$$

In the limit that the b quark mass is large compared to the scale of the strong interaction $m_b \gg \Lambda_{QCD}$, we can express the hadronic matrix element of a dimension 6 operator as the factorized product of two matrix elements of quark bilinears, up to non factorizable corrections of order α_s and power corrections [92, 93, 94], as follows

$$\langle J/\psi \bar{K}^0 | \mathcal{O}_i^c | \bar{B}^0 \rangle = \langle J/\psi | \bar{c} \Gamma_i c | 0 \rangle \langle \bar{K}^0 | \bar{s} \Gamma_i b | \bar{B}^0 \rangle \left(1 + \mathcal{O}(\alpha_s) + \mathcal{O}\left(\frac{\Lambda}{m_c \alpha_s} \right) \right). \tag{5.124}$$

Equation (5.124) requires some explanation. On the lhs is the full hadronic matrix element of the operator $\mathcal{O}_i$. On the rhs, at leading order is the factorized form of the matrix element where by it is assumed that interactions between the J/ψ meson and the BK system can be neglected in the heavy quark limit and we can therefore parameterize the matrix element in terms of a decay constant and a form factor. The next term occurs for gluon exchange between the J/ψ meson and the BK system and whilst are perturbatively calculable in some frameworks, are non factorizable. The third term is associated with power corrections and where this is usually $\mathcal{O}\left(\frac{\Lambda}{m_b}\right)$ for other classes of decays, in this decay the corrections are found to be larger due to the size of charmonium being small in the heavy quark limit but its Bohr radius being larger than $\frac{1}{m_b}$ [93]. In what follows we restrict ourselves to considering the first term in (5.124). Let us write down the naive estimate for the matrix element of $\mathcal{O}_1$. For the vector and tensor decay constants and form factors we have the following definitions from [95] and [96]

$$\langle J/\psi(p)|c(0)\gamma_\mu c(0)|0\rangle = f_{J/\psi} M_{J/\psi} \epsilon^*_\mu(p) \tag{5.125}$$

$$\langle J/\psi(p)|c(0)\sigma_{\mu\nu} c(0)|0\rangle = i f^T_{J/\psi}(\epsilon^*_\nu(p) p_\mu - \epsilon^*_\mu(p) p_\nu) \tag{5.126}$$

$$\langle \bar{K}^{(0)}(p')|\bar{s}(0)\gamma_\mu b(0)|\bar{B}^{(0)}(p_B)\rangle = [(p_B + p')_\mu - \frac{M_B^2}{p^2} p_\mu] F^+_{B\to K} + \frac{M_B^2}{p^2} p_\mu F^0_{B\to K} \tag{5.127}$$

$$p^\nu \langle \bar{K}^{(0)}(p')|\bar{s}(0)\sigma_{\mu\nu} b(0)|\bar{B}^{(0)}(p_B)\rangle = \frac{i F^T_{B\to K}}{M_B}[p^2(p_B + p')_\mu - M_B^2 p_\mu] \tag{5.128}$$

and $p' = p_B - p$ being the four-momentum of the J/ψ meson and $p^2 = M^2_{J\psi}$. We work in the frame of reference in which the B meson is at rest. So that

$$p^\mu_B = (M_B, \vec{0}) \tag{5.129}$$

$$p'^\mu = (M_K, \vec{p}') \tag{5.130}$$

$$p^\mu = (M_{J/\psi}, \vec{p}) \tag{5.131}$$

The decay is back to back with $\vec{p} = -\vec{p}' = -|\vec{p}|\hat{z}$, and the charmonium state with helicity $\lambda = 0$ is described by the polarization vector

$$\varepsilon^*_\mu(p) = \frac{(|\vec{p}|, 0, 0, M_{J/\psi})}{M_{J/\psi}} \tag{5.132}$$

Moreover, neglecting the mass of the strange quark and the Kaon gives the simplified relation between the form factors

$$F^0_{B\to K} = \left(1 - \frac{p^2}{M_B^2}\right) F^+_{B\to K} \tag{5.133}$$

Then, applying the Lorenz condition $\varepsilon_\mu p^\mu = 0$ the simple factorization approximation gives

$$\begin{aligned}\langle J/\psi \bar{K}^0 | \mathcal{O}_i^c | \bar{B}^0 \rangle_{NF} &= \frac{1}{4} \langle J/\psi | \bar{c}(0)\gamma_\mu c(0) | 0 \rangle \langle \bar{K}^0 | \bar{s}(0)\gamma^\mu b(0) | \bar{B}^0 \rangle \\ &= \frac{1}{4} f_{J/\psi} M_{J/\psi} (2\varepsilon^*(p) \cdot p_B) F^+_{B\to K}\end{aligned} \tag{5.134}$$

Thus we have for the naive factorization estimate of the magnitude of the matrix element of operator $\mathcal{O}_1$

$$|\langle O_1^c \rangle|_{NF} = \frac{M_B}{2} |\vec{p}| f_{J/\psi} F^+_{B\to K} + \mathcal{O}\left(\frac{1}{N_c^2}\right), \tag{5.135}$$

with

$$|\vec{p}| = \frac{\sqrt{M_B^4 + (M_K^2 - M_{J/\psi}^2)^2 - 2M_B^2(M_K^2 + M_{J/\psi}^2)]}}{2M_B}. \tag{5.136}$$

considering all corrections to be proportional to an $\mathcal{O}(1)$ number suppressed by two powers of the number of colours in the large N limit [97], gives the estimate

$$|\langle O_1^c \rangle|_{NF} = (1.23 \pm 0.11 \pm \mathcal{O}\left(\frac{1}{N_c^2}\right)) GeV^3 \tag{5.137}$$

5.5.2 The time dependent CP asymmetry

Adopting notation similar to that of [38], as a measure of CP violation we may consider the time dependent CP asymmetry given by

$$A_{CP}(t) = \frac{\Gamma(\bar{B}(t) \to f_{CP}) - \Gamma(B(t) \to f_{CP})}{\Gamma(\bar{B}(t) \to f_{CP}) + \Gamma(B(t) \to f_{CP})} \tag{5.138}$$

which describes the difference in rate between the decay of a B_d meson into a CP eigenstate with the anti-B_d meson into the same CP eigenstate. If the symmetry CP is indeed violated, this quantity will be non zero, as it is in the SM. We may express the above in terms of the mass difference and decay rate difference as defined in (2.64) and (2.65) of

section 2.2

$$A_{CP}(t) = \frac{S_f \sin(\Delta M_d t) - C_f \cos(\Delta M_d t)}{\cosh(\frac{\Delta\Gamma_d t}{2}) + D_f \sinh(\frac{\Delta\Gamma_d t}{2})} \tag{5.139}$$

where the coefficients of the sine, cosine and sinh functions are defined as

$$S_f = \frac{2\mathrm{Im}(\lambda_f)}{1+|\lambda_f|^2} \tag{5.140}$$

$$C_f = \frac{1-|\lambda_f|^2}{1+|\lambda_f|^2} \tag{5.141}$$

$$D_f = \frac{2\mathrm{Re}(\lambda_f)}{1+|\lambda_f|^2} \tag{5.142}$$

S_f is associated with the CP violation in the interference between neutral meson mixing and decay, C_f is associated with direct CP violation. In the case where $\Delta\Gamma\tau_d \ll 1$ the above expression simplifies to

$$A_{CP}(t) = S_f \sin(\Delta M_d t) - C_f \cos(\Delta M_d t) \tag{5.143}$$

Generically, let the amplitude for a B meson to decay to a final state f and an anti B meson to decay to the same state be

$$A_f = \langle f|\mathcal{H}^{\mathrm{eff}}|B\rangle, \tag{5.144}$$

$$\bar{A}_f = \langle f|\mathcal{H}^{\mathrm{eff}}|\bar{B}\rangle, \tag{5.145}$$

then the quantity important in the study of CP violation in the quark sector λ_f is

$$\lambda_f = \left(\frac{q}{p}\right)_B \frac{\bar{A}(B^0 \to f)}{A(B^0 \to f)}. \tag{5.146}$$

with $\frac{p}{q}$ defined generically in chapter 2 section 2.2. Having specified definitions and relations, let us now specialise to the final CP eigenstate $f_{CP} = J/\psi K_S$. In (5.146) we will have

$$\lambda_{J/\Psi K_S} = \frac{q_{B_d}}{p_{B_d}} \frac{\bar{\mathcal{A}}_{J/\Psi K_S}}{\mathcal{A}_{J/\Psi K_S}} \tag{5.147}$$

and we define the following hadronic amplitudes for $B^0 \to J/\psi K_S$ and $\bar{B}^0 \to J/\psi K_S$ as

$$\mathcal{A}_{J/\Psi K_S} = \langle J/\Psi K_S|\mathcal{H}^{\mathrm{eff}}|B^0_d\rangle \qquad \bar{\mathcal{A}}_{J/\Psi K_S} = \langle J/\Psi K_S|\mathcal{H}^{\mathrm{eff}}|\bar{B}^0_d\rangle. \tag{5.148}$$

The hadronic states for the long K_L and short K_S lived physical eigenstates are linear combinations of the neutral Kaon $K^0, \bar{K}^0$ flavour eigenstates, as is given generically in section 2.2.

$$|K_L\rangle = p_K|K^0\rangle + q_K|\bar{K}^0\rangle \tag{5.149}$$

$$|K_S\rangle = p_K|K^0\rangle - q_K|\bar{K}^0\rangle \tag{5.150}$$

In what follows we assume no CP violation in Kaon mixing, so that we assume $\left(\frac{q_K}{p_K}\right) \approx 1$ which is a reasonable approximation [98]. The operators in $\mathcal{H}_{\text{eff}}$ which contribute to $\bar{\mathcal{A}}_{J/\Psi K_S}$ are $\mathcal{O}_i$, and those contributing to $\mathcal{A}_{J/\Psi K_S}$ their hermitian conjugates $\mathcal{O}_i^\dagger$, so that (5.148) in (5.147) gives

$$\lambda_{J/\Psi K_S} = \frac{q_B}{p_B}\frac{\lambda_c}{\lambda_c^*}\frac{\sum_{i=1}^{10}\langle J/\Psi K_S|(C_i^c\mathcal{O}_i^c + C_i^{c\prime}\mathcal{O}_i^{c\prime})|\bar{B}_d^0\rangle}{\sum_{i=1}^{10}\langle J/\Psi K_S|((C_i^c)^*\mathcal{O}_i^{c\dagger} + (C_i^{c\prime})^*\mathcal{O}_i^{c\dagger\prime})|B_d^0\rangle}. \tag{5.151}$$

Upon factoring out the ratio of the operator matrix element of $\mathcal{O}_1^c$ to that of $\mathcal{O}_1^{c\dagger}$ and using the CP conservation of the strong interactions we find that

$$\lambda_{J/\Psi K_S} = \frac{q_B}{p_B}\frac{\lambda_c}{\lambda_c^*}\frac{1}{\eta_{CP}}\frac{(C_1^c + \sum_{i=2}^{10}(C_i^c r_{i1} + C_i^{c\prime} r'_{i1})}{((C_1^c)^* + \sum_{i=2}^{10}((C_i^c)^* r_{i1} + (C^{c\prime})_i^* r'_{i1}))}. \tag{5.152}$$

Finally, we make the approximation that $\frac{\lambda_c}{\lambda_c^*} \approx 1 \in \mathbb{R}$, which is justified in our phase convention, further we take $\frac{q_B}{p_B} = \frac{V_{tb}^* V_{td}}{V_{tb} V_{td}^*} \approx e^{-2i\beta + \mathcal{O}(\lambda^4)}$ [33] where the Wolfenstein paramater $\lambda \approx 0.22$ which amounts to neglecting CP violation in mixing. With $\eta_{CP} = -1$ we get

$$\lambda_{J/\psi K} = -e^{-2i\beta}\frac{(C_1^c + \sum_{i=2}^{10}(C_i^c r_{i1} + C_i^{c\prime} r'_{i1}))}{((C_1^c)^* + \sum_{i=2}^{10}((C_i^c)^* r_{i1} + (C^{c\prime})_i^* r'_{i1}))}. \tag{5.153}$$

In the above we express the Wilson coefficients as complex quantities

$$\Delta C_i = \text{Re}(\Delta C_i) + i\text{Im}(\Delta C_i) \qquad\qquad i = 1, ..., 10, \tag{5.154}$$

and the ratio of the matrix elements of the i^{th} operator $i = 1, 2, ..., 10$ to that of the matrix element of the colour singlet operator $\mathcal{O}_1^c$ as

$$r_{i1}^{(\prime)} = \frac{\langle J/\psi K_S|\mathcal{O}_i^{c(\prime)}|\bar{B}_d^0\rangle}{\langle J/\psi K_S|\mathcal{O}_1^c|\bar{B}_d^0\rangle} e^{i(\delta_i - \delta_1)} \qquad\qquad i = 1, ..., 10 \tag{5.155}$$

where the phases δ_i and ϕ_i are strong CP conserving phases and weak CP violating phases respectively. There are three observable quantities which we will use to obtain a further

constraint from this process. From (5.143) with $f = J/\psi K_S$, the first two are

$$S_{J/\psi K_S} = \frac{2\mathrm{Im}\left(-e^{-2i\beta}\frac{(C_1^c+\sum_{i=2}^{10}(C_i^c r_{i1}+C_i^{c\prime}r'_{i1}))}{((C_1^c)^*+\sum_{i=2}^{10}((C_i^c)^* r_{i1}+(C^{c\prime})_i^* r'_{i1}))}\right)}{\left(1+\left|\frac{(C_1^c+\sum_{i=2}^{10}(C_i^c r_{i1}+C_i^{c\prime}r'_{i1}))}{((C_1^c)^*+\sum_{i=2}^{10}((C_i^c)^* r_{i1}+(C^{c\prime})_i^* r'_{i1}))}\right|^2\right)}, \tag{5.156}$$

$$C_{J/\psi K_S} = \frac{\left(1-\left|\frac{(C_1^c+\sum_{i=2}^{10}(C_i^c r_{i1}+C_i^{c\prime}r'_{i1}))}{((C_1^c)^*+\sum_{i=2}^{10}((C_i^c)^* r_{i1}+(C^{c\prime})_i^* r'_{i1}))}\right|^2\right)}{\left(1+\left|\frac{(C_1^c+\sum_{i=2}^{10}(C_i^c r_{i1}+C_i^{c\prime}r'_{i1}))}{((C_1^c)^*+\sum_{i=2}^{10}((C_i^c)^* r_{i1}+(C^{c\prime})_i^* r'_{i1}))}\right|^2\right)}. \tag{5.157}$$

5.5.3 The branching ratio $\mathcal{B}(B_d^{(0)} \to J/\psi K_d^{(0)})$

For the third observable used in this study we consider the branching ratio $\mathcal{B}(B_d^{(0)} \to J/\psi K_d^{(0)})$, in a similar manner as is done in the SM case in [99], and [100]. It is obtained by calculating the decay rate $\Gamma(B_d^{(0)} \to J/\psi K_d^{(0)})$ in the usual manner by performing a two-body phase space integral over the modulus squared of the amplitude. The differential decay rate is

$$d\Gamma = \frac{1}{2E_B}|\mathcal{M}(B_d^{(0)} \to J/\psi K_d^{(0)})|^2 d\Phi^{(2)}, \tag{5.158}$$

with the differential two-body phase space given by

$$d\Phi^{(2)} = \int \frac{d^3p'}{(2\pi)^3 2E_K}\int \frac{d^3p}{(2\pi)^3 2E_\psi}(2\pi)^4\delta^{(4)}(p_B - p - p'). \tag{5.159}$$

Replacing four dimensional Dirac delta distribution with

$$\delta^{(4)}(p_B - p - p') = \delta(M_B - (E_K + E_\psi))\delta^{(3)}(\vec{p} + \vec{p'}), \tag{5.160}$$

and performing the integration over d^3p' and moving to spherical polar coordinates, we find

$$d\Gamma = \frac{1}{(2\pi)^2}\frac{1}{8M_B^2}|\vec{p}||\mathcal{M}(B_d^{(0)} \to J/\psi K_d^{(0)})|^2 d\Omega. \tag{5.161}$$

Subsequently, as the $B_d^{(0)}$ meson is spin zero, performing the integral over the solid angle gives only a factor of 4π and this yields

$$\Gamma(B_d^{(0)} \to J/\psi K_d^{(0)}) = \frac{1}{8\pi M_B^2}|\vec{p}||\langle J/\psi K^{(0)}|\mathcal{H}_{\text{eff}}^{cc}|B_d^{(0)}\rangle|^2. \tag{5.162}$$

for the branching ratio then, we use the lifetime of the $B_d^{(0)}$ meson to give the final result for our theoretical prediction of the branching ratio

$$\mathcal{B}(B_d^{(0)} \to J/\psi K_d^{(0)}) = \frac{\tau_B p_c^3 G_F^2 |\lambda_c|^2}{\pi} |\langle \mathcal{O}_1^{c\dagger} \rangle|^2 |((C_1^c)^* + \sum_{i=2}^{10} ((C_i^c)^* r_{i1} + (C_i^{c\prime})^* r'_{i1}))|^2. \tag{5.163}$$

Chapter 6

Phenomenology

In this chapter results obtained from calculations in Chapter 5 are presented in graphical and tabular format. The theoretical predictions for the collection of observables are compared with their average experimental values, and constraints upon scenarios of modified CBSM couplings are obtained. The chapter is laid out as follows: In section 6.1 the statistical methods for obtaining bounds and constraints are introduced. In section 6.3 results constraining scenarios involving pairs of Wilson coefficients $\Delta C_1 - \Delta C_4$ are shown at renormalization scales μ_b and M_W and rare decay anomalies related to the Wilson coefficient C_{9V} are addressed and discussed. In section 6.4 scenarios involving pairs of Wilson coefficients $\Delta C_1' - \Delta C_4'$ are presented and constrained by additional pseudo observables $\bar{C}'_{7\gamma}$ and $\bar{C}'_{9V}$. In section 6.7 complex SM Wilson coefficients are studied and the CP violating effects which are constrained by flavour specific CP asymmetry and hadronic decay observables are shown, and finally in section 6.8 we present best fit ranges for individual coefficients both in the case of individual observables providing constraint, and combined constraints which lead to naive estimates for the scale at which BSM physics could occur.

6.1 Statistical treatment

Following a procedure outlined in [101] we define the following quantities

$$X^{Exp} = \left\{ X_1^{Exp}, ..., X_{N_{exp}}^{Exp} \right\} \tag{6.1}$$

$$X^{Th} = \left\{ X_1^{Th}, ..., X_{N_{th}}^{Th} \right\} \tag{6.2}$$

$$\theta = \{\theta_1, ..., \theta_{N_\theta}\} \tag{6.3}$$

$$\nu = \{\nu_1, ..., \nu_{N_\nu}\} \tag{6.4}$$

Where (6.1) is a set of N_{exp} experimental measurements, (6.2) is a set of N_{th} corresponding theoretical expressions which predict values for the measurements, and which are functions of the N_θ parameters θ and N_ν parameters ν of (6.3) and (6.4) respectively. Individually, for each X_i^{Exp}, X_i^{Th} we determine regions of the parameter space using a simple function

$$\chi_i^2(\vec{\theta},\vec{\nu}) = \frac{(X_i^{Exp} - X_i^{Th}(\vec{\theta},\vec{\nu}))^2}{\sigma(X_i^{Exp})^2 + \sigma(X_i^{Th})^2}, \tag{6.5}$$

and when combining constraints we will use the sum of the individual functions given above

$$\chi^2(\vec{\theta},\vec{\nu}) = \sum_{i=1}^{N_{Exp}} \frac{(X_i^{Exp} - X_i^{Th}(\vec{\theta},\vec{\nu}))^2}{\sigma(X_i^{Exp})^2 + \sigma(X_i^{Th})^2}. \tag{6.6}$$

For the study of real Wilson coefficients, we will only consider the parameters of interest θ which are the Wilson coefficients ΔC_j and we will set all other parameters to their experimental averages. In general when plotting results and obtaining best fit points we will refer to the offset corrected χ^2 denoted as

$$\Delta\chi^2(\vec{\theta},\vec{\nu}) = \chi^2(\vec{\theta},\vec{\nu}) - \chi^2_{min;\theta;\nu}, \tag{6.7}$$

where the last term in (6.7) is the absolute minimum of $\chi^2(\vec{\theta},\vec{\nu})$, obtained by allowing all parameters $\vec{\theta}$ and $\vec{\nu}$ to be freely varied. This quantity gives a measure of the quality of agreement of a given theoretical model with the data, assuming the SM to be correct. For the study of hadronic decay we will use the following definitions. Define the profile χ^2 as a function of the relevant parameters $\vec{\theta}$ at the values of $\vec{\nu}$ which minimize (6.6), at each point in θ space.

$$\chi^2(\vec{\theta}) = \chi^2_{min;\nu}(\vec{\theta}) \tag{6.8}$$

We aim to set Confidence Levels (CL) in the space of relevant parameters θ irrespective of what values the parameters ν might take. Then the quantity which gives confidence levels for the parameters of interest in θ space is the offset corrected χ^2

$$\Delta\chi^2(\vec{\theta}) = \chi^2(\vec{\theta})_{min;\nu} - \chi^2_{min;\theta;\nu}. \tag{6.9}$$

Here the first term on the LHS of (6.9) is the minimal value of the $\chi^2(\vec{\theta})$ function with respect to parameters $\vec{\nu}$ for fixed $\vec{\theta}$, and the second term is the same as that described above for (6.7). For each case it will be made clear which approaches we are using to represent and analyse results.

6.2 Numerical inputs

In this section, we describe all the numerical inputs that are used in this work, along with the experimental results and their corresponding uncertainties. We break these down into a set of fundamental inputs that are common to all our different observables, and then some specific input values required for the prediction of BSM contributions to individual observables.

6.2.1 Common inputs

We show in Table 6.1 input parameters that are common to all our theoretical predictions. These inputs are taken from the PDG [33] and CKMfitter [102]

Parameter	Value	Reference
$\alpha_s(M_Z)$	0.1181 ± 0.0011	PDG 2018
M_{K_S}	$(0.497\,611 \pm 0.000\,013)$ GeV	PDG 2018
$M_{J/\psi}$	$(3.096\,900 \pm 0.000\,006)$ GeV	PDG 2018
M_{B_d}	$(5.279\,55 \pm 0.000\,26)$ GeV	PDG 2018
M_{B_s}	$(5.366\,84 \pm 0.000\,30)$ GeV	PDG 2018
$\bar{m}_b(\bar{m}_b)$	$4.18^{+0.04}_{-0.03}$ GeV	PDG 2018
$m_{c,\text{pole}}$	(1.67 ± 0.07) GeV	PDG 2018
$\bar{m}_c(\bar{m}_b)$	(0.924 ± 0.07)GeV	from $m_{c,\text{pole}}$ and $\alpha_s(M_Z)$ via RunDec [103, 104]
$m_s(2\text{GeV})$	95^{+9}_{-3} MeV	PDG 2018
$\lvert V_{ub}/V_{cb}\rvert$	$0.08835^{+0.00221}_{-0.00281}$	CKMfitter (ICHEP 2018)
V_{cb}	$0.04240^{+0.00030}_{-0.00115}$	CKMfitter (ICHEP 2018)
V_{us}	$0.2254745^{+0.000254}_{-0.000059}$	CKMfitter (ICHEP 2018)
γ	$65.81^{+0.99}_{-1.66}\,^\circ$	CKMfitter (ICHEP 2018)

Table 6.1: List of general input parameters needed for our theoretical predictions.

6.2.2 Theoretical inputs

Shown in table 6.2 are the SM predictions for our mixing, lifetime and radiative decay observables and their references. In tables 6.5 and 6.4 are the non perturbative inputs for the $\Delta B = 0$ and $\Delta B = 2$ matrix elements required for prediction of the lifetime ratio and mixing observables respectively.

Quantity	Value	Reference
$\Delta\Gamma_s^{SM}$	(0.088 ± 0.02) ps^{-1}	[38]
$a_{fs}^{s,SM}$	$(2.22 \pm 0.27) \times 10^{-5}$	[38]
$(\tau_{B_s}/\tau_{B_d})^{SM}$	0.9994 ± 0.0025	[88]
$\mathcal{B}(B \to X_s\gamma)^{SM}$	$(3.36 \pm 0.23) \times 10^{-4}$	[69]

Table 6.2: List of SM values needed for our theoretical predictions.

Quantity	Value	Reference
f_{B_s}	(227.2 ± 3.4)MeV	[91]
$\bar{B}_1(\bar{m}_b)$	$1.028^{+0.064}_{-0.056}$	[88]
$\bar{B}_2(\bar{m}_b)$	$0.988^{+0.087}_{-0.079}$	[88]
$\bar{\epsilon}_1(\bar{m}_b)$	$-0.107^{+0.028}_{-0.029}$	[88]
$\bar{\epsilon}_2(\bar{m}_b)$	$-0.033^{+0.021}_{-0.021}$	[88]

Table 6.3: Non- perturbative inputs for $\Delta B = 0$ matrix elements.

Quantity	Value	Reference
$\sqrt{\hat{B}} f_{B_s}$	270(16)MeV	[91]
$\hat{B}$	1.32(6)	[91]
$\frac{\tilde{B}_s(\overline{m}_b)}{B(\overline{m}_b)}$	1.07(6)	[38]

Table 6.4: Non- perturbative inputs for $\Delta B = 2$ matrix elements.

Quantity	Value	Reference
$f_{J/\psi}$	(407 ± 6)MeV	[105]
$F^{B\to K}(q^2 = M_{J/\psi}^2)$	0.68 ± 0.06	[106]

Table 6.5: Non - perturbative inputs for $B \to J\psi K$ matrix elements.

As part of our theoretical calculation of $S_{J/\psi K_S}$ and $C_{J/\psi K_S}$, we use the most recent CKMfitter [102] value

$$\sin 2\beta = 0.738^{+0.027}_{-0.030}\,, \tag{6.10}$$

where the experimental measurement is not included in their fit. We note there is a very slight tension between the HFLAV average and the CKMfitter result, at the level of $\sim 1.1\,\sigma$.

The non perturbative inputs in table 6.4 contain the following definitions and conversions.

The RGI B parameter $\hat{B}$ is given in [91] as

$$\hat{B}_{B_q} = \left(\frac{\bar{g}(\mu)^2}{4\pi}\right)^{-\frac{\gamma_0}{(2\beta_0)}} \left\{1 + \frac{\bar{g}(\mu)^2}{(4\pi)^2}\left[\frac{\beta_1\gamma_0 - \beta_0\gamma_1}{2\beta_0^2}\right]\right\} B_{B_q}(\mu) \tag{6.11}$$

for $m_b < \mu < m_t$, the following values are $N_f = 5$, and $N_c = 3$, $\gamma_0 = 4, \beta_0 = \frac{23}{3}$, $\gamma_1 = \frac{116}{3}, \beta_1 = -\frac{43}{9}$.

6.2.3 Experimental inputs

Quantity	Value	Reference
$\Delta\Gamma_s^{exp}$	(0.088 ± 0.006) ps^{-1}	[78]
$a_{fs}^{s,exp}$	-0.0006 ± 0.0028	[78]
$(\tau_{B_s}/\tau_{B_d})^{exp}$	0.993 ± 0.004	[78]
$\mathcal{B}(B \to X_s\gamma)^{exp}$	$(3.32 \pm 0.15) \times 10^{-4}$	[78]
$\tau_{B_s}^{exp}$	1.509 ± 0.004 ps	[78]
$S_{J/\psi K_S}$	0.699 ± 0.017	[78]
$C_{J/\psi K_S}$	-0.005 ± 0.015	[78]
$\mathcal{B}(B_d \to J/\psi K_S)$	$(8.73 \pm 0.32) \times 10^{-4}$	[33]
$\mathcal{B}(\bar{B} \to X_c e\bar{\nu})^{\text{exp}}$	0.1061 ± 0.0017	[81]

Table 6.6: List of experimental values needed for our theoretical predictions.

6.2.4 Rare decay Wilson coefficients

For our study of new physics in rare decay and constraints upon all four fermion coefficients we use the following best fit values for $C_9^{(\prime)}$ and $C'_{7\gamma}$ from global fits performed by [19] and [107], respectively.

$$C_9^{NP} = -1.21 \pm 0.2 \tag{6.12}$$

$$C'_9 = 0.19 \pm 0.2 \tag{6.13}$$

$$C'_{7\gamma} = 0.018 \pm 0.037 \tag{6.14}$$

The observables included in these fits for $C_9^{(\prime)}$ are; angular observables in $B^0 \to K^{*0}\mu^+\mu^-$ [9, 108], [109, 5] , $B^{0,\pm} \to K^{*0,\pm}\mu^+\mu^-$ branching ratios [4, 110, 5, 9], $B^{0,\pm} \to K^{0,\pm}\mu^+\mu^-$ branching ratios [4, 9], $B_s \to \phi\mu^+\mu^-$ branching ratio [111, 9], $B_s \to \phi\mu^+\mu^-$ angular observables [111, 9], the branching ratio of inclusive decay $B \to X_s\mu^+\mu^-$ [112], with the standard model predictions of these [18, 113]. For $C'_{7\gamma}$ the measurements are for

the exclusive semileptonic angular observables $\langle P_1 \rangle (B^0 \to K^{*0} e^+ e^-)$ and A_T^{Im} [114], the mixing induced CP asymmetry in $B^0 \to K^* \gamma$ given by $S_{K^* \gamma}$ [115, 116] , and the $\mathcal{B}(B \to X_s \gamma)$ [117, 118, 119, 120, 121], $\mathcal{B}(B^+ \to K^* \gamma)$,$\mathcal{B}(B^0 \to K^* \gamma)$ [120, 122, 123], and $\mathcal{B}(B_s \to \phi \gamma)$ [124] branching ratios.

6.3 Constraints on BSM in C_{9V} : $\Delta C_1 - \Delta C_4$

In this section we focus upon the study carried out in [1] concerning the impact of operators $Q_1^c - Q_4^c$ upon the partonic $\mathcal{A}(b \to s \bar{\mu} \mu)$ by investigating whether it is possible to achieve a shift to Wilson coefficient $C_{9V} \approx -1$ subject to constraints from mixing and lifetime data. Currently global fits performed by [19] predict a best fit value of $C_9^{NP} = -1.21 \pm 0.2$. Here, constraints imposed by the $B_s^{(0)}$ meson width difference and the ratio of the $B_s^{(0)}$ to the $B_d^{(0)}$ lifetimes are used to determine the viability of such a shift being due to modified coefficients in the CBSM Hamiltonian.

6.3.1 Low scale scenarios and q^2 dependence

In Figures 6.1 - 6.3 are shown six plots representing scenarios where two Wilson coefficients are "switched on" and all of the rest are set to their SM values. In all figures the regions are determined by individual constraints overlaid using (6.5) and best fit points correspond to points which minimize (6.6). The experimental quantities, their respective theoretical predictions and parameters of interest are

$$X^{Exp} = \{\Delta\Gamma_s^{Exp}, C_9^{bs\mu\mu}, (\tau_s/\tau_d)^{Exp}\} \tag{6.15}$$

$$X^{Th} = \{\Delta\Gamma_s, \bar{C}_{9V}(\mu_b), (\tau_{B_s}/\tau_{B_d})\} \tag{6.16}$$

$$\vec{\theta} = \{\Delta C_1(\mu_b), \Delta C_2(\mu_b), \Delta C_3(\mu_b), \Delta C_4(\mu_b)\} \tag{6.17}$$

and the theoretical predictions in (6.16) are given by (5.81), (5.22) and (5.85) in Chapter 5. In these scenarios we consider the scale of new physics to be around the scale of the B meson mass, M_B. At this scale it is not necessary to employ renormalization group improvement, as the logarithms appearing in the loop calculations are not large. Such a situation could be due to "hidden" new particles which although are within the range of energies probed by current experiments, are for some reason not detectable.

In this "low scale" scenario, (5.22) reduces to (5.18) as without renormalization group improvement, $C_{9V}(\mu_b)$ does not contain a BSM contribution and so it does not mix

with CBSM coefficients. In all plots the black and red dashed lines are contours of $\bar{C}_{9V}(\mu_b) = -1.21 \pm 0.2$ for two choices of dilepton invariant mass squared $q^2 = 5GeV^2$ and $q^2 = 2GeV^2$ respectively. For values of q^2 above this, the charmonium resonances are the dominant signal detected and therefore for consideration of rare decay anomalies, it is most reliable to remain in the region $q^2 \in [1, 5]GeV^2$.

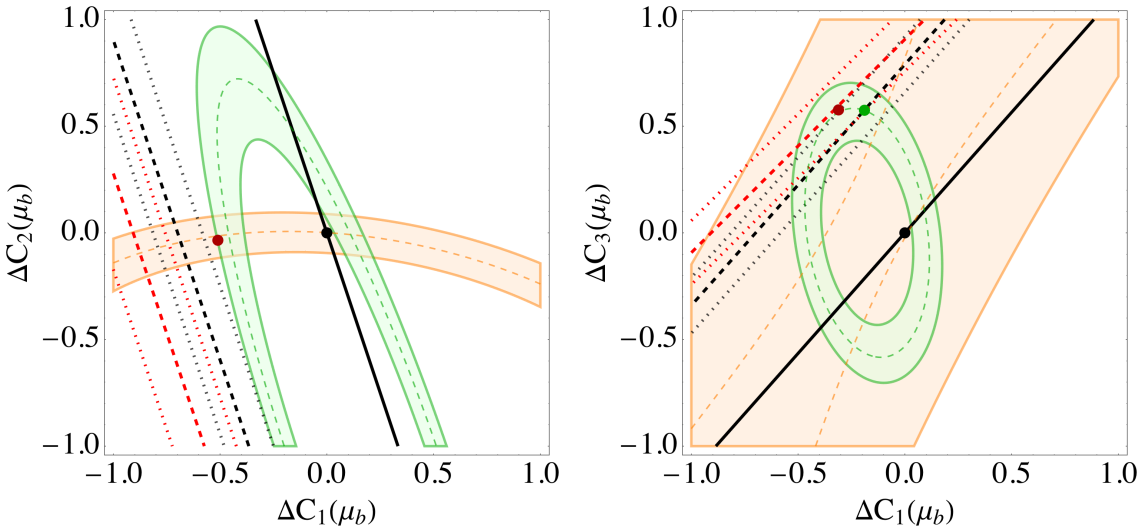

Figure 6.1: Two parameter scenarios for $\Delta C_1(\mu_b), \Delta C_2(\mu_b)$ (left), $\Delta C_1(\mu_b), \Delta C_3(\mu_b)$ (right). Red dashes and black dashes correspond to $q^2 = 2\text{GeV}^2$ and $q^2 = 5\text{GeV}^2$ respectively. Overlaid are individual 1σ constraints from $\Delta\Gamma_s$ (orange shaded) and $\frac{\tau_{B_s}}{\tau_{B_d}}$ (green shaded) with the (orange and green) dashed lines the experimental central value for each respectively.

In Figure 6.1 (left) of $(\Delta C_1(\mu_b), \Delta C_2(\mu_b))$ we are considering shifts to the SM coefficients C_1, C_2. The width difference (orange) here constrains new physics in C_2 and the lifetime ratio (green) new physics in C_1 at 1σ. There is a current 1.4σ discrepancy between the SM prediction computed recently in [88] shown in Table 6.2 and the measured value [78] given in Table 6.6, and this is why the lifetime ratio does not pass through the SM point. The best fit points lie outside the 1σ regions for C_{9V} at $(C_1(\mu_b), \Delta C_2(\mu_b)) = (-0.5, -0.03)$ and $(C_1(\mu_b), \Delta C_2(\mu_b)) = (-0.51, -0.04)$ for the higher and lower q^2 values respectively. There is no region for which a shift of $\bar{C}_{9V} = -1.21 \pm 0.2$ is achievable and in agreement with both mixing and lifetimes, however $\Delta\Gamma_s$ easily accommodates a negative shift for both q^2 values. In the next panel (right hand) we consider BSM effects as a shift to SM C_1 and NP ΔC_3. Indeed this is a favourable scenario, it would be possible to produce a shift by as much as $\bar{C}_{9V} = -1.21$ for $(\Delta C_1(\mu_b), \Delta C_3(\mu_b)) = (-0.19, 0.57)$ in the higher q^2 for and $(\Delta C_1(\mu_b), \Delta C_3(\mu_b)) = (-0.31, 0.58)$ for lower q^2 and remain well within allowed values imposed by the lifetime ratio.

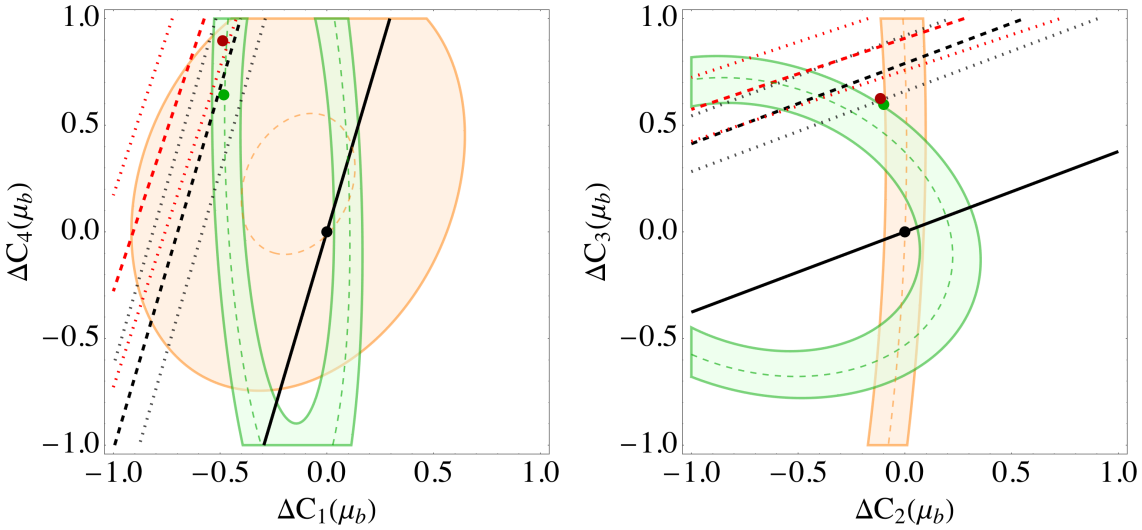

Figure 6.2: Two parameter scenarios for $\Delta C_1(\mu_b), \Delta C_4(\mu_b)$ (left), $\Delta C_2(\mu_b), \Delta C_3(\mu_b)$ (right). Red dashes and black dashes correspond to $q^2 = 2\text{GeV}^2$ and $q^2 = 5\text{GeV}^2$ respectively. Overlaid are individual 1σ constraints from $\Delta\Gamma_s$ (orange shaded) and $\frac{\tau_{B_s}}{\tau_{B_d}}$ (green shaded) with the (orange and green) dashed lines the experimental central value for each respectively.

In Figure 6.2 (left) of $(\Delta C_1(\mu_b), \Delta C_4(\mu_b))$ this scenario is again quite favoured with points in the plane where all observables agree, and achieve the desired shift of $\bar{C}_{9V} = -0.95 \pm 0.2$. It is clear the $\Delta C_4(\mu_b)$ is not constrained much by the observables, yet a preference for a negative shift to SM $C_1^c(\mu_b)$ is observed. The data prefers best fit points of $(\Delta C_1(\mu_b), \Delta C_4(\mu_b)) = (-0.48, 0.64)$ and $(\Delta C_1(\mu_b), \Delta C_4(\mu_b)) = (-0.49, 0.90)$ in the $q^2 = 5\text{GeV}^2$ and $q^2 = 2\text{GeV}^2$ cases respectively.The q^2 dependence of $\bar{C}_{9V}(\mu_b)$ leads to contours closer to the origin for higher q^2. In the right hand panel, as is the case with $(\Delta C_1(\mu_b), \Delta C_2(\mu_b))$ the even coefficient is constrained by the mixing and lifetime observables, and the odd coefficient by rare decay. For this scenario the best fit points lie close to the if not just outside the region allowed by the lifetime ratio $(\Delta C_2(\mu_b), \Delta C_3(\mu_b)) = (-0.11, 0.63)$, and $(\Delta C_2(\mu_b), \Delta C_3(\mu_b)) = (-0.10, 0.60)$ for $q^2 = 5\text{GeV}^2$ and $q^2 = 2\text{GeV}^2$ respectively.

In Figure 6.3 (left) of $(\Delta C_2(\mu_b), \Delta C_4(\mu_b))$ this is the least viable of the scenarios, the contours of constant $\bar{C}_{9V}$ are only just visible in the top left hand corner and nowhere in the plane agree with the width difference and lifetime ratio. ΔC_2 is constrained by mixing and lifetimes but these impose no constraints at all for ΔC_4. Finally the $(\Delta C_3(\mu_b), \Delta C_4(\mu_b))$ plane has best fit points very closely placed together at $(\Delta C_3(\mu_b), \Delta C_4(\mu_b)) = (0.37, 0.69)$ for the higher q^2 value and $(\Delta C_3(\mu_b), \Delta C_4(\mu_b)) = (0.36, 0.68)$ for the lower. Neither are in agreement with all observables. This scenario again implies a possible shift of $\Delta C_3(\mu_b) \approx 0.3$, if we consider only $\Delta\Gamma_s$.

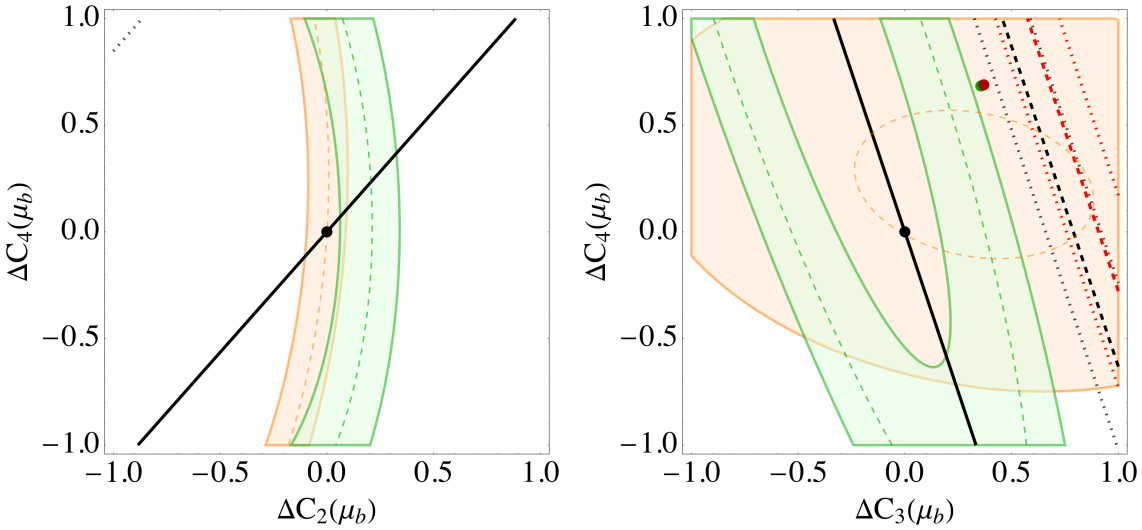

Figure 6.3: Two parameter scenarios for $\Delta C_2(\mu_b), \Delta C_4(\mu_b)$ (left), $\Delta C_3(\mu_b), \Delta C_4(\mu_b)$ (right). Red dashes and black dashes correspond to $q^2 = 2\text{GeV}^2$ and $q^2 = 5\text{GeV}^2$ respectively. Overlaid are individual 1σ constraints from $\Delta\Gamma_s$ (orange shaded) and $\frac{\tau_{B_s}}{\tau_{B_d}}$ (green shaded) with the (orange and green) dashed lines the experimental central value for each respectively.

6.3.2 High scale scenarios

In Figures 6.4-6.6 are shown 2-parameter planes in one to one correspondence with those in Figures 6.1-6.3 respectively, but in this case the coefficients are evaluated at the weak scale $\mu = M_W$ and evolved down to the scale of the b quark mass through RG improvement [1]. Again, in all figures the regions are determined by individual constraints overlaid using (6.5) and best fit points correspond to points which minimize (6.6). The experimental quantities, their respective theoretical predictions and parameters of interest are

$$X^{Exp} = \{\Delta\Gamma_s^{Exp}, C_9^{bs\mu\mu}, (\tau_s/\tau_d)^{Exp}, \mathcal{B}(B \to X_s\gamma)^{Exp}\} \tag{6.18}$$

$$X^{Th} = \{\Delta\Gamma_s, \bar{C}_{9V}(\mu_b), (\tau_{B_s}/\tau_{B_d}), \mathcal{B}(B \to X_s\gamma)\} \tag{6.19}$$

$$\vec{\theta} = \{\Delta C_1(M_W), \Delta C_2(M_W), \Delta C_3(M_W), \Delta C_4(M_W)\} \tag{6.20}$$

and the theoretical predictions in (6.19) are given by (5.81), (5.22), (5.85) and (5.37) in Chapter 5. In all panels, 1σ constraints from $\Delta\Gamma_s$ (orange shading), $\mathcal{B}(\bar{B} \to X_s\gamma)$ (blue shading), $\frac{\tau_s}{\tau_d}$ (green shading) are given, with the dashed lines in the corresponding colours being the experimental central value respectively. For these scenarios, our pseudo observable $\bar{C}_{9V}(\mu)$ given in (5.22) contains contributions from $\Delta C_1(M_W) - \Delta C_4(M_W)$, in addition to those which are due to $\mathcal{C}_{9V}(q^2, \mu)$, which appear because of mixing between Q_{9V} and $Q_1^c - Q_4^c$ upon renormalization. Again in red dashed lines are contours of con-

stant $\bar{C}_{9V}(\mu_b) = -1.21 \pm 0.2$.

The branching ratio of the inclusive $\bar{B} \to X_s\gamma$ decay has now been included as an additional constraint. As can be seen by comparing the three sets of plots, the effect of the evolution of $C_{9V}(\mu_b)$ upon $\bar{C}_{9V}$ is powerful and considerably improves the prospects of achieving a negative shift to the SM coefficient C_{9V}, without being excluded due to mixing, lifetime and radiative decay data. The contours are tightly spaced and closer to the SM point implying a very small BSM contribution could be hidden in CBSM coefficients and yet still give rise to a negative shift to C_{9V}.

In the left hand panel of 6.4, if there were agreement between the lifetime ratio and the SM, a small negative ΔC_1 and very slight shift to ΔC_2 would satisfy this requirement. In the right hand panel is shown a scenario where ΔC_1 and ΔC_3 are modified by NP. This scenario is favourable, all of the observables agree at the best fit point and allow a shift to C_{9V} for a $\Delta C_3(M_W) \approx 0.3$ and $\Delta C_1 < 0.1$. In the left hand panel of 6.5, in the

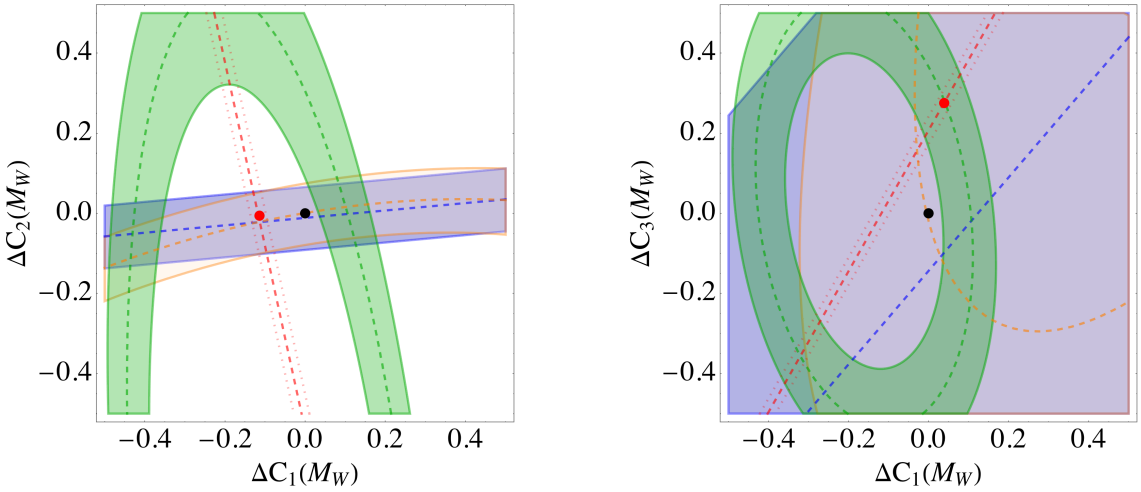

Figure 6.4: Two parameter planes of: left $\Delta C_1(M_W), \Delta C_2(M_W)$ and right $\Delta C_1(M_W), \Delta C_3(M_W)$

$\Delta C_1(M_W) - \Delta C_4(M_W)$ plane the $\bar{B} \to X_s\gamma$ branching ratio constrains only ΔC_4 but the lifetime ratio constrains ΔC_1. In this scenario a negative shift $\Delta C_1 \approx -0.1$ and a very slight negative $\Delta C_4(M_W)$ achieve agreement with radiative decay and the $\Delta\Gamma_s$, whereas the lifetime ratio with it's current discrepancy would not support our hypothesis. In the right hand panel of the $\Delta C_2(M_W) - \Delta C_3(M_W)$ plane again is found a favourable scenario. All of the observables agree with a a shift $\bar{C}_{9V} = -1.21$ within 1σ and again, this requires a positive non vanishing $\Delta C_3(M_W) \in [0.1, 0.2]$ and very slight positive $\Delta C_2(M_W)$. None of the observables constrain ΔC_3 at all with vertical bands from radiative decay and mixing constraints, but these do impose a region of allowed values for $\Delta C_2(M_W)$. These

statements will be made quantitative in subsection 6.8.1. In the left hand panel of 6.6, is

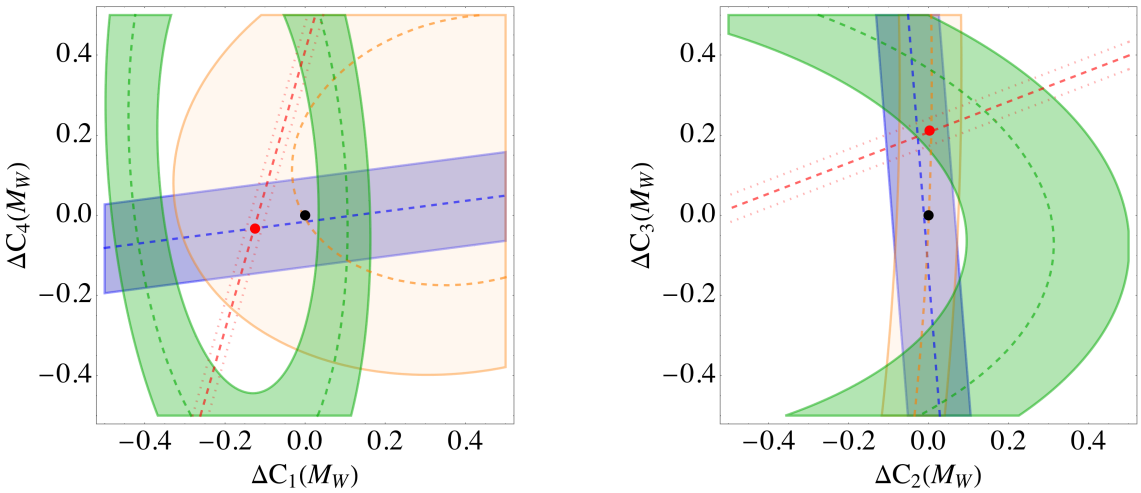

Figure 6.5: Two parameter planes of: left $\Delta C_1(M_W), \Delta C_4(M_W)$ and right $\Delta C_2(M_W), \Delta C_3(M_W)$

shown the $\Delta C_2(M_W) - \Delta C_4(M_W)$ plane which is less favoured by the data. None of the observables constrain $\Delta C_4(M_W)$ and in addition there is no point in the plane where all observables agree with a negative shift to C_{9V}. In the right hand panel showing the $\Delta C_3(M_W) - \Delta C_4(M_W)$ plane again the pattern of favoured new physics in $\Delta C_3(M_W)$ is confirmed. There is a point in the plane where all observables support the hypothesis for a positive $\Delta C_3(M_W) \in [0.2, 0.3]$ and a very slight negative $\Delta C_4(M_W)$. Viewing this "High

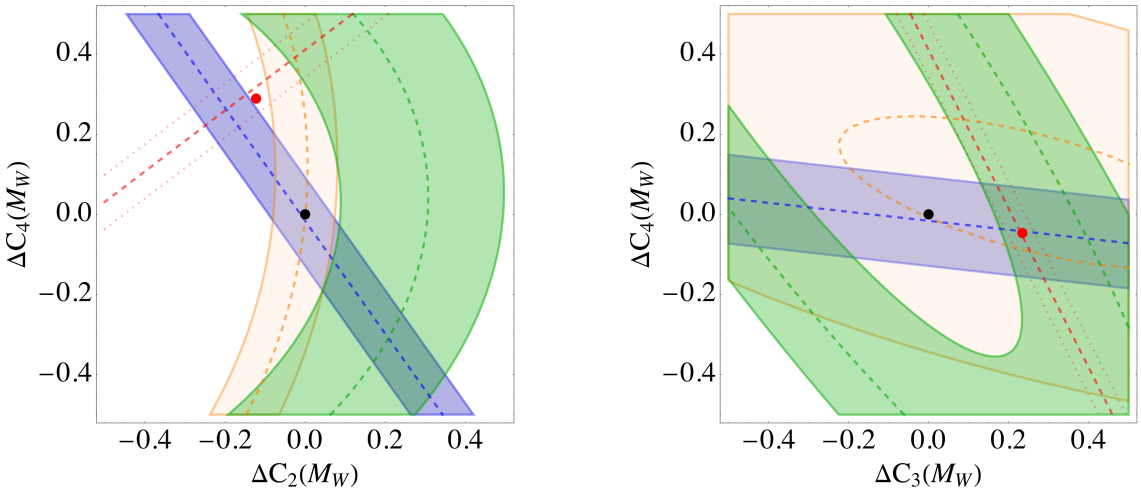

Figure 6.6: Two parameter planes of: left $\Delta C_2(M_W), \Delta C_3(M_W)$ and right $\Delta C_2(M_W), \Delta C_4(M_W)$

scale" BSM in C_{9V} from $\Delta C_1(M_W) - \Delta C_4(M_W)$ scenario the distinguishing features are that a non zero coefficient ΔC_3 at the weak scale is highly favoured, as is demonstrated in the right hand panels of 6.4, 6.5 and 6.6. All these point to a positive $\Delta C_3(M_W)$ accompanied by either a small shift to SM coefficients or a pure new physics scenario involving just $\Delta C_3(M_W)$,$\Delta C_4(M_W)$. The least favoured combinations are $\Delta C_2(M_W)$,$\Delta C_4(M_W)$

for which there is nowhere agreement from any of our chosen observables. It remains to be seen whether $\Delta C_1(M_W)$,$\Delta C_2(M_W)$ and $\Delta C_1(M_W)$,$\Delta C_4(M_W)$ could become viable but this is dependent upon future measurement, and SM calculations of the lifetime ratio, converging.

6.4 BSM in right handed currents: $\Delta C_1'(M_W) - \Delta C_4'(M_W)$

This subsection focuses upon the constraints that the right handed coefficients $C_9' = 0.19 \pm 0.2$ and $C_{7\gamma}' = 0.018 \pm 0.037$ which are associated with the "wrong chirality" semileptonic and dipole operators respectively, place upon new physics in $b \to c\bar{c}s$ coefficients $\Delta C_1'(M_W) - \Delta C_4'(M_W)$. In this case our "pseudo observables" are the coefficients $\bar{C}_{9V}'$ and $\bar{C}_{7\gamma}^{\prime\text{eff}}$ and rather than assuming BSM physics could be hidden in these coefficients, we instead use their best fit points obtained from global fits from [19] and [107] to angular observables as our "experimental central value". Regions are determined by individual constraints overlaid using (6.5) and best fit points correspond to points which minimize (6.6). The experimental quantities, their respective theoretical predictions and parameters of interest are

$$X^{Exp} = \{\Delta\Gamma_s^{Exp}, C_9^{\prime bs\mu\mu}, C_{7\gamma}', (\tau_s/\tau_d)^{Exp}, \mathcal{B}(B \to X_s\gamma)^{Exp}\} \tag{6.21}$$

$$X^{Th} = \{\Delta\Gamma_s, \bar{C}_{9V}(\mu_b), \bar{C}_{7\gamma}^{\prime\text{eff}}(\mu_b), (\tau_{B_s}/\tau_{B_d}), \mathcal{B}(B \to X_s\gamma)\} \tag{6.22}$$

$$\vec{\theta} = \{\Delta C_1'(M_W), \Delta C_2'(M_W), \Delta C_3'(M_W), \Delta C_4'(M_W)\} \tag{6.23}$$

and the theoretical predictions in (6.22) are given by (5.81), (5.22), (5.41), (5.85) and (5.37) in Chapter 5. In all the panels in figures 6.7, 6.8 and 6.9 are shown contours of $\bar{C}_{9V}' = 0.19 \pm 0.2$ in red dashed at central value and dotted at 1σ, and $\bar{C}_{7\gamma}^{\prime\text{eff}} = 0.018 \pm 0.037$ in blue dashed (central value) and dotted (1σ). The observables already mentioned above are shown according to the same colour scheme. The radiative decay constraint for the primed coefficients is much weaker than in the previous case due to (assuming parity symmetry) the mixing of operators $Q_1', ..., Q_4'$ with $Q_{7\gamma}'$ under renormalization occurring first at two-loop, and in addition, to the primed coefficient $\bar{C}_7^{\prime\text{eff}}$ only entering (5.38) quadratically with no linear dependence upon $C_7^{\text{eff,SM}}$. For combinations of these coefficients it is found that the strongest constraint comes from the experimental fits of angular observables to C_9'. This is due to a strong dependence of $C_{9V}^{\prime,\text{BSM}}(m_b)$ upon $\Delta C_1'(M_W) - \Delta C_4'(M_W)$ which results in closely spaced contours (red dashes).

In the $(\Delta C_1'(M_W), \Delta C_2'(M_W))$ plane shown in Figure 6.7 (left), the radiative decay does not constrain the scenario, and the width difference only mildly constrains $\Delta C_2'$ and the lifetime ratio constrains mildly $\Delta C_1'$. In the right panel $(\Delta C_1'(M_W), \Delta C_3'(M_W))$ does achieve a best fit point for which all observables agree, however this would imply a large $\Delta C_3' < -0.4$ and $\Delta C_1' \approx -0.3$ which has been pulled down to the left hand corner by the non visible contours of $\bar{C}_7'^{\text{eff}}$ for which the central value is beyond the right bottom hand corner. The central values for the rare and radiative decay agree for large negative values of $(\Delta C_1, \Delta C_3) \approx (-2.1, -3.5)$. In Figure 6.8 the radiative decay

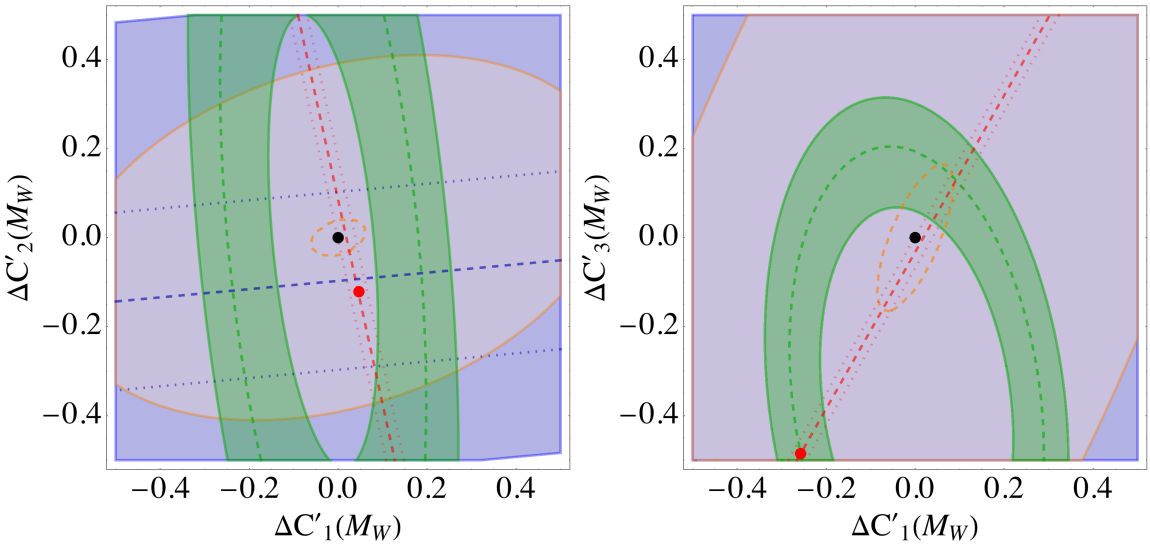

Figure 6.7: Contours of $\bar{C}_{9V}'$ (red, dashed) and $\bar{C}_{7\gamma}'^{\text{eff}}$ (blue, dashed) for best fit, and 1 sigma ranges, along with radiative decay (blue), lifetime ratio (green) and width difference (orange) 1 sigma constraints on coefficients $\Delta C_1'(M_W), \Delta C_2'(M_W)$ and $\Delta C_1'(M_W), \Delta C_3'(M_W)$.

constrains the even coefficients and the rare decay, very tightly the odd coefficients. In the $(\Delta C_1'(M_W), \Delta C_4'(M_W))$ plane (left) there is a best fit point for which all observables agree implying that for this scenario new physics is slightly favoured over the SM. In the $(\Delta C_2(M_W), \Delta C_3(M_W))$ plane and in Figure 6.9 the $(\Delta C_2(M_W), \Delta C_4(M_W))$ plane (left) the best fit value is very close to zero which appears to be due to the pull of the lifetime ratio somewhat cancels out the effect of the radiative decay. Finally in Figure 6.9 right there is no point in the plane where all observables agree but a $(\Delta C_3'(M_W), \Delta C_4'(M_W)) \approx (0.03, -0.1)$ are the best fit for the current data.

6.5 General constraints on BSM: $\Delta C_5^{(\prime)}(M_W) - \Delta C_{10}^{(\prime)}(M_W)$

In figure 6.10 are shown three examples of two parameter scenarios involving combinations of the coefficients $\Delta C_5 - \Delta C_{10}$ evaluated at the weak scale. For this case regions

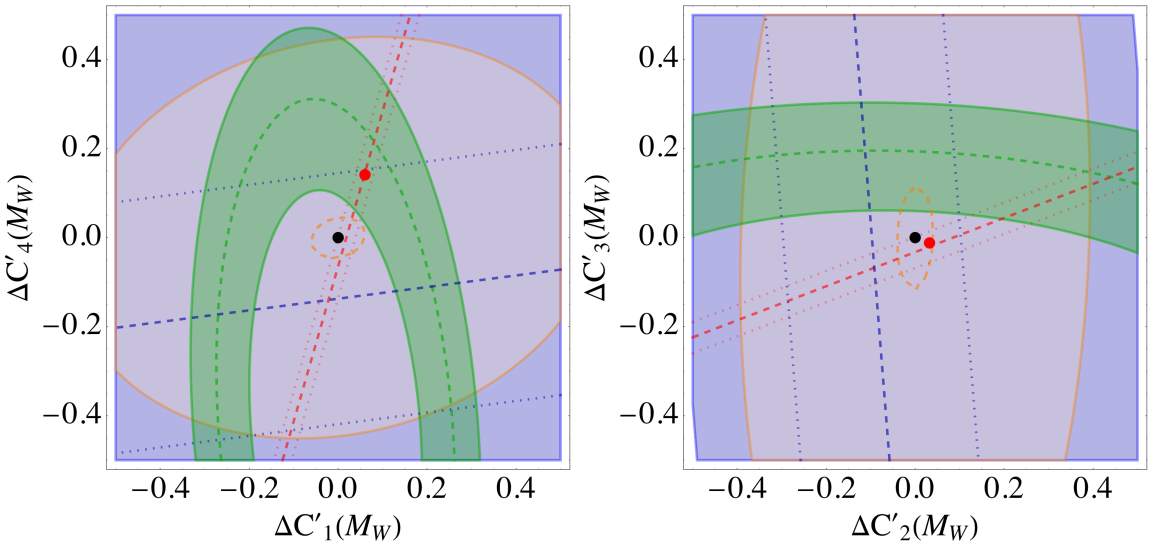

Figure 6.8: Contours of $\bar{C}'_{9V}$ (red, dashed) and $\bar{C}'^{\text{eff}}_{7\gamma}$ (blue, dashed) for best fit, and 1 sigma ranges, along with radiative decay (blue), lifetime ratio (green) and width difference (orange) 1 sigma constraints on coefficients $\Delta C'_1(M_W), \Delta C'_4(M_W)$ and $\Delta C'_2(M_W), \Delta C'_3(M_W)$.

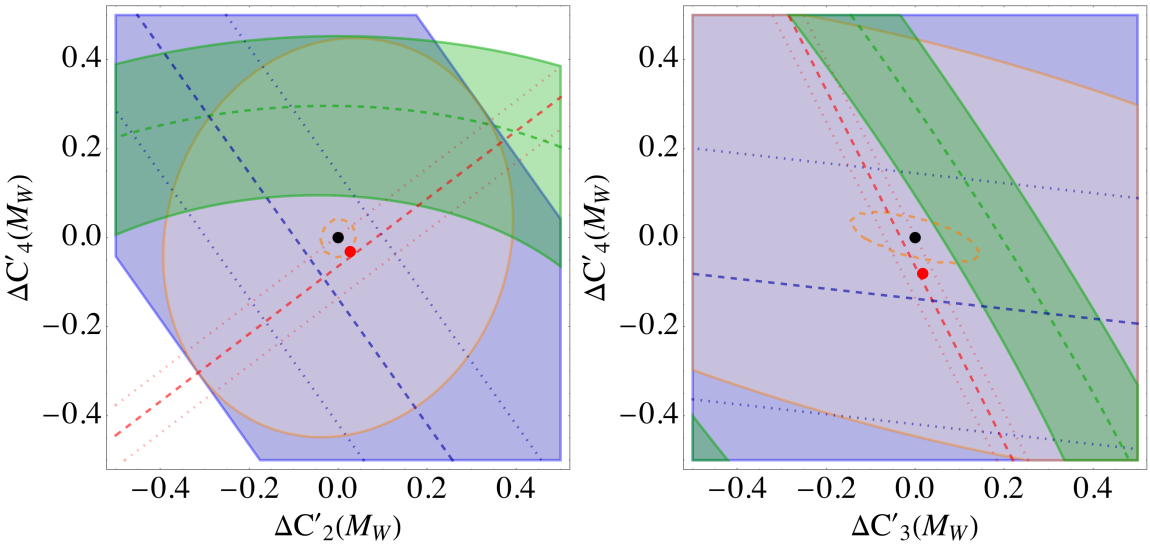

Figure 6.9: Contours of $\bar{C}'_{9V}$ (red, dashed) and $\bar{C}'^{\text{eff}}_{7\gamma}$ (blue, dashed) for best fit, and 1 sigma ranges, along with radiative decay (blue), lifetime ratio (green) and width difference (orange) 1 sigma constraints on coefficients $\Delta C'_2(M_W), \Delta C'_4(M_W)$ and $\Delta C'_3(M_W), \Delta C'_4(M_W)$.

are determined as are the cases above, experimental quantities, their respective theoretical predictions and parameters of interest are

$$X^{Exp} = \{\Delta\Gamma_s^{Exp}, (\tau_s/\tau_d)^{Exp}, \mathcal{B}(B \to X_s\gamma)^{Exp}\} \tag{6.24}$$

$$X^{Th} = \{\Delta\Gamma_s, (\tau_{B_s}/\tau_{B_d}), \mathcal{B}(B \to X_s\gamma)\} \tag{6.25}$$

$$\vec{\theta} = \{\Delta C_5(M_W), ..., \Delta C_{10}(M_W), \Delta C'_5(M_W), ..., \Delta C'_{10}(M_W)\} \tag{6.26}$$

and the theoretical predictions in (6.25) are given by (5.81),(5.85) and (5.37) in Chapter 5. The presiding feature in all of these panels is the stringent constraint placed upon values

that these coefficients could take, by $\mathcal{B}(B \to X_s\gamma)$.

6.5.1 $\Delta C_5 - \Delta C_{10}$

As explained in chapter 4, the mixing of operators $Q_5, ..., Q_{10}$ with $Q_{7\gamma}$ first at one-loop gives rise to strong RG effects which enter $\bar{C}_7^{\text{eff}}$ and result in the dominant constraint for such scenarios coming from radiative decays. As the coefficient $\bar{C}_7^{\text{eff}}$ enters (5.38) both quadratically as well as linearly, it receives a contribution from $C_7^{\text{eff,SM}}$ which at the scale $\mu_b = 4.2\,\text{GeV}$ we take to be $C_7^{\text{eff,SM}}(\mu_b) = -0.385$. This combination results in a much narrower 1 sigma region, as is shown in all panels of Figure 6.10 as the blue shaded area. In the first and third panel, the presence of another purple band corresponds to contours where $\bar{C}_7^{\text{eff}} = \pm C_7^{\text{eff},SM}$. In terms of the lifetime ratio, shown in the green shaded area, the contours slightly miss the SM point due to the current 1.4σ discrepancy between theory and experiment. For the $B_s - \bar{B}_s$ width difference the scenarios consisting of coefficients of left and right handed vector currents and coefficients of tensor operators are the most restrictive. In all cases scenarios between even numbered coefficients are favoured owing to the $\frac{1}{N_c}$ suppression which always accompanies colour singlet operators in the calculations.

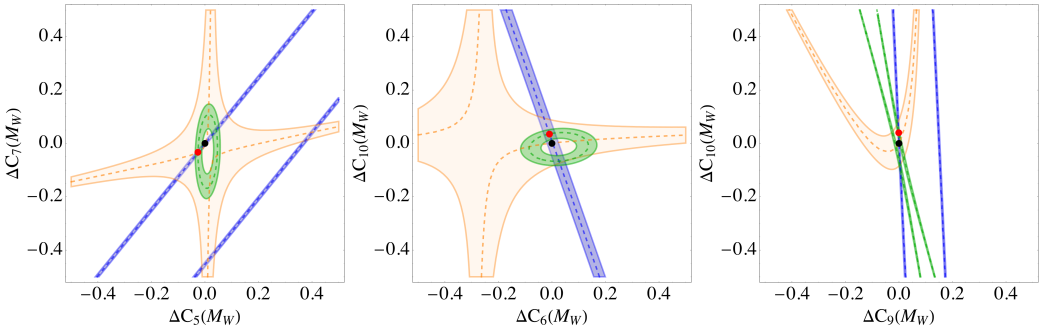

Figure 6.10: Overlaid individual constraints from radiative decay (blue), lifetime ratio (green), width difference (orange) upon $\Delta C_5 - \Delta C_7$ plane (left), $\Delta C_6 - \Delta C_{10}$ plane (middle), $\Delta C_9 - \Delta C_{10}$ plane (right). The SM point and best fit point are shown as the black and red dots respectively.

6.5.2 $\Delta C_5' - \Delta C_{10}'$

Three examples of possible 2 parameter scenarios are shown in Figure 6.11 and are the right handed counter parts in one to one correspondence with those of Figure 6.10. Although as for coefficients $\Delta C_5 - \Delta C_{10}$, it is also true in this case that the one-loop mixing under renormalization of $Q_5', ..., Q_{10}'$ with $Q_{7\gamma}'$ results in a stronger dependence of $\bar{C}_7'^{\text{eff}}$ upon $\Delta C_5' - \Delta C_{10}'$ than is true for coefficients $\Delta C_1' - \Delta C_4'$, here $\bar{C}_7'^{\text{eff}}$ only contributes

quadratically to the $B \to X_s\gamma$ branching ratio so the radiative decay constraint bands are wider. All plots show very similar constraints from the lifetime ratio and the width difference, although differences are more pronounced in $\Delta\Gamma_s$ due to primed and unprimed coefficients not mixing in the theoretical prediction for Γ_{12}^{NP} and hence there is no linear contribution from SM Wilson coefficients C_1 and C_2 here.

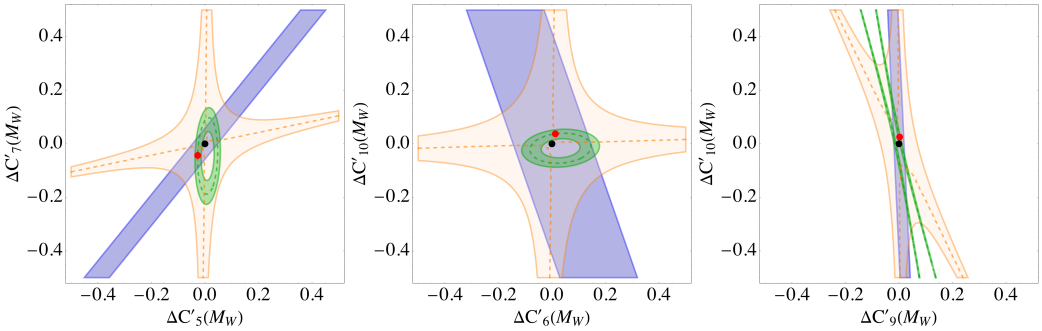

Figure 6.11: Overlaid individual constraints from radiative decay (blue), lifetime ratio (green), width difference (orange) upon $\Delta C_5' - \Delta C_7'$ plane (left), $\Delta C_6' - \Delta C_{10}'$ plane (middle), $\Delta C_9' - \Delta C_{10}'$ plane (right). The SM point and best fit point are shown as the black and red dots respectively.

6.6 Prospects for mixing and lifetime observables

In this section we turn our attention to the precision with which we may know exactly the predicted and measured value of the width difference, the lifetime ratio and the $\mathcal{B}(\bar{B} \to X_s\gamma)$ branching ratio. Here, it is investigated whether in the case where the predictions and the measurements coincide, such observables could discriminate between different scenarios of Wilson coefficients, and even completely rule some of them them out.

In Figures 6.12-6.14 are shown contours of constant width difference (brown) and lifetime ratio (green) corresponding to the SM central values respectively. The dashed and dotted lines are spaced either side of this in such a way that any spacing between two contours corresponds to a prospective 1σ region, where we have assumed a combined experimental and theoretical error of 0.001 on the lifetime ratio and an error of 5% on the width difference. These future errors are representative of expected theoretical and experimental progress. For the width difference, the experimental error in table 6.6 is already 6%, but in this observable it is the theoretical error which requires most improvement. Since publication of [1], the state of the art SM prediction is $\Delta\Gamma_s = 0.091 \pm 0.014$ [125] with a current error of 14% which is a marked improvement on 23% as given by table 6.2 [38]. The main source of theoretical error is due to the lattice determination of dimension 7 operators [126], however it is realistic to expect a future reduction in uncertainty to be-

low 5%, given further effort from both sum rules and lattice QCD. For the lifetime ratio, the theoretical error is already 2.5 per mille, and current work in reducing this error by including $SU(3)_F$ violating corrections and inclusion of extra, previously undetermined terms is in progress [125]. For further reduction, again this would require determination of dimension 7 operator matrix elements. Experimentally, the error is greater at 4 per mille, however a recent ATLAS measurement of the B_s^0 width difference has been presented [127] with reduced errors, indicating a B_s^0 lifetime with accordingly reduced errors at approximately around 2.5 per mille. Other collaborations such as CMS and LHCb providing independent measurements could result in halving the current uncertainty. With future developments 1 per mille is achievable.

In addition, we have shown the $\mathcal{B}(\bar{B} \to X_s\gamma)$ overlaid as the blue shaded region corresponding to a 1σ difference between measurement and SM. In Figure 6.12 the left hand

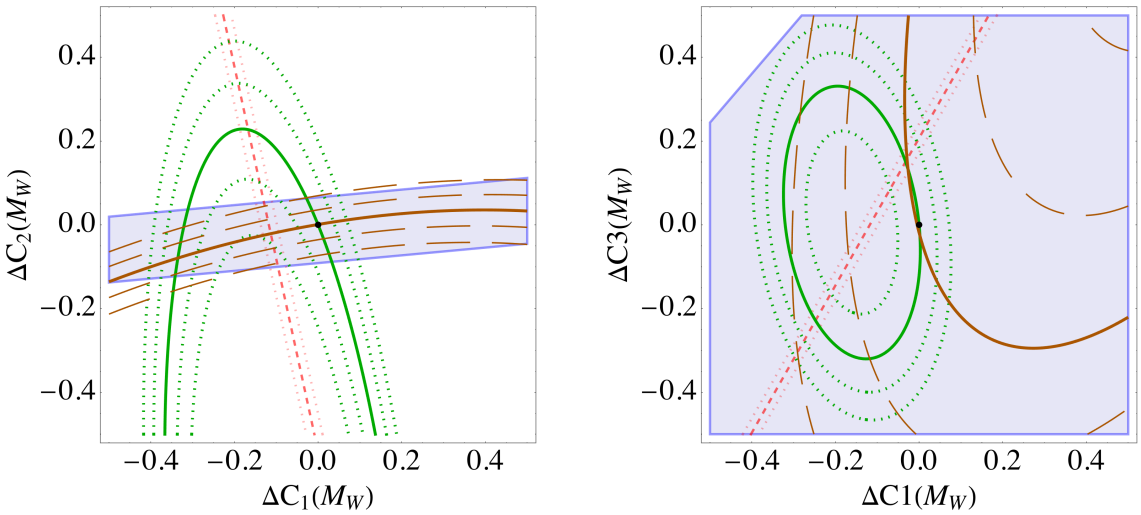

Figure 6.12: Future prospects for lifetime and mixing observables. Left hand panel: real $\Delta C_1 - \Delta C_2$ plane, right hand panel: real $\Delta C_1 - \Delta C_3$ plane. Solid lines are the SM prediction for width difference (brown) and lifetime ratio (green). Brown dashed and green dotted lines are contours of constant width difference and lifetime ratio respectively.

panel shows a point in the $(\Delta C_1, \Delta C_2)$ plane where $\bar{C}_{9V} = -1.21$ at a 2σ deviation in the lifetime ratio and a 1σ deviation in $\Delta\Gamma_s$ which is just within the constraints imposed by radiative decay. In the right hand panel showing the combination $\Delta C_1 - \Delta C_3$, contours of $\bar{C}_{9V} = -1.21$, and the SM contours for both mixing and lifetime coincide within 1σ in this scenario favoured already in Figure 6.4. In Figure 6.13 left hand panel, there are not any points in the $(\Delta C_1, \Delta C_4)$ plane which simultaneously allow a new contribution to semi-leptonic decay and still lie within 1σ of the other constraints. One could consider that this scenario is potentially ruled out by the lifetime ratio which requires a larger value of ΔC_4 than can be accommodated by radiative decay. In the right hand

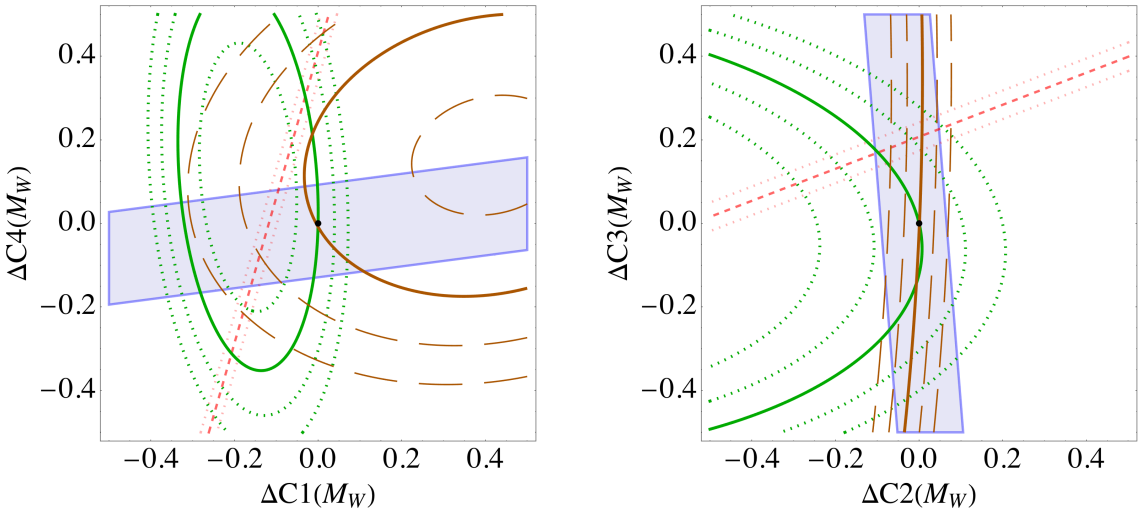

Figure 6.13: Future prospects for lifetime and mixing observables. Left hand panel: real $\Delta C_1 - \Delta C_4$ plane, right hand panel: real $\Delta C_2 - \Delta C_3$ plane. Solid lines are the SM prediction for width difference (brown) and lifetime ratio (green). Brown dashed and green dotted lines are contours of constant width difference and lifetime ratio respectively.

panel we observe that a smaller combined error on the mixing and lifetime observables can more accurately pinpoint preferred values for couplings in this scenario of approximately $(\Delta C_2, \Delta C_3) \approx (-0.05, 0.15)$. In Figure 6.14 left hand panel, there are no points for

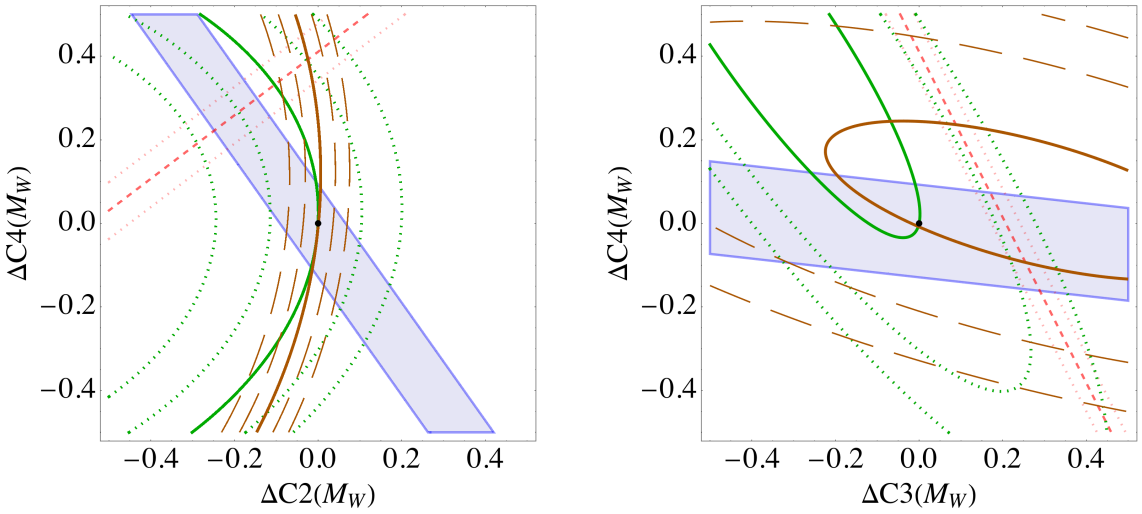

Figure 6.14: Future prospects for lifetime and mixing observables. Left hand panel: real $\Delta C_2 - \Delta C_4$ plane, right hand panel: real $\Delta C_3 - \Delta C_4$ plane. Solid lines are the SM prediction for width difference (brown) and lifetime ratio (Green). Brown dashed and green dotted lines are contours of constant width difference and lifetime ratio respectively.

which all observables considered can accommodate $\bar{C}_{9V} = -1.21$ within 1σ. Interestingly, although the better agreement between experiment and theory in the lifetime ratio helps this scenario, the more ambitious future error estimates for the width difference prevent a negative contribution to our pseudo observable $\bar{C}_{9V}$ which is accommodated by $\mathcal{B}(\bar{B} \to X_s\gamma)$ and one might therefore conclude that this is a case where more precise knowledge would rule out this scenario. Finally, in the right hand panel we find again that

a situation which involves ΔC_3 is favoured and with the $\bar{C}_{9V} = -1.21$ contour running almost parallel with, but just outside the limits of, the lifetime ratio 1σ contour, we might consider the possibility that a further precise determination of $\Delta\Gamma_s$ could really pinpoint the place on this line which offers a candidate for a viable new physics scenario.

6.7 CP Violation: Complex Wilson coefficients ΔC_1, ΔC_2

In this section we determine bounds upon the size of complex shifts to SM Wilson coefficients C_1^c and C_2^c by introducing a new weak CP violating phase for each coefficient. The observables which are sensitive to CP violation are the flavour specific CP asymmetry a_{fs}^s and the time dependent CP asymmetry $A_{CP}(B_d^{(0)} \to J/\psi K_S)$. In subsection 6.7.1 are shown constraints from $a_{fs}^s, \mathcal{B}(\bar{B} \to X_s\gamma), \frac{\tau_s}{\tau_d}$ and $\Delta\Gamma_s$, in the complex ΔC_i plane for $i = 1, ..., 4$. In subsection 6.7.2 we show the above constraints and in addition, a further set of three constraints from the hadronic $B_d^0 \to J/\psi K_{(S)}$ decay.

6.7.1 CP violating constraints on NP in SM coefficients

Figure 6.15 shows the complex $\Delta C_1(M_W)$ plane (left hand side) and the complex $\Delta C_2(M_W)$ plane (right hand side). In the complex $\Delta C_1(M_W)$ plane are shown in red the width difference, in purple the flavour specific asymmetry and in green the lifetime ratio. For a scenario where CP violation is accounted for by a complex phase in this coefficient the best observable to discriminate possible values is the lifetime ratio which constrains the real and imaginary parts to lie in the set of points $\{\Delta C_1(M_W) \in \mathbb{C} : 0.21 < |\Delta C_1(M_W) + 0.16| < 0.31\}$. Taking into account the other constraints leads to an approximate constraint on the complex phase of $\Delta C_1(M_W)$ of $\phi_1 \in [-\frac{3\pi}{4}, \frac{3\pi}{4}]$. In the right hand panel there is a stronger constraint upon the imaginary part of $\Delta C_2(M_W)$ from the flavour specific asymmetry, and constraints upon the real part from the lifetime ratio, width difference and inclusive radiative branching ratio. There is no point in the plane where all observables agree upon a particular value, however the precisely measured and theoretically well controlled branching ratio and width difference along with the CP asymmetry require a complex $Re(\Delta C_2)(M_W) \in [-0.1, 0.1]$ and $\mathrm{Im}\Delta C_2(M_W) \in [-0.2, 0.2]$ for agreement at the level of 1σ. In Figure 6.16 (left) are shown constraints upon a complex $\Delta C_3(M_W)$, which are dominated by the lifetime ratio. The lifetime ratio requires that complex values of $\Delta C_3(M_W)$ are included in the set $\{\Delta C_3(M_W) \in \mathbb{C} : 0.35 < |\Delta C_3(M_W) + 0.02| < 0.54\}$ and here there are no restrictions on the complex phase. In the right hand panel are

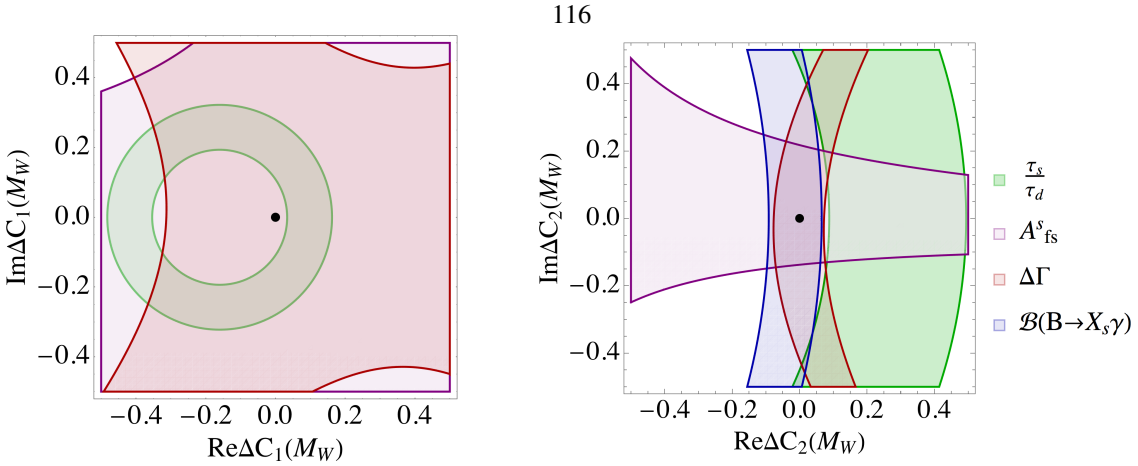

Figure 6.15: Complex Wilson coefficients $\Delta C_1(M_W)$, $\Delta C_2(M_W)$

shown regions of the complex $\Delta C_4(M_W)$ plane allowed by all of the observables. In this case, the radiative inclusive branching ratio constrains the real part and the lifetime ratio and width difference, the imaginary part. For this coefficient there are points in the plane for which all observables agree at 1σ and these are approximately $Re\Delta C_4(M_W) \in [-0.2, 0.1]$ and $\mathrm{Im}\Delta C_4(M_W) \in [-0.5, -0.3], [0.25, 0.5]$.

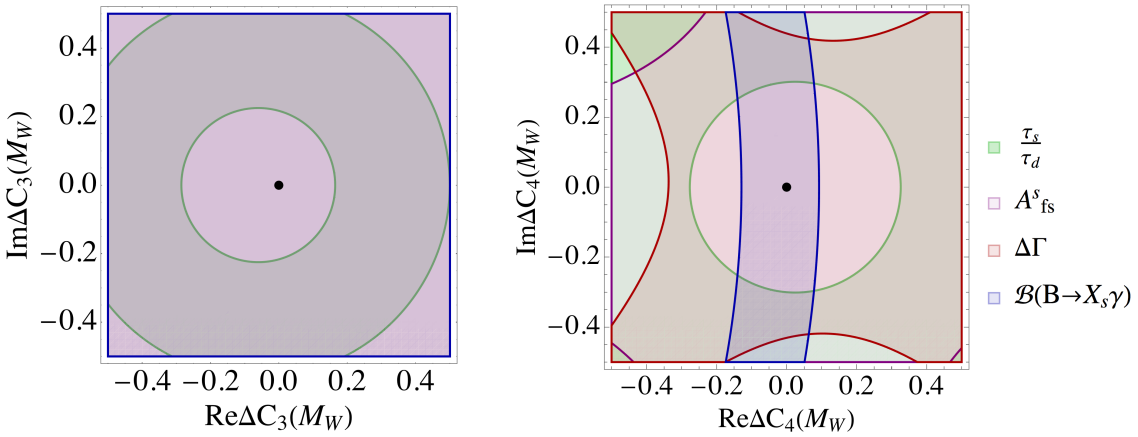

Figure 6.16: Complex Wilson coefficients $\Delta C_3(M_W)$, $\Delta C_4(M_W)$

6.7.2 Constraints from hadronic decay

In the study of the SM Wilson coefficients $C_1(\mu), C_2(\mu)$ in the non leptonic decay $B \to J/\psi K_S$, we assume these be shifted relative to their SM values by amount $\Delta C_1(\mu), \Delta C_2(\mu)$ and allow them to take on complex values. Here, we will be using the profile χ^2 in (6.9) and equations (6.3) and (6.4) take the form

$$\vec{\theta} = (\mathrm{Re}(\Delta C_1(M_W)), \mathrm{Im}(\Delta C_1(M_W)), \mathrm{Re}(\Delta C_2(M_W)), \mathrm{Im}(\Delta C_2(M_W)))^T \quad (6.27)$$

$$\vec{\nu} = (\mathrm{Re}(r_{21}), \mathrm{Im}(r_{21}), |\langle \mathcal{O}_1^c \rangle|)^T \quad (6.28)$$

and the experimental measured values and their corresponding theoretical predictions are

$$X^{Exp} = \{S^{exp}_{J/\psi K}, C^{exp}_{J/\psi K}, \mathcal{B}(B \to J/\psi K)^{exp}\} \tag{6.29}$$

$$X^{Th} = \{S_{J/\psi K}, C_{J/\psi K}, \mathcal{B}(B \to J/\psi K)\} \tag{6.30}$$

where the central values of (6.1) are taken from [78] and [33]

$$S^{exp}_{J/\psi K} = 0.699 \pm 0.017 \tag{6.31}$$

$$C^{exp}_{J/\psi K} = -0.005 \pm 0.015 \tag{6.32}$$

$$\mathcal{B}(B \to J/\psi K)^{exp} = (8.73 \pm 0.32)10^{-4} \tag{6.33}$$

and the analytical functional form of the observables in are given by (5.156), (5.157) and (5.163).

Complex ΔC_1 plane

Let us now consider what constraints may be obtained in the complex ΔC_1 plane. The naive factorization estimate for the ratio of matrix elements defined in (5.155) with $i = 2$ is

$$r^{NF}_{21} = \frac{1}{N}, \tag{6.34}$$

with $N = 3$. Our first result shown in Figure 6.17, depicts the departure of the complex parameter r_{21} from the naive factorization estimate shown above, for all angles $\phi_{21} \in [-\pi, \pi]$ at a given radius corresponding to contours of $\frac{\tau(B_s)}{\tau(B_d)}^{\text{th}} = 0.993 \pm 1\sigma$, in the the annulus given by the shaded green region in Figure 6.15 (left). The phase ϕ_{21} is given by

$$\phi_{21} = \text{Arg}\left(\frac{\text{Im}(\Delta C_1)}{\text{Re}(\Delta C_1 - \delta)}\right) \tag{6.35}$$

with $\delta = -0.16$, the offset of the center of the concentric circles from the SM point at $(0, 0)$. Figure 6.17 shows four distinct points (there are only four because $\pm\pi$ is the same point) within the region allowed by lifetime data at 1σ, for which the χ^2 is minimized to give a value of r_{21} in agreement with (6.34). Table 6.7 shows the angles for which the value of r_{21} at the minimum coincides with the naive factorization prediction, along with the corresponding points in the ΔC_1 plane.

Analogously, in Figure 6.18 is shown the departure of the $|\langle \mathcal{O}^c_1 \rangle|$ from the NF prediction. In the left hand panel we see the surprising result that there are four distinct points for

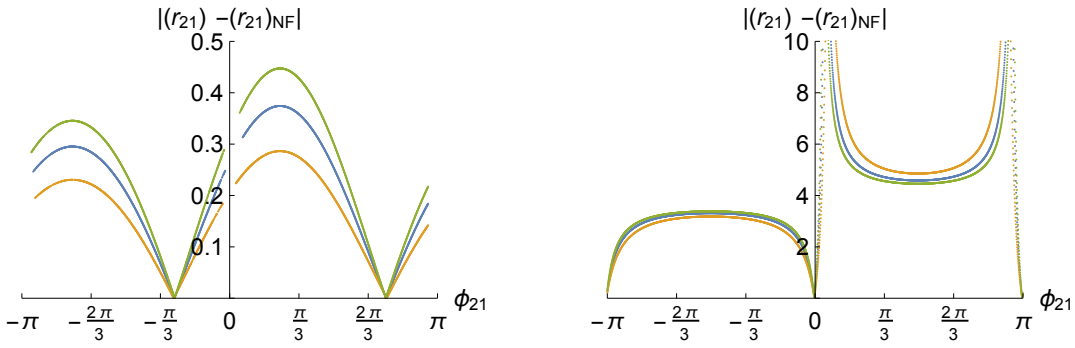

Figure 6.17: Left: Solution 1 and Right: Solution 2 showing the difference between the naive estimate for r_{21} and the point wise minimum values of r_{21} for fixed $\frac{\tau_s}{\tau_d} \in \{0.988, 0.993, 0.998\}$ shown as green, blue, yellow lines respectively.

ϕ_{21}	$\mathrm{Re}(\Delta C_1) + i\mathrm{Im}(\Delta C_1)$
Solution 1	
$\phi_{21} = -0.85\,\mathrm{rad}\,(-49.4°)$	$0.01 - 0.2i$
$\phi_{21} = 2.37\,\mathrm{rad}\,(136°)$	$-0.35 + 0.2i$
Solution 2	
$\phi_{21} = 0.013\,\mathrm{rad}\,(-0.75°)$	$0.1 + 0i$
$\phi_{21} = 3.13\,\mathrm{rad}\,(179.3°)$	$-0.4 + 0i$

Table 6.7: ϕ_{21} and ΔC_1 values where r_{21} agrees with Naive Factorization

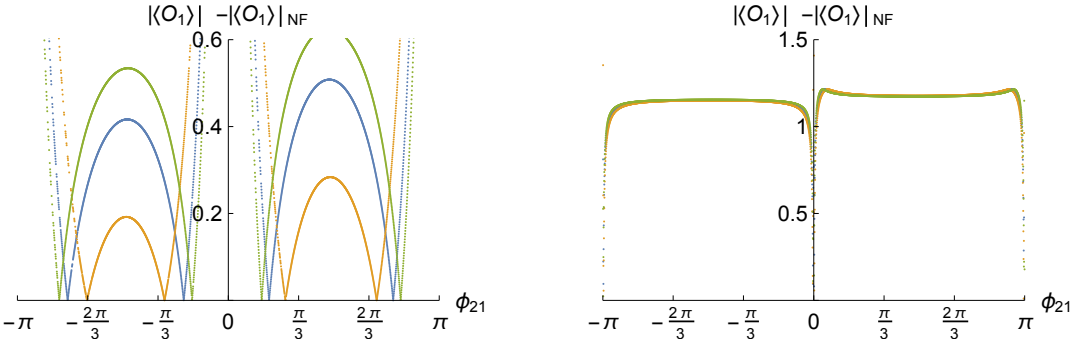

Figure 6.18: Left: Solution 1 and Right: Solution 2 showing the difference between the naive estimate for $|\langle \mathcal{O}_1^c \rangle|$ and the point wise minimum values of $|\langle \mathcal{O}_1^c \rangle|$ for fixed $\frac{\tau_s}{\tau_d} \in \{0.988, 0.993, 0.998\}$ shown as green, blue, yellow lines respectively

which the value of $|\langle \mathcal{O}_1^c \rangle|$ at the minimum coincides with the naive factorization prediction of $|\langle \mathcal{O}_1^c \rangle|_{NF} = 1.23\mathrm{GeV}^3$. In the right hand panel there are again only two points at $\phi_{21} = 0, \pm\pi$. The corresponding angles and points in the complex plane are shown in Table 6.8.

ϕ_{21}	$\mathrm{Re}(\Delta C_1) + i\mathrm{Im}(\Delta C_1)$
Solution 1	
$\phi_{21} = 0.85\,\mathrm{rad}\,(48.8°)$	$0.5 + 0.15i$
$\phi_{21} = 2.21\,\mathrm{rad}\,(126.6°)$	$-0.35 + 0.2i$
$\phi_{21} = -2.1\,\mathrm{rad}\,(-120.6°)$	$-0.35 - 0.2i$
$\phi_{21} = -0.95\,\mathrm{rad}\,(-54.4°)$	$0.4 - 0.18i$
Solution 2	
$\phi_{21} = 0.01\,\mathrm{rad}\,(0.43°)$	$0.1 + 0i$
$\phi_{21} = 3.13\,\mathrm{rad}\,(179.2°)$	$-0.37 + 0i$

Table 6.8: ϕ_{21} and ΔC_1 values where $|\langle \mathcal{O}_1^c \rangle|$ agrees with Naive Factorization

In Figure 6.19 are shown the solutions for the values of $|\langle \mathcal{O}_1^c \rangle|$ again with the phase ϕ_{21}, and over this is shown the theoretical prediction for $|\langle \mathcal{O}_1^c \rangle|_{NF}$ given in (5.137) including parametric error bars plus a correction of $\mathcal{O}^c\left(\frac{1}{N^2}\right)$, which we include to parameterize our ignorance of the hadronic effects using the large N counting rules of [97]. The purple

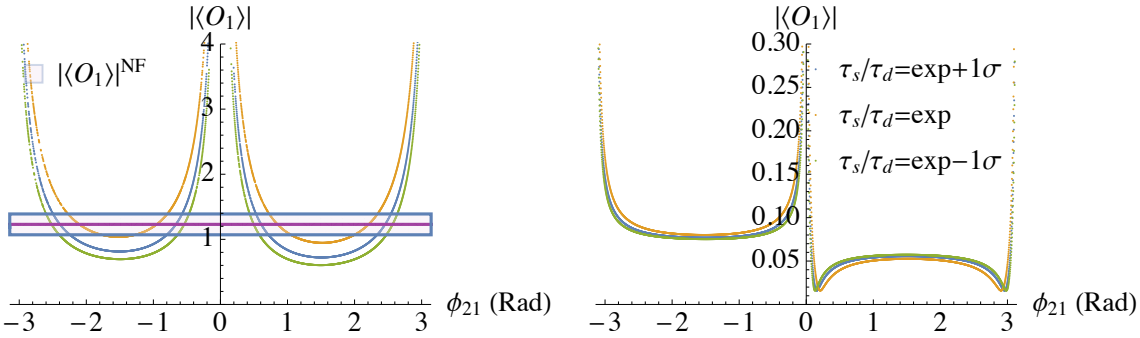

Figure 6.19: Left: Solution 1 and Right: Solution 2 showing the values of the hadronic matrix element $|\langle \mathcal{O}_1^c \rangle|$ with phase ϕ_{12} for contours of constant lifetime ratio $\frac{\tau_s}{\tau_d} \in \{0.988, 0.993, 0.998\}$ shown as green, blue, yellow lines respectively. Theoretical estimate for $|\langle \mathcal{O}_1^c \rangle|$ in purple with errors in blue.

line is the central value and the blue shaded area represents the error. In the left hand panel it is clear that there are four points where the numerical solution crosses the NF estimate. In the right hand panel it is less clear to the eye, but there are in fact solutions at $\phi_{21} = 0, \pm\pi$ as was the case with r_{21}. These are the same points as those shown in Figure 6.18. All in all, this parameter allows six regions in the complex ΔC_1 plane which further constrain the possibility of physics BSM in C_1^c. All the above results are summarized in Figure 6.20 which shows all points determined by the above analysis in one figure in the complex ΔC_1 plane. In this graph are shown angular and radial regions which correspond

to the constraints we can obtain from our minimization procedure as described above. The squares represent the points in the plane where r_{21} agrees with the naive factorization estimate exactly. As r_{21} is less well theoretically controlled due to the uncertainty in the matrix element of $\mathcal{O}_2^c$ being considered to be greater (as it would receive corrections of $\mathcal{O}(\alpha_s)$) we do not estimate errors but simply show points of agreement. These occur at the angles and points shown in table 6.7. The solid lines represent angular regions where the solutions in Figure 6.19 coincide with the NF prediction and it's error at the given radius. What is interesting about this plot is that there seems to be some sort of degeneracy in the points allowed in the upper and lower plane, which is broken by a strict agreement of r_{21} with the NF prediction.

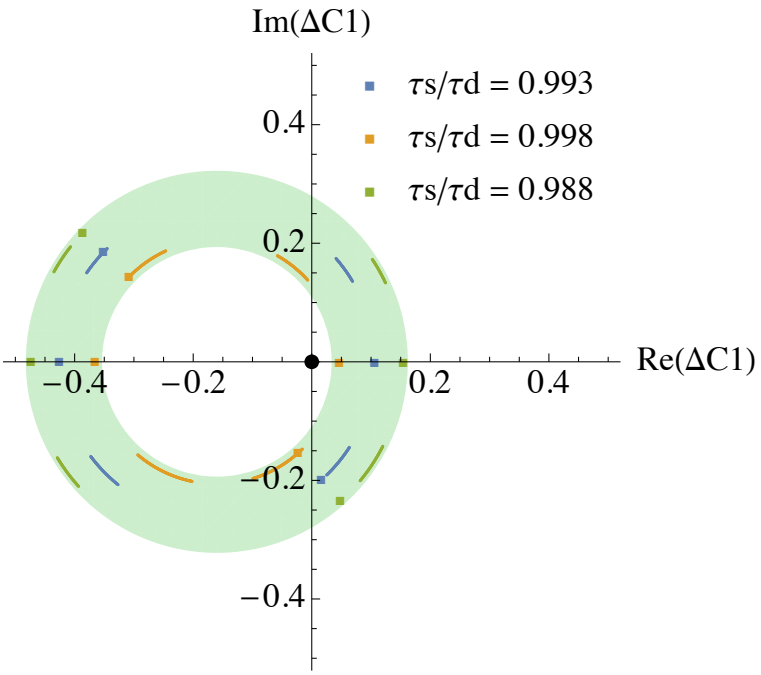

Figure 6.20: Naive factorization predictions for $|\langle\mathcal{O}_1^c\rangle|, \mathrm{Re}(r_{21}), \mathrm{Im}(r_{21})$ in complex $\Delta C_1(M_W)$ plane

In Table 6.9 are given the angular regions and the corresponding allowed real and imaginary parts of ΔC_1 shown in Figure 6.20. As can be seen in the figure, there are four continuous angular ranges corresponding to each of the contours of the lifetime ratio, which can be distinctly separated in the region $\{\Delta C_1(M_W) \in \mathbb{C} : 0.21 < |\Delta C_1(M_W) + 0.16| < 0.31\}$.

Complex ΔC_2 plane

We turn our attention now to the complex ΔC_2 plane and find a rather different picture emerge. The same analysis is performed as is done for the coefficient ΔC_1 however when

$\Delta\phi_{21}$	$\mathrm{Re}(\Delta C_1)$	$\mathrm{Im}(\Delta C_1)$
$25^\circ \leqslant \phi_{21} \leqslant 60^\circ$	$\mathrm{Re}\Delta C_1 \in [-0.06, 0.12,]$	$\mathrm{Im}\Delta C_1 \in [0.13, 0.18]$
$115^\circ \leqslant \phi_{21} \leqslant 151^\circ$	$\mathrm{Re}\Delta C_1 \in [-0.34, -0.29]$	$\mathrm{Im}\Delta C_1 \in [0.10, 0.29]$
$-149^\circ \leqslant \phi_{21} \leqslant -102^\circ$	$\mathrm{Re}\Delta C_1 \in [-0.43, -0.20]$	$\mathrm{Im}\Delta C_1 \in [-0.20, -0.16]$
$-73^\circ \leqslant \phi_{21} \leqslant -37^\circ$	$\mathrm{Re}\Delta C_1 \in [-0.09, 0.12]$	$\mathrm{Im}\Delta C_1 \in [-0.2, -0.14]$

Table 6.9: $\Delta\phi_{21}$ and ΔC_1 values where $|\langle \mathcal{O}_1^c \rangle|$ agrees with Naive Factorization

regarding Figure 6.15 we see that there is no region wherein all the observables under consideration agree which would provide an obvious region over which to minimize the χ^2 containing $B \to J/\psi K$ predictions.

The closest region of overlap appears to be along the line $\mathrm{Re}(\Delta C_2) = 0.1$ thus we minimize for each point on that line to obtain the values of the uncertain hadronic parameters which give the best description of the data. In Figure 6.21 in the left hand panel there is a solution to the minimization problem which favours a value of $\mathrm{Re}(r_{21})$ in agreement with naive factorization of a small negative value of $\mathrm{Im}(\Delta C_2)$. The right hand panel however has no points where there is agreement with naive factorization. In Figure 6.22 in the

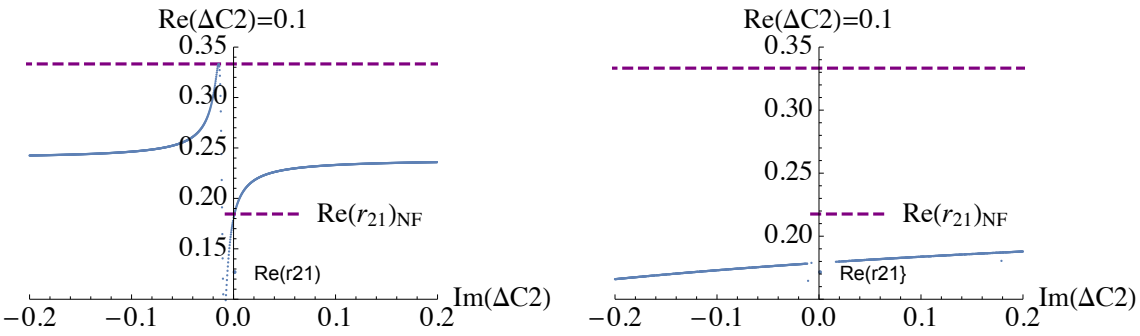

Figure 6.21: Solution 1 (left) and solution 2 (right) for the value of $\mathrm{Re}(r_{21})$ at fixed $\mathrm{Re}(\Delta C_2) = 0.1$ and $\Delta C_2 \in [-0.2, 0.2]$ (blue solid) and the naive factorization prediction of $\mathrm{Re}(r_{21})$ (purple dashes).

left hand panel there is a solution to the minimization problem which assymptotes to the naive factorization prediction for $\mathrm{Im}(\Delta C_2) \to \pm 0.2$ and crosses from positive to negative at $\mathrm{Im}(\Delta C_2) = 0$. In the right hand panel the solution is everywhere small but agrees with naive factorization again at $\mathrm{Im}(\Delta C_2) = 0$.

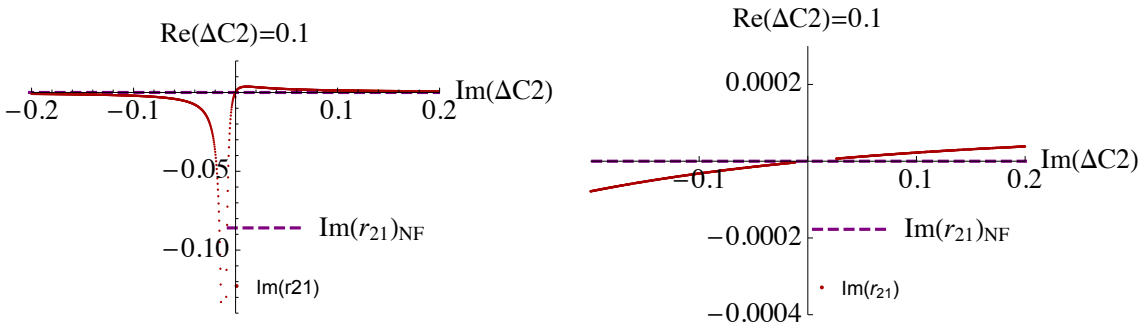

Figure 6.22: Solution 1 (left) and solution 2 (right) for the value of $\mathrm{Im}(r_{21})$ at fixed $\mathrm{Re}(\Delta C_2) = 0.1$ and $\Delta C_2 \in [-0.2, 0.2]$ (Red solid) and the naive factorization prediction of $\mathrm{Im}(r_{21})$ (purple dashes).

In Figure 6.23 are the two solutions for the value of the hadronic matrix element of $\mathcal{O}_1^c$ at the minimum of the χ^2 for varying $\mathrm{Im}(\Delta C_2)$. In the left hand panel there is again one place where the solution agrees with naive factorization for small negative $\mathrm{Im}(\Delta C_2)$ and this corresponds roughly with the agreement found in the left hand panel (same solution) of Figure 6.21. The right hand panel shows the solution for which there are no points of agreement with naive factorization and the values found for $|\langle \mathcal{O}_1^c \rangle|$ in this solution are too large to be realistic.

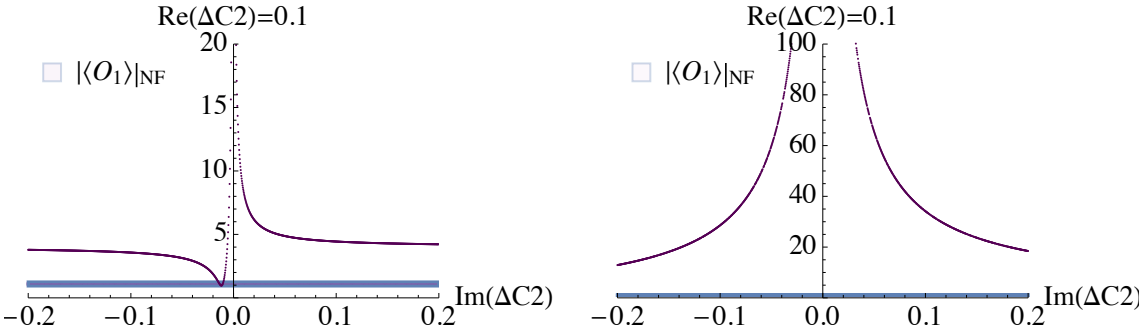

Figure 6.23: Solution 1 (left) and solution 2 (right) for the value of $|\langle \mathcal{O}_1^c \rangle|$ at fixed $\mathrm{Re}(\Delta C_2) = 0.1$ and $\Delta C_2 \in [-0.2, 0.2]$ (purple solid) and the naive factorization prediction of $|\langle \mathcal{O}_1^c \rangle| = (1.23 \pm 0.16)\mathrm{GeV}^3$ (blue shaded area).

Full results for ΔC_1 and ΔC_2

In Figure 6.24 this work is extended to find whole regions of the complex ΔC_1 plane which receive a further constraint from the $B_d^{(0)} \to J/\psi K_S$ time dependent CP asymmetry $B_d^{(0)} \to J/\psi K_d^{(0)}$ branching ratio. In the left hand panel of Figure 6.24 are shown regions in the complex ΔC_1 plane for which $\Delta\chi^2(\mathrm{Re}\Delta C_1, \mathrm{Im}\Delta C_1)$ is minimized with respect to $\mathrm{Re}r_{21}, \mathrm{Im}r_{21}$ subject to the constraint that $|\langle \mathcal{O}_1^c \rangle| \in [1.07, 1.39]$ which corresponds to a 1σ band given by the naive factorization prediction and it's error. There are

three regions in the plane which further constrain ΔC_1: The upper and lower bands constrain the imaginary part to be $\mathrm{Im}(\Delta C_1(M_W) \approx -0.2$ or $\mathrm{Im}(\Delta C_1(M_W) \approx 0.2$. The third region requires a zero imaginary part. Taken together with the lifetime ratio constraint, we find that the real part is $\mathrm{Re}(\Delta C_1(M_W) \in [-0.4, 0.1]$ with CP violating phase and $\mathrm{Re}(\Delta C_1(M_W) \in [-0.45, -0.35], [0.02, 0.12]$ with no CP violation present.

In the right hand panel the picture is less clear, owing to the absence of any points in the complex $\Delta C_2(M_W)$ plane for which all of the observables agree. None the less, should the SM value predicted for the lifetime ratio and the measured value obtain more precise agreement, the region for which the hadronic decay observables and the radiative decay and width difference could allow a value of $\mathrm{Re}(\Delta C_2(M_W) \in [-0.1, 0.1]$ and a very small $\mathrm{Im}(\Delta C_2(M_W) \in [-0.05, 0.05]$. The red diagonal band of values in the lower left hand corner is ruled out by the other constraints.

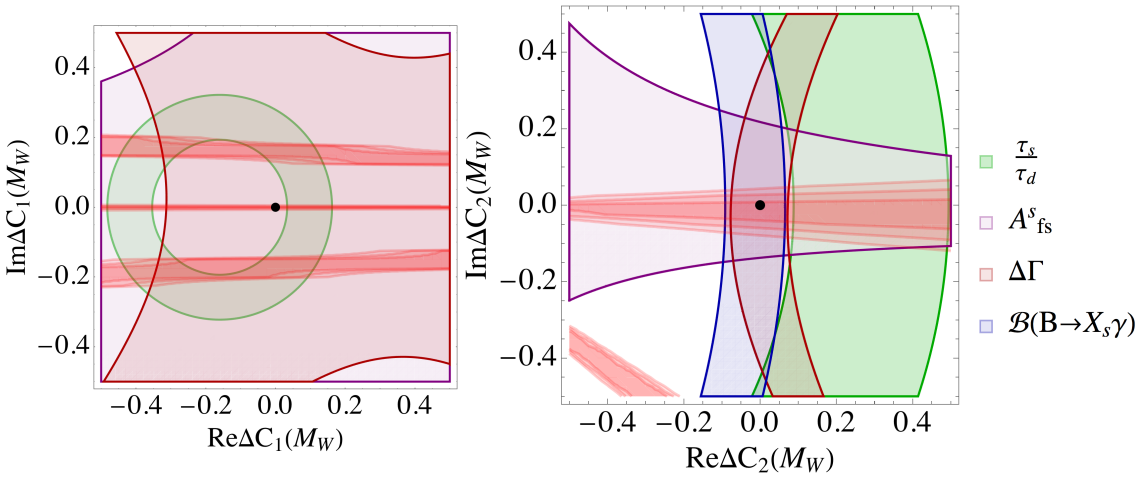

Figure 6.24: $B_d^0 \to J/\psi K$ constraints on (left) $\Delta C_1(M_W), (right)\Delta C_2(M_W)$. Regions for which data agree with naive factorization prediction for $|\langle \mathcal{O}_1^c \rangle|$ at $1, 2$ and 3σ shown as horizontal red bands.

6.8 Constraints on 1 parameter scenarios

In this section we present best fit ranges for one parameter scenarios in two cases. The first case is shown and discussed in subsection 6.8.1 for which we set all Wilson coefficients to zero except the one we are considering and find the best fit point for that coefficient according to each individual observable separately. The second case is presented in subsection 6.8.2 where we combine all of the observables and find the best fit point for each coefficient and the energy scale we could naively expect the coefficient to be generated at. The ranges allowed by individual observables as shown in Tables 6.10 and 6.11 are found using (6.5), while for the combined quantities (Table 6.12), we sum up the individual χ^2.

In both cases we normalise to the best fit point by subtracting the relevant χ^2 minima.

6.8.1 Best fit ranges for 1 parameter models

In Table 6.10 are shown possible ranges for each coefficient taking into account only one observable at a time. Considering $\Delta C_5 - \Delta C_{10}$ in the first column of Table 6.10, there are best fit ranges which correspond to those that pass through the SM point and those that do not. This can be understood by considering the functional form with which $\bar{C}_7^{\text{eff}}$ enters (5.38) and the impact that larger coefficients in $C_7^{\text{eff},BSM}$ have upon reducing the parameter space allowed by radiative decay. This results in there being two bands instead of one for each $\Delta\chi_i^2 \leq 1$. Some of these are unphysically large, such as is the case for $\Delta C_1 - \Delta C_4$ and these points could not be representative of genuine BSM effects as they would be ruled out upon consideration alongside other observables. The second column of Table 6.10 does not for any coefficient include the SM point, and this is simply due to the current disagreement between measurement and theory for the lifetime ratio. Column 3 containing ranges accommodated by $\Delta\Gamma_s$ always includes the SM point.

In Table 6.11 we show 1σ ranges accommodated by C_9' and $C_{7\gamma}'$ for the primed coeffi-

Table 6.10: 1σ Best fit ranges for scenarios with one Wilson coefficient.

Coeff.	$\Delta\chi^2_\gamma \leq 1$	$\Delta\chi^2_\tau \leq 1$	$\Delta\chi^2_{\Delta\Gamma} \leq 1$
ΔC_1	$[-0.71, 0.99], [44.0, 46.0]$	$[-0.48, -0.35], [0.03, 0.16]$	$[-0.32, 1.1]$
ΔC_2	$[-4.2, -4.1], [-0.09, 0.07]$	$[-2.7, -2.3], [0.09, 0.49]$	$[-2.0, -1.9], [-0.08, 0.08]$
ΔC_3	$[-53.0, -51.0], [-1.2, 0.83]$	$[-0.62, -0.29], [0.16, 0.50]$	$[-0.84, 1.5]$
ΔC_4	$[-6.0, -5.7], [-0.13, 0.09]$	$[-0.75, -0.28], [0.33, 0.80]$	$[-0.34, 0.58]$
ΔC_5	$[-0.01, 0.01], [0.36, 0.37]$	$[-0.03, -0.01], [0.03, 0.06]$	$[-0.13, 0.34]$
ΔC_6	$[-0.02, 0.03], [1.1, 1.2]$	$[-0.11, -0.03], [0.09, 0.17]$	$[-1.5, 0.49]$
ΔC_7	$[-0.46, -0.45], [-0.01, 0.01]$	$[-0.21, -0.11], [0.04, 0.14]$	$[-1.7, 0.44]$
ΔC_8	$[-0.92, -0.88], [-0.02, 0.014]$	$[-0.26, -0.12], [0.06, 0.20]$	$[-0.27, 0.27]$
ΔC_9	$[-0.002, 0.003], [0.15, 0.15]$	$[-0.02, -0.01], [0.003, 0.011]$	$[-0.14, 0.035]$
ΔC_{10}	$[-0.05, 0.07], [3.2, 3.3]$	$[-0.08, -0.05], [0.02, 0.05]$	$[-0.09, 0.09]$
$\Delta C_1'$	$[-5.7, 5.7]$	$[-0.32, -0.15], [0.08, 0.25]$	$[-0.58, 0.58]$
$\Delta C_2'$	$[-0.53, 0.53]$	$[-1.2, -0.51], [0.39, 1.1]$	$[-0.39, 0.39]$
$\Delta C_3'$	$[-6.7, 6.7]$	$[-1.0, -0.79], [0.06, 0.30]$	$[-1.1, 1.1]$
$\Delta C_4'$	$[-0.75, 0.75]$	$[-1.3, -0.96], [0.09, 0.45]$	$[-0.44, 0.44]$
$\Delta C_5'$	$[-0.05, 0.05]$	$[-0.03, -0.01], [0.03, 0.06]$	$[-0.21, 0.21]$
$\Delta C_6'$	$[-0.15, 0.15]$	$[-0.10, -0.03], [0.10, 0.18]$	$[-0.85, 0.85]$
$\Delta C_7'$	$[-0.06, 0.06]$	$[-0.23, -0.13], [0.03, 0.13]$	$[-0.86, 0.86]$
$\Delta C_8'$	$[-0.12, 0.12]$	$[-0.30, -0.17], [0.04, 0.17]$	$[-2.0, 2.0]$
$\Delta C_9'$	$[-0.02, 0.02]$	$[-0.02, -0.01], [0.003, 0.011]$	$[-0.07, 0.07]$
$\Delta C_{10}'$	$[-0.42, 0.42]$	$[-0.09, -0.05], [0.01, 0.05]$	$[-1.2, 1.2]$

cients. The primed coefficients $\Delta C_1' - \Delta C_4'$ are tightly constrained by the right handed C_{9V}', which has no expectation of new physics and thus stringently constrains the parameter space for these coefficients. Of all the coefficients, the largest value a non SM

coupling can take is $|\Delta C_2'| = 0.17$. In terms of the pseudo observable $C_{7\gamma}'$, the constraints for the 1 parameter scenarios are much less severe for $\Delta C_1' - \Delta C_4'$ but similarly stringent for $\Delta C_5' - \Delta C_{10}'$ for the same reasons as are explained in subsection 6.5.2.

Table 6.11: 1σ Best fit ranges for scenarios with one primed Wilson coefficient. These correspond to $\bar{C}_7'^{\text{eff}}(m_b)$ and $\bar{C}_9'(m_b)$ at $\pm 1\sigma$ from fitted values of C_7' and C_9' respectively.

Coeff.	$\Delta\chi^2_{\bar{C}_9'} \leq 1$	$\Delta\chi^2_{\bar{C}_7'^{\text{eff}}} \leq 1$
$\Delta C_1'$	$[-0.001, 0.04]$	$[-1.11, 3.21]$
$\Delta C_2'$	$[-0.004, 0.17]$	$[-0.30, 0.10]$
$\Delta C_3'$	$[-0.07, 0.002$	$[-3.74, 1.29]$
$\Delta C_4'$	$[-0.13, 0.003]$	$[-0.42, 0.14]$
$\Delta C_5'$	$-$	$[-0.01, 0.03]$
$\Delta C_6'$	$-$	$[-0.03, 0.08]$
$\Delta C_7'$	$-$	$[-0.03, 0.01]$
$\Delta C_8'$	$-$	$[-0.06, 0.02]$
$\Delta C_9'$	$-$	$[-0.03, 0.01]$
$\Delta C_{10}'$	$-$	$[-0.08, 0.23]$

6.8.2 Best fit ranges and corresponding bounds

By combining the individual constraints we can proceed further and make predictions upon the possible scale at which new physics generates the $b \to c\bar{c}s$ operators. We employ a simple approximation to the BSM scale, estimating that at tree level

$$\Lambda^2_{NP} \geq \frac{U_{cb}U^*_{cs}}{V_{cb}V^*_{cs}} \frac{\sqrt{2}}{4G_F} \frac{g^2_{NP}}{|\Delta C_i(M_W)|}. \tag{6.36}$$

where $U_{cb}U^*_{cs}$ are the quark mixing matrix elements which are generic and represent some BSM model. The g_{NP} is the coupling at the high scale, in the full theory. If we assume the value of these is 1 then the simplified expression is

$$\Lambda^2_{NP} \geq \frac{\sqrt{2}}{4G_F} \frac{1}{V_{cb}V^*_{cs}} \frac{1}{|\Delta C_i(M_W)|}. \tag{6.37}$$

In column 2 of Table 6.12 the coefficients $\Delta C_5 - \Delta C_{10}$ have 1σ ranges according to the sum of the individual χ^2 including the radiative decay branching ratio. The 1σ ranges for the primed coefficients $\Delta C_1' - \Delta C_{10}'$ include the sum of χ^2 excluding the radiative decay branching ratio, as this is already contained in the fitted value of $C_{7\gamma}'$. In columns 3 and 4 of Table 6.12 are shown allowed ranges for each coefficient according to the sum of the individual χ^2. In the following columns we take the modulus of the bound corresponding to the negative value of ΔC_i in the best fit range, if it exists, and call it Λ_-. We take the

modulus of the bound corresponding to the positive value of ΔC_i in the same range and call it Λ_+. This way we allow the possibility of a negative coefficient, corresponding to new heavy quanta at the associated scale. If there is no negative value because the range does not include the SM point, then the Λ_- is left blank as the scale in this case will be greater than Λ_+ and Λ_- has no meaning. Where there are two ranges per coefficient, as is the case for $\Delta C'_{10}$ the bounds in the 3rd and 4th column correspond to the magnitude of the largest negative and positive values in each range, respectively. Adopting a completely

Table 6.12: Allowed ranges and corresponding bounds on NP for Wilson coefficients from all observables combined at 1σ

Coeff.	$\Delta\chi^2 \leq 1$	Λ_-(TeV)	Λ_+(TeV)
ΔC_1	$[0.03, 0.161]$	-	2.1
ΔC_2	$[-0.04, 0.06]$	4.1	3.4
ΔC_3	$[-0.60, -0.25], [0.14, 0.49]$	2.3	1.7
ΔC_4	$[-0.14, 0.09]$	2.3	2.8
ΔC_5	$[-0.01, 0.01]$	9.7	10.5
ΔC_6	$[-0.02, 0.02]$	5.6	5.8
ΔC_7	$[-0.01, 0.01]$	8.8	9.7
ΔC_8	$[-0.02, 0.02]$	6.2	6.9
ΔC_9	$[-0.001, 0.01]$	22.3	12.6
ΔC_{10}	$[0.01, 0.05]$	-	3.8
$\Delta C'_1$	$[0, 0.04]$	-	4.3
$\Delta C'_2$	$[-0.03, 0.14]$	5.5	2.3
$\Delta C'_3$	$[-0.06, 0.01]$	3.6	8.4
$\Delta C'_4$	$[-0.12, 0.02]$	2.5	6.4
$\Delta C'_5$	$[-0.02, 0.04]$	5.8	4.5
$\Delta C'_6$	$[-0.07, 0.11]$	3.3	2.6
$\Delta C'_7$	$[-0.03, 0.02]$	5.1	6.6
$\Delta C'_8$	$[-0.06, 0.04]$	3.6	4.3
$\Delta C'_9$	$[0.002, 0.010]$	-	8.5
$\Delta C'_{10}$	$[-0.08, -0.06], [0.02, 0.05]$	7.1	3.5

agnostic view of the type of BSM physics generating the operators in (5.123) we make some general observations about the lower bounds obtained in Table 6.12. Scenarios involving Wilson coefficients $\Delta C_9^{(\prime)}$ which correspond to tensor operators, show possible sensitivity to scales as high as $\Lambda \sim (8.5 - 22.3)\,\mathrm{TeV}$ and above. Whereas the colour singlet operator coefficient $\Delta C_{10}^{(\prime)}$ is sensitive already to lower scales $\Lambda \sim 3.8\,\mathrm{TeV}$ and above. Operator coefficients $\Delta C_{5(6)}^{(\prime)}$ are sensitive to the lowest scales with $\Lambda \sim (5.6 - 10.5)\,\mathrm{TeV}$ and $\Lambda \sim (2.6 - 5.8)\,\mathrm{TeV}$ in the unprimed and primed cases respectively. Operators corresponding to these coefficients could be generated in the full theory by vector gauge bosons which couple to left and right handed fermions. Operators which could be generated by scalar bosons in the full theory are associated with coefficients $\Delta C_{7(8)}^{(\prime)}$ and $\Delta C'_{3(4)}$. Of these $\Delta C_{7(8)}^{(\prime)}$ have lower bounds in the region $\Lambda \sim (6.2 - 9.7)\,\mathrm{TeV}$

and $\Lambda \sim (3.6 - 6.6)\,\mathrm{TeV}$ for unprimed and primed coefficients respectively. $\Delta C'_{3(4)}$ correspond to lower scales of $\Lambda \sim (2.5 - 8.4)\,\mathrm{TeV}$. Finally the right handed $\Delta C'_{1(2)}$ which would also be associated with a vector boson coupling to a right handed fermion in the full theory have a lower bound of $\Lambda \sim (2.1 - 5.5)\,\mathrm{TeV}$.

Chapter 7

BSM in dipole operator mixing

This chapter presents the technical result of a calculation of two and one loop diagrams, carried out for a project which is still ongoing. These results are partial, but will be used in the calculation of the anomalous dimension matrix element which governs the mixing of certain dimension six operators with the dipole operators of the SM EFT basis.

7.1 SM EFT Lagrangian and operator basis

Dimension six dipole operators contribute to several processes, including radiative decay and electron and neutron dipole moments and are sensitive probes of BSM physics at high energy scales. Dipoles are important in setting bounds upon CP violation and in exploring the flavour structure of BSM models. Through renormalization, certain classes of operators mix with Dipole operators, possibly generating non-negligible effects which contribute to observables associated with these processes. Some of the operators under consideration however, such as the $\psi^2 H^3$ class, have vanishing ADM entries at one loop, necessitating higher order perturbative calculations to capture effects generated by this mixing.

The goal of this project is to calculate the ADM entry which governs the mixing of operators with $\psi^2 H^3$ structure (where $\psi \in \{q, u, d, \ell, e\}$ and H is the Higgs doublet as described in chapter 2), with dipole operators with $\psi^2 H X$ structure (with $X \in \{B^{\mu\nu}, F^{\mu\nu}, G^{\mu\nu}\}$). The ultimate aim, is to determine phenomenological bounds on BSM physics generated by $\psi^2 H^3$ operators, through their associated effective coefficients, which we label generically as $C_{\psi H}$.

Results presented in this chapter include the two loop diagrams with $\psi^2 H^3$ operator insertions, which evaluate to scalar loop integrals multiplying Dirac structure corresponding to

that of the dipole operators, and one loop diagrams which will contribute to their counter terms.

To begin, we define the Lagrangian we use as the $\mathcal{L}_{SM}$ which contains dim $d = 2$ and dim $d = 4$ operators and is given in (2.1), and further higher dimensional effective operators which are necessarily suppressed by a power of the heavy particle which has been integrated out at the high scale Λ_{NP}.

$$\mathcal{L} = \mathcal{L}_{SM} + \frac{1}{\Lambda_{NP}^2} \sum_k C_k^{(6)} Q_k^{(6)} \tag{7.1}$$

Below, in Table 7.1 are shown the dimension six $\psi^2 H^3$ operators and the dimension six dipole operators, as taken from the basis used in [128]. The subscripts p, r are flavour indices.

Table 7.1: Operator basis: Dimension six $\psi^2 H^3$ operators (left) and dimension six dipole operators (right)

$\psi^2 H^3 + \text{h.c}$	$\psi^2 X H + \text{h.c}$
$Q_{eH} = (H^\dagger H)(\bar{\ell}_p e_r H)$	$Q_{eW} = (\bar{\ell}_p \sigma^{\mu\nu} e_r)\tau^I H W^I_{\mu\nu}$
$Q_{uH} = (H^\dagger H)(\bar{q}_p u_r H)$	$Q_{eB} = (\bar{\ell}_p \sigma^{\mu\nu} e_r) H B_{\mu\nu}$
$Q_{dH} = (H^\dagger H)(\bar{q}_p d_r H)$	$Q_{uG} = (\bar{q}_p \sigma^{\mu\nu} T^A u_r)\tilde{H} G^A_{\mu\nu}$
	$Q_{uW} = (\bar{\ell}_p \sigma^{\mu\nu} u_r)\tau^I \tilde{H} W^I_{\mu\nu}$
	$Q_{uB} = (\bar{\ell}_p \sigma^{\mu\nu} u_r)\tilde{H} B_{\mu\nu}$
	$Q_{dG} = (\bar{q}_p \sigma^{\mu\nu} T^A d_r) H G^A_{\mu\nu}$
	$Q_{dW} = (\bar{\ell}_p \sigma^{\mu\nu} d_r) H W^I_{\mu\nu}$
	$Q_{dB} = (\bar{\ell}_p \sigma^{\mu\nu} d_r) H B_{\mu\nu}$

7.2 Calculation

7.2.1 Conventions

We work in a basis of operators not reduced by the equations of motion (EOM) and in all cases work in Feynman gauge. At each interaction vertex the coupling assigned may

be complex and contains group theory factors if it is a gauge coupling. These are left unspecified, table 7.2 gives the generic prescriptions. In addition, where there are more than one vertex with the same type of coupling, the number of the vertex is put in brackets as a superscript and the corresponding vertex of the diagram will be labelled accordingly.

Table 7.2: Interaction vertices

Coupling	Interactions
g_{ffs}	Yukawa
g_{ffb}	Gauge - fermion
g_{ssb}	Gauge - scalar
g_{ssbb}	Gauge - scalar
g_{ssss}	Quartic scalar
g_{bbbb}	Quartic gauge
g_{bbb}	Cubic gauge

7.2.2 Technical procedure

The two and one loop integrals are simplified and Infra Red (IR) regulated using the propagator decomposition procedure outlined in [129]. In this procedure the IR divergences are regulated by introducing an artificial mass parameter to each denominator of each propagator in a diagram. Following this, an expansion in all the particle masses and external momenta is carried out. The result of this is that all integrals are reduced to those with only a single mass - the regulator mass in all the propagator denominators and loop momenta.

$$\frac{1}{(k+p)^2 - M^2} = \frac{1}{k^2 - m^2} + \frac{(M^2 - p^2 - 2k \cdot p - m^2)}{(k^2 - m^2)} \frac{1}{(k+p)^2 - M^2} \tag{7.2}$$

The expansion takes the form of (7.2) where k is a linear combination of loop momenta, p is a linear combination of external momenta, M is the particle mass and m is the regulator mass. We define the superficial degree of Ultra Violet (UV) divergence, denoted as as $\Delta\omega$, in a naive sense as the number of powers of loop momenta in the numerator minus the number of powers of loop momenta in the denominator. We note that the first term on the lhs of (7.2) has superficial degree of divergence $\Delta\omega = -2$ as does the first term on the rhs, however this term depends only upon the regulator mass and the loop momenta.

The second term on the lhs has $\Delta\omega = -3$ overall and the denominator of the last term in the product has the identical form as the original propagator. Performing the expansion iteratively two times more leads to the expression

$$\frac{1}{(k+p)^2 - M^2} = \frac{1}{k^2 - m^2} + \frac{(M^2 - p^2 - 2k\cdot p - m^2)}{(k^2 - m^2)^2} + \frac{(M^2 - p^2 - 2k\cdot p - m^2)^2}{(k^2 - m^2)^3} + \frac{(M^2 - p^2 - 2k\cdot p - m^2)^3}{(k^2 - m^2)^3}\frac{1}{(k+p)^2 - M^2} \tag{7.3}$$

Again, counting the superficial degree of divergence of the terms on the rhs we find the first term as before has $\Delta\omega = -2$, the second term has $\Delta\omega = -3$ and the third term has $\Delta\omega = -4$. The last term then has $\Delta\omega = -5$. Through this procedure we have IR regulated the integrals and in addition, we have simplified the terms in the expansion so that now all integrands contain only loop momenta and mass regulator in the denominators and polynomials of the particle masses, external momenta and regulator mass in the numerators which can be factored out and the resultant simplified tensor integrals reduced further in a next step.

The typical one and two loop integrals arising from the diagrams shown in Figures 7.1-7.3 are rank 0 to rank 4 tensor integrals in the Minkowski metric, of the form

$$(I_n^{(1)\ell})_{\mu_1\ldots\mu_\ell} = \frac{1}{(2\pi)^D}\int \frac{d^Dk\; k_{\mu_1}\ldots k_{\mu_\ell}}{(k^2 - m^2)^n}, \tag{7.4}$$

$$(I^{(2)\ell m}_{n_1n_2n_3})_{\mu_1\ldots\mu_\ell,\nu_1\ldots\nu_m} = \frac{1}{(2\pi)^{2D}}\int\!\!\int \frac{d^Dk\; d^Dq\; k_{\mu_1}\ldots k_{\mu_\ell}q_{\nu_1}\ldots q_{\nu_m}}{(k^2 - m^2)^{n_1}(q^2 - m^2)^{n_2}((k-q)^2 - m^2)^{n_3}}. \tag{7.5}$$

Next, we outline the steps taken to reduce the tensor integrals to scalar integrals.

One loop integrals

The one loop tensor integrals reduce as

$$(I_n^{(1)1}) = A_n^{(D)}, \tag{7.6}$$

$$(I_n^{(1)1})_{\mu_1} = 0, \tag{7.7}$$

$$(I_n^{(1)2})_{\mu_1\mu_2} = \frac{\eta_{\mu_1\mu_2}}{D}(A_{n-1}^{(D)} + m^2A_n^{(D)}), \tag{7.8}$$

$$(I_n^{(1)3})_{\mu_1\mu_2\mu_3} = 0, \tag{7.9}$$

$$(I_n^{(1)4})_{\mu_1\mu_2\mu_3\mu_4} = (\eta_{\mu_1\mu_2}\eta_{\mu_3\mu_4} + \eta_{\mu_1\mu_3}\eta_{\mu_2\mu_4} + \eta_{\mu_1\mu_4}\eta_{\mu_2\mu_3})\frac{(A_{n-2}^{(D)} + 2m^2A_{n-1}^{(D)} + 3m^4A_n^{(D)})}{D(D+2)}. \tag{7.10}$$

Where the basis integral $A_n^{(D)}$ is given by

$$A_n^{(D)} = \frac{1}{(2\pi)^D}\int \frac{d^Dk}{(k^2-m^2)^n}. \tag{7.11}$$

Two loop integrals

The two loop tensor integrals are more complicated to reduce, we give an example for (7.5) with $\ell = 2, m = 2$.

$$(I_{n_1n_2n_3}^{(2)22})_{\mu_1\mu_2\nu_1\nu_2} = F_1\eta_{\mu_1\mu_2}\eta_{\nu_1\nu_2} + F_2(\eta_{\mu_1\nu_1}\eta_{\mu_2\nu_2} + \eta_{\mu_1\nu_2}\eta_{\mu_2\nu_1}) \tag{7.12}$$

To obtain the coefficients F_1, F_2 we contract both sides once with $\eta_{\mu_1\nu_1}\eta_{\mu_2\nu_2}$ and then with $\eta_{\mu_1\mu_2}\eta_{\nu_1\nu_2}$ giving the following set of equations for scalar integrals X_1, X_2

$$X_1 = DF_1 + D(D+1)F_2, \tag{7.13}$$

$$X_2 = D^2F_1 + 2DF_2, \tag{7.14}$$

with the integrals now

$$X_1 = \int\int d^Dkd^Dq\frac{(k\cdot q)^2}{((k^2-m^2)^{n_1}(q^2-m^2)^{n_2}((k-q)^2-m^2)^{n_3}}, \tag{7.15}$$

$$X_2 = \int\int d^Dkd^Dq\frac{k^2q^2}{((k^2-m^2)^{n_1}(q^2-m^2)^{n_2}((k-q)^2-m^2)^{n_3}}. \tag{7.16}$$

To obtain the coefficient then we must invert the matrix to give

$$\begin{pmatrix} F_1 \\ F_2 \end{pmatrix} = \begin{pmatrix} D & D(D+1) \\ D^2 & 2D \end{pmatrix}^{-1}\begin{pmatrix} X_1 \\ X_2 \end{pmatrix}. \tag{7.17}$$

The integrals X_1, X_2 are reduced to linear combinations of basis integrals of the form

$$K_{n_1,n_2,n_3}^{(D)} = \frac{1}{\pi^D}\int\int \frac{d^Dkd^Dq}{(k^2-m^2)^{n_1}((k-q)^2-m^2)^{n_2}(q^2-m^2)^{n_3}}, \tag{7.18}$$

by re-expressing the scalar products in the numerators using

$$k\cdot q = \frac{1}{2}((k-q)^2 - m^2 - (k^2-m^2) - (q^2-m^2) - 2m^2), \tag{7.19}$$

$$k^2q^2 = (k^2 - m^2)(q^2 - m^2) + m^2(k^2 - m^2) + m^2(q^2 - m^2) + m^4. \tag{7.20}$$

This procedure is implemented in a mathematica workbook by programming all possible combinations of ℓ, m in the two loop integrals arising and programming their reduction to scalar integrals, through relations obtained analytically in a similar manner as is shown above. After the above relations are obtained, further contractions of metric tensors and Dirac matrices are performed using the FeynCalc package [130], [131]. Then, in the two loop case, these scalar integrals are simplified using the Tarcer package [132].

Computational procedure

1. All diagrams are analytically expressed and input to a mathematica notebook using graph theory techniques to obtain conservation of momentum at vertices
2. The propagator decomposition is performed and the integrals IR regulated
3. Dirac structure, external momentum are factored out and integrals are isolated
4. Tensor integrals are reduced to scalar integrals
5. Results are expressed in terms of a small basis of basic one and two loop integrals with Dirac structure and external momenta dependence factored out

7.3 Results

In this section we present the results obtained by the methods described above, for a set of two and one loop graphs with $\psi^2 H^3$ operator insertion. Below in Tables 7.3 - 7.6 are shown the combination of couplings and the integral and Dirac structure resulting from calculation of the two loop graphs and their symmetric counterparts [1] in terms of the integrals defined in (7.11) and (7.18) we find only the following are necessary

$$A_1^D = \frac{1}{(2\pi)^D} \int \frac{d^D k}{(k^2 - m^2)}, \tag{7.21}$$

$$K_{1,1,1}^D = \frac{1}{(2\pi)^{2D}} \int\int \frac{d^D k_1 d^D k_2}{(k_1^2 - m^2)((k_1 - k_2)^2 - m^2)(k_2^2 - m^2)}, \tag{7.22}$$

where D is the number of spacetime dimensions, k_i are loop momenta and m are the regulator masses. The parts of the above integrals which will be retained are the divergent $\frac{1}{\epsilon}$

[1] Not all symmetric diagrams are shown

poles, as it is these which will allow us to construct the ADM element.

7.3.1 Two loop results

We begin by presenting the results from calculation of the Greens functions of $\psi^2 H^3$ operators represented by graphs in figures 7.1 - 7.3 and their symmetric counterparts (not all shown). All of these diagrams represent the calculation of Greens functions with $H\bar{\psi}\psi X$ fields as external states, and are classified according to their different topologies. In all figures, the black square represents the insertion of a $\psi^2 H^3$ operator.

Figure 7.1 correspond to the results in table 7.3. The diagrams 7.1a and 7.1d vanish, whilst 7.1d and 7.1d yield dipole Dirac structure with divergent integrals. These contributions involve gauge-scalar, and gauge-fermion couplings.

Figure 7.2 correspond to the results in table 7.4. All these diagrams are non vanishing, and except for 7.2d, contain dipole Dirac structure and divergent integrals. Results of figures 7.2a and 7.2b contribute Yukawa and gauge-fermion couplings, whilst figures 7.2c and 7.2d contribute gauge-scalar and Yukawa couplings.

Figure 7.3 correspond to the results in table 7.5. All these diagrams are non vanishing, contain dipole Dirac structure and only include simple integrals of the form (7.21). Results of figures 7.3a contribute Yukawa and gauge-fermion couplings, whilst figure 7.3b contribute gauge-scalar and Yukawa couplings.

Figure 7.4 correspond to the results in table 7.6 and unlike those above, correspond to Greens functions with $H\psi\psi$ as external states. Figure 7.4a corresponds to a result with dipole - like $\sigma^{\mu\nu}$ structure and divergent integral of type (7.21) only. Figures 7.4b and 7.4c have no dipole structure and are polynomial in the external momenta. They depend upon both types of integrals. All Class 4 results contribute Yukawa couplings.

7.3.2 One loop results

These one loop results are computed in order to form part of the counter terms for the two loop results. All one loop graphs are shown in Figure 7.5 and the resultant expressions and couplings are given in Table 7.7.

Figure 7.5a corresponds to a Greens function with $H\bar{\psi}\psi X$ external states and vanishes identically. Figures 7.5b and 7.5c correspond to Greens functions with $H\bar{\psi}\psi XX$ external

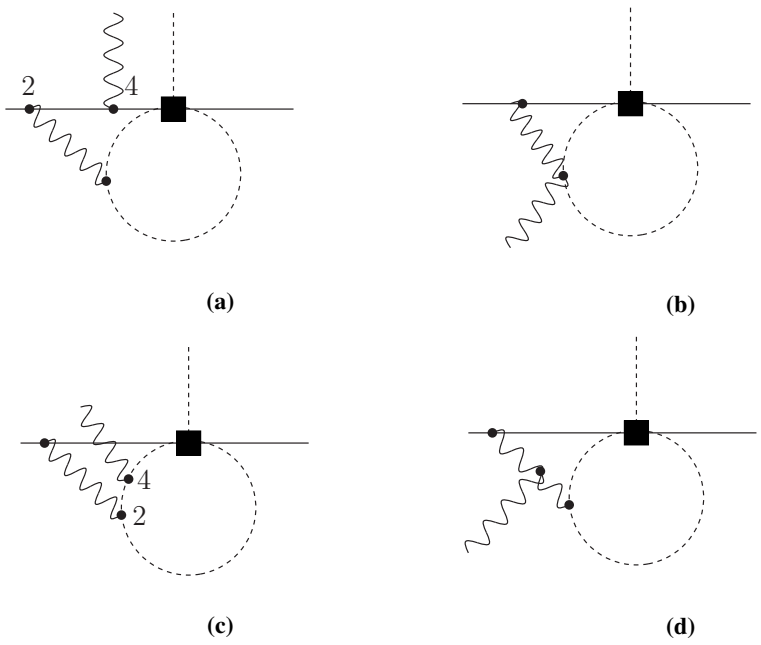

Figure 7.1: Class 1 topologies of two loop graphs

Table 7.3: Class 1 contributions from two-loop Feynman diagrams and their couplings

Fig.	Couplings	Contribution
7.1a	$C_{\psi H} g^{(4)}_{ffb} g^{(2)}_{ffb} g_{ssb}$	0
	$C_{\psi H} g^{(4)}_{ffb} g^{(2)}_{ffb} g_{ssb}$	0
7.1b	$C_{\psi H} g_{ffb} g_{ssbb}$	$\frac{(D-2)^2}{6Dm^4}((p_1^\mu + i\sigma^{\mu p_1})P_R - 2(q_2^\mu + i\sigma^{\mu q_2})P_R)(A_1^{(D)})^2 +$ $\frac{(D-3)}{9Dm^2}(-2(D+1)(p_1^\mu + i\sigma^{\mu p_1})P_R + (D+4)(q_2^\mu + i\sigma^{\mu q_2})P_R)K_{111}^{(D)}$
	$C_{\psi H} g_{ffb} g_{ssbb}$	$\frac{(D-2)^2}{6Dm^4}((p_2^\mu - i\sigma^{\mu p_2})P_R + 2(q_2^\mu - i\sigma^{\mu q_2})P_R)(A_1^{(D)})^2$ $+ \frac{(D-3)}{9Dm^2}(2(D+1)(i\sigma^{\mu p_2} - p_2^\mu)P_R + (D+4)(i\sigma^{\mu q_2} - q_2^\mu)P_R)K_{111}^{(D)}$
7.1c	$C_{\psi H} g^{(4)}_{ssb} g^{(2)}_{ssb} g_{ffb}$	$\frac{(D-2)^2}{6Dm^4}(2q_2^\mu P_R - (p_1^\mu + i\sigma^{\mu p_1})P_R)(A_1^{(D)})^2$ $+ \frac{(D-3)}{9Dm^2}(2(D+1)(p_1^\mu + i\sigma^{\mu p_i})P_R - (D+4)q_2^\mu P_R)K_{111}^{(D)}$
	$C_{\psi H} g^{(4)}_{ssb} g^{(2)}_{ssb} g_{ffb}$	$\frac{(D-2)^2}{6Dm^4}(2q_2^\mu P_R + (p_2^\mu - i\sigma^{\mu p_2})P_R)(A_1^{(D)})^2$ $+ \frac{(D-3)}{9Dm^2}(2(D+1)(i\sigma^{\mu p_2} - p_2^\mu)P_R - (D+4)q_2^\mu P_R)K_{111}^{(D)}$
7.1d	$C_{\psi H} g_{ffb} g_{bbb} g_{ssb}$	0
	$C_{\psi H} g_{ffb} g_{bbb} g_{ssb}$	0

states, have tensor structure and contribute gauge-scalar couplings. Figures 7.5d-7.5i correspond to Greens functions with $HHH\bar{\psi}\psi$ external states. These all have Lorentz scalar structure and contribute different combinations of gauge-scalar, gauge-fermion, Yukawa and scalar quartic couplings. Figure 7.5j correspond to Greens functions with $HH\bar{\psi}\psi$

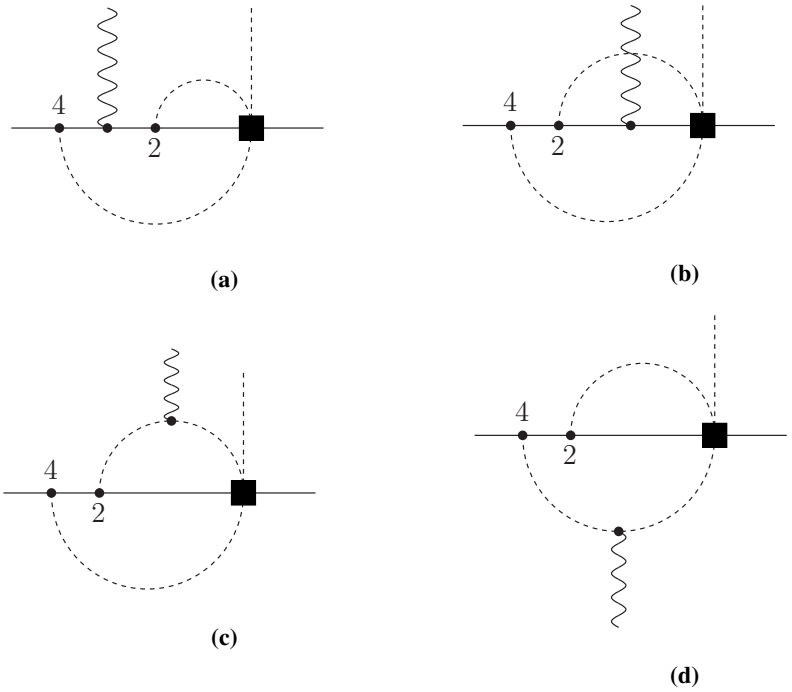

Figure 7.2: Class 2 topologies of two loop graphs

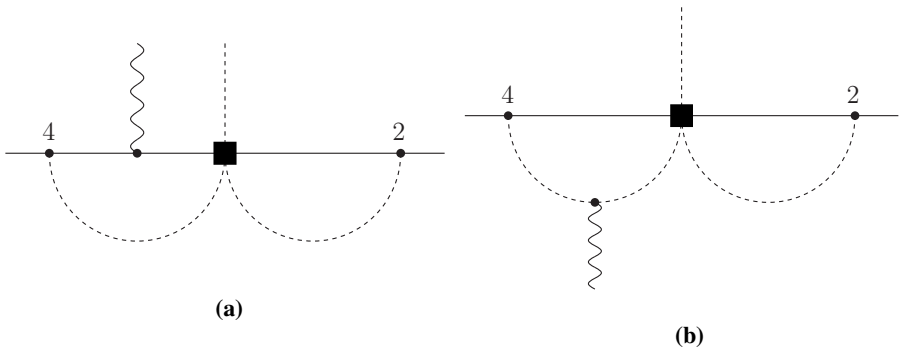

Figure 7.3: Class 3 topologies of two loop graphs

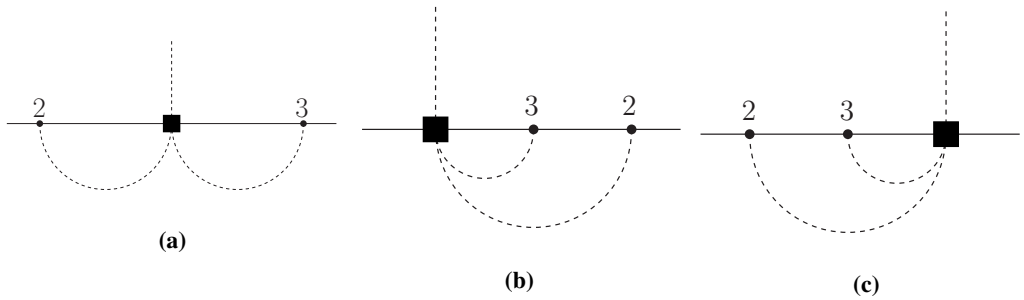

Figure 7.4: Class 4 topologies of two loop graphs

external states. This graph gives a Yukawa coupling, is of vector structure and is dependent upon external momenta. Figure 7.5k and 7.5l correspond to Greens functions with $HH\bar{\psi}\psi X$ external states. These have vectorial structure and contribute Yukawa and

Table 7.4: Class 2 contributions from two-loop Feynman diagrams and their couplings

Fig.	Couplings	Contribution
7.2a	$C_{\psi H} g^{(2)}_{ffs} g_{ffb} g^{(4)}_{ffs}$	$\frac{(D-2)^2}{216Dm^4}\left(5(D+2)(p_1^\mu - i\sigma^{\mu p_1})P_R \right.$ $\left. -(D+20)(q_2^\mu - i\sigma^{\mu q_2}))\, P_R (A_1^{(D)})^2 \right.$ $+ \frac{(D-3)}{324Dm^2}\left(2(D-5)(D+2)(p_1^\mu - i\sigma^{\mu p_1})P_R \right.$ $\left. +(5D^2-6D+40)(q_2^\mu - i\sigma^{\mu q_2})P_R\right) K^{(D)}_{111}$
	$C_{\psi H} g^{(2)}_{ffs} g_{ffb} g^{(4)}_{ffs}$	$-\frac{(D-2)^2}{216Dm^4}\left(5(D+2)(p_2^\mu - i\sigma^{\mu p_2})P_R \right.$ $\left. +(D+20)(q_2^\mu + i\sigma^{\mu q_2}))\, P_R (A_1^{(D)})^2 \right.$ $+ \frac{(D-3)}{324Dm^2}\left(-2(D-5)(D+2)(p_2^\mu + i\sigma^{\mu p_2})P_R \right.$ $\left. +(5D^2-6D+40)(q_2^\mu + i\sigma^{\mu q_2})\, P_R\right) K^{(D)}_{111}$
7.2b	$C_{\psi H} g_{ffb} g^{(2)}_{ffs} g^{(4)}_{ffs}$	$\frac{(D-2)^2}{72Dm^4}\left[i(D-10)\sigma^{\mu p_1}P_R \right.$ $\left. +(2-5D)p_1^\mu P_R + 8(D-1)(q_2 + i\sigma^{\mu q_2})P_R\right](A_1^{(D)})^2$ $+ \frac{(D-3)}{54Dm^2}\left[i(2D^2-3D+10)\sigma^{\mu p_1}P_R - (D^2-9D+2)p_1^\mu P_R \right.$ $\left. -2(D-1)(D+4)(q_2^\mu + i\sigma^{\mu q_2})P_R\right] K^{(D)}_{111}$
	$C_{\psi H} g_{ffb} g^{(2)}_{ffs} g^{(4)}_{ffs}$	$\frac{(D-2)^2}{72Dm^4}\left[i(D-10)\sigma^{\mu p_2}P_R + (2-5D)p_2^\mu P_R \right.$ $\left. +8(D-1)(q_2 - i\sigma^{\mu q_2})P_R\right](A_1^{(D)})^2$ $+ \frac{(D-3)}{54Dm^2}\left[i(2D^2-3D+10)\sigma^{\mu p_2}P_R + (D^2-9D+2)p_2^\mu P_R \right.$ $\left. -2(D-1)(D+4)(q_2^\mu - i\sigma^{\mu q_2})P_R\right] K^{(D)}_{111}$
7.2c	$C_{\psi H} g_{ssb} g^{(2)}_{ffs} g^{(4)}_{ffs}$	$\frac{(D-2)^2}{36Dm^4}\left[(2D+7)p_1^\mu P_R - 2(D+2)q_2^\mu P_R - 3i\sigma^{\mu p_1}P_R\right](A_1^{(D)})^2$ $+ \frac{(D-3)}{54Dm^2}\left[(D+2)(D+4)q_2^\mu P_R - (D(D+3)+14)p_1^\mu P_R \right.$ $\left. -3i(D-2)\sigma^{\mu p_1}P_R\right] K^{(D)}_{111}$
	$C_{\psi H} g_{ssb} g^{(2)}_{ffs} g^{(4)}_{ffs}$	$-\frac{(D-2)^2}{36Dm^4}\left[(2D+7)p_2^\mu P_R + 2(D+2)q_2^\mu P_R + 3i\sigma^{\mu p_2}P_R\right](A_1^{(D)})^2$ $+ \frac{(D-3)}{54Dm^2}\left[(D+2)(D+4)q_2^\mu P_R + (D(D+3)+14)p_2^\mu P_R \right.$ $\left. -3i(D-2)\sigma^{\mu p_2}P_R\right] K^{(D)}_{111}$
7.2d	$C_{\psi H} g_{ssb} g^{(2)}_{ffs} g^{(4)}_{ffs}$	$-\frac{(D-2)^2}{216Dm^4}\left[(D+20)(q_2^\mu - 2p_1^\mu)P_R\right](A_1^{(D)})^2$ $+ \frac{(D-3)}{324Dm^2}\left[(D(5D-6)+40)(q_2^\mu - 2p_1^\mu)P_R\right] K^{(D)}_{111}$
	$C_{\psi H} C_{ssb} g^{(2)}_{ffs} g^{(4)}_{ffs}$	$-\frac{(D-2)^2}{216Dm^4}\left[(D+20)(q_2^\mu + 2p_2^\mu)P_R\right](A_1^{(D)})^2$ $+ \frac{(D-3)}{324Dm^2}\left[(D(5D-6)+40)(q_2^\mu + 2p_2^\mu)P_R\right] K^{(D)}_{111}$

Table 7.5: Class 3 contributions from two-loop Feynman diagrams and their couplings

Fig.	Couplings	Contribution
7.3a	$C_{\psi H} g^{(2)}_{ffs} g_{ffb} g^{(4)}_{ffs}$	$-\frac{(D-2)^3}{32m^4}(p_2^\mu + i\sigma^{\mu p_2})P_R(A_1^{(D)})^2$
	$C_{\psi H} g^{(2)}_{ffs} g_{ffb} g^{(4)}_{ffs}$	$\frac{(D-2)^3}{32m^4}(p_1^\mu - i\sigma^{\mu p_1})P_R(A_1^{(D)})^2$
7.3b	$C_{\psi H} g^{(2)}_{ffs} g_{ssb} g^{(4)}_{ffs}$	$\frac{(D-2)^2}{16m^4}P_R(p_2^\mu + i\sigma^{\mu p_2})(A_1^{(D)})^2$
	$C_{\psi H} g^{(2)}_{ffs} g_{ssb} g^{(4)}_{ffs}$	$-\frac{(D-2)^2}{16m^4}P_R(p_1^\mu - i\sigma^{\mu p_1})(A_1^{(D)})^2$

Table 7.6: Class 4 contributions from two-loop Feynman diagrams and their couplings

Fig.	Couplings	Contribution
7.4a	$C_{\psi H} g^{(2)}_{ffs} g^{(3)}_{ffs}$	$\frac{(D-2)^2}{16m^4}(p_1 \cdot p_2 + i\sigma^{p_1 p_2}) P_R (A^{(D)}_1)^2$
7.4b	$C_{\psi H} g^{(2)}_{ffs} g^{(3)}_{ffs}$	$\frac{(D-2)^2(D+20)}{216Dm^4} p_2^2 P_R (A^{(D)}_1)^2 - \frac{\left(54(D-4)D^2 + \frac{(D-3)(D(5D-6)+40)p_2^2}{m^2}\right)}{324D} P_R K^{(D)}_{111}$
7.4c	$C_{\psi H} g^{(2)}_{ffs} g^{(3)}_{ffs}$	$\frac{(D-2)^2(D+20)}{216Dm^4} p_1^2 P_R (A^{(D)}_1)^2 - \frac{\left(54(D-4)D^2 + \frac{(D-3)(D(5D-6)+40)p_1^2}{m^2}\right)}{324D} P_R K^{(D)}_{111}$

gauge-scalar, gauge-fermion couplings. Figure 7.5m correspond to Greens functions with $H\bar{\psi}\psi$ external states. This result is finite and does not contribute a pole.

Table 7.7: Contributions from one-loop Feynman diagrams and their couplings

Graph	Couplings	Contribution
7.5a	$C_{fH} g_{ssb}$	0
7.5b	$C_{fH} g_{ssbb}$	$\frac{(D-2)}{2m^2}\eta^{\mu\nu} P_R A^{(D)}_1$
7.5c	$C_{fH} g_{ssb} g_{ssb}$	$\frac{(D-2)}{2m^2} P_R \eta^{\mu\nu} A^{(D)}_1$
7.5d	$C_{fH} g_{ssb} g_{ffb}$	$-\frac{D(D-2)}{8m^2} P_R A^{(D)}_1$
7.5e	$C_{fH} g_{ffb} g_{ffb}$	$-\frac{D^2(D-2)}{8m^2} P_R A^{(D)}_1$
7.5f	$C_{fH} g_{ffs} g_{ffs}$	$\frac{D(D-2)}{8m^2} P_R A^{(D)}_1$
7.5g	$C_{fH} g_{ssb} g_{ssb}$	$-\frac{(D-2)D}{8m^2} P_R A^{(D)}_1$
7.5h	$C_{fH} g_{ssss}$	$\frac{(D-2)}{2m^2} P_R A^{(D)}_1$
7.5i	$C_{fH} g_{ffs} g_{ffs}$	$\frac{D(D-2)}{8m^2} P_R A^{(D)}_1$
7.5j	$C_{fH} g_{ffs}$	$\frac{(D-2)}{4m^2} \not{p}_1 P_R A^{(D)}_1$
7.5k	$C_{fH} g_{ffs} g_{ssb}$	$-\frac{(D-2)}{4m^2}\gamma_\mu P_R A^{(D)}_1$
7.5l	$C_{fH} g_{ffs} g_{ffb}$	$-\frac{(D-2)^2}{8m^2}\gamma_\mu P_R A^{(D)}_1$
7.5m	C_{fH}	finite

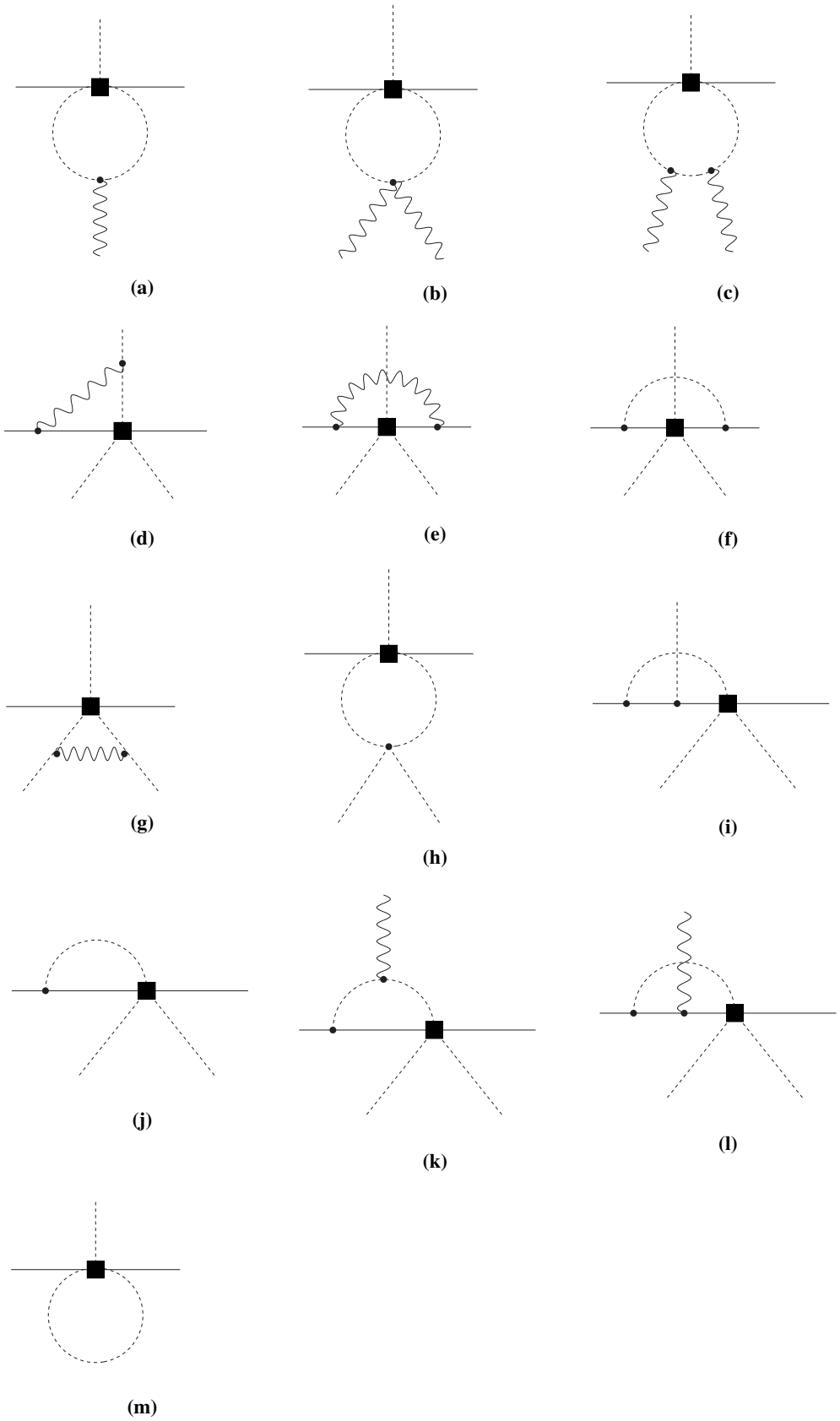

Figure 7.5: One loop diagrams with $\psi^2 H^3$ operator insertion

Chapter 8

Conclusions

In this thesis we have made a thorough study of the possible effects of new physics arising in tree-level in the strong coupling $b \to c\bar{c}s$ decays. This decay mode contributes to a wide variety of different observables. In this work we have focused on seven: the branching ratio for radiative B meson decay $\mathcal{B}(B_s \to X_s\gamma)$, the B_s^0 to B_d^0 meson lifetime ratio $\tau(B_s)/\tau(B_d)$, the B_s^0 mixing observables $\Delta\Gamma_s$ and a_{sl}^s, the branching ratio $\mathcal{B}(B_d^0 \to J/\psi K_d^0)$ and the hadronic $B_d^0 \to J/\psi K_S$ time dependent CP asymmetry observables $S_{B_d^0 \to J/\psi K_S}$ and $C_{B_d^0 \to J/\psi K_S}$.

The radiative branching ratio is an example of an inclusive decay mode that is under good theoretical control and is well measured experimentally, while similarly the lifetime ratio and mixing observables are controlled through the HQE. Whilst the remaining observables are less well theoretically understood, we have adopted a new approach for extracting further limits upon BSM effects which does not depend upon any particular theoretical method for estimation of hadronic matrix elements. Taken together, effects in this set of observables are connected through our "Charming BSM" scenario providing very complementary constraints.

Our basis of four quark operators contributing to $b \to c\bar{c}s$ transitions is comprised of twenty dimension six operators, defined in (3.2). We have calculated the contribution from the full basis to all of our observables; the most complex result being that obtained for mixing and the lifetime ratio which involved a high degree of detail and required intense analytical and computational effort. We have further calculated the renormalisation group evolution for our basis, and results are summarised in the full evolution matrix given in (4.77).

First we summarise our results for BSM in Wilson coefficients $\Delta C_1 - \Delta C_4$, which form

some of the most important findings of this thesis. We have shown that it is possible to generate an effect in rare semi-leptonic decays compatible with hints from LHCb and B-factory data, while satisfying the $B \to X_s\gamma$ constraint. Such an effect can originate from different $b \to c\bar{c}s$ operators, with scenarios including coefficient ΔC_3 distinctly favoured. Considering renormalization scales $\mu \sim M_B$ we find a mild q^2 dependence of the pseudo observable $\bar{C}_{9V}$ and show that negative shifts of $\mathcal{O}(1)$ are achievable in certain scenarios whilst still respecting the measured width difference and lifetime ratio. However, considerable theoretical progress in the understanding of long distance charm effects would be required to identify these as genuine new physics effects.

If new physics enters at $\mu \sim M_W$ or above, strong renormalization group enhancements are present. Whilst the q^2 dependence is then lost, we find the striking result that $\mathcal{O}(1)$ shifts to C_{9V} are indeed readily achievable for very small shifts to our $b \to c\bar{c}s$ coefficients. In short, we find it possible to provide a new physics explanation to the rare decay anomalies coming from operators $Q_1^c - Q_4^c$ by considering only short distance effects. Again however, until theoretical methods for calculation of long distance effects are under better control, we cannot make any stronger statements.

Another important result includes our study of future prospects for constraining BSM in the lifetime ratio and width difference observables with improvements in experimental and theoretical uncertainties. We find indications that a convergence of the SM predictions and experimental measurements for the lifetime ratio and mixing observables could confirm or exclude Charming-BSM scenarios and indeed discriminate between different new physics couplings.

We consider next our results for and $\Delta C'_{1-4}$ and $\Delta C^{(\prime)}_{5-10}$, which provide general constraints upon BSM effects in combinations of these coefficients, which could be useful to model builders, but which do not confront any particular flavour anomaly. We group them into three categories exhibiting similar behaviour. In scenarios involving coefficients $\Delta C'_{1-4}$ the strongest constraint upon these coefficients comes indirectly from angular observables through the pseudo observables $\bar{C}'_{9V}, \bar{C}'^{\text{eff}}_{7\gamma}$ for which data from global fits of C'_{9V} and $C'_{7\gamma}$ sets stringent bounds [1]. As is the case above, at higher scales there are strong RG enhancements but in contrast in this case they create a constraining effect due to the smallness of C'_{9V}. Of all the scenarios, we find that scenarios involving the pairs of coefficients $\Delta C'_1$ and $\Delta C'_3$, and $\Delta C'_1$ and $\Delta C'_4$, stand out as scenarios where agreement with all data can be found.

[1] under assumptions regarding hadronic effects

In contrast, in coefficients ΔC_{5-10} the mixing of $\bar{C}_{7\gamma}^{\text{eff}}$ with ΔC_{5-10} occurs at 1-loop, resulting in these coefficients being very highly constrained by radiative decay, and this indicates that our study disfavours models involving combinations of these coefficients.

Finally, the coefficients $\Delta C'_{5-10}$ are constrained in a complementary fashion by each of our observables, the crucial difference between scenarios involving these effective couplings and that of their unprimed counterparts is again the quadratic dependence of the radiative decay rate upon $\bar{C}_{7\gamma}^{\prime\text{eff}}$, which relaxes the constraints imposed by radiative decay relative to the unprimed case.

As a step towards converting our many constraints into statements on the viability of more definite NP models, we considered what the equivalent NP scale Λ_{NP} we are probing when we place limits on our Wilson coefficients, and our results were shown in Table 6.12. The tensor operators $Q_9^{(\prime)c}$ are sensitive to the highest scales, with the best fit to those coefficients corresponding to scales in excess of 20TeV. Importantly, all our operators probe energy scales above 1.5TeV, showing how our choice of observables can complement direct LHC searches for NP effects.

When considering the introduction of new weak CP violating phases to $C_1^c - C_4^c$ we have first considered the observables already employed in our CP conserving study but with an emphasis upon the flavour specific CP asymmetry which in the complex case, comes into play. We find that a_{fs}^s leads to constraints on the imaginary part in the complex ΔC_2 plane, but that it does not give much further constraint for the remaining coefficients. The $\mathcal{B}(B \to X_s\gamma)$ constrains the real part of the even coefficients and the lifetime ratio dictates the region of allowed parameter space in the odd coefficients.

To go a step further and study more closely the SM coefficients C_1^c and C_2^c we used the sine and cosine coefficients $S_{J/\psi K_S}$ and $C_{J/\psi K_S}$ of the time dependent CP asymmetry $A_{CP}(B_d^0 \to J/\psi K_S)$, alongside the branching ratio $\mathcal{B}(B_d^0 \to J/\psi K_d^0)$ to constrain the parameter space. Since the theoretical predictions for this hadronic decay depend upon non-perturbative parameters which are theoretically problematic to calculate, we adopted a different approach to constrain our BSM Wilson coefficients. We profiled over the non-hadronic parameters, fixing the magnitude of the matrix element $\langle O_1 \rangle$ to agree with the naive factorisation prediction and its error whilst allowing the ratio $r_{21}$to float freely, and studied resultant constraints.

For the possibility of a non standard shift to C_1^c, our result (shown in Figure 6.24) proves very interesting – whereas in the SM naive factorisation is not expected to well describe

this decay mode, we have shown that a small complex BSM contribution with an imaginary part of around $\mathrm{Im}\Delta C_1 = \pm 0.2$ is sufficient to achieve agreement between the full compliment of observables and their respective experimental averages. Furthermore, we find that there are distinct points in the complex ΔC_1 plane where r_{21} coincides with its NF prediction (shown in Figure 6.20) breaking the approximate sign degeneracy of the imaginary part. This is indeed a striking and unexpected result, and demonstrates that including $B \to J/\psi K_S$ observables in our analysis does not imply large violations of naive factorization. We find the best agreement (within 1 standard deviation) between all our observables and data, favours a small negative imaginary shift to C_1^c.

For C_2^c, we found that the results, whilst clear, were less interesting. A broad band centred on real shifts is compatible with the NF result for $\langle O_1 \rangle$, as well as a diagonal region with negative real and imaginary parts. Unfortunately the other constraints we consider have no clear region of overlap where all the predictions can be brought into agreement with data.

In chapter 7 we have presented the calculation of a set of two and one loop graphs which contribute to the ADM governing the mixing of $\psi^2 H^3$ dimension six operators with $\psi^2 HX$ dipole operators in the SMEFT framework. For this partial result, we have shown that the propagator decomposition method of [129] is effectively implemented to calculate the two loop Greens functions for $\psi^2 H^3$ operators, and that many of these do result in a dipole Dirac structure, signalling the mixing between these operators.

To summarise, we have shown in this work that new physics in $b \to c\bar{c}s$ operators can lead to a set of complimentary effects in several well known and studied observables. We have produced a full set of expressions for these effects which will be of use for any further study in this area, as well as calculating the leading order renormalisation group running for the full set of operators. Our results show that a complex $\Delta C_1(M_W)$ can give agreement with all the observables considered, including those associated with $B_d^0 \to J/\psi K_S$. We have placed limits on the real contributions to the coefficients $C_{5-10}^{(\prime)c}$ and $C_{1-4}^{(\prime)c}$ and shown that these operators can probe NP scales above $10\mathrm{TeV}$ in several cases. We also showed how possible BSM effects in grouped combinations of coefficients are constrained by data, classifying the various groups according to the similar patterns of constraints imposed upon them by our chosen set of observables.

Bibliography

[1] Sebastian Jäger, Kirsten Leslie, Matthew Kirk, and Alexander Lenz. Charming new physics in rare b decays and mixing? *Phys. Rev. D*, 97:015021, Jan 2018. pages ii, 2, 43, 44, 45, 55, 63, 102, 105, 112, 160

[2] S. Jäger, M. Kirk, A. Lenz, and K. Leslie. Charming New B-Physics. 2019. arXiv:1910.12924. pages ii, 2, 43, 44, 49, 51, 55, 56, 58, 61, 63

[3] S. Jäger, K. Leslie, and L. Vale-Silva. to appear. pages ii, 3

[4] R. Aaij et al. Differential branching fractions and isospin asymmetries of $B \to K^{(*)}\mu^+\mu^-$ decays. *JHEP*, 06:133, 2014. pages 2, 43, 101

[5] Vardan Khachatryan et al. Angular analysis of the decay $B^0 \to K^{*0}\mu^+\mu^-$ from pp collisions at $\sqrt{s} = 8$ TeV. *Phys. Lett.*, B753:424–448, 2016. pages 2, 43, 101

[6] J. P. Lees et al. Measurement of angular asymmetries in the decays $B \to K^{*+-}$. *Phys. Rev.*, D93(5):052015, 2016. pages 2, 43

[7] J. T. Wei et al. Measurement of the Differential Branching Fraction and Forward-Backword Asymmetry for $B \to K^{(*)}\ell^+\ell^-$. *Phys. Rev. Lett.*, 103:171801, 2009. pages 2, 43

[8] T. Aaltonen et al. Measurements of the Angular Distributions in the Decays $B \to K^{(*)}\mu^+\mu^-$ at CDF. *Phys. Rev. Lett.*, 108:081807, 2012. pages 2, 43

[9] Roel Aaij et al. Angular analysis of the $B^0 \to K^{*0}\mu^+\mu^-$ decay using 3 fb^{-1} of integrated luminosity. *JHEP*, 02:104, 2016. pages 2, 43, 101

[10] A. Abdesselam et al. Angular analysis of $B^0 \to K^*(892)^0\ell^+\ell^-$. In *Proceedings, LHCSki 2016 - A First Discussion of 13 TeV Results: Obergurgl, Austria, April 10-15, 2016*, 2016. pages 2, 43

[11] S. Wehle et al. Lepton-Flavor-Dependent Angular Analysis of $B \to K^* \ell^+ \ell^-$. *Phys. Rev. Lett.*, 118(11):111801, 2017. pages 2, 43

[12] Morad Aaboud et al. Angular analysis of $B_d^0 \to K^* \mu^+ \mu^-$ decays in pp collisions at $\sqrt{s} = 8$ TeV with the ATLAS detector. *JHEP*, 10:047, 2018. pages 2, 43

[13] Albert M Sirunyan et al. Measurement of angular parameters from the decay $\mathrm{B}^0 \to \mathrm{K}^{*0} \mu^+ \mu^-$ in proton-proton collisions at $\sqrt{s} = 8$ TeV. *Phys. Lett.*, B781:517–541, 2018. pages 2, 43

[14] Sebastien Descotes-Genon, Joaquim Matias, and Javier Virto. Understanding the $B \to K^* \mu^+ \mu^-$ Anomaly. *Phys. Rev.*, D88:074002, 2013. pages 2, 43

[15] Wolfgang Altmannshofer and David M. Straub. New Physics in $B \to K^* \mu\mu$? *Eur. Phys. J.*, C73:2646, 2013. pages 2, 43

[16] Tobias Hurth and Farvah Mahmoudi. On the LHCb anomaly in B $\to K^* \ell^+ \ell^-$. *JHEP*, 04:097, 2014. pages 2, 43

[17] Frederik Beaujean, Christoph Bobeth, and Danny van Dyk. Comprehensive Bayesian analysis of rare (semi)leptonic and radiative B decays. *Eur. Phys. J.*, C74:2897, 2014. [Erratum: Eur. Phys. J.C74,3179(2014)]. pages 2, 43

[18] Wolfgang Altmannshofer and David M. Straub. New physics in $b \to s$ transitions after LHC run 1. *Eur. Phys. J.*, C75(8):382, 2015. pages 2, 43, 101

[19] Wolfgang Altmannshofer, Christoph Niehoff, Peter Stangl, and David M. Straub. Status of the $B \to K^* \mu^+ \mu^-$ anomaly after Moriond 2017. *Eur. Phys. J.*, C77(6):377, 2017. pages 2, 43, 101, 102, 108

[20] Jason Aebischer, Wolfgang Altmannshofer, Diego Guadagnoli, M'eril Reboud, Peter Stangl, and David M. Straub. B-decay discrepancies after Moriond 2019. 2019. pages 2, 43

[21] A. Khodjamirian, Th. Mannel, A. A. Pivovarov, and Y. M. Wang. Charm-loop effect in $B \to K^{(*)} \ell^+ \ell^-$ and $B \to K^* \gamma$. *JHEP*, 09:089, 2010. pages 2

[22] Sebastian Jäger and Jorge Martin Camalich. Reassessing the discovery potential of the $B \to K^* \ell^+ \ell^-$ decays in the large-recoil region: SM challenges and BSM opportunities. *Phys. Rev.*, D93(1):014028, 2016. pages 2

[23] Christoph Bobeth, Marcin Chrzaszcz, Danny van Dyk, and Javier Virto. Long-distance effects in $B \to K^* \ell\ell$ from analyticity. *Eur. Phys. J.*, C78(6):451, 2018. pages 2

[24] A. Arbey, T. Hurth, F. Mahmoudi, and S. Neshatpour. Hadronic and New Physics Contributions to $b \to s$ Transitions. *Phys. Rev.*, D98(9):095027, 2018. pages 2

[25] S. L. Glashow. Partial Symmetries of Weak Interactions. *Nucl. Phys.*, 22:579–588, 1961. pages 4, 9, 10

[26] F. Englert and R. Brout. Broken Symmetry and the Mass of Gauge Vector Mesons. *Phys. Rev. Lett.*, 13:321–323, 1964. [,157(1964)]. pages 4, 8

[27] Peter W. Higgs. Broken Symmetries and the Masses of Gauge Bosons. *Phys. Rev. Lett.*, 13:508–509, 1964. [,160(1964)]. pages 4, 8

[28] G. S. Guralnik, C. R. Hagen, and T. W. B. Kibble. Global Conservation Laws and Massless Particles. *Phys. Rev. Lett.*, 13:585–587, 1964. [,162(1964)]. pages 4, 8

[29] Abdus Salam and John Clive Ward. Electromagnetic and weak interactions. *Phys. Lett.*, 13:168–171, 1964. pages 4

[30] Steven Weinberg. A Model of Leptons. *Phys. Rev. Lett.*, 19:1264–1266, 1967. pages 4, 9, 10

[31] Nicola Cabibbo. Unitary Symmetry and Leptonic Decays. *Phys. Rev. Lett.*, 10:531–533, 1963. [,648(1963)]. pages 12

[32] Makoto Kobayashi and Toshihide Maskawa. CP Violation in the Renormalizable Theory of Weak Interaction. *Prog. Theor. Phys.*, 49:652–657, 1973. pages 12

[33] M. Tanabashi et al. Review of Particle Physics. *Phys. Rev.*, D98(3):030001, 2018. pages 13, 14, 94, 99, 101, 117

[34] Lincoln Wolfenstein. Parametrization of the kobayashi-maskawa matrix. *Phys. Rev. Lett.*, 51:1945–1947, Nov 1983. pages 13

[35] Gustavo C. Branco, Luis Lavoura, and Joao P. Silva. CP Violation. *Int. Ser. Monogr. Phys.*, 103:1–536, 1999. pages 14, 19

[36] V. Weisskopf and Eugene P. Wigner. Calculation of the natural brightness of spectral lines on the basis of Dirac's theory. *Z. Phys.*, 63:54–73, 1930. pages 14

[37] V. Weisskopf and E. Wigner. Over the natural line width in the radiation of the harmonius oscillator. *Z. Phys.*, 65:18–29, 1930. pages 14

[38] Marina Artuso, Guennadi Borissov, and Alexander Lenz. CP Violation in the B_s^0 System. 2015. pages 17, 18, 80, 92, 100, 112

[39] Gerard 't Hooft and M. J. G. Veltman. Regularization and Renormalization of Gauge Fields. *Nucl. Phys.*, B44:189–213, 1972. pages 22

[40] C. G. Bollini and J. J. Giambiagi. Lowest order divergent graphs in nu-dimensional space. *Phys. Lett.*, 40B:566–568, 1972. pages 22

[41] J. F. Ashmore. A Method of Gauge Invariant Regularization. *Lett. Nuovo Cim.*, 4:289–290, 1972. pages 22

[42] G. M. Cicuta and E. Montaldi. Analytic renormalization via continuous space dimension. *Lett. Nuovo Cim.*, 4:329–332, 1972. pages 22

[43] ER Speer and MJ Westwater. Generic feynman amplitudes. In *Annales de l'IHP Physique théorique*, volume 14, pages 1–55, 1971. pages 22

[44] Gerhard Buchalla, Andrzej J. Buras, and Markus E. Lautenbacher. Weak decays beyond leading logarithms. *Rev. Mod. Phys.*, 68:1125–1144, 1996. pages 23, 35

[45] L. D. Faddeev and V. N. Popov. Feynman Diagrams for the Yang-Mills Field. *Phys. Lett.*, 25B:29–30, 1967. [,325(1967)]. pages 23

[46] Ernst Carl Gerlach Stueckelberg de Breidenbach and Andreas Petermann. La normalisation des constantes dans la thorie des quantaNormalization of constants in the quanta theory. *Helv. Phys. Acta*, 26:499–520, 1953. pages 25

[47] Murray Gell-Mann and F. E. Low. Quantum electrodynamics at small distances. *Phys. Rev.*, 95:1300–1312, 1954. pages 25

[48] R. P. Feynman and Murray Gell-Mann. Theory of Fermi interaction. *Phys. Rev.*, 109:193–198, 1958. [,417(1958)]. pages 27

[49] R. E. Marshak, S. Okubo, and G. Sudarshan. V-A theory and the decay of the hyperon. *Phys. Rev.*, 113:944–954, 1959. pages 27

[50] E. C. G. Sudarshan and R. e. Marshak. Chirality invariance and the universal Fermi interaction. *Phys. Rev.*, 109:1860–1860, 1958. pages 27

[51] Kenneth G. Wilson. Nonlagrangian models of current algebra. *Phys. Rev.*, 179:1499–1512, 1969. pages 29

[52] K. G. Wilson and W. Zimmermann. Operator product expansions and composite field operators in the general framework of quantum field theory. *Commun. Math. Phys.*, 24:87–106, 1972. pages 29

[53] Wolfhart Zimmermann. Composite operators in the perturbation theory of renormalizable interactions. *Annals of Physics*, 77(1):536 – 569, 1973. pages 29

[54] Edward Witten. Short Distance Analysis of Weak Interactions. *Nucl. Phys.*, B122:109–143, 1977. pages 29, 30

[55] Aneesh V. Manohar and Mark B. Wise. Heavy quark physics. *Camb. Monogr. Part. Phys. Nucl. Phys. Cosmol.*, 10:1–191, 2000. pages 29

[56] H. David Politzer and Mark B. Wise. Effective Field Theory Approach to Processes Involving Both Light and Heavy Fields. *Phys. Lett.*, B208:504–507, 1988. pages 37

[57] H. David Politzer and Mark B. Wise. Leading Logarithms of Heavy Quark Masses in Processes with Light and Heavy Quarks. *Phys. Lett.*, B206:681–684, 1988. pages 37

[58] Nathan Isgur and Mark B. Wise. Weak Decays of Heavy Mesons in the Static Quark Approximation. *Phys. Lett.*, B232:113–117, 1989. pages 37

[59] Matthias Neubert. Heavy quark effective theory. In *Nonperturbative particle theory and experimental tests. Proceedings, 20th Johns Hopkins Workshop on Current Problems in Particle Theory, Heidelberg, Germany, June 27-29, 1996*, pages 39–78, 1996. pages 37

[60] V. Khoze and Mikhail A. Shifman. Heavy Quarks. *Soviet Physics Uspekhi*, 26:387–424, 1983. pages 40

[61] Valery A. Khoze, Mikhail A. Shifman, N. G. Uraltsev, and M. B. Voloshin. On Inclusive Hadronic Widths of Beautiful Particles. *Sov. J. Nucl. Phys.*, 46:112, 1987. [Yad. Fiz.46,181(1987)]. pages 40

[62] Ikaros I. Y. Bigi, B. Blok, Mikhail A. Shifman, N. Uraltsev, and Arkady I. Vainshtein. Nonleptonic decays of beauty hadrons: From phenomenology to theory. 1994. pages 40

[63] Ikaros I. Y. Bigi, Mikhail A. Shifman, and N. Uraltsev. Aspects of heavy quark theory. *Ann. Rev. Nucl. Part. Sci.*, 47:591–661, 1997. pages 40

[64] Alexander Lenz. Lifetimes and heavy quark expansion. *Int. J. Mod. Phys.*, A30(10):1543005, 2015. [,63(2014)]. pages 40

[65] Matthias Neubert. B decays and CP violation. *Int. J. Mod. Phys.*, A11:4173–4240, 1996. pages 40

[66] Hai-Yang Cheng. Phenomenological Study of Heavy Hadron Lifetimes. *JHEP*, 11:014, 2018. pages 40

[67] M. Beneke, G. Buchalla, and I. Dunietz. Width Difference in the $B_s - \bar{B}_s$ System. *Phys. Rev.*, D54:4419–4431, 1996. [Erratum: Phys. Rev.D83,119902(2011)]. pages 41, 71, 79

[68] Daniel King, Alexander Lenz, and Thomas Rauh. Bs mixing observables and Vtd/Vts from sum rules. *JHEP*, 05:034, 2019. pages 43

[69] M. Misiak et al. Updated NNLO QCD predictions for the weak radiative B-meson decays. *Phys. Rev. Lett.*, 114(22):221801, 2015. pages 43, 70, 100

[70] Konstantin G. Chetyrkin, Mikolaj Misiak, and Manfred Munz. Weak radiative B meson decay beyond leading logarithms. *Phys. Lett.*, B400:206–219, 1997. [Erratum: Phys. Lett.B425,414(1998)]. pages 46, 49, 51, 56, 58, 159, 160

[71] A. J. Buras, M. Misiak, M. Munz, and S. Pokorski. Theoretical uncertainties and phenomenological aspects of $B \to X(s)$ gamma decay. *Nucl. Phys.*, B424:374–398, 1994. pages 49, 50

[72] Andrzej J. Buras, Mikolaj Misiak, and Jorg Urban. Two loop QCD anomalous dimensions of flavor changing four quark operators within and beyond the standard model. *Nucl. Phys.*, B586:397–426, 2000. pages 56, 58, 159, 161

[73] Paolo Gambino, Martin Gorbahn, and Ulrich Haisch. Anomalous dimension matrix for radiative and rare semileptonic B decays up to three loops. *Nucl. Phys.*, B673:238–262, 2003. pages 56, 58, 160, 161

[74] Christoph Bobeth, Paolo Gambino, Martin Gorbahn, and Ulrich Haisch. Complete NNLO QCD analysis of $\bar{B} \to X_s l^+ l^-$ and higher order electroweak effects. *JHEP*, 04:071, 2004. pages 56, 58, 160

[75] H. Lehmann, K. Symanzik, and W. Zimmermann. On the formulation of quantized field theories. *Nuovo Cim.*, 1:205–225, 1955. pages 65, 73

[76] G. Passarino and M. J. G. Veltman. One Loop Corrections for e+ e- Annihilation Into mu+ mu- in the Weinberg Model. *Nucl. Phys.*, B160:151–207, 1979. pages 65

[77] M. Beneke, T. Feldmann, and D. Seidel. Systematic approach to exclusive $B \to V l^+ l^-$, $V\gamma$ decays. *Nucl. Phys.*, B612:25–58, 2001. pages 66

[78] Y. webupdate of Amhis et al. Averages of b-hadron, c-hadron, and τ-lepton properties as of summer 2016. *Eur. Phys. J.*, C77(12):895, 2017. pages 70, 101, 103, 117

[79] G. Buchalla, G. Isidori, and S. J. Rey. Corrections of order Λ^2_{QCD}/m^2_c to inclusive rare B decays. *Nucl. Phys.*, B511:594–610, 1998. pages 70

[80] Michael Benzke, Seung J. Lee, Matthias Neubert, and Gil Paz. Factorization at Subleading Power and Irreducible Uncertainties in $\bar{B} \to X_s\gamma$ Decay. *JHEP*, 08:099, 2010. pages 70

[81] Mikolaj Misiak and Matthias Steinhauser. NNLO QCD corrections to the $\bar{B} \to X_s\gamma$ matrix elements using interpolation in m(c). *Nucl. Phys.*, B764:62–82, 2007. pages 70, 101

[82] Paolo Gambino and Mikolaj Misiak. Quark mass effects in $\bar{B} \to Xs\gamma$. *Nucl. Phys.*, B611:338–366, 2001. pages 70

[83] Michal̃ Czakon, Paul Fiedler, Tobias Huber, Mikol̃aj Misiak, Thomas Schutzmeier, and Matthias Steinhauser. The $(Q_7, Q_{1,2})$ contribution to $\overline{B} \to X_s\gamma$ at $\mathcal{O}(\alpha_s^2)$. *JHEP*, 04:168, 2015. pages 71

[84] M. Beneke, G. Buchalla, C. Greub, A. Lenz, and U. Nierste. Next-to-leading order QCD corrections to the lifetime difference of B(s) mesons. *Phys. Lett.*, B459:631–640, 1999. pages 71, 79

[85] Martin Beneke, Gerhard Buchalla, Alexander Lenz, and Ulrich Nierste. CP asymmetry in flavor specific B decays beyond leading logarithms. *Phys. Lett.*, B576:173–183, 2003. pages 79

[86] Alexander Lenz and Ulrich Nierste. Theoretical update of $B_s - \bar{B}_s$ mixing. *JHEP*, 06:072, 2007. pages 79

[87] M. Neubert and Christopher T. Sachrajda. Spectator effects in inclusive decays of beauty hadrons. *Nucl. Phys.*, B483:339–370, 1997. pages 88

[88] M. Kirk, A. Lenz, and T. Rauh. Dimension-six matrix elements for meson mixing and lifetimes from sum rules. *JHEP*, 12:068, 2017. pages 89, 100, 103

[89] E. Franco, V. Lubicz, F. Mescia, and C. Tarantino. Lifetime ratios of beauty hadrons at the next-to-leading order in QCD. *Nucl. Phys.*, B633:212–236, 2002. pages 89

[90] Martin Beneke, Gerhard Buchalla, Christoph Greub, Alexander Lenz, and Ulrich Nierste. The B+ - B0(d) lifetime difference beyond leading logarithms. *Nucl. Phys.*, B639:389–407, 2002. pages 89

[91] S. Aoki et al. Review of lattice results concerning low-energy particle physics. *Eur. Phys. J.*, C77(2):112, 2017. pages 89, 100, 101

[92] M. Beneke, G. Buchalla, M. Neubert, and Christopher T. Sachrajda. QCD factorization for $B \to \pi\pi$ decays: Strong phases and CP violation in the heavy quark limit. *Phys. Rev. Lett.*, 83:1914–1917, 1999. pages 90

[93] M. Beneke, G. Buchalla, M. Neubert, and Christopher T. Sachrajda. QCD factorization for exclusive, nonleptonic B meson decays: General arguments and the case of heavy light final states. *Nucl. Phys.*, B591:313–418, 2000. pages 90, 91

[94] M. Beneke, G. Buchalla, M. Neubert, and Christopher T. Sachrajda. QCD factorization in $B \to \pi K$, $\pi\pi$ decays and extraction of Wolfenstein parameters. *Nucl. Phys.*, B606:245–321, 2001. pages 90

[95] Hai-Yang Cheng and Kwei-Chou Yang. $B \to J/\psi K$ decays in QCD factorization. *Phys. Rev.*, D63:074011, 2001. pages 91

[96] Junegone Chay and Chul Kim. Analysis of the QCD improved factorization in $B \to J/\psi K$. 2000. pages 91

[97] Edward Witten. Baryons in the 1/n Expansion. *Nucl. Phys.*, B160:57–115, 1979. pages 92, 119

[98] Michael Gronau. CP Violation. *Nucl. Phys. Proc. Suppl.*, 38:136–151, 1995. pages 94

[99] Damir Bečirević, Goran Duplančić, Bruno Klajn, Blaženka Melić, and Francesco Sanfilippo. Lattice QCD and QCD sum rule determination of the decay constants of η_c, J/ψ and h_c states. *Nucl. Phys.*, B883:306–327, 2014. pages 95

[100] Hai-Yang Cheng. Can $B \to J/\psi K$ (K*) decays be described by factorization? *Phys. Lett.*, B395:345–354, 1997. pages 95

[101] Andreas Hocker, H. Lacker, S. Laplace, and F. Le Diberder. A New approach to a global fit of the CKM matrix. *Eur. Phys. J.*, C21:225–259, 2001. pages 97

[102] J. Charles, Andreas Hocker, H. Lacker, S. Laplace, F. R. Le Diberder, J. Malcles, J. Ocariz, M. Pivk, and L. Roos. CP violation and the CKM matrix: Assessing the impact of the asymmetric B factories. *Eur. Phys. J.*, C41(1):1–131, 2005. pages 99, 100

[103] K. G. Chetyrkin, Johann H. Kuhn, and M. Steinhauser. RunDec: A Mathematica package for running and decoupling of the strong coupling and quark masses. *Comput. Phys. Commun.*, 133:43–65, 2000. pages 99

[104] Florian Herren and Matthias Steinhauser. Version 3 of RunDec and CRunDec. *Comput. Phys. Commun.*, 224:333–345, 2018. pages 99

[105] Gabriela Bailas, Benoît Blossier, and Vincent Morénas. Some hadronic parameters of charmonia in $\boldsymbol{N_{\rm f} = 2}$ lattice QCD. *Eur. Phys. J.*, C78(12):1018, 2018. pages 100

[106] Alexander Khodjamirian and Aleksey V. Rusov. $B_s \to K\ell\nu_\ell$ and $B_{(s)} \to \pi(K)\ell^+\ell^-$ decays at large recoil and CKM matrix elements. *JHEP*, 08:112, 2017. pages 100

[107] Ayan Paul and David M. Straub. Constraints on new physics from radiative B decays. *JHEP*, 04:027, 2017. pages 101, 108

[108] The ATLAS collaboration. Angular analysis of $B_d^0 \to K^*\mu^+\mu^-$ decays in pp collisions at $\sqrt{s} = 8$ TeV with the ATLAS detector. 2017. pages 101

[109] CMS Collaboration. Measurement of the P_1 and P_5' angular parameters of the decay $\mathrm{B}^0 \to \mathrm{K}^{*0}\mu^+\mu^-$ in proton-proton collisions at $\sqrt{s} = 8$ TeV. 2017. pages 101

[110] Roel Aaij et al. Measurements of the S-wave fraction in $B^0 \to K^+\pi^-\mu^+\mu^-$ decays and the $B^0 \to K^*(892)^0\mu^+\mu^-$ differential branching fraction. *JHEP*, 11:047, 2016. [Erratum: JHEP04,142(2017)]. pages 101

[111] Roel Aaij et al. Angular analysis and differential branching fraction of the decay $B_s^0 \to \phi\mu^+\mu^-$. *JHEP*, 09:179, 2015. pages 101

[112] J. P. Lees et al. Measurement of the $B \to X_s l^+ l^-$ branching fraction and search for direct CP violation from a sum of exclusive final states. *Phys. Rev. Lett.*, 112:211802, 2014. pages 101

[113] Aoife Bharucha, David M. Straub, and Roman Zwicky. $B \to V\ell^+\ell^-$ in the Standard Model from light-cone sum rules. *JHEP*, 08:098, 2016. pages 101

[114] Roel Aaij et al. Angular analysis of the $B^0 \to K^{*0}e^+e^-$ decay in the low-q^2 region. *JHEP*, 04:064, 2015. pages 102

[115] Bernard Aubert et al. Measurement of Time-Dependent CP Asymmetry in $B^0 \to K_S^0\pi^0\gamma$ Decays. *Phys. Rev.*, D78:071102, 2008. pages 102

[116] Y. Ushiroda et al. Time-Dependent CP Asymmetries in $B^0 \to K_S^0\pi^0\gamma$ transitions. *Phys. Rev.*, D74:111104, 2006. pages 102

[117] S. Chen et al. Branching fraction and photon energy spectrum for $b \to s\gamma$. *Phys. Rev. Lett.*, 87:251807, 2001. pages 102

[118] Kazuo Abe et al. A Measurement of the branching fraction for the inclusive $B \to X_s\gamma$ decays with BELLE. *Phys. Lett.*, B511:151–158, 2001. pages 102

[119] Bernard Aubert et al. Measurement of the $B \to X_s\gamma$ branching fraction and photon energy spectrum using the recoil method. *Phys. Rev.*, D77:051103, 2008. pages 102

[120] J. P. Lees et al. Exclusive Measurements of $b \to s\gamma$ Transition Rate and Photon Energy Spectrum. *Phys. Rev.*, D86:052012, 2012. pages 102

[121] J. P. Lees et al. Measurement of B($B \to X_s\gamma$), the $B \to X_s\gamma$ photon energy spectrum, and the direct CP asymmetry in $B \to X_{s+d}\gamma$ decays. *Phys. Rev.*, D86:112008, 2012. pages 102

[122] M. Nakao et al. Measurement of the $B \to K^*\gamma$ branching fractions and asymmetries. *Phys. Rev.*, D69:112001, 2004. pages 102

[123] Bernard Aubert et al. Measurement of Branching Fractions and CP and Isospin Asymmetries in $B \to K^*(892)\gamma$ Decays. *Phys. Rev. Lett.*, 103:211802, 2009. pages 102

[124] R Aaij et al. Measurement of the ratio of branching fractions $BR(B_0 \to K^{\star 0}\gamma)/BR(B_{s0} \to \phi\gamma)$ and the direct CP asymmetry in $B_0 \to K^{\star 0}\gamma$. *Nucl. Phys.*, B867:1–18, 2013. pages 102

[125] A Lenz. private communication. pages 112, 113

[126] Christine T. H. Davies, Judd Harrison, G. Peter Lepage, Christopher J. Monahan, Junko Shigemitsu, and Matthew Wingate. Lattice QCD matrix elements for the $B_s^0 - \bar{B}_s^0$ width difference beyond leading order. 2019. pages 112

[127] The ATLAS collaboration. Measurement of the CP violation phase ϕ_s in $B_s \to J/\psi\phi$ decays in ATLAS at 13 TeV. 2019. pages 113

[128] Elizabeth E. Jenkins, Aneesh V. Manohar, and Michael Trott. Renormalization Group Evolution of the Standard Model Dimension Six Operators I: Formalism and lambda Dependence. *JHEP*, 10:087, 2013. pages 129

[129] Konstantin G. Chetyrkin, Mikolaj Misiak, and Manfred Munz. Beta functions and anomalous dimensions up to three loops. *Nucl. Phys.*, B518:473–494, 1998. pages 130, 143

[130] R. Mertig, M. Bohm, and Ansgar Denner. FEYN CALC: Computer algebraic calculation of Feynman amplitudes. *Comput. Phys. Commun.*, 64:345–359, 1991. pages 133

[131] Vladyslav Shtabovenko, Rolf Mertig, and Frederik Orellana. New Developments in FeynCalc 9.0. *Comput. Phys. Commun.*, 207:432–444, 2016. pages 133

[132] R. Mertig and R. Scharf. TARCER: A Mathematica program for the reduction of two loop propagator integrals. *Comput. Phys. Commun.*, 111:265–273, 1998. pages 133

Appendix A

Definitions and conventions

Definitions

$$\not{p} = \gamma^\mu p_\mu \tag{A.1}$$

$$\not{\partial} = \gamma^\mu \partial_\mu \tag{A.2}$$

In the Chiral/Weyl representation the Dirac matrices are given by

$$\gamma^0 = \begin{pmatrix} 0 & \mathbb{1} \\ \mathbb{1} & 0 \end{pmatrix}, \qquad \gamma^i = \begin{pmatrix} 0 & \sigma^i \\ -\sigma^i & 0 \end{pmatrix}, \qquad \gamma^5 = \begin{pmatrix} -\mathbb{1} & 0 \\ 0 & \mathbb{1} \end{pmatrix}. \tag{A.3}$$

The relation between the Dirac representation and the Chiral representation is

$$\gamma^\mu_{chiral} = U\gamma^\mu_{Dirac}, \qquad U = \frac{1}{\sqrt{2}}(\mathbb{1} - \gamma^5\gamma^0). \tag{A.4}$$

Conventions

$$\hbar = c = 1 \tag{A.5}$$

$$\eta^{\mu\nu} = \mathrm{diag}(1, -1, -1, -1) \tag{A.6}$$

$$\sigma^{\mu\nu} = \frac{i}{2}[\gamma^\mu, \gamma^\nu] \tag{A.7}$$

$$P_L = \frac{1}{2}(1 - \gamma^5) \tag{A.8}$$

$$P_R = \frac{1}{2}(1 + \gamma^5) \tag{A.9}$$

Covariant and contravariant four-vectors

$$x^\mu = (x^0, \vec{x}) \tag{A.10}$$

$$x_\mu = (x^0, -\vec{x}) \tag{A.11}$$

Particles with mass m have

$$p^2 = p^\mu p_\mu = E^2 - |\vec{p}|^2 = m^2 \tag{A.12}$$

The Feynman propagator for the Dirac fermion is

$$S^F(x) = \int \frac{d^4p}{(2\pi)^4} \frac{i(\not{p} + m)}{(p^2 - m^2 + i\epsilon)} e^{-ip\cdot x}. \tag{A.13}$$

The time ordering symbol is defined through

$$\langle 0|T[\phi(x)\phi(y)|0\rangle \equiv \theta(x^0 - y^0)\langle 0|\phi(x)\phi(y)|0\rangle + \theta(y^0 - x^0)\langle 0|\phi(y)\phi(x)|0\rangle \tag{A.14}$$

Fierz relations

$$(\gamma^\mu P_L)_{ij}(\gamma_\mu P_L)_{kl} = -(\gamma^\mu P_L)_{il}(\gamma_\mu P_L)_{kj} \tag{A.15}$$

$$(\gamma^\mu P_L)_{ij}(\gamma_\mu P_R)_{kl} = 2(P_R)_{il}(P_L)_{kj} \tag{A.16}$$

$$(P_L)_{ij}(P_L)_{kl} = \frac{1}{2}(P_L)_{il}(P_L)_{kj} + \frac{1}{8}(\sigma_{\mu\nu}P_L)_{il}(\sigma^{\mu\nu}P_L)_{kj} \tag{A.17}$$

$$(\sigma_{\mu\nu}P_L)_{ij}(\sigma^{\mu\nu}P_L)_{kl} = 6(P_L)_{il}(P_L)_{kj} - \frac{1}{2}(\sigma_{\mu\nu}P_L)_{il}(\sigma^{\mu\nu}P_L)_{kj} \tag{A.18}$$

The fierz relations between operators, in $d \to 4$ dimensions, with operators defined as

$$\mathcal{O}_{VLL} = (\bar{s}_1^i \gamma_\mu P_L b_1^i)(\bar{s}_2^j \gamma^\mu P_L b_2^j) \tag{A.19}$$

$$\mathcal{O}_{VLR} = (\bar{s}_1^i \gamma_\mu P_L b_1^i)(\bar{s}_2^j \gamma^\mu P_R b_2^j) \tag{A.20}$$

$$\mathcal{O}_{SLR} = (\bar{s}_1^i P_L b_1^i)(\bar{s}_2^j P_R b_2^j) \tag{A.21}$$

$$\mathcal{O}_{TLL} = (\bar{s}_1^i \sigma_{\mu\nu} P_L b_1^i)(\bar{s}_2^j \sigma^{\mu\nu} P_L b_2^j) \tag{A.22}$$

$$\mathcal{O}_{SLL} = (\bar{s}_1^i P_L b_1^i)(\bar{s}_2^j P_L b_2^j) \tag{A.23}$$

$$\tilde{\mathcal{O}}_{VLL} = (\bar{s}_1^i \gamma_\mu P_L b_2^j)(\bar{s}_2^j \gamma^\mu P_L b_1^i) \tag{A.24}$$

$$\tilde{\mathcal{O}}_{VLR} = (\bar{s}_1^i \gamma_\mu P_L b_2^j)(\bar{s}_2^j \gamma^\mu P_R b_1^i) \tag{A.25}$$

$$\tilde{\mathcal{O}}_{SLR} = (\bar{s}_1^i P_L b_2^j)(\bar{s}_2^j P_R b_1^i) \tag{A.26}$$

$$\tilde{\mathcal{O}}_{TLL} = (\bar{s}_1^i \sigma_{\mu\nu} P_L b_2^j)(\bar{s}_2^j \sigma^{\mu\nu} P_L b_1^i) \tag{A.27}$$

$$\tilde{\mathcal{O}}_{SLL} = (\bar{s}_1^i P_L b_2^j)(\bar{s}_2^j P_L b_1^i) \tag{A.28}$$

$$\tilde{\mathcal{O}}_{VLL} = \mathcal{O}_{VLL} \tag{A.29}$$

$$\tilde{\mathcal{O}}_{VLR} = -2\mathcal{O}_{SLR} \tag{A.30}$$

$$\tilde{\mathcal{O}}_{TLL} = -6\mathcal{O}_{SLL} + \frac{1}{2}\mathcal{O}_{TLL} \tag{A.31}$$

$$\tilde{\mathcal{O}}_{SLL} = -\frac{1}{2}\mathcal{O}_{SLL} - \frac{1}{8}\mathcal{O}_{TLL} \tag{A.32}$$

Appendix B

Anomalous dimension matrix entries

Here are listed the sources from which some of the anomalous dimension matrix elements were obtained in the literature in order to calculate the evolution for the coefficients in Chapter 4. Some elements were obtained from calculations performed for this thesis and where this is the case, it has been stated.

Case I

This corresponds to the solution for case I obtained in section 4.2. The entries to $\hat{\gamma}_{cc,I}$ are obtained from [72]

$$\hat{\gamma}_{cc,I} = \begin{pmatrix} -\frac{6}{N} & 6 & 0 & 0 & 0 & 0 \\ 6 & -\frac{6}{N} & 0 & 0 & 0 & 0 \\ 0 & 0 & \frac{6}{N} & -6 & 0 & 0 \\ 0 & 0 & 0 & -6N + \frac{6}{N} & 0 & 0 \\ 0 & 0 & 0 & 0 & -6N + \frac{6}{N} & 0 \\ 0 & 0 & 0 & 0 & -6 & \frac{6}{N} \end{pmatrix} \tag{B.1}$$

entries for $\hat{\gamma}_{pp}$ are obtained from [70]

$$\hat{\gamma}_{pp} = \begin{pmatrix} 0 & -\frac{52}{3} & 0 & 2 \\ -\frac{40}{9} & -\frac{100}{9} & \frac{4}{9} & \frac{5}{6} \\ 0 & -\frac{256}{3} & 0 & 20 \\ -\frac{256}{9} & \frac{56}{9} & \frac{40}{9} & -\frac{2}{3} \end{pmatrix} \tag{B.2}$$

entries to $\vec{\gamma}_{p7,I}$ and $\vec{\gamma}_{p8,I}$ are from [73] and note that due to rescaling of their operators these are part of the $\hat{\gamma}^{(1)}$ matrix.

$$\vec{\gamma}_{p7,I} = \left(\begin{array}{cccc} \frac{64}{81}, & \frac{-200}{243}, & -\frac{6464}{81}, & -\frac{11408}{243} \end{array} \right)^T \tag{B.3}$$

$$\vec{\gamma}_{p8,I} = \left(\begin{array}{cccc} \frac{368}{27}, & -\frac{1409}{162}, & \frac{13052}{27}, & -\frac{2740}{81} \end{array} \right)^T \tag{B.4}$$

$\vec{\gamma}_{p9,I}$ is from [74]

$$\vec{\gamma}_{p9,I} = \left(\begin{array}{cccc} -\frac{16}{9}, & \frac{32}{27}, & -\frac{112}{9}, & \frac{512}{27} \end{array} \right)^T \tag{B.5}$$

The first 4 entries of $\vec{\gamma}^{\text{eff}}_{c7,I}$ are 2 loop entries and from [70] and [1]. The last 2 entries are from my own calculations.

$$\vec{\gamma}_{c7,I} = \left(\begin{array}{cccccc} 0, & \frac{464}{81}, & 0, & \frac{200}{81}, & 0, & 0 \end{array} \right)^T \tag{B.6}$$

The first 2 entries of $\vec{\gamma}^{\text{eff}}_{c8,I}$ are 2 loop entries and from [70].

$$\vec{\gamma}_{c8,I} = \left(\begin{array}{cccccc} 3, & \frac{76}{27}, & 0, 0, & 0, & 0 \end{array} \right)^T \tag{B.7}$$

All entries of $\vec{\gamma}_{c9,I}$ and $\hat{\gamma}_{cp,I}$ are from my own calculations.

$$\vec{\gamma}_{c9,I} = \left(\begin{array}{cccccc} -\frac{8N}{9}, & -\frac{8}{9}, & \frac{4N}{9}, & \frac{4}{9}, & 0 & 0 \end{array} \right)^T$$

$$\hat{\gamma}_{cp,I} = \begin{pmatrix} 0 & 0 & 0 & 0 \\ 0 & \frac{4}{3} & 0 & 0 \\ 0 & 0 & 0 & 0 \\ 0 & -\frac{2}{3} & 0 & 0 \\ 0 & 0 & 0 & 0 \\ 0 & 0 & 0 & 0 \end{pmatrix} \tag{B.8}$$

The first 6 elements are from [70] and $\gamma_{99,I}$ in the normalization specified in 4.2.2 from my own calculations.

$$\gamma_{77,I} = \frac{32}{3}, \qquad \gamma_{87,I} = -\frac{32}{9}, \tag{B.9}$$

$$\hat{\gamma}_{88,I} = \frac{28}{3}, \qquad \gamma_{99,I} = -2\beta^{(0)} \tag{B.10}$$

Case II

This corresponds to the solution for case II obtained in section 4.2. The entries to $\hat{\gamma}_{cc,II}$ are obtained from [72]

$$\hat{\gamma}_{cc,II} = \begin{pmatrix} \frac{6}{N} & -6 & \frac{1}{N} - \frac{N}{2} & -\frac{1}{2} \\ 0 & \frac{6}{N} - 6N & -1 & \frac{1}{N} \\ \frac{48}{N} - 24N & -24 & 4N - \frac{2}{N} & 6 \\ -48 & \frac{48}{N} & 0 & 2N - \frac{2}{N} \end{pmatrix} \tag{B.11}$$

The below elements are from adaptation of my own results.

$$\hat{\gamma}_{cp,II} = \begin{pmatrix} 0 & 0 & 0 & 0 \\ 0 & 0 & 0 & 0 \\ 0 & 0 & 0 & 0 \\ 0 & 0 & 0 & 0 \\ 0 & 0 & 0 & 0 \\ 0 & 0 & 0 & 0 \end{pmatrix}. \tag{B.12}$$

Entries to $\vec{\gamma}_{p7,II}$ and $\vec{\gamma}_{p8,II}$ are from [73],

$$\vec{\gamma}_{p7,II} = \begin{pmatrix} 0, & 0, & 0, & 0 \end{pmatrix}^T \tag{B.13}$$

$$\vec{\gamma}_{p8,II} = \begin{pmatrix} 0, & 0, & 0, & 0 \end{pmatrix}^T \tag{B.14}$$

$$\vec{\gamma}_{c7,II} = \begin{pmatrix} 2\frac{Nx_c}{3}, & \frac{2x_c}{3}, & -8\frac{Nx_c}{3}, & -8\frac{x_c}{3} \end{pmatrix}^T \tag{B.15}$$

$$\vec{\gamma}_{c8,II} = \begin{pmatrix} 0, & x_c, & 0, & -4x_c \end{pmatrix}^T \tag{B.16}$$

All entries of $\vec{\gamma}_{c9,II}$ and $\hat{\gamma}_{cp}$ are from my own calculations.

$$\vec{\gamma}_{c9,II} = \begin{pmatrix} 0, & 0, & 0, & 0, \end{pmatrix}^T \tag{B.17}$$

These elements are from the above sources but are changed in the normalization employed in 4.1 from own calculations.

$$\gamma_{77,II} = \frac{32}{3} - 2\beta^{(0)}, \qquad \gamma_{87,II} = -\frac{32}{9} - 2\beta^{(0)}, \tag{B.18}$$

$$\gamma_{88,II} = \frac{28}{3} - 2\beta^{(0)}, \qquad \gamma_{99,II} = -2\beta^{(0)} \tag{B.19}$$

All of the other elements are the same as those in case I.

Appendix C

Integrals

Veltman and Passarino integrals

$$B_0, B_\sigma, B_{\sigma\lambda} = \int \frac{d^d k}{(2\pi)^d} \frac{1; k_\sigma; k_{\sigma\lambda}}{((k-q)^2 - m^2 + i\epsilon)(k^2 - m^2 + i\epsilon)} \tag{C.1}$$

$$A(m^2) = \int \frac{d^d k}{(4\pi)^d} \frac{1}{k^2 - m^2 + i\epsilon} \tag{C.2}$$

and where The Veltman and Passarino reduction yields

$$B_1(m^2, m^2, q^2) = \frac{1}{2} B_0(m^2, m^2, q^2) \tag{C.3}$$

$$B_{00}(m^2, m^2, q^2) = \frac{1}{(1-d)} \left[\left(\frac{1}{4} q^2 - m^2 \right) B_0(m^2, m^2, q^2) - \frac{A(m^2)}{2} \right] \tag{C.4}$$

$$B_{11}(m^2, m^2, q^2) = -\frac{1}{q^2(1-d)} \left[\left(\frac{d}{4} q^2 - m^2 \right) B_0(m^2, m^2, q^2) + \frac{(d-2)}{2} A(m^2) \right] \tag{C.5}$$

Appendix D

Complete set of constraints

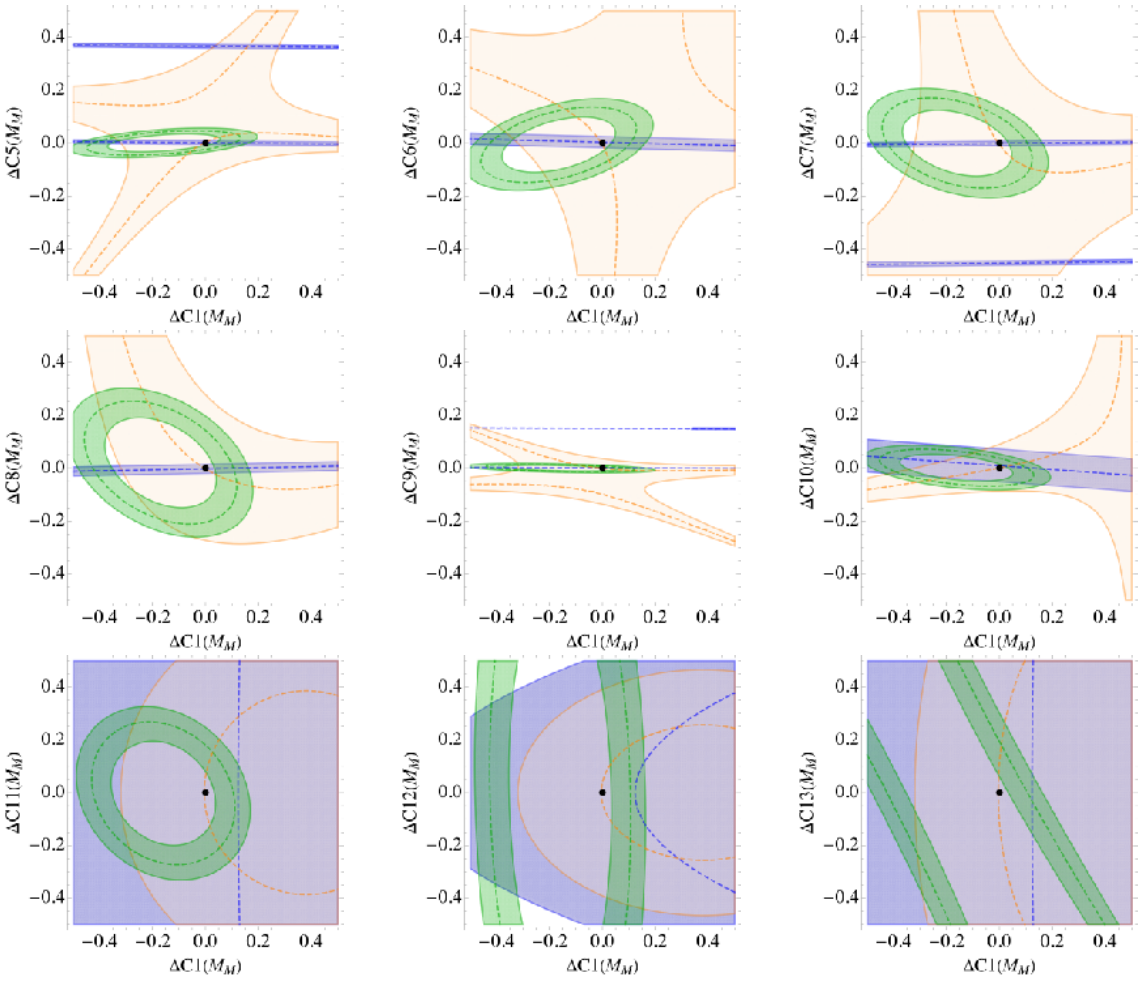

Figure D.1

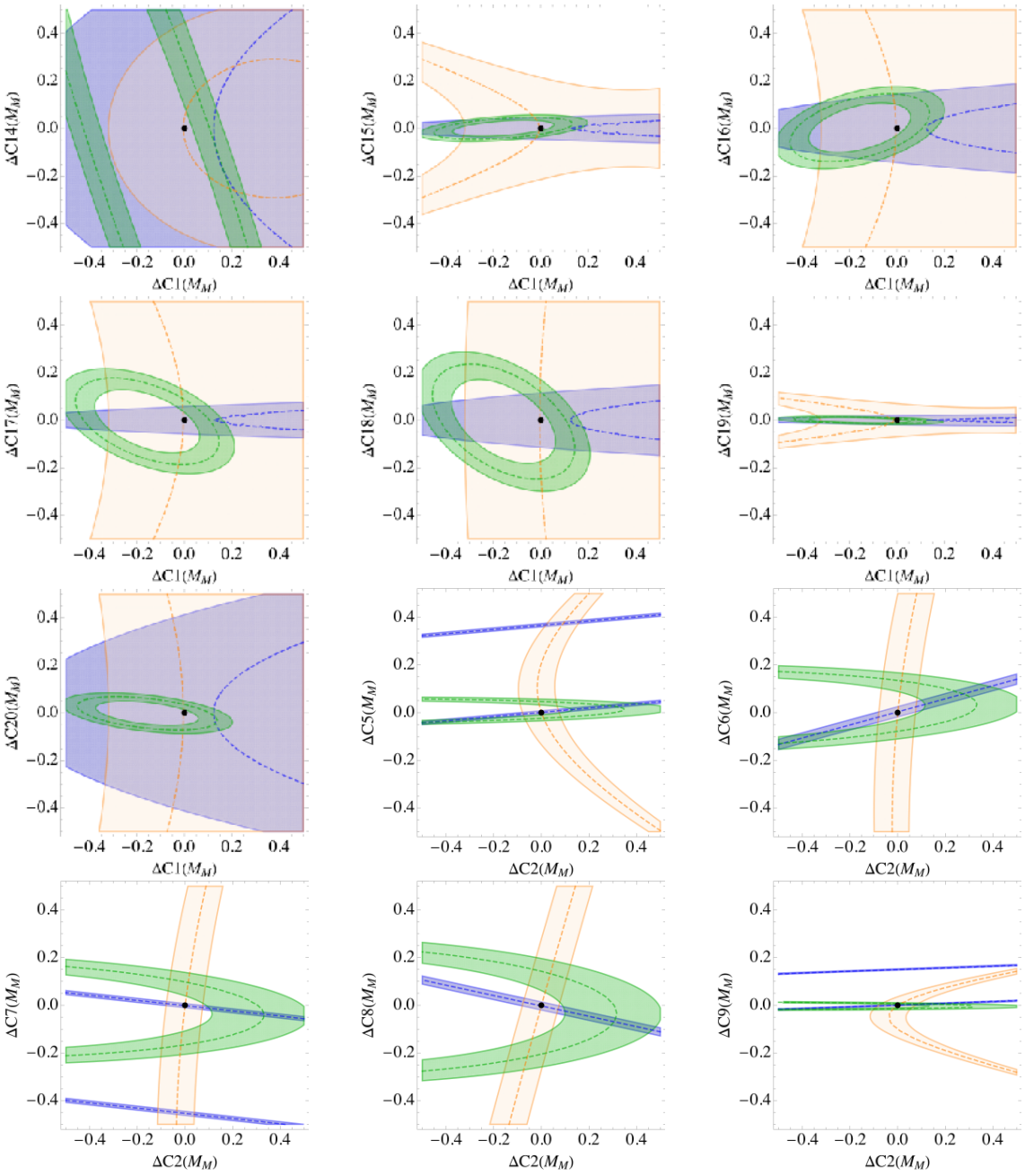
ΔC14(M_M)
ΔC15(M_M)
ΔC16(M_M)
ΔC17(M_M)
ΔC18(M_M)
ΔC19(M_M)
ΔC20(M_M)
ΔC5(M_M)
ΔC6(M_M)
ΔC7(M_M)
ΔC8(M_M)
ΔC9(M_M)
ΔC1(M_M)
ΔC2(M_M)
0.4
0.2
0.0
−0.2
−0.4

Figure D.2

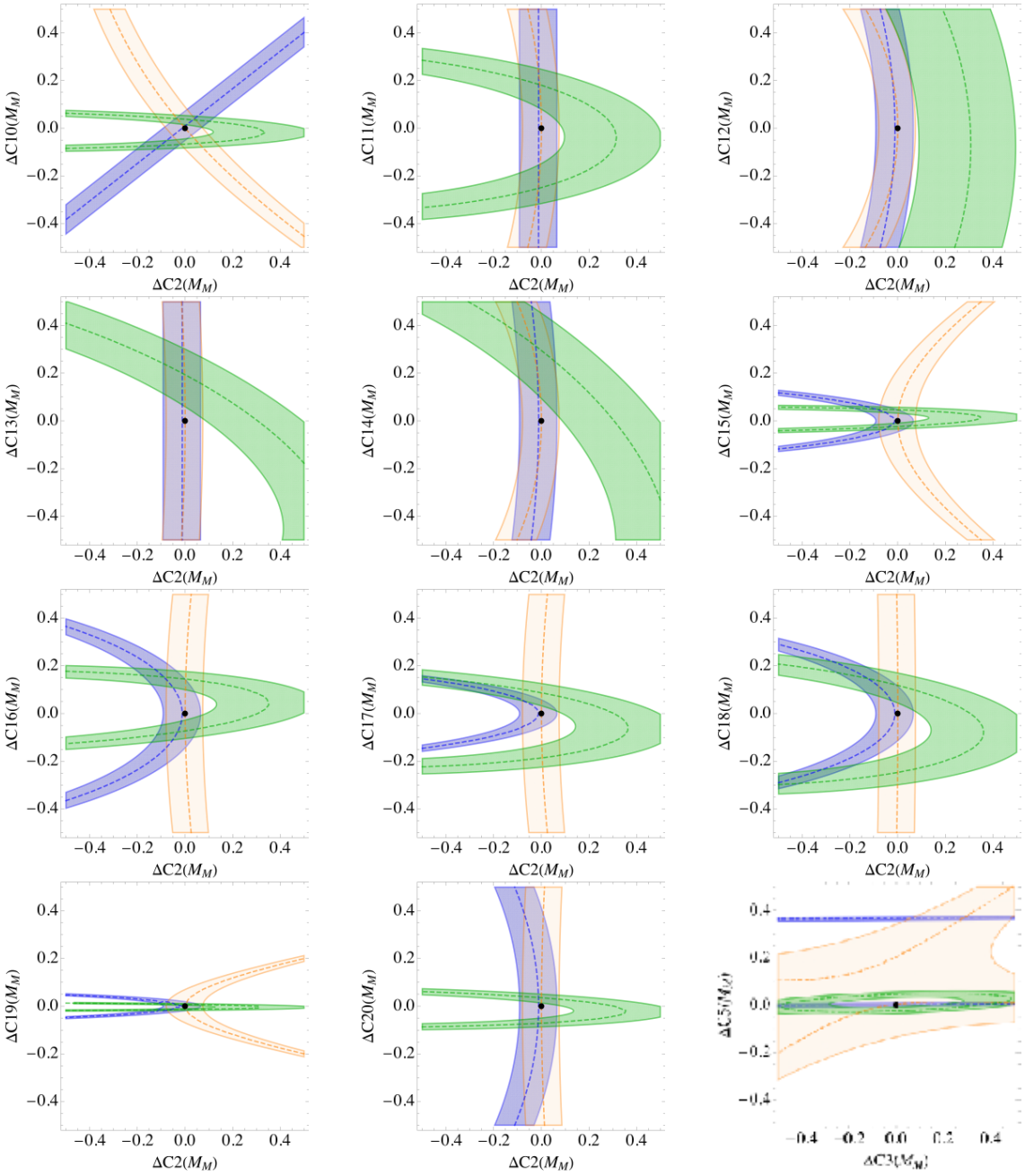
ΔC10(M_M)
ΔC11(M_M)
ΔC12(M_M)
ΔC13(M_M)
ΔC14(M_M)
ΔC15(M_M)
ΔC16(M_M)
ΔC17(M_M)
ΔC18(M_M)
ΔC19(M_M)
ΔC20(M_M)
ΔC2(M_M)
0.4
0.2
0.0
−0.2
−0.4

Figure D.3

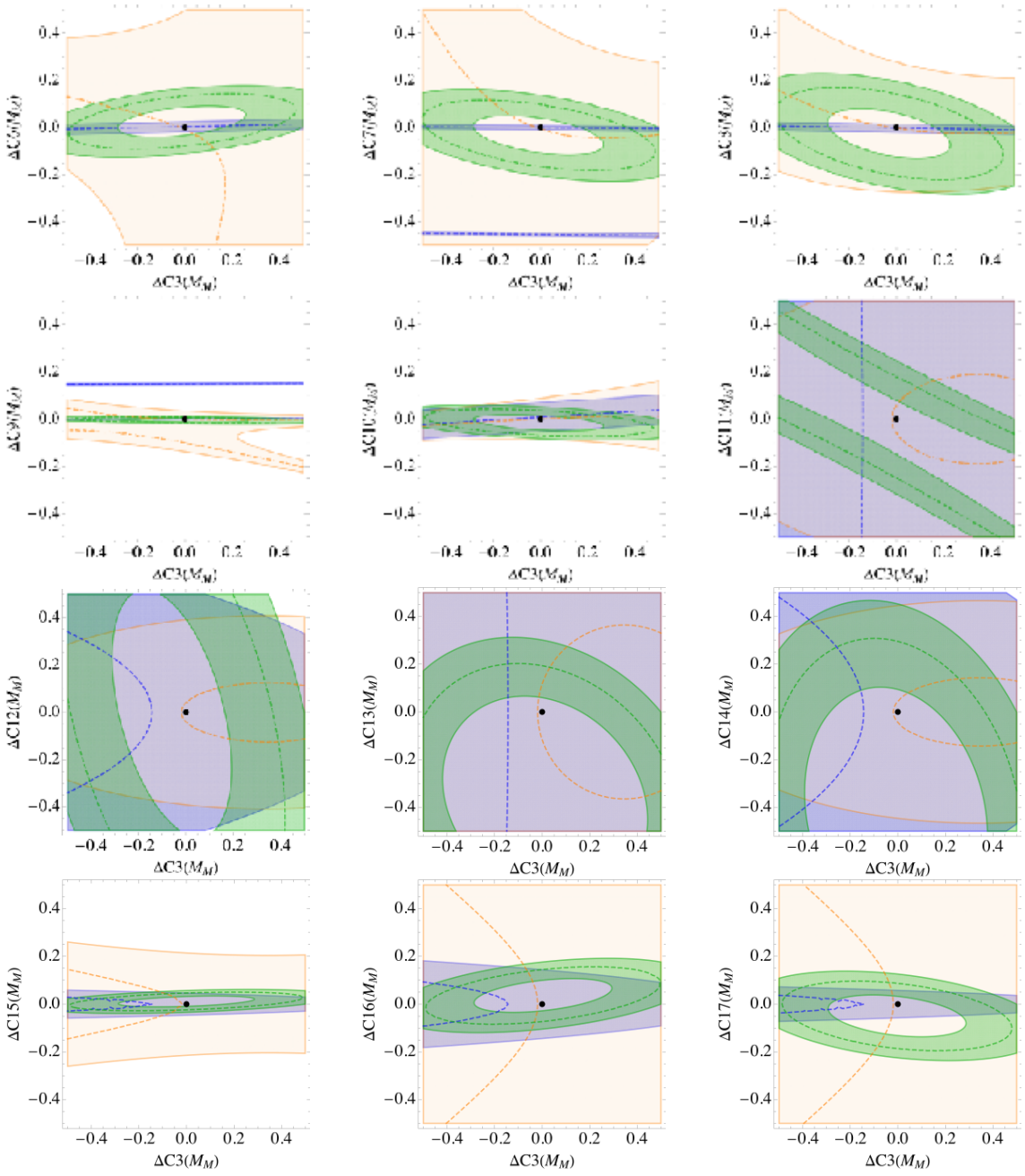
ΔC3(M_M)
ΔC12(M_M)
ΔC13(M_M)
ΔC14(M_M)
ΔC15(M_M)
ΔC16(M_M)
ΔC17(M_M)
−0.4 −0.2 0.0 0.2 0.4

Figure D.4

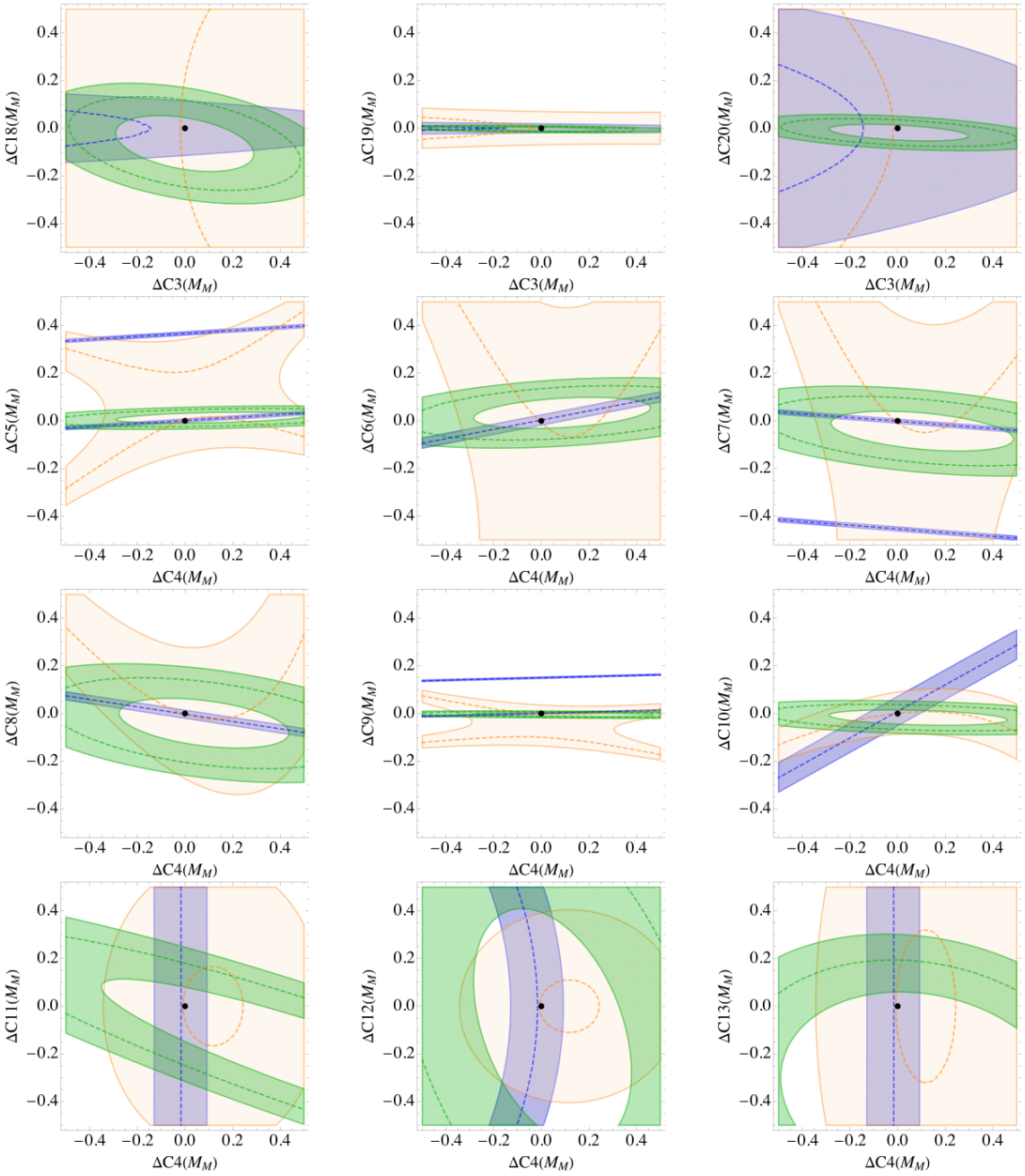
ΔC18(M_M)
ΔC19(M_M)
ΔC20(M_M)
ΔC5(M_M)
ΔC6(M_M)
ΔC7(M_M)
ΔC8(M_M)
ΔC9(M_M)
ΔC10(M_M)
ΔC11(M_M)
ΔC12(M_M)
ΔC13(M_M)
ΔC3(M_M)
ΔC4(M_M)
0.4
0.2
0.0
−0.2
−0.4

Figure D.5

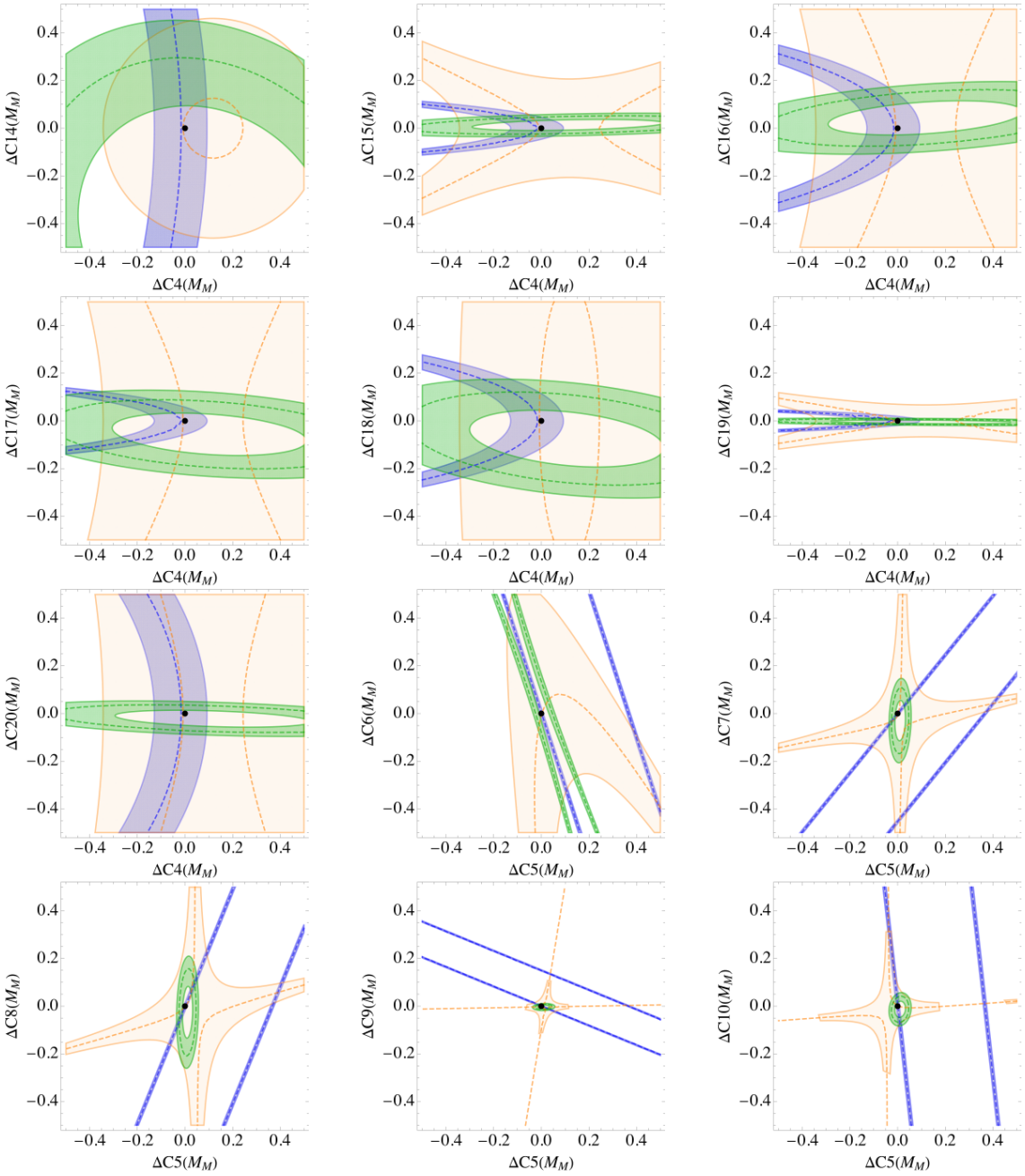
ΔC14(M_M)
ΔC4(M_M)
ΔC15(M_M)
ΔC4(M_M)
ΔC16(M_M)
ΔC4(M_M)
ΔC17(M_M)
ΔC4(M_M)
ΔC18(M_M)
ΔC4(M_M)
ΔC19(M_M)
ΔC4(M_M)
ΔC20(M_M)
ΔC4(M_M)
ΔC6(M_M)
ΔC5(M_M)
ΔC7(M_M)
ΔC5(M_M)
ΔC8(M_M)
ΔC5(M_M)
ΔC9(M_M)
ΔC5(M_M)
ΔC10(M_M)
ΔC5(M_M)

Figure D.6

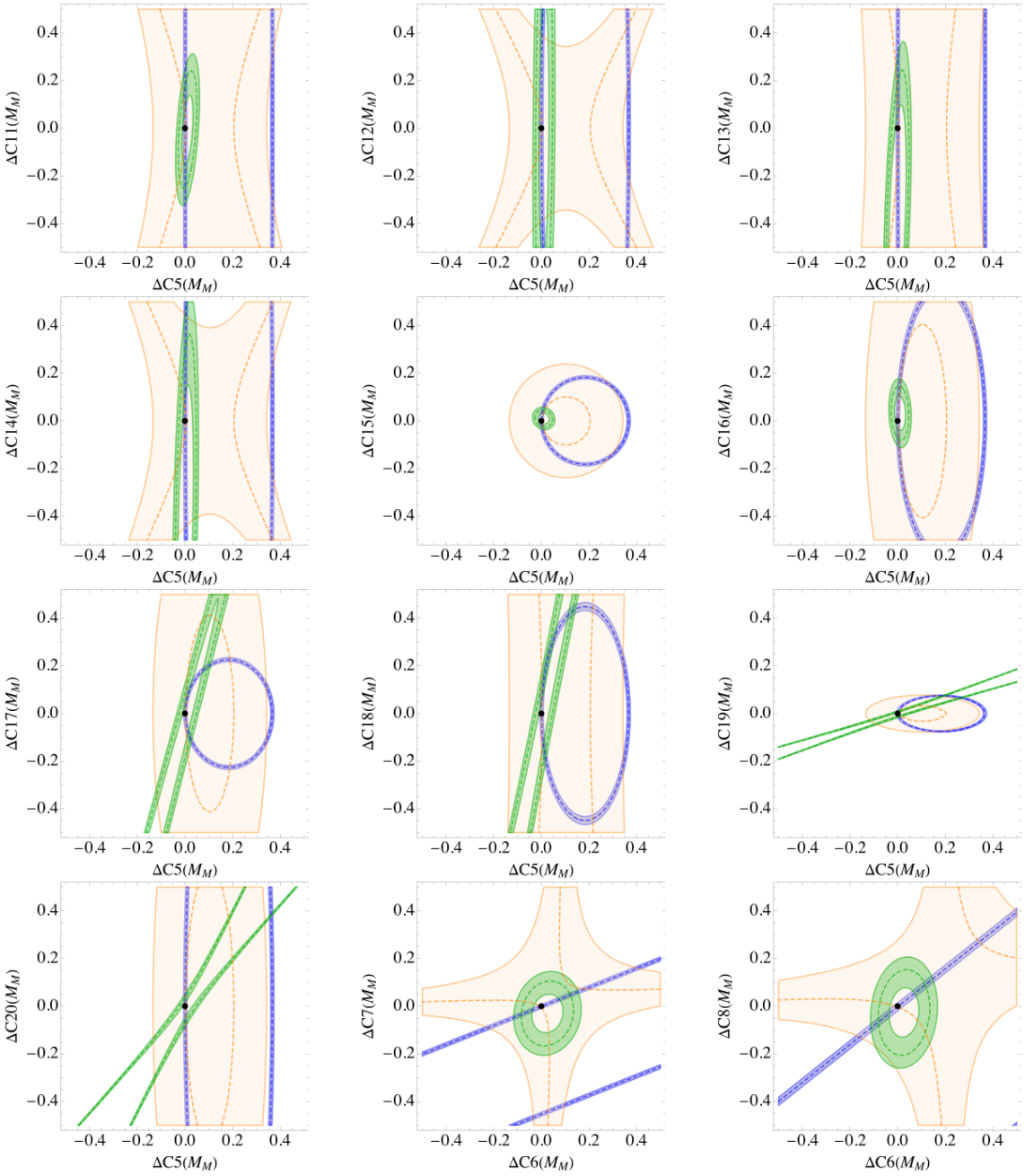
ΔC11(M_M)
ΔC12(M_M)
ΔC13(M_M)
ΔC14(M_M)
ΔC15(M_M)
ΔC16(M_M)
ΔC17(M_M)
ΔC18(M_M)
ΔC19(M_M)
ΔC20(M_M)
ΔC7(M_M)
ΔC8(M_M)
ΔC5(M_M)
ΔC6(M_M)
0.4
0.2
0.0
−0.2
−0.4

Figure D.7

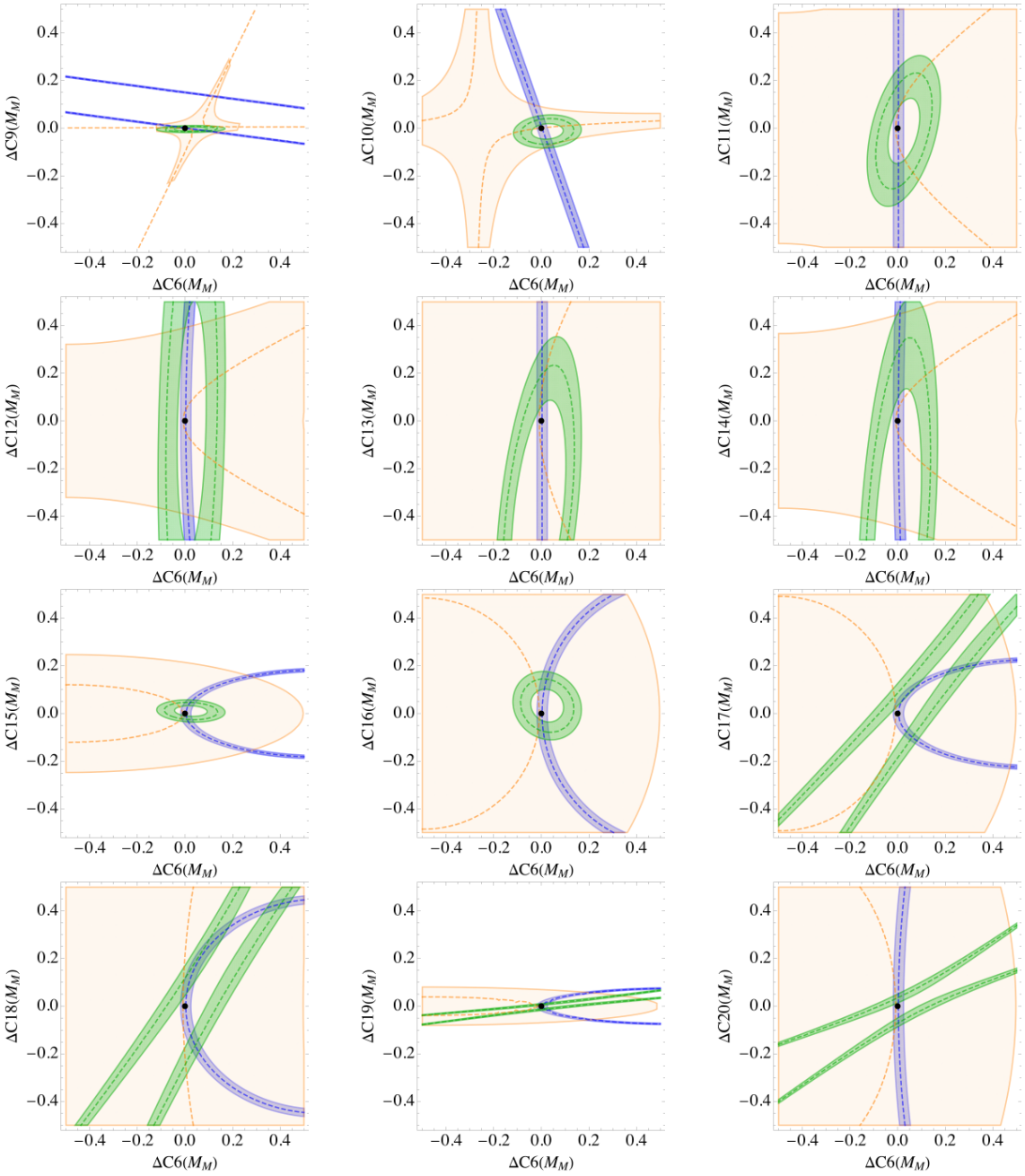
ΔC9(M_M)
ΔC10(M_M)
ΔC11(M_M)
ΔC12(M_M)
ΔC13(M_M)
ΔC14(M_M)
ΔC15(M_M)
ΔC16(M_M)
ΔC17(M_M)
ΔC18(M_M)
ΔC19(M_M)
ΔC20(M_M)
ΔC6(M_M)
0.4
0.2
0.0
−0.2
−0.4

Figure D.8

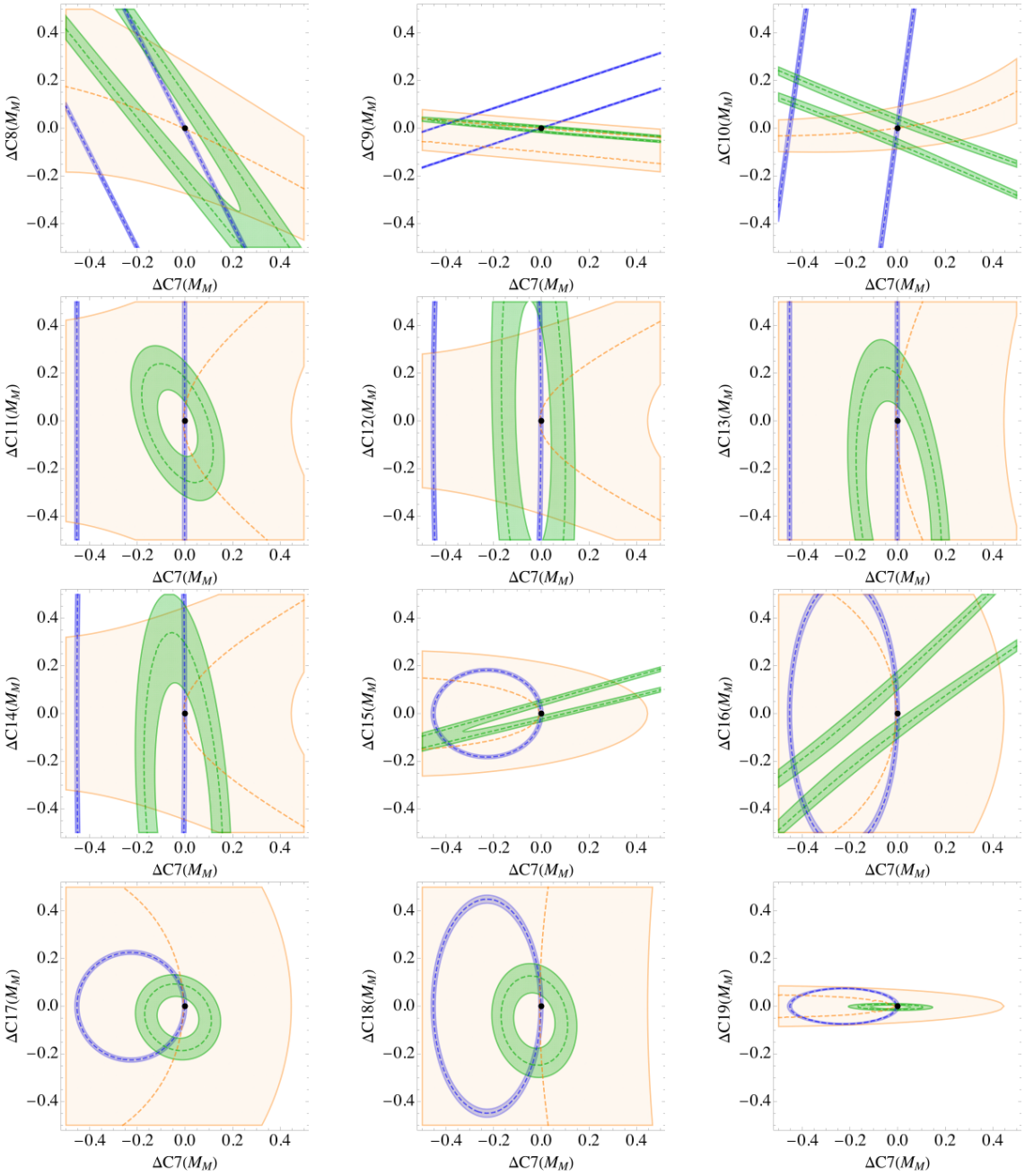
ΔC8(M_M)
ΔC9(M_M)
ΔC10(M_M)
ΔC11(M_M)
ΔC12(M_M)
ΔC13(M_M)
ΔC14(M_M)
ΔC15(M_M)
ΔC16(M_M)
ΔC17(M_M)
ΔC18(M_M)
ΔC19(M_M)
ΔC7(M_M)
0.4
0.2
0.0
−0.2
−0.4

Figure D.9

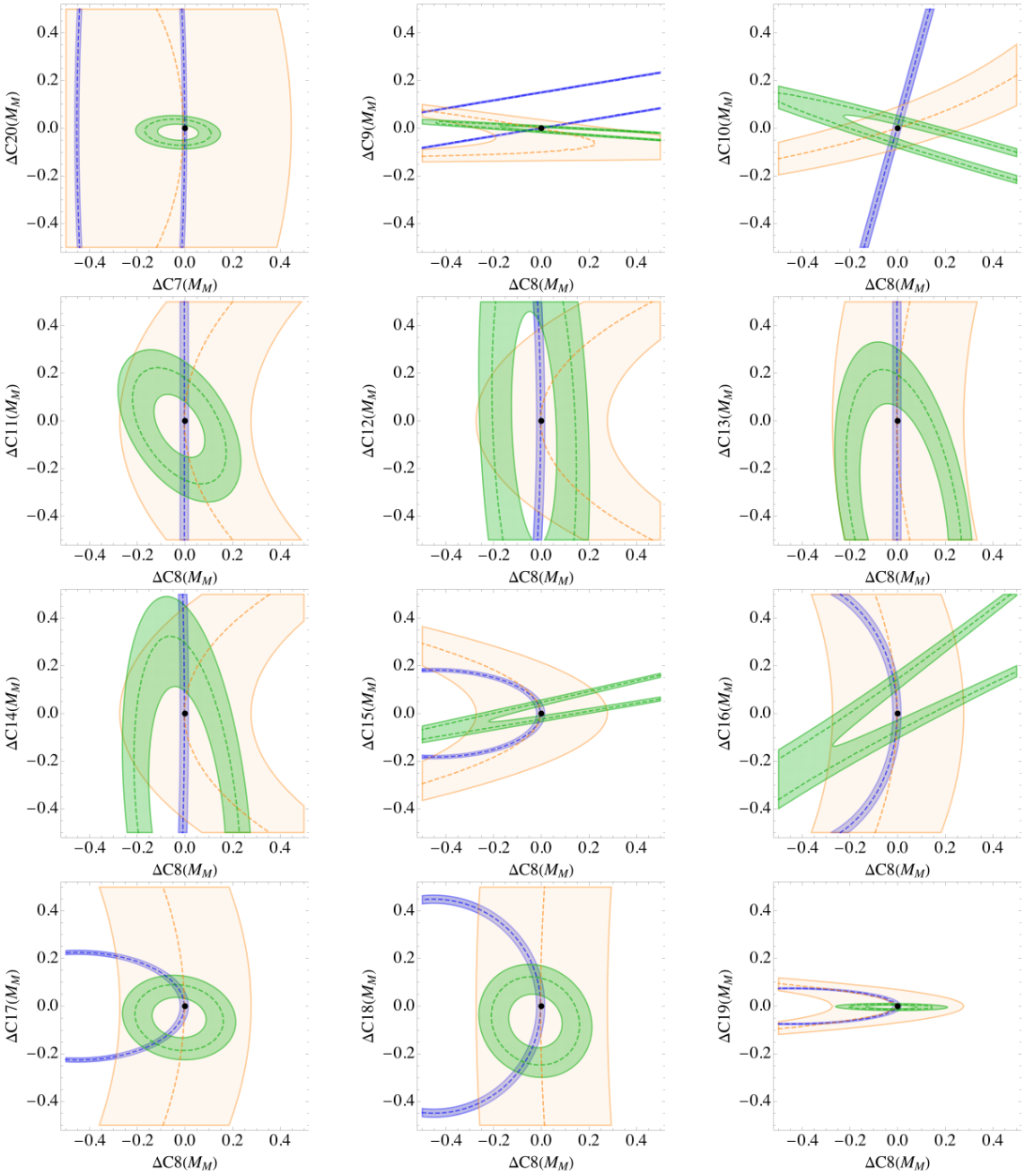
ΔC20(M_M)
ΔC7(M_M)
ΔC9(M_M)
ΔC8(M_M)
ΔC10(M_M)
ΔC8(M_M)
ΔC11(M_M)
ΔC8(M_M)
ΔC12(M_M)
ΔC8(M_M)
ΔC13(M_M)
ΔC8(M_M)
ΔC14(M_M)
ΔC8(M_M)
ΔC15(M_M)
ΔC8(M_M)
ΔC16(M_M)
ΔC8(M_M)
ΔC17(M_M)
ΔC8(M_M)
ΔC18(M_M)
ΔC8(M_M)
ΔC19(M_M)
ΔC8(M_M)

Figure D.10

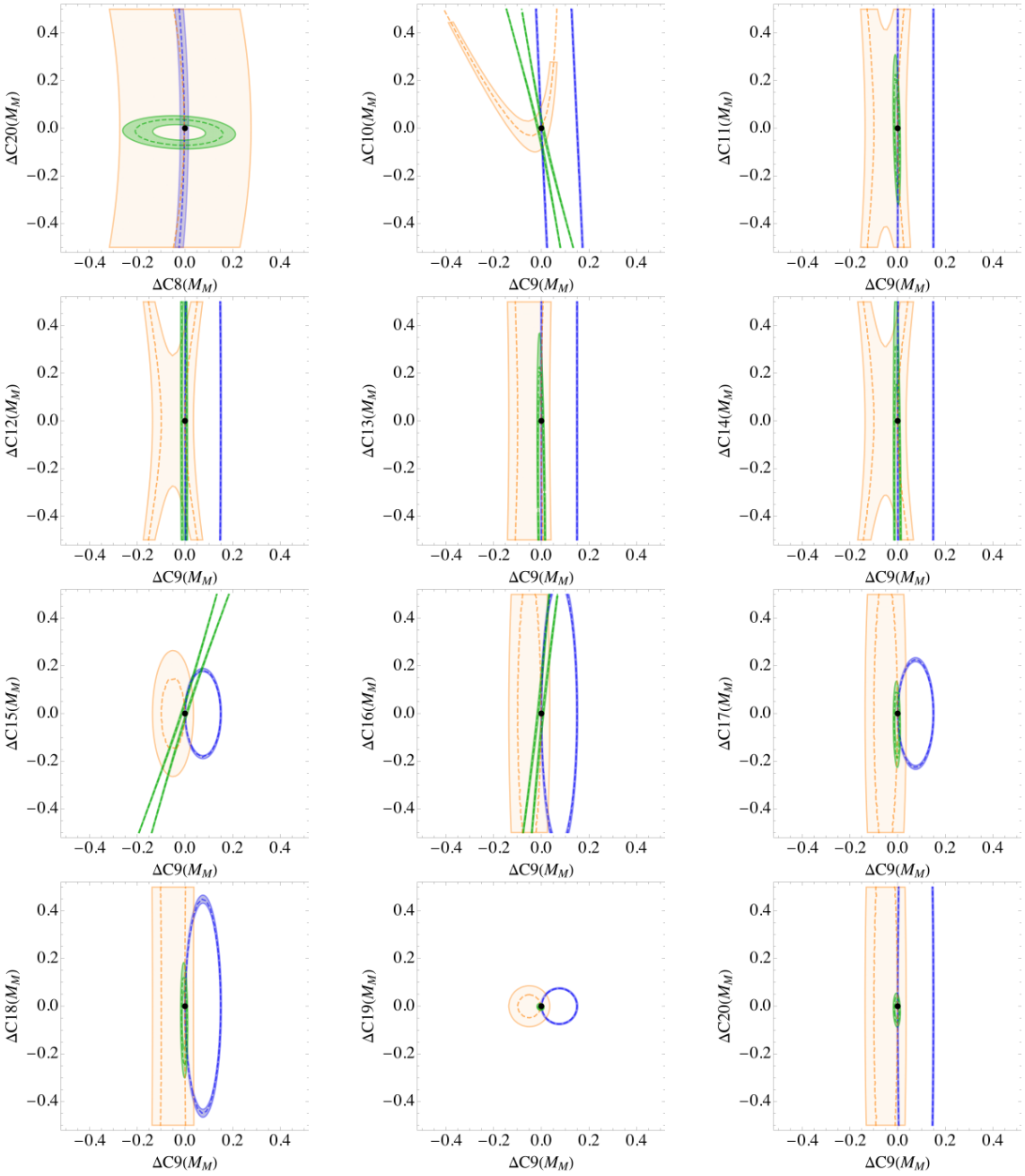
ΔC20(M_M)
ΔC8(M_M)
ΔC10(M_M)
ΔC9(M_M)
ΔC11(M_M)
ΔC9(M_M)
ΔC12(M_M)
ΔC9(M_M)
ΔC13(M_M)
ΔC9(M_M)
ΔC14(M_M)
ΔC9(M_M)
ΔC15(M_M)
ΔC9(M_M)
ΔC16(M_M)
ΔC9(M_M)
ΔC17(M_M)
ΔC9(M_M)
ΔC18(M_M)
ΔC9(M_M)
ΔC19(M_M)
ΔC9(M_M)
ΔC20(M_M)
ΔC9(M_M)

Figure D.11

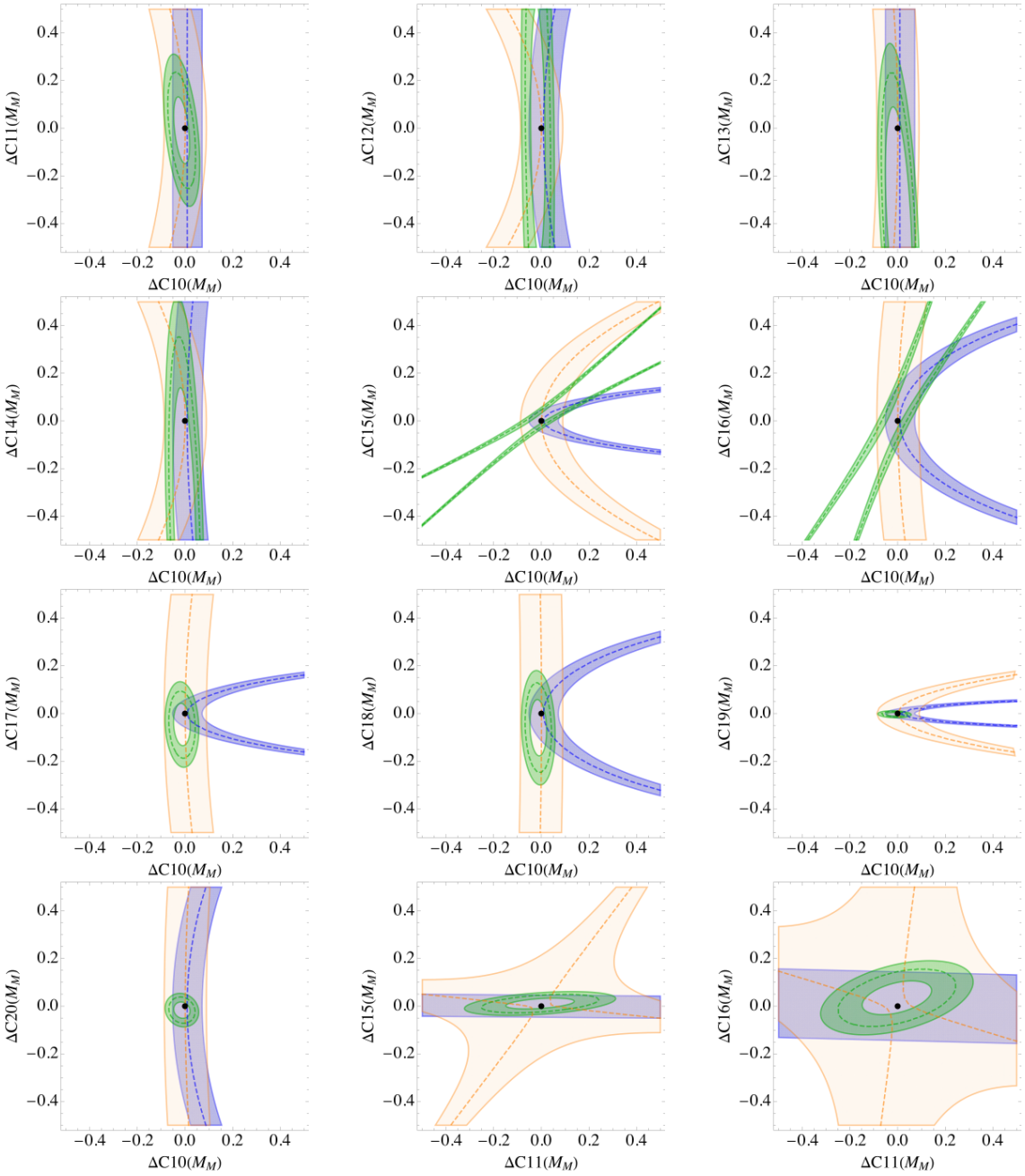
ΔC11(M_M)
ΔC12(M_M)
ΔC13(M_M)
ΔC14(M_M)
ΔC15(M_M)
ΔC16(M_M)
ΔC17(M_M)
ΔC18(M_M)
ΔC19(M_M)
ΔC20(M_M)
ΔC15(M_M)
ΔC16(M_M)
ΔC10(M_M)
ΔC11(M_M)
0.4
0.2
0.0
−0.2
−0.4

Figure D.12

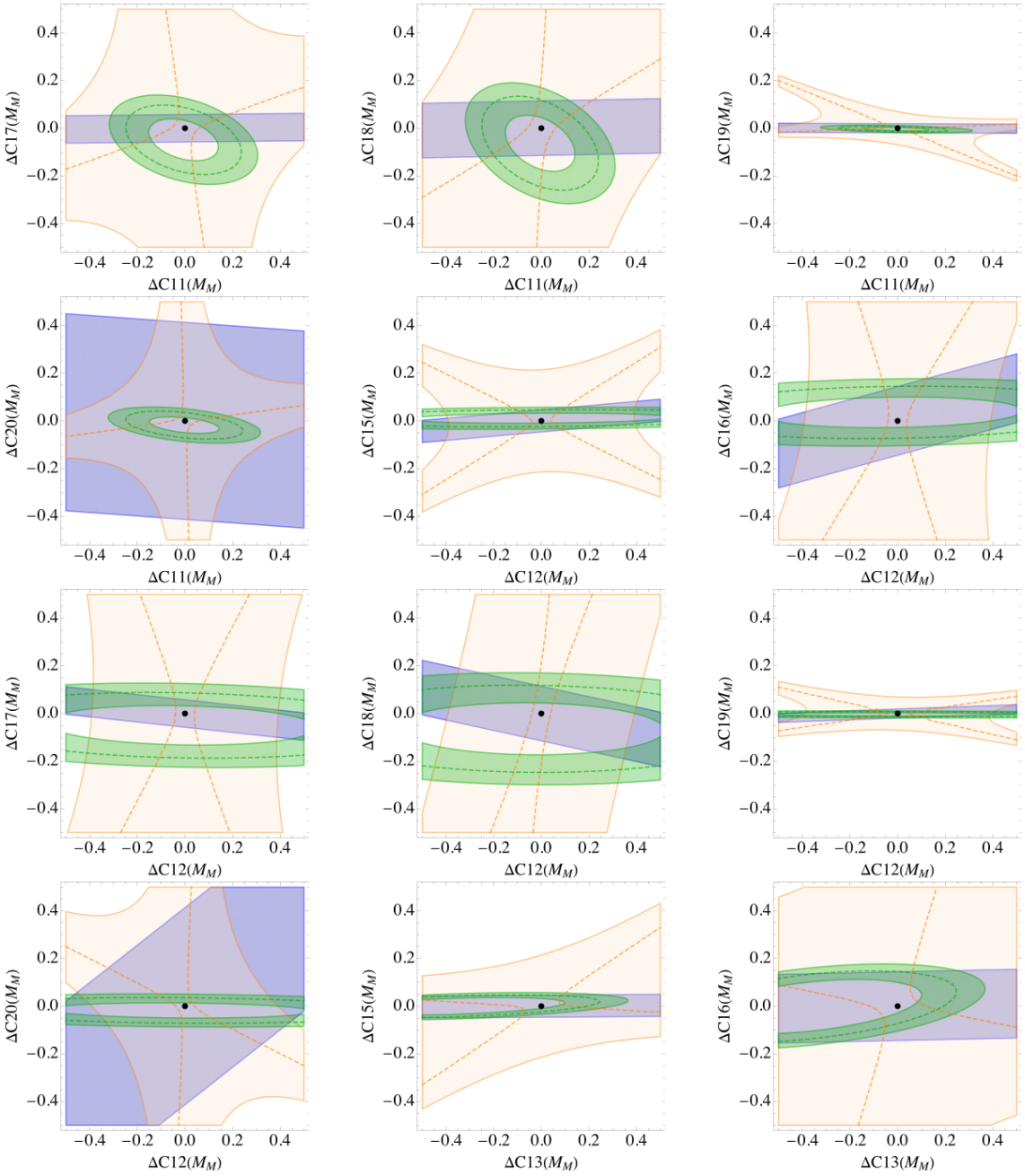
ΔC17(M_M)
ΔC11(M_M)
ΔC18(M_M)
ΔC11(M_M)
ΔC19(M_M)
ΔC11(M_M)
ΔC20(M_M)
ΔC11(M_M)
ΔC15(M_M)
ΔC12(M_M)
ΔC16(M_M)
ΔC12(M_M)
ΔC17(M_M)
ΔC12(M_M)
ΔC18(M_M)
ΔC12(M_M)
ΔC19(M_M)
ΔC12(M_M)
ΔC20(M_M)
ΔC12(M_M)
ΔC15(M_M)
ΔC13(M_M)
ΔC16(M_M)
ΔC13(M_M)

Figure D.13

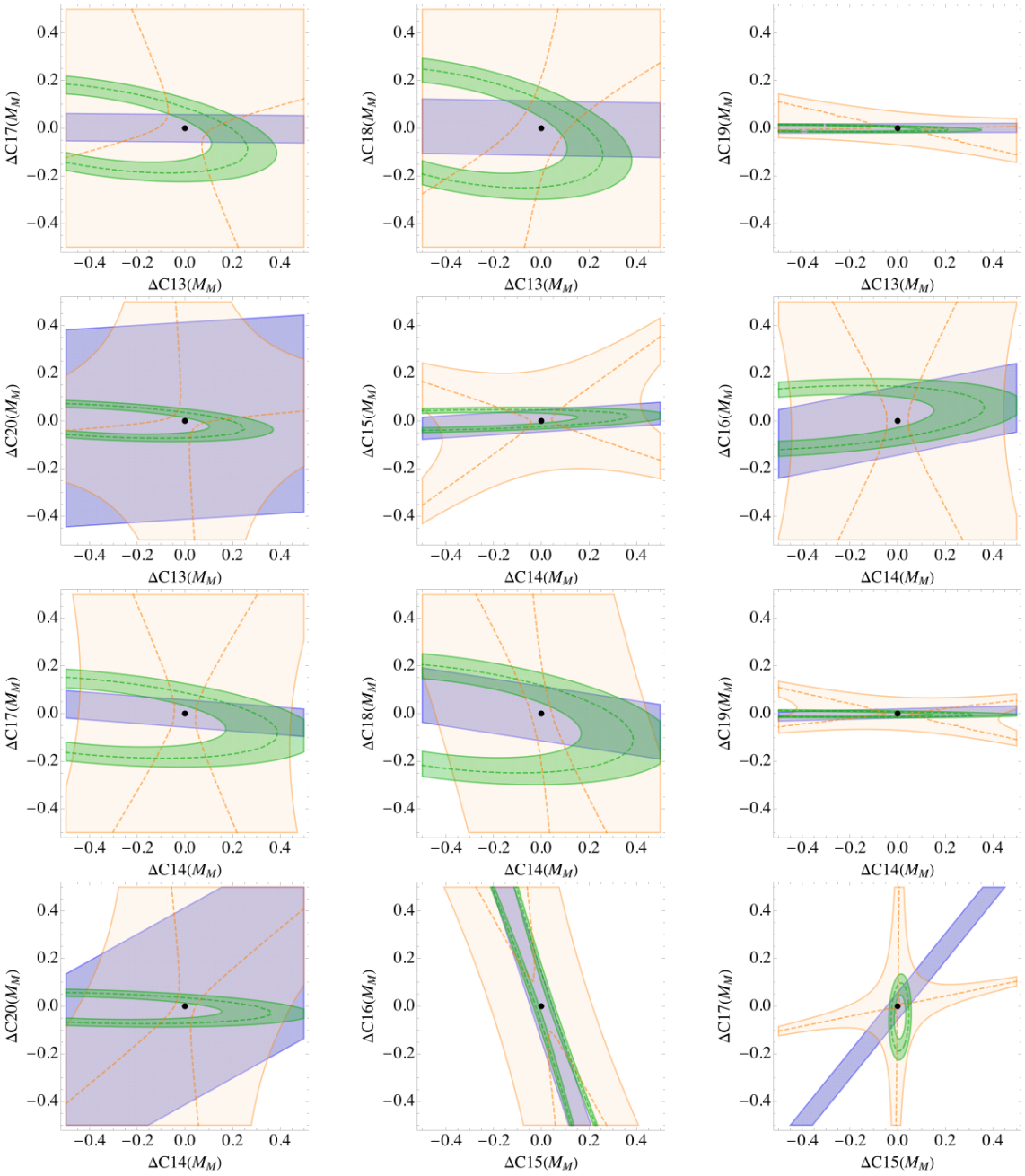
ΔC17(M_M)
ΔC13(M_M)
ΔC18(M_M)
ΔC13(M_M)
ΔC19(M_M)
ΔC13(M_M)
ΔC20(M_M)
ΔC13(M_M)
ΔC15(M_M)
ΔC14(M_M)
ΔC16(M_M)
ΔC14(M_M)
ΔC17(M_M)
ΔC14(M_M)
ΔC18(M_M)
ΔC14(M_M)
ΔC19(M_M)
ΔC14(M_M)
ΔC20(M_M)
ΔC14(M_M)
ΔC16(M_M)
ΔC15(M_M)
ΔC17(M_M)
ΔC15(M_M)

Figure D.14

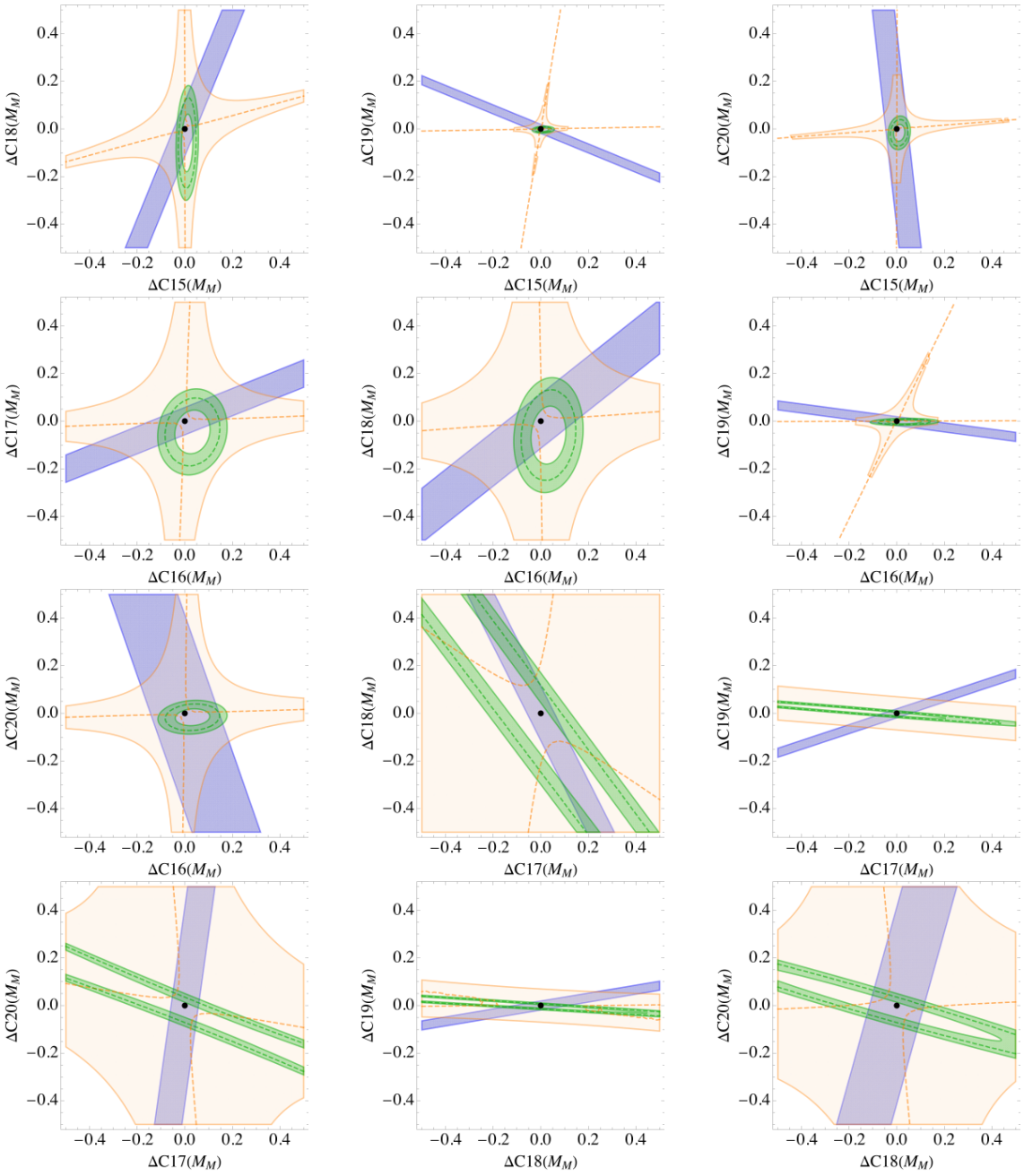

Figure D.15

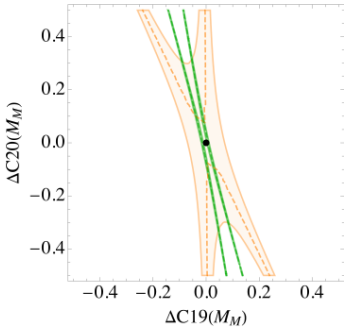

Figure D.16